The face of *Homo floresiensis*: An investigation of scale

Michael Duncan

A thesis presented to Lakehead University

in partial fulfillment of the requirements of

Master of Science in Archaeological Science

Thunder Bay, Ontario, Canada, 2023

Table of contents

Acknowledgements

First, I would like to thank Dr. Matt Tocheri for all of your time, effort, and support during the course of this research project. Thank you for getting me started on this project and helping me reach my full potential as a graduate student. This work would have not been possible without your constant support and guidance throughout. The skills I have learnt here will remain with me throughout the rest of my career and life. Thank you to Dr. Tamara Varney for agreeing to serve on my committee and for your critical comments and suggestions on my thesis. Dr. Adam Gordon, thank you for providing your fabulous R code, which gave me a fantastic head start in performing the scaling analyses. Without this code to get started, it would have taken me much longer to figure out what I needed to do to perform these analyses correctly and on command. Finally, a special thank you to Dr. Bernard Wood for serving as my external examiner.

I would also like to thank Lakehead University's Anthropology Department. Thank you to Jennifer McKee for her constant reliability and willingness to help by answering my questions and providing expert administrative guidance. Thank you to all my graduate course instructors throughout the last two years: Drs. Scott Hamilton, Jessica Metcalfe, Matt Tocheri, and Adam Cornwell. I am thankful to have had the opportunity to advance my knowledge with all of you. Thank you to everyone in the Human Origins Laboratory who attended the weekly meetings and shared their work, even on holidays. I have learned so much listening to the many different research projects. Thank you to my fellow MSc in Archaeological Science cohort members: Holly Ascroft, Shane Teasdale, Steph Skelton, Maddison Mancusa, Claire Woodley, and Taylor Belot. It has been great getting to work and learn with all of you.

I am grateful for all the financial support this project received. Thank you to the Ontario Graduate Scholarship Program (OGS) (to Michael Duncan), SSHRC Insight award No. 435-2017-1234 (to Dr. Matt Tocheri), Lakehead University Ontario Graduate Scholarship committee, and Lakehead University for supporting and funding this project.

Lastly, I would like to thank all my family for dealing with my rants about craniofacial scaling, locomotion, and the evolution of our species. Thank you to my friends Brandon McKinlay, Giuseppe Tullio, and Mitchell Legault for always being willing to listen to my research and give helpful advice. A very special thank you to my parents, Michelle and David, and my partner Veronika Thomas for your unwavering support and motivation to pursue the career of my dreams.

List of tables

List of figures

Abstract

The face of *Homo floresiensis* has been described as small in absolute and relative size, comparable to the condition observed in modern humans (*Homo sapiens*). It has even been claimed that LB1's relative facial dimensions are broadly similar to other fossil hominin crania that have extremely small faces in relation to their cranial vaults, such as Asian *Homo erectus* and the Dali cranium. The idea that LB1 shares a proportionately small face with some but not all species in the genus *Homo* is a key component of the hypothesis that *Homo floresiensis* is an island-dwarfed descendant of Asian *Homo erectus*. Here I test two specific questions in terms of the relative external size/shape of LB 1's facial skeleton. First, can LB 1's relative facial size and shape be accommodated within the ranges of variation for a worldwide sample of normal, nonpathological, modern humans? If not, then which hominin taxon or subset of hominin crania does LB 1 most closely resemble in terms of relative facial size and shape? Results show that when LB 1 is properly scaled against other measures of cranial size, its face is actually relatively large and comparable to the facial sizes of various australopith and early *Homo* specimens, not including *Homo erectus sensu lato*, yet it retains a facial shape that is shared among all *Homo*. Although reduced facial size in hominins is typically considered to be the result of decreased masticatory stresses, it has also been linked to the evolution of running, wherein a smaller face makes it energetically easier for the head to remain stabilized during movements at faster speeds. The combination of a relatively large face, short legs, and long feet suggests that *Homo floresiensis* most likely evolved from an early *Homo* ancestry that does not include Asian *Homo erectus* and had yet to accrue any morphological adaptations (either cranial or postcranial) for bipedal running. Moreover, evolution of the face in the genus *Homo* may be the result of a two-stage process: 1) initial reduction in facial and dentognathic size as well as modifications to

facial shape relative to facial size and shape in australopiths due to changes in diet, followed by 2) subsequent reduction in facial size (length especially) due to increased commitment to terrestrial bipedality, including running.

Introduction

Homo floresiensis, an extinct small-bodied and small-brained hominin species found on the Indonesian island of Flores, has stimulated many intense debates and discussions in paleoanthropology during the past two decades since its unexpected discovery (Brown et al., 2004; Morwood et al., 2004). One unresolved question about this species involves competing hypotheses about its ancestry. Is *Homo floresiensis* an island-dwarfed descendant of Asian *Homo erectus* or does it trace its ancestry to some other species of early *Homo* (e.g., *Homo habilis*, *Homo rudolfensis*, etc.) (Kaifu et al., 2011a; Baab, 2016; Tocheri et al., 2022)? Evidence from its skull, the teeth and face in particular, has been used to support the former (Brown et al., 2004; Kaifu et al., 2011a, 2015a,b; van den Bergh et al., 2016) whereas evidence from its postcrania (e.g., limb proportions and pelvic, wrist, and foot morphology) has been used to support the latter (Brown et al., 2004; Morwood et al., 2004; Tocheri et al., 2007; Jungers et al., 2009a,b; Orr et al., 2013). In this thesis, I focus on this apparent discrepancy between the cranium and postcranium in *Homo floresiensis* by closely reexamining the evidence from its face. It is generally accepted that *Homo floresiensis* has a face that is absolutely and relatively small in relation to the size of its neurocranium (Kaifu et al., 2011a; Cook et al., 2021) and that this derived morphology is shared (i.e., a synapomorphy) with Asian *Homo erectus* and other Asian *Homo* specimens such as the Dali cranium (Kaifu et al., 2011a). However, studies have yet to consider how scaling (i.e., how proportional changes in body size impact other morphological changes within and between species) may impact comparisons of facial size and shape between an extremely small taxon like *Homo floresiensis* and other larger hominin taxa both fossil and extant. Scaling analyses are a critical component of evolutionary biology generally (Kingslover and Koehl, 1985; Macfadden, 1986) and have been used successfully to increase knowledge and

understanding of hominin biology and evolution specifically (Gordon et al. 2008; Singleton, 2012; Kubo et al., 2013; Du et al., 2018; Ruff and Wood, 2023).

Hominin evolution is characterized by multiple major changes in anatomy and behaviour that occurred during the past ~8–6 million years (Ma). Among these changes, a reduction in canine size coupled with the loss of the maxillary canine-mandibular 3rd premolar honing complex (Brunet et al., 2002; Selassie et al., 2004; Suwa et al., 2009; Delezene, 2015) and the adoption of terrestrial bipedal locomotion, differentiate the earliest hominins from nonhominin primates (Stern and Susman 1983; Pickford et al., 2002; Nagano et al., 2005; Richmond and Jungers, 2009; Lovejoy et al., 2009a,b; Daver et al., 2022). Subsequent changes, such as increases in relative brain size (Elton et al., 2001; Navarette et al., 2011; Holloway, 2015), the use and manufacture of stone tools (Marzke, 1997; Semaw et al., 1997; Susman, 1998; Harmand et al., 2015; Shea, 2017; Kunze et al., 2022; Plumber et al., 2023), and the emergence of endurance running (Bramble and Lieberman, 2004; Pontzer et al., 2010; Lieberman, 2011; Ruxton and Wilkinson, 2011), appear to characterize various species placed in the genus *Homo*, with many of these traits presumably occurring together for the first time in *Homo erectus sensu lato* as early as ~1.47 Ma (Antón, 2003; Ruxton and Wilkinson, 2011; McDougall et al., 2012).

The idea that endurance running played an important role during human evolution is based on the fact that the anatomy of modern humans differs from that of australopiths (i.e., specimens typically attributed to genera such as *Australopithecus* and *Paranthropus*) and *Homo habilis* in several substantial ways. For instance, in addition to having a tall narrow body form (Bramble and Lieberman, 2004), modern humans have legs that are long in relation to their arms as well as feet that are short in relation to the rest of their hindlimb (Susman et al., 1984; Richmond et al., 2002; Aiello and Wells, 2002; Jungers, 2009; Jungers et al., 2009a,b). The feet

of modern humans also have long achilles tendons, plantar arches, short toes relative to the metatarsals, adducted non-grasping halluces, enlarged calcaneal tubers, and close-packed calcaneocuboid joints, enabling the foot to act efficiently as a propulsive lever during prolonged terrestrial bipedal locomotion (D'Août and Aerts, 2008; Jungers et al., 2009a; Holowaka and Lieberman, 2018). Other features that contribute to a more energetically efficient gait for running rather than walking bipedally include a low and wide pectoral girdle, increased lordosis of the spine, a barrel shaped trunk with a narrow waist and enlarged iliac pillars, shorter femoral necks, a stronger and larger *gluteus maximus* area, and an expanded hindlimb joint area (Bramble and Lieberman, 2004; Lieberman and Bramble, 2007; Larson et al., 2007; Lieberman, 2011).

There are also a number of ways that modern human cranial shape is thought to be adapted for endurance running. For instance, the cranium as a whole is decoupled from the pectoral girdle to handle the counter rotation of the head versus the trunk (Bramble and Lieberman, 2004). The posterior semicircular canals are enlarged relative to those of chimpanzees and australopiths and are thought to help stabilize the head as it pitches forward during running, while the neurovenous regions are expanded for thermoregulation (Bramble and Lieberman, 2004; Lieberman, 2011). Moreover, the head is well balanced atop the vertebral column with reduced nuchal attachment areas—where soft tissues connect the cranial base to the cervical vertebrae and parts of the pectoral girdle—while the face is ventrally positioned and tucked under the calvaria (Bramble and Lieberman, 2004; Lieberman, 2011). In combination, these cranial features create a more stable and kinesthetically efficient relationship between the head and the body for endurance running in modern humans and other similarly derived hominin species (e.g., Neandertals), resulting in sustained energy output and minimal energy/heat loss in comparison to those of great apes and various early hominin species (Bramble and Lieberman,

2004). For example, a cranium with a face that is relatively short and orthognathic in combination with a less posteriorly-projected occipital bone helps counteract forces that destabilize the cranium during running (Bramble and Lieberman, 2004; Yegian et al., 2021). These features enable the head to be pitched closer to the trunk resulting in energetically more efficient and/or less strenuous bipedal endurance running (Bramble and Lieberman, 2004).

Lieberman (2011) suggested that a reduction in facial length (i.e., a reduced face that is 'tucked' underneath the anterior cranial vault) is observed first in early *Homo* or *Homo habilis*, ending with the condition seen in modern *Homo sapiens*. Yet compared to *Homo erectus sensu lato* (specifically, KNM-WT 15000), *Homo habilis* and other early *Homo* lack many other distinguishing traits related to endurance running such as modern human-like body and/or limb proportions, appearing more as 'transitional' hominins between australopiths and more derived species of *Homo* such as modern humans and Neandertals (Ohman et al., 2002; Richmond et al., 2002; Haeusler and McHenry, 2004; Ruff, 2009; Wood, 2019). It is possible that these evolutionary trends in craniofacial form are tightly linked to trends for other endurance running-related traits in the postcranial skeleton, where they first begin to appear in early *Homo* but only become clearly modern human-like in hominins such as *Homo erectus sensu lato* (Bramble and Liebrman, 2004; Ruff, 2009; Ruxton and Wilkinson, 2011). A potential way to test this idea is to examine how facial size scales in relation to neurocranial size in various fossil hominin specimens in comparison with the scaling patterns of extant humans and great apes.

Scaling analyses are used in evolutionary biology to examine how characteristics or features vary in relation to size (usually body size but other measures of size can be included) across a set of taxa (Pilbeam and Gould, 1978; Pagel and Harvey, 1988; McCarthy, 2001; Gordon et al., 2008; Spence, 2009; Campione and Evans, 2012; Singleton, 2013; Pérez-Carlos et

al., 2015; Pérez-Carlos and Palmqvist, 2022). In other words, are specimens or taxa scaled down or scaled up versions of one another, meaning that they are the same relative size and otherwise increase or decrease in size at the same or similar rate (Pilbeam and Gould, 1978; Pagel and Harvey, 1988; McCarthy, 2001; Gordon et al., 2008; Spence, 2009; Campione and Evans, 2012; Singleton, 2013; Pérez-Carlos et al., 2015; Pérez-Carlos and Palmqvist, 2022)?

A number of different methods can be applied to research questions about scaling in order to observe rates of change in relative size space, but most often these involve some kind of regression analysis, usually with logged variables. Since the variables of interest are usually measured in units that differ from that for mass (e.g., mm versus kg), a regression method that is scale invariant is required. Logging variables prior to analysis acts to reduce the order of magnitude and generates a linear relationship between two variables (Pilbeam and Gould, 1978; Pagel and Harvey, 1988; McCarthy, 2001; Gordon et al., 2008; Spence, 2009; Campione and Evans, 2012; Singleton, 2013; Pérez-Carlos et al., 2015; Pérez-Carlos and Palmqvist, 2022). Components or factors that describe a percentage of variation generated from multiple variables can also be logged and examined using bivariate regressions to describe variation in relative size/shape (Kubo et al., 2013; Pérez-Claros et al., 2015; Pérez-Claros and Palmqvist, 2022). Reducing the order of magnitude helps represent specimens of drastically different sizes in a reduced space, making it easier to interpret the empirical scaling relationships compared with using only absolute measurements/values (Pilbeam and Gould, 1978; Pagel and Harvey, 1988; McCarthy, 2001; Gordon et al., 2008; Spence, 2009; Campione and Evans, 2012; Singleton, 2013; Pérez-Carlos et al., 2015; Pérez-Carlos and Palmqvist, 2022). In essence, reducing the order of magnitude by using logged values better describes the relative size/shape variation of included specimens.

In evolutionary biology, scaling methods typically use ordinary least squares (OLS), major axis (MA), and/or reduced major axis (RMA) regression analyses, all of which are suitable for examining scaling relationships (Dhona et al., 2016). However, OLS can only function properly when assumptions of errors in the dependant variable (y) are permitted and the independent variable (x) is confidently defined with no errors, creating an asymmetrical relationship between the two variables used (White et al., 2007; Dhona et al., 2016; Kilmer and Rodríguez, 2017). An asymmetrical relationship occurs when the residuals (i.e., the linear distances from each observation to the predicted value based on the slope of the regression line) are measured perpendicular to the x axis (or parallel to the y axis) (Dhona et al., 2016). However, measurement of bone/soft tissues, mass estimations (vis a vis from other measurements), and other calculated values to describe multidimensional surfaces are all subject to errors because they may not represent the 'true' condition of the observed variable. Kilmer and Rodríguez (2017) suggest that OLS should be used uniformly across evolutionary biological studies of allometry, "because: (i) the problem of slope attenuation by OLS regression can realistically be mitigated by ensuring that measurement error is low, or by correcting for it; and (ii) OLS regression actually describes allometric scaling, whereas RMA regression does so only in a narrow range of conditions" (2017:11). However, this argument is contingent upon the notion that all measurements used for x can be mitigated for error (Kilmer and Rodríguez, 2017) and this is unfortunately not possible when comparing fossil specimens with living species because any measurement or extrapolated value is in essence a measurement that is subject to error (Dhona et al., 2016). Even with error mitigation, issues based on multiple observations (sometimes by multiple observers) create errors with unknown variance that violate the OLS

assumption that the independent variable has no error (Dhona et al., 2016). Therefore, not all scaling studies in evolutionary biology can reliably use OLS.

Scaling relationships that depend on using variables that are prone to error and variance, as is most often the case when observing differences in scale between known species and fossil specimens, are instead typically analyzed using MA or RMA regressions (Pilbeam and Gould, 1978; Pagel and Harvey, 1988; McCarthy, 2001; Gordon et al., 2008; Spence, 2009; Campione and Evans, 2012; Pérez-Claros et al., 2015; Dhona et al., 2016; Pérez-Claros and Palmqvist, 2022). In MA, the residuals are measured as the perpendicular distance to the slope of the regression line whereas in RMA the residuals are measured as the area of the triangle created by each point to the regression line. In both instances, the desired outcome is the ability to describe the relationship the two variables have with one another, assuming that both variables have some kind of associated error (Pilbeam and Gould, 1978; Pagel and Harvey, 1988; McCarthy, 2001; Gordon et al., 2008; Spence, 2009; Campione and Evans, 2012; Pérez-Carlos et al., 2015; Pérez-Carlos and Palmqvist, 2022). Since MA/RMA regressions assume errors in both x and y, they each describe a symmetrical relationship between these two selected variables. In other words, a symmetrical relationship occurs when the residuals of x and y are equidistant from the measured slope (Dhonas et al., 2016; Kilmer and Rodríguez, 2017). MA/RMA scaling regressions also observe more natural variation than when using the same variables in an OLS regression because of the assumptions of error in both x and y (Kilmer and Rodríguez, 2017). For example, a previous MA scaling analysis of body mass over femoral or humeral length in terrestrial quadrupeds revealed a linear relationship across all species sampled (Campione and Evans, 2012). These results demonstrated that the body mass of a terrestrial quadruped increases

at the same rate as femoral or humeral lengths across all of the species observed (Campiones and Evans, 2012).

If specimens or species do not scale equivalently with one another, then the two variables will not scale in relative space equally. For example, Pérez-Carlos et al. (2015) scaled the crania of extant great apes as well as modern humans and extinct hominins using six linear measurements (three facial, two neurocranial, one facial projection), by first conducting a factor analysis to describe the covariation of their samples. This factor analysis reduced the six variables used into two factors that described 93.7% of the total variance (Factor 1 = 61.2%, Factor 2 = 32.5%), while attempting to describe the correlation between each variable observed (Pérez-Carlos et al., 2015). The first factor described a separation of facial size over neurocranial size with the relatively large faces and small neurocrania of australopiths and great apes (with orangutans as the most extreme) on one end, and the relatively small faces and large crania of modern humans on the other, with fossil *Homo* plotting in between these two groups (Pérez-Carlos et al., 2015). The second factor described separation of general size, with male gorillas representing the largest crania and *Pan* the smallest crania. RMA regressions of each known species (and all fossil specimens) were then plotted over this factor analysis to describe if each species (and the fossil specimens) not only differentiated from each other in this factorial space, but that the predicted size relationships of each species, fossil and extant, were in fact, also different (Pérez-Carlos et al., 2015).

Their results suggested that the scaling relationships of great apes and modern humans were different from one another, and that all of the included fossil hominin specimens described a 'transitional' scaling relationship with australopiths showing the most great ape-like relationship, and Neandertals, Asian *Homo erectus* (Sangiran 17), and *Homo heidelbergensis*

(Steinhiem, Petralona) plotting with modern humans (recent and Pleistocene) (Pérez-Carlos et al., 2015). In other words, it is fundamentally impossible based on the differences in observed scaling relationships to achieve the relative size of a modern human by scaling a great ape (or vice versa) because the respective scaling relationships are fundamentally different from one another (Pérez-Claros et al., 2015).

In studies of hominin evolution, the relationship between body mass and the size or proportions of specific variables of the skeleton is important when claiming that a hominin species is different not only in absolute size/shape but also in relative size/shape. Among relatively recent hominin discoveries, none arguably better encapsulates the need for careful analyses of scale than does *Homo floresiensis*. The discovery in the early 2000s of this extinct small-bodied and small-brained species thus far known only from the Indonesian island of Flores (Brown et al., 2004; Morwood et al., 2004, 2005) has prompted intense debates about its taxonomy and ancestry. Initially, these taxonomic debates centered around whether to treat this new discovery and its holotype (LB 1) as a novel species or a pathological modern human (Brown et al., 2004; Lahr and Foley, 2004; Morwood et al., 2004; Falk et al., 2005a,b; Morwood et al., 2005; Jacob et al., 2006). However, continued research of material attributed to this taxon has strongly favored treating it as a novel species (Argue, et al., 2006; Falk et al., 2006, 2007; Larson et al., 2007; Tocheri et al., 2007; Gordon et al., 2008; Jungers et al., 2009a,b; Kaifu et al., 2011a; Brown, 2012; Kaifu et al., 2015a,b; Baab et al., 2016; Cook et al., 2021).

There have also been several analyses showing that LB 1's relative cranial, endocranial, and postcranial size is more similar to that of other fossil hominins and unlike that of modern humans (Argue et al., 2006; Falk et a., 2007; Gordon et al., 2008; Baab and McNulty, 2009; Falk et al., 2009a,b; Kaifu et al., 2011a; Baab et al., 2013; Pérez-Carlos et al., 2015; Pérez-Carlos and

Palmqvist, 2022). For example, LB 1 appeared more similar to fossil species than modern humans based on six cranial measurements (four neurocranial, two facial projection) when these were first scaled using their geometric mean (Gordon et al., 2008). Similarly, 3D geometric morphometric analyses of the neurocranium and the neurocranium together with the face showed that LB 1 was more similar with early *Homo* and australopiths than with modern humans or extant great apes (Baab and McNulty, 2009). Another study (Kaifu et al., 2011a) included a principal component analysis (PCA) using eight neurocranial measurements and plotted the first four components against the geometric mean of these eight measurements in an OLS regression. Each of the four resulting scaling regressions showed LB 1 shared more in common with various fossil specimens of *Homo* than with modern humans (Kaifu et al., 2011a).

Some studies have also included modern humans with some form of microcephaly (i.e., brain size of modern human equivalent) in the sample for comparison with LB 1 (Argue et al., 2006; Falk et a., 2007; Falk et al., 2009a; Baab et al., 2013; Pérez-Carlos et al., 2015). For instance, Baab et al. (2013) used PCA and Procrustes distances to examine the calvarial shape of LB 1 with those of modern humans with normal brain sizes, modern humans with some form of microcephaly (including individuals with Laron syndrome, myxoedematous endemic cretinism, hypothyroidism, and primary microcephaly), and other fossil hominins. Their results showed further support that LB 1's cranial shape is more similar to that of other fossil *Homo* than it is to that of modern humans, including those with microcephaly (Baab et al., 2013). Other studies (Pérez-Carlos et al., 2015; Pérez-Carlos and Palmqvist, 2022) examined the relationship between the calvaria and the face and found a general trend demonstrating that great apes have larger faces relative to their neurocranium in comparison to all modern and fossil humans in their sample. These studies (based on three neurocranial, two facial, and one facial projection

measurement) also found that LB1's cranial shape is more similar to that of early *Homo* such as *Homo habilis* rather than *Homo erectus sensu lato* (Pérez-Carlos et al., 2015; Pérez-Carlos and Palmqvist, 2022). However, these results were not considered particularly surprising because these studies assumed that LB 1 is more closely related to *Homo habilis* rather than possibly representing an island-dwarfed descendant of Asian *Homo erectus* (Pérez-Carlos et al., 2015; Pérez-Carlos and Palmqvist, 2022). Due to the wide variety of interpretations drawn from the skeletal remains of *Homo floresiensis*, the ancestry of this enigmatic species is still a topic of intense debate among paleoanthropologists, and few would argue that such a question has been satisfactorily resolved.

Debates over the ancestry of *Homo floresiensis* are centered on how exactly this species is related to *Homo sapiens* and other extinct hominin taxa. For example, is it an evolutionary descendant or sister taxon of Asian *Homo erectus* or some other species of *Homo*? The possibility of a close phylogenetic relationship with Asian, and especially Indonesian *Homo erectus* is favored by many (Kaifu et al., 2011a; Baab et al., 2013; Kaifu et al., 2015a,b; Cook et al., 2021) because at the time *Homo floresiensis* was discovered, Asian *Homo erectus* was the only non-modern hominin species widely recognized from this geographical region. However, with new discoveries, such as *Homo luzonensis* from the Philippines (Detroit et al., 2019), and as further details have emerged about the anatomy and behavior of *Homo floresiensis* (Tocheri et al., 2007; Gordon et al., 2008; Jungers et al., 2009; Baab and McNulty 2009; Orr et al., 2013; Tocheri et al., 2022), the possibility that it might share a closer phylogenetic relationship with hominin species currently known only from Africa (e.g., early *Homo* such as *Homo habilis* or perhaps even australopiths) has gained traction (Dembo et al., 2015, 2016; Argue et al., 2017). Both of these hypotheses regarding the ancestry of *Homo floresiensis* have received support from

various aspects of the available evidence, including when comparative scaling analyses have been performed (Baab, 2016).

Given that LB 1 has an estimated stature and body mass of 106 cm (Brown et al., 2004) and 27.5 kg (Grabowski et al. 2015), respectively, as well as a cranial capacity of ~420 cubic centimeters (Falk et al., 2005; Kubo et al., 2013), hypotheses involving Asian *Homo erectus* ancestry typically invoke scenarios that include some degree of insular dwarfism (Brown et al., 2004; Broham and Cardillo, 2007; Weston and Lister, 2009). Based on cranial morphology, Kaifu et al. (2011a) concluded that *Homo floresiensis* is most similar to early Javanese *Homo erectus* and other South East Asian hominins, such as the Dali cranium, than to African *Homo erectus* or *Homo habilis*, especially in terms of relative facial size, facial gracilization, and overall cranial shape. According to Kaifu et al. (2011a), "the face of LB 1 is small both absolutely and relatively to its neurocranial size in all dimensions except for the orbital height" and "one parsimonious explanation for the markedly reduced face of LB 1 is that it originated from the small face of Asian *H. erectus*" (2011a:678). However, this conclusion was based primarily on bivariate analyses of absolute size measurements in combination with qualitative assessments and no empirical scaling analyses were conducted. In contrast, when six cranial measurements were empirically scaled using a geometric mean (as a proxy for overall cranial size) and examined in log-log space, *Homo floresiensis* more closely resembled *Homo habilis* and African *Homo erectus* rather than Asian *Homo erectus* (Gordon et al., 2008). Similarly, scaling analyses using MA and RMA regressions of logged endocranial volume over logged femoral head diameters demonstrated that the brain size of *Homo floresiensis* scales more closely to that of *Homo habilis* and australopiths than that of *Homo erectus* or modern humans (Kubo et al., 2013).

In this thesis research, I investigate the generally accepted idea that LB 1 has a gracile face that is small in both absolute and relative size (Kaifu et al., 2011a) using MA regression analyses of craniofacial measurements from recent modern humans and comparing how they scale in comparison with measurements from LB 1, other fossil hominin specimens, and extant great ape taxa. Similar to a previous study of neurocranial scaling of LB 1 (Gordon et al., 2008), I address two specific questions in terms of the relative external size/shape of LB 1's facial skeleton. First, can LB 1's relative facial size and shape be accommodated within the ranges of variation for a worldwide sample of normal, nonpathological, modern humans? If not, then which hominin taxon or subset of hominin crania does LB 1 most closely resemble in terms of relative facial size and shape?

The reason these questions are important to investigate is because various cladistic analyses based on suites of craniodental characters have typically found that *Homo floresiensis* is more similar to early African *Homo* than it is to later Asian *Homo* (Argue et al., 2009; Dembo et al., 2015, 2016; Argue et al., 2017). However, Kaifu et al. (2011a) specifically described the face of LB 1 (*Homo floresiensis*) as gracile and similar to Asian *Homo erectus* in terms of its relative size, morphology, and robusticity. Therefore, if the interpretations of Kaifu et al. (2011a) are accurate, then the face of *Homo floresiensis* should scale in a similar way to that of Asian *Homo erectus*.

Methods

This project utilizes 11 craniofacial osteometric measurements of extant hominids (i.e., modern humans and great apes) and extinct hominins compiled from the literature (Weidenrieich, 1943; Howell, 1960; Tobias, 1967; Howells, 1973; Kimbel et al., 1982; Rak et al., 1983;

Rightmire, 1983; Clarke, 1985; Leakey and Walker, 1988; Clarke, 1990; Wood, 1991; Condemi, 1992; Arsuaga et al., 1997; Suwa et al., 1997; Lockwood, 1999; Lockwood and Tobias, 1999; Arif et al., 2002; Asfaw et al., 2002; Widianto and Zeitoun, 2003; Brown et al., 2004; Kimbel et al., 2004; Liu et al., 2005; Curnoe and Tobias, 2006; Lordkipanidze et al., 2006; Rightmire et al., 2006; Lockwood et al., 2007; Spoor et al., 2007; Gordon et al., 2008; Kaifu et al., 2008; Berger et al., 2010; Benazzi et al., 2011; Rightmire, 2013; Kaifu et al., 2011a, b; Kaifu et al., 2015c; Weaver and Stringer, 2015; Hawks et al., 2017; Kaifu, 2017; Laird et al., 2017; Selassie et al., 2019; Ni et al., 2021; Rak et al., 2021; Pérez-Claros and Palmqvist, 2022). The measurements for the extant taxa derive from 2,524 modern humans, representing populations worldwide, including those of small body size (Howells, 1973), and from 14 orangutans, 29 gorillas, 20 bonobos, and 291 chimpanzees (Weaver and Stringer, 2015; Pérez-Claros and Palmqvist, 2022). The fossil hominin data represent various species of australopith (i.e., specimens attributed to *Australopithecus* or *Paranthropus*) and *Homo*. In cases where measurements of particular fossil specimens have been published by different researchers, a number of these different sets of measurements have been included so as not to necessarily bias or favor one set over another. The full data set, including the various sources of the measurements used, is provided in Appendix A.

Of the 11 craniofacial variables, four measure the neurocranium, five measure the face, and two measure facial projection relative to the neurocranium (Figure 1). The neurocranium variables capture length (greatest cranial length, GOL), width (cranial and asterionic breadth, XCB and ASB, respectively), and height (cranial height, BBH); the facial variables capture facial height (nasion-prosthion height, NPH), upper midfacial breadth (zygomatic breadth, ZYB), lower midfacial breadth (zygomaxillary breadth, ZMB), lower facial breadth (maxilloalveolar breadth, MAB), and bi-orbital outer breadth (BOB); the remaining two variables capture upper

and lower facial projection relative to the neurocranium (basion-nasion and basion-prosthion length, BNL and BPL, respectively).

Defined as the linear distance between glabella and opisthocranion, GOL is the most reliably repeatable way to measure maximum neurocranial length. Although supraorbital torus size affects the location of glabella and occipital/nuchal process orientation affects the location of opisthocranion, these two landmarks are almost always the most anterior and posterior points, respectively, of the neurocranium. Cranial breadth is measured in two ways: the maximum linear distance between the right and left supramastoid crests (XCB) and the linear distance between both asterion landmarks, the point where the occipital, temporal, and parietal bones meet, on the right and left side of the basicranium (ASB). Neurocranial height (BBH) is measured as the linear distance between basion, the most anterior point of the foramen magnum, and bregma, the point where the coronal and sagittal sutures meet. Both BNL and BPL are typically used to quantify facial projection relative to the neurocranium (Gordon et al., 2008; Bastir and Rosas 2016). For the upper face, BNL is measured as the linear distance between basion and nasion, which is located where the interorbital and internasal sutures meet. For the lower face, BPL is measured as the linear distance between basion and prosthion, the most anteroinferior point on the maxilla that occurs between the left and right central maxillary incisors.

Nasion-prosthion height (NPH) measures the combined height of the upper and middle face and is defined as the linear distance between nasion and prosthion. This measurement in combination with BNL and BPL creates a facial triangle that captures the height and projection of the upper and lower face in relation to the position of the foramen magnum. Zygomatic breadth (ZYB) is measured as the maximum linear distance between the most lateral points of the left and right zygomatic arches (also known as zygion) and is often used to describe

masticatory potential in hominins (Pearson and Lieberman, 2004; Weber and Kren, 2017; Rak and Marom, 2017; Ledogar et al., 2016, 2017). Zygomaxillary breath (ZMB) is measured as the maximum linear distance between the two most inferior points where the zygomatic and the maxillary processes meet (also known as zygomaxillare). It is generally used to represent the breadth of the midface while still including part of the masticatory apparatus. In combination, ZYB and ZMB provide a reasonable, repeatable way to quantitatively describe the masticatory potential of a hominin specimen. Maxilloalveolar breadth (MAB) is measured as the linear distance between the two most lateral points of the alveolar borders on the left and right maxilla (also known as ectomalare) (Kaifu et al., 2011a). This measurement is typically used to represent lower facial breadth as it is unaffected by the temporal region (i.e., MAB is reasonably independent of ZMB and ZYB). Finally, bi-orbital outer breadth (BOB) captures the breadth of the upper face and is measured as the linear distance between the right and left frontomalare temporale landmarks, which occur where the temporal bone meets the orbital arch.

In this study, the main aim was to explore how facial size and shape, as expressed by various combinations of five linear distances (NPH, BOB, ZYB, ZMB, and MAB), scales in relation to relative cranial size, which was used here as a proxy for body mass and was quantified as a geometric mean of selected cranial measurements. A geometric mean is a numerical value used to represent overall 'size' based on a set of selected variables, ideally ones that are measured in three-dimensional space and can approximate a true volume (e.g., linear measurements of height, width, and breadth). It is calculated using the following formula, which multiplies a set of three or more variables by one another to the power of one over the number of variables:

$$\left(\prod_{i=1}^{n} x_i\right)^{1/n} = \sqrt[n]{x_1 x_2 \ldots x_n},$$

where Π = the geometric mean, n = the number of variables, and x_i = the variables to average.

The use of geometric means is necessary because unfortunately, body mass may not always be known or directly measurable for a given specimen or sample. This is especially the case for extinct hominin species wherein body mass can only ever be estimated based on equations derived from extant comparative samples and even this may not be possible if appropriate comparative data are not available. For this reason, reasonable proxies for body mass are required and the most practical solution is to use a geometric mean.

For this study, geometric means were calculated in three different ways. First, GOL, XCB, ASB, BBH, BNL, and BPL were used to represent overall cranial size (GM1). The other two geometric means represent neurocranial size and enabled additional specimens that lack particular measurements to be incorporated into the analyses. The first combination used GOL, XCB, and BBH (GM2), while the second used GOL, ASB, and BBH only (GM3). Facial shape variables were calculated by dividing each face measurement by these three geometric means (GM1, GM2, and GM3) of other cranial measurements for a given specimen and are denoted by one or more prime symbol (GOL′, GOL″, and GOL‴, respectively). All statistical analyses were performed in R studio (R core team, 2021) and the following packages were used: scatterplot3d (Ligges and Mächler, 2003), smatr (Warton et al., 2012), and ggplot2 (Wickham, 2016). Univariate comparisons between LB 1 and the recent modern human sample for these five raw and size-adjusted facial measurements as well as the six raw and size-adjusted neurocranial measurements (Brown et al., 2004; Kaifu et al., 2011a) were conducted using a single case t test function and a sequential Bonferroni for multiple comparisons (Target α / (n – rank + 1)) (Holm, 1979) was used to assess statistical significance. Multivariate comparisons using principal

components analysis of the size-adjusted facial measurements were also performed to evaluate overall shape affinities among the samples.

For the scaling analyses, a number of fossil hominin specimens lacked one or more of the measurements required to calculate any of the three GMs. Thus, additional analyses examined the relationship between each facial variable and GOL as it was one of the measurements used in the calculation of all three GMs used here and it maximized the number of fossil hominins that could be included for comparison. Each facial variable was scaled against each geometric mean and GOL using MA regression of the recent modern human dataset (n=2,524). In this study, MA regression was used because this method assumes there are errors in both x and y variables and minimizes the perpendicular distances of the residuals to the created slope (Dhona et al., 2016; Kilmer and Rodríguez, 2017).

To determine how LB 1 and other fossil hominin specimens compared to modern humans in terms of relative facial size, MA regressions of all logged facial variables against each logged geometric mean (GM1–3) were calculated for all 2,524 modern humans. For MA regressions of all great apes, only GM2 was used as measurements were not available to calculate GM1 or GM3. Minor axis residuals of LB 1 and the other fossil hominin specimens from these empirical scaling lines were examined individually for each bivariate relationship as well as squared and summed across several regression analyses to produce a measure of morphological dissimilarity from expected cranial shapes for modern humans and great apes, respectively. Residuals for modern humans and great apes were then standardized by dividing by the standard deviation of the residuals for each regression for each of the six cranial and five facial variables respectively. Sums of the standardized residuals and means for the absolute values of the standardized residuals were then also calculated and compared among modern humans and great apes, with

the lowest values indicating greatest morphological similarity between LB 1 and the expected shape for either modern humans or great apes as determined by the empirical scaling patterns.

Results

The univariate comparisons between LB 1 and the recent modern human sample for the five raw and size-adjusted facial measurements are shown in Table 1 and Figures 2–6. In terms of absolute size, LB 1 was significantly smaller than the recent modern human sample for ZMB, MAB, and BOB ($p < .0167$) but not for NPH and ZYB ($p > .025$). When adjusted by GM1, LB 1 was not significantly different from the recent modern human sample for any of the five facial measurements. However, when adjusted either by GM2 or GM3, ZYB′ and ZYB″ in LB 1 were both significantly wider than in the recent modern human sample ($p < .01$) but none of the other measurements differed significantly from those of the recent modern human sample. For the six raw and size-adjusted neurocranial measurements, the univariate comparisons for both sets of data for LB 1 (Brown et al., 2004; Kaifu et al., 2011a) are also shown in Table 1 and Figures 7–12, with similar results as reported previously by Gordon et al. (2008).

Plots of the first three principal components (PCs) for analyses of the size-adjusted facial measurements for LB 1 and modern humans only, and for LB 1, modern humans, and fossil hominins are shown in Figures 13 and 14–17, respectively. In these PC plots, LB 1 and other fossil specimens attributed to the genus *Homo* fall well inside the observed range of modern humans based on size-adjusted facial variables (Figures 14 and 15). Specimens attributed to the genus *Australopithecus* fall outside the observed range of modern humans based on the size-adjusted facial variables (Figures 14 and 15).

The bivariate empirical scaling relationship results are shown in Figures 18–37 and the MA regression slopes, intercepts, and coefficients of determination (R^2) are provided in Table 2. Raw and squared residuals, sum of the squared residuals, sum of the standardized squared residuals, and mean of the absolute value of the standardized residuals are shown in Tables 3–14 for the analyses using GM1–3 and in Tables 15–18 for those using GOL.

For facial height (NPH), each of the three regression slopes is significantly positively allometric (Table 2) and reveals that LB 1 exhibits a tall face relative to its cranial or neurocranial size compared to that of recent modern humans. In relation to GM1 (Figure 16), NPH raw residuals (i.e., perpendicular distances to the fitted line) for the recent modern human sample range between –0.104 and +0.108 whereas LB 1 has a raw residual of +0.153, which is similar to those of early *Homo* (KNM-ER 1813, OH 24) and australopiths (STS 5, OH 5). This pattern for NPH is even more marked in relation to GM2 (Figure 17) and GM3 (Figure 18) wherein LB 1's raw residuals (+0.202 and +0.192, respectively) exceed the recent modern human range (-0.106–0.096 and -0.113–0.095, respectively) even further, as do those of multiple early *Homo* and australopith specimens. African *Homo erectus* (KNM-WT 15000, KNM-ER 3733) also have large positive raw residuals whereas Asian *Homo erectus* (Sangiran 17, Zhoukoudian 11) and other Asian *Homo* (Dali, Harbin) do not. Figure 17 is particularly informative in this regard because extant great apes (*Pan*, *Gorilla*, and *Pongo*) can be included for comparison. Great apes plot the furthest to the left (raw residual range = 0.285–0.523) of the fitted line for the recent modern human sample because they have the tallest faces in the total sample relative to their neurocrania. A similar pattern and significantly positively allometric slope was observed when NPH was scaled with GOL to include more fossil specimens such as KNM-ER 1470 (*Homo rudolfensis*) (Figure 19). All fossil hominins, including LB 1, plot

between the extant great ape and recent modern human clusters (raw residual ranges of 0.264–0.543 and -0.132–0.140, respectively) except for some australopiths that overlap the former and all Asian *Homo erectus* and several other *Homo* specimens (e.g., all Neandertals, Kabwe, Dali) that overlap the latter.

For ZYB, each of the three regression slopes is significantly positively allometric (Table 2) and reveals that LB 1 exhibits a wide face relative to its cranial or neurocranial size compared to that of recent modern humans. In relation to GM1 (Figure 20), only the ZYB raw residuals of LB 1 (+0.123), KNM-ER 1813 (+0.089), KNM-ER 406 (+0.174), and OH 5 (+0.131 or +0.142) exceed the range for recent modern humans (-0.101–0.068). In relation to GM2 (Figure 21), which enables comparisons with extant great apes and a considerable number of additional fossil hominins, LB 1 plots between the clusters for extant great apes (raw residuals = 0.220–0.426) and recent modern humans (raw residuals = -0.086–0.070) as do a number of australopith (STS 5, STW 573) and early *Homo* specimens (KNM-ER 1813, STW 53), as well as African (KNM-ER 3883) and Georgian (D2700, D2282, D3444) *Homo erectus* and *Homo naledi* (LES 1). Fossils with raw residuals within the recent modern human range include Asian *Homo erectus* (Sangiran 17*,* Zhoukoudian 11), African *Homo erectus* (KNM-ER 3733), and other *Homo* (Kabwe, Dali, Harbin, Steinheim, all Neandertals, Skhul 5). Similar results as above for GM1 and GM2 are observed for ZYB in relation to GM3 (Figure 22) and GOL (Figure 23), the latter of which also showed a significantly positively allometric slope. In relation to GOL, all fossil hominins, including LB 1, plot between the extant great ape and recent modern human clusters (raw residual ranges of 0.172–0.302 and -0.106–0.120, respectively) except for some australopiths that overlap the former as well as Asian *Homo erectus* (Sangiran 17, Zhoukoudian 11) and several other *Homo* specimens (e.g., all Neandertals, Kabwe, Dali) that overlap the latter.

For ZMB, each of the three regression slopes was significantly positively allometric (Table 2) and reveals that LB 1 again exhibits a wide midface relative to its cranial or neurocranial size compared to that of recent modern humans. In relation to GM1 (Figure 24), the ZMB residuals of LB 1 (+0.017), australopiths (OH 5, KNM-ER 406, STS 5), and early *Homo* (OH 24, KNM-ER 1813) exceed the range for recent modern humans (-0.101–0.068). In relation to GM2 (Figure 25), *Pan* plots the furthest to the left (raw residual range = 0.208–0.348) of the fitted line for the recent modern human sample (-0.111–0.098) due to having the widest midfaces in the total sample relative to their neurocrania. LB 1 plots between the respective clusters of *Pan* and recent modern humans, along with australopiths (MRD-VP-1/1, OH 5), early *Homo* (KNM-ER 1813, OH 24, STW 53), as well as African (KNM-ER 3883) and Georgian *Homo erectus* (D3444). Fossils with residuals within the *Pan* range include australopiths (STS 5, SK 48, KNM-ER 406) and Georgian *Homo erectus* (D2700) whereas those within the recent modern human range include African (KNM-WT 15000, KNM-ER 3733) and Asian (Sangiran 17, Zhoukoudian 11) *Homo erectus* as well as other *Homo* (Sima de los Huesos 5, Steinheim, Kabwe, Dali, Harbin, all Neandertals, Skhul 5). Similar results as above for GM1 and GM2 are observed for ZMB in relation to GM3 (Figure 26). When ZMB was scaled with GOL, the slope remained significantly positively allometric and the plotted positions of the various fossil hominins were again similar to those of the previous three regression plots (Figure 27).

For MAB, each of the three regression slopes is significantly positively allometric (Table 2) and reveals that LB 1's maxilla is wide relative to its cranial and neurocranial size compared to that of modern humans. In relation to GM1 (Figure 28), the raw MAB residuals of LB 1 (+0.114), australopiths (OH 5, KNM-ER 406), and early *Homo* (OH 24, KNM-ER 1813) exceed the range for recent modern humans (-0.100–0.103). In relation to GM2 (Figure 29), *Pan* plots

the furthest to the left (raw residual range = 0.204–0.372) of the fitted line for the recent modern human sample (raw residual range = -0.096–0.098) due to having the widest maxillae in the total sample relative to their neurocrania. LB 1 plots between the ranges of *Pan* and the recent modern humans, along with Georgian *Homo erectus* (D2700). The residuals of australopiths (STS 5, SK 48, OH 5, KNM-ER 406), early *Homo* (OH 24, KNM-ER 1813), and *Homo naledi* (LES 1) are within the *Pan* range whereas those of African (KNM-ER 3733) and Asian (Zhoukoudian 11) *Homo erectus* as well as other *Homo* (Sima de los Huesos 5, Steinheim, Petralona, Kabwe, Dali, Harbin, all Neandertals, Skhul 5) are within the recent modern human range. In relation to GM3 (Figure 30), results similar to those for GM1 and GM2 are observed. In relation to GOL, the slope was again significantly positively allometric and the plotted positions of the various fossil hominin specimens remained similar to that seen for GM2. However, scaling MAB with GOL enabled the inclusion of *Australopithecus afarensis* (A.L. 444-2) and *Homo rudolfensis* (KNM-ER 1470), both of which plotted near other australopith and early *Homo* specimens, respectively (Figure 31).

For BOB, each of the three regression slopes is significantly positively allometric (Table 2). In relation to GM1 (Figure 32), the BOB residuals of LB 1 and all other fossil hominins except OH 24 have outer orbital margins that are within the range of recent modern humans (-0.082–0.081). In relation to GM2 (Figure 33) and GM3 (Figure 34), the residuals of LB 1 are well within the recent modern human ranges (-0.087–0.95 and -0.080–0.085, respectively) whereas those of most other fossil hominins are near to or slightly exceed the positive limits of these ranges. When BOB was scaled with GOL, the slope was significantly negatively allometric (slope = 0.85) and the plotted positions of the various fossil hominin specimens remained similar to that seen for GM2 (Figure 35).

To further assess morphological dissimilarity from expected cranial shapes for modern humans and great apes, the residuals of these groups as well as those of LB 1 and the other fossil hominin specimens were squared and summed across several combinations of the bivariate empirical scaling analyses (Tables 4, 8, 12, and 16). Sums of the standardized residuals and means for the absolute values of the standardized residuals were then also calculated and compared (Tables 5, 6, 9, 10, 13, 14, 17, 18). Results reveal a clear and consistent pattern regardless of which geometric mean or GOL was used (Figures 36–74).

When regression lines were fitted to facial variables for the recent modern human sample using either GM1, GM2, or GM3, the only fossil hominin specimens that fell outside all 12 of the observed ranges for the sums of the standardized squared residuals in recent modern humans were the following: LB 1, KNM-ER 1813, STS 5, and OH 5 (Tables 5, 9, and 13). MRD-VP-1/1 (2 out of 2), OH 24 (3 out of 3), and D2700 (7 out of 8) also consistently fell outside these ranges but due to missing measurements not all of the variable combinations could be assessed for these three specimens. In contrast, KNM-ER 3733 and Steinheim each fell outside three of the 12 ranges, all of which involved GM2, whereas Sangiran 17 and Zhoukoudian 11 did not fall outside any (0 out of 6 and 0 out of 12, respectively). Similarly, all of the remaining other *Homo* specimens (Sima de los Huesos 5, Petralona, Kabwe, Dali, Harbin, all Neandertals, Skhul 5) fell within the ranges for recent modern humans in all instances where they could be observed. Identical results as above also occurred for the means of the absolute values of the standardized residuals (Tables 6, 10, and 14). If the regression lines were instead fitted to facial variables for the extant great ape sample using either GM1, GM2, or GM3, then only STS 5, OH 5, KNM-ER 1813, and LB 1 had squared residual values that summed below both observed ranges of GM2 for recent modern humans whereas D2700 and Steinheim each fell outside one of the two ranges

while MRD-VP-1/1 fell outside the one range for which it could be observed. All other fossil hominin specimens fell within the observed ranges for recent modern humans (Table 8).

Discussion

This study assessed how the faces of recent modern humans, extant great apes, LB 1, and other fossil hominins empirically scale with various measures of cranial size. The results put into stark relief how previous descriptions, analyses, and interpretations of the face of *Homo floresiensis* have been greatly influenced by the small, absolute size of the LB 1 cranium overall. Indeed, in all five raw measurements of the face used here (NPH, ZYB, ZMB, BOB, and MAB), LB 1 falls within or slightly beyond the lower part of the recent modern human range and yet this has somehow led to a generally accepted notion that the face of *Homo floresiensis* is small in both absolute and relative size and is thus derived like that in Asian *Homo erectus* as well as other Asian *Homo* specimens such as Dali (Kaifu et al., 2011a; Cook et al., 2021). Even size-adjusted, all of these measures fall well within the recent modern human ranges (Figures 2, 4–12) and ZYB′ and ZYB″ are both even significantly wider in LB 1 than the recent modern human means for these two metrics ($p < .01$) (Figure 3).

This raises an important question that, until the current study, has yet to be addressed: why does LB 1, which is estimated to have had a stature of 106 cm tall (Brown et al., 2004) and a body mass of 27.5 kg (Grabowski et al., 2015), have facial measurements that largely overlap in absolute and relative size with those of recent modern humans? Perhaps the extremely small brain size (~417 cm^3) of LB 1 (Falk et al., 2009b; Kubo et al., 2013) and its overall absolutely small cranial vault size in general have distracted previous research from asking this specific question about its face. Regardless of why this question has been overlooked, previous work has

often stressed that scaling analyses should play a major role in investigations of LB 1 given its small absolute size (Lieberman, 2005; Gordon et al., 2008; Baab and McNulty, 2009).

In terms of how facial height (NPH) scales with cranial size, australopiths and extant great apes were the furthest removed from the recent modern human range demonstrating that they have tall faces relative to overall cranial size (Figures 18–21; Tables 3, 7, 11, 15). Falling between these two extremes in relative facial height in hominids are a number of early *Homo* specimens, including LB 1, whereas Asian *Homo erectus* (Sangiran 17, Zhoukoudian 11) and other *Homo* specimens from Asia (Dali, Harbin) have facial heights that scale to cranial size as they do in recent modern humans, Neandertals, and other *Homo* specimens from Africa and Europe (Kabwe, Sima de los Huesos 5, Petralona, Steinheim). These empirical scaling results contrast sharply with Kaifu et al.'s (2011a) conclusions that, based essentially on non-scaled comparisons of absolute size, LB 1's facial height is most similar to the reduced facial heights seen in Asian hominin specimens like Dali, Sangiran 17, and Zhoukoudian 11.

Kaifu et al. (2011a) also concluded that in terms of relative facial breadth, LB 1 possessed morphology similar to that of Asian *Homo erectus* and other Asian *Homo* specimens like the Dali cranium. However, when facial breadth (ZYB) is empirically scaled against cranial size, *Homo floresiensis* does not appear particularly small at all as its facial breadth is relatively much wider than in Dali or Asian *Homo erectus* (Sangiran 17, Zhoukoudian 11) as well as other *Homo* specimens (Kabwe, Dali, Harbin, Steinheim, all Neandertals, Skhul 5) including KNM-ER 3733 (African *Homo erectus*), all of which scale similarly to recent modern humans (Figures 22–25). Indeed, in this scaled measure LB 1 is most similar to australopith (STS 5, STW 573, KNM-ER 406, OH 5) and early *Homo* specimens (KNM-ER 1813, STW 53), as well as African (KNM-ER 3883) and Georgian (D2700, D2282, D3444) *Homo erectus* and *Homo naledi* (LES

1). In other words, LB 1 and these particular fossil specimens all have wide faces relative to cranial size in comparison to recent modern humans (and the other fossil specimens mentioned above) but narrower than in extant great apes (Figures 23 and 25).

If these two maximum dimensions of the face (NPH and ZYB) are considered in combination using their sum of squared, sum of standardized squared, and mean of standardized squared residuals, then it becomes even clearer that LB 1's relative facial size is large and most similar to that of KNM-ER 1813 overall (Figures 36, 41, and 46). Depending on the particular measure of cranial size, similarities with some Dmanisi and australopith specimens are also evident. Specimens of *Homo erectus sensu lato* (Sangiran 17, Zhoukoudian 11, KNM-ER 3733) and other *Homo* (Dali, Harbin), all show relative facial sizes that are similar to those of recent modern humans against all measures of cranial size (Figures 36, 41, and 46). LB 1, KNM-ER 1813, LES 1, and australopiths consistently fall outside of the relative facial size ranges of recent modern humans with australopiths generally falling closest to the relative facial sizes of extant great apes (Figures 36, 41, and 46). However, other facial dimensions such as midfacial breadth (ZMB) have also been described as "remarkably narrow (present in Dali)" in LB 1 (Kaifu et al., 2011a:675).

In this study, when midfacial breadth (ZMB) is empirically scaled against cranial size, *Homo floresiensis* appears more similar to early *Homo* (KNM-ER 1813, OH 24, Stw 53, KNM-ER 1470, D2700, D3444) and some australopiths (STS 5, MRD VP-1/1, DNH 7, A.L. 444-2, OH 5), all of which have midfaces that are relatively wider than in recent modern humans and other *Homo* specimens including Dali and Asian *Homo erectus* (Sangiran 17, Zhoukoudian 11) (Figures 24–27). Several other australopiths (KNM-ER 406, A.L. 888-2, SK 48, STW 573, STS 71), African *Homo erectus* (KNM-ER 3883), and chimpanzees show even wider midfaces

relative to cranial size. In terms of how lower facial breadth (MAB) scales with cranial size, chimpanzees as well as specimens of australopith (STS 5, SK 48, KNM-ER 406, OH 5), early *Homo* (KNM-ER 1813, OH 24, KNM-ER 1470), and *Homo naledi* (LES 1) were the furthest removed from the recent modern human range demonstrating that they have the widest lower faces relative to overall cranial size. LB 1 and D2700 (Dmanisi) both fall in between these two extremes of hominid lower facial relative size, whereas Asian *Homo erectus* (Zhoukoudian 11), Dali, and Harbin have lower facial breadths that scale to cranial size as they do in recent modern humans, Neandertals, and other *Homo* specimens from Africa and Europe (Kabwe, Sima de los Huesos 5, Petralona, Steiheim) (Figures 28–31). These empirical scaling results are consistent with the description of LB 1's dental arcade as displaying "a near-parallel arrangement of the canine-molar rows that makes its lateral maxillary surface relatively flat and directly laterally facing" (Kaifu et al., 2011a: 676), similar to the squarish maxillary arch shapes of early *Homo*.

If these two dimensions of the middle and lower face (ZMB and MAB, respectively) are considered in combination with facial height (NPH), LB 1 appears most similar to D2700 in terms of relative facial size (Figures 39, 44, and 49). Both of these specimens fall in between the relatively large faces of chimpanzees, australopiths, and some early *Homo* specimens (KNM-ER 1813, OH 24) on one extreme and the relatively small faces of recent modern humans on the other. In contrast, specimens of *Homo erectus sensu lato* (Zhoukoudian 11, KNM-ER 3733) and other *Homo* (Dali, Harbin) display relative facial sizes that overlap with the recent modern human range (Figures 39, 44, and 49).

Of all the facial measurements examined in this study, only upper facial breadth (BOB) shows a scaling pattern with GM1 (and to some extent GOL as well) in which LB 1 and all other fossil hominin specimens except OH 24 overlap with the recent modern human range (Figures 32

and 35). However, when BOB is scaled to either GM2 or GM3, however, only LB 1, STS 5, Sima de los Huesos 6, Ngawi 1, and Neandertals fall within the recent modern human range while other fossil specimens fall near to the relatively wider end (i.e., positive residuals) of the recent modern human range (Figures 33 and 34; Tables 3, 7, 11, 15). These results are reasonably consistent with previous studies that have suggested that BOB in hominins remains relatively constant in relation to cranial size across a wide range of geographical and temporal contexts (Lieberman, 2011; Kaifu et al., 2011a; Pérez-Claros et al., 2015; Pérez-Claros, 2022).

Kaifu et al. (2011a) concluded that the "overall facial configuration of LB1 is generally similar to Asian groups of pre-modern *Homo*" (2011a:676) particularly in terms of overall facial size. However, in the current study when all five facial dimensions are considered in combination, LB 1 falls in between the relatively small faces of recent modern humans and the relatively large faces of extant great apes and/or australopiths (STS 5, OH 5) (Figures 38, 43, and 47). Depending on the cranial size proxy, LB 1 is either very similar to KNM-ER 1813 (GM1 and GOL) or smaller than this particular hominin cranium (GM2 and GM3) in terms of overall relative facial size. Because GM1 includes BNL and BPL, facial prognathism contributes to overall cranial size whereas for GM2 and GM3 it does not. Therefore, more prognathic faces—and KNM-ER 1813 is more prognathic than LB 1—will look larger relative to cranial size when facial projection measures are not included in the calculation of the size proxy. In contrast, specimens of *Homo erectus sensu lato* (Zhoukoudian 11, KNM-ER 3733) and other *Homo* (Dali, Harbin) fall within the range of recent modern humans (Figures 38, 43, and 47). If MAB is excluded in order to include Sangiran 17 in the comparisons, then the results are essentially the same as above with Sangiran 17 also overlapping the recent modern human range (Figure 37, 42, and 48). If the MA regression lines are instead fitted to extant great apes rather

than recent modern humans, then the calculated residuals result in the same pattern as above with the exception that LB 1 more consistently plots nearest to KNM-ER 1813 and OH 24 (Figures 51, 52, 55, 56, 59, 60, 63, 64, 67, 68, 71, 72). Overall, these scaling results demonstrate that LB 1 has a relatively large face whereas Asian *Homo erectus* does not. African *Homo erectus* appears to be more variable in this regard depending on the facial dimension or combination of measures examined but specimens attributed to this taxon still consistently display relatively smaller faces than does LB 1. In terms of facial scaling, LB 1 is most similar to early *Homo* specimens (KNM-ER 1813, OH 24, KNM-ER 1470), *Homo naledi* (LES 1), and some Georgian *Homo erectus* (D2700, D2282, but not D3444 or D4500). In this regard, LB 1 appears to have a relative facial size that is roughly the same as the probable primitive condition for the genus *Homo*.

Given the results of the scaling analyses, why does LB 1 cluster with recent modern humans in the PCA, which used size-adjusted facial shape variables (Figures 13–15)? Although the PCA should provide a mostly scale-free perspective it is not completely immune from issues of scale because it assumes that cranial shape is isometric and not affected by overall cranial size (Gordon et al., 2008). The fact that LB 1 and other fossil *Homo* specimens overlap with the recent modern human cluster indicates that all of these specimens are similar to one another in terms of facial shape, particularly in comparison to australopiths (STS 5, OH 5), which fall outside this cluster. The question, however, is whether these observed shapes should be predicted based on the significant difference in absolute cranial size between LB 1 and recent modern humans. To investigate this question, the PCA was rerun with three additional hypothetical recent modern human specimens whose size-adjusted facial shape values were generated using the MA regression equations (Table 2). One of these specimens was predicted to have the same cranial size (GM1) as LB 1, one was predicted to have the same cranial size as Harbin, and the

other was predicted to have the same cranial size as the recent modern human average. As seen in Figures 75 and 76, the predicted 'average' specimen falls within the recent modern human cluster. However, the predicted 'small' and 'large' specimens each fall well outside the cluster. These results demonstrate that to maintain the predicted facial shapes for recent modern humans scaled to the size of either LB 1 or Harbin, the recent modern human cluster would need to extend further negatively and positively along PC1. In other words, LB 1's relatively large face causes its facial shape to overlap with that of recent modern humans. However, this is not the facial shape that would be predicted for a modern human with the same cranial size as LB 1 because facial shape, as demonstrated by the scaling analyses of individual facial dimensions, does not scale isometrically in recent modern humans. Facial shape in the genus *Homo* is probably under various kinds of adaptive constraint related to mastication and/or locomotion and is thus being maintained despite the pattern of positive allometric scaling of relative facial size documented in this study.

Previous studies of the LB 1 and LB 6 mandibles (Daegling et al., 2014) and the LB 1 cranium (Cook et al., 2021) have shown that the feeding biomechanics of *Homo floresiensis* was neither australopith-like nor ape-like. Although Daegling et al. (2014) found that masticatory loads would have been elevated in *Homo floresiensis* in relation to those of modern humans, as suggested elsewhere (Brown and Maeda, 2009), Cook et al. (2021) found that strain levels across the face of LB 1 would have closely resembled those experienced by modern humans. The latter study also concluded that their "biomechanical simulations are consistent with morphological evidence demonstrating a midfacial gracilization in *H. floresiensis* like that of later *Homo* and a corresponding reduction in masticatory loads (Kaifu et al., 2011)" (Cook et al., 2021: 5), perhaps related to dietary shifts that began sometime after the first appearance of *Homo erectus* (Barr et

al., 2022). However, as shown here in this study, such characterizations of LB 1's midface failed to consider the influence of scale, which instead indicates that its midface along with its face overall is relatively large and therefore robust for its size. Thus, the smaller relative facial size and robusticity observed in early *Homo* (and which LB 1 appears to share) compared to that in australopiths (Daegling et al., 2014; Ledogar et al., 2016; 2017; Weber and Kren, 2017; Rak and Marom, 2017; Stelzer et al., 2017; Cook et al., 2021; Rak et al., 2021) may represent the key morphological changes that result in the reduced masticatory ability in the genus *Homo* rather than the additional facial size reductions that occurred in some lineages (e.g., *Homo erectus sensu lato*, modern humans, etc.). This might also explain why LB 1 showed "elevated strains observed for modern humans across much of the facial skeleton, while exhibiting chimpanzee-like levels of increased strains in the zygomatic body and arch" (Cook et al., 2021: 5). Further biomechanical studies such as Cook et al. (2021) that include specimens of early *Homo* are required to resolve this interesting question. However, if the masticatory biomechanics of *Homo floresiensis* (with a relatively large face) and modern humans (with a relatively small face) are indeed the same, then why is relative facial size reduced even further in so many other species of *Homo*? Could continued reduction in the relative size of the face be related to locomotor adaptation rather than mastication alone (Bramble and Lieberman, 2004; Lieberman, 2011; Bastir and Rosas, 2016; Ledogar et al., 2016)?

Limb length proportions are excellent predictors of locomotor behavior in extant and extinct vertebrates (Jungers, 1982, Aiello, 1990; Leakey and Walker, 1993; Aiello and Wells, 1994; Berger and Tobias, 1996; Richmond et al., 2002; Haeusler and McHenry, 2004; 2007; Green et al., 2007; Lieberman, 2011; McDougall et al., 2012; Marchi, 2015; Wills et al., 2017; Ruff et al., 2018; Ryan et al., 2018; Traynor et al, 2022). The fragmentary nature of the fossil

record, however, often makes reconstructing limb length proportions in fossil taxa or specimens an extremely challenging task. This is especially the case within hominin evolution, as very few fossil specimens with well preserved elements from both the fore and hindlimb have been recovered (e.g., A.L. 288-1, KNM-WT 15000, LB 1). Nonetheless, significant effort has been expended to reconstruct the limb proportions of more fragmentary hominin specimens, such as OH 62 and KNM-ER 3735 (Richmond et al., 2002; Haeusler and McHenry, 2004; 2007; Green et al., 2007). Despite the limited fossil evidence, it seems that modern human-like limb proportions had evolved at least as early as ~1.47 Ma based on the KNM-WT 15000 partial skeleton (Brown et al., 1985; Ruff and Walker, 1993; Richtsmeier and Walker, 1993; McDougall et al., 2012). Prior to ~1.5 Ma, early hominins show either more ape-like limb proportions (e.g., OH 62) or proportions that fall intermediate between those of modern humans and extant great apes (e.g., A.L. 288-1) (Jungers, 1982; Richmond et al., 2002). To date, the strongest working hypothesis for explaining these changes in anatomical form is that hominins evolved adaptations to endurance running at the cost of climbing efficiency (Bramble and Lieberman, 2004; Lieberman, 2011).

Predicted changes to cranial form that increase endurance running efficiency by stabilizing the cranium from the forces generated and absorbing the inertial acceleration superimposed on the head include a shorter and less prognathic face, a reduced occipital projection behind the foramen magnum, a reduced nuchal region, and nuchal ligaments reoriented and lengthened (Bramble and Lieberman, 2004; Lieberman, 2011). In the present study, extant great apes display the tallest relative facial sizes followed by australopiths (Figures 16–19). If these australopith specimens share the humerofemoral limb proportions of A.L. 288-1

as generally assumed, then initial reduction of relative facial length may indeed be closely linked to changes in postcranial form related to the evolution of bipedal locomotion.

Within the genus *Homo*, the relatively tallest faces are observed in KNM-ER 1813, OH 24, D2282, D4500, LES 1, and LB 1 (NPH squared residuals ≥ 0.04) (Table 7). For these specimens, limb length proportions are only known with certainty for LB 1 (86.8), which has a similar humerofemoral index as A.L. 288-1 (85.4) (Jungers et al., 2016). However, a humerus and femur from Dmanisi (D4507 and D4167) result in an index (76.4) just beyond the observed upper ranges for modern human small-bodied populations (Jungers et al., 2016) and *Homo naledi* is also considered to have had slightly greater but not significantly different relative upper limb size compared to the modern human mean (Feuerriegel et al., 2015; Prabhat et al., 2021; Traynor et al., 2022). In contrast, other fossil *Homo* specimens examined here have NPH squared residuals that either overlap with the recent modern human range (0.00–0.01) or fall just beyond it (≤ 0.03) (Table 7). This includes KNM-WT 15000, which has a known humerofemoral index of 73.8 (Richmond et al., 2002) and a NPH squared residual of 0.013 (Table 7), and the other Dmanisi specimens (D2700, D3444) along with other African and Asian *Homo erectus* (KNM-ER 3733, Sangiran 17, Zhoukoudian 11), Dali, Harbin, Kabwe, Petralona, Steinheim, Sima de los Huesos 5, and all Neandertals. If these specimens share the humerofemoral limb proportions of KNM-WT 15000 or recent modern humans as generally assumed, then subsequent reduction of relative facial length in *Homo* may indeed be closely linked to changes in postcranial form related to the evolution of bipedal running. For instance, specific muscle groups connecting the cranial base, clavicle, and radius elbow joint, are only activated during running and not walking (Yegian et al., 2021) and reduced facial lengths in hominins may improve endurance running capabilities by creating a center of gravity closer to the

trunk/foramen magnum by pitching the head forward and towards the trunk (e.g., see Figure 5 in Yegian et al., 2021).

To conclude, the results of this study demonstrate two important details about facial size relative to neurocranial size in LB 1. First, contrary to previous interpretations (Brown et al., 2004; Kaifu et al., 2011a), the relative facial size of *Homo floresiensis* is clearly not small. Instead, based on empirically scaled analyses, the face of LB 1 is relatively large, and consistently most similar to that of early *Homo* specimens from Africa such as KNM-ER 1813 and OH 24. This is especially the case if only the maximum dimensions of the face (NPH and ZYB) are considered (Figures 16–31, 36, 41, 46, and Tables 4–6, 8–10, 12–14, 16–18). In some cases, similarities to some but not all of the Dmanisi cranial specimens are also seen but generally several of these specimens fall closer to or within the recent modern human ranges in terms of relative facial size (Figures 16–35 and Tables 4–6, 8–10, 12–14, 16–18). Perhaps most importantly, however, no clear similarities between LB 1 and Asian *Homo erectus* or Dali are observed from these scaling analyses of the face (Figures 16–31). Instead Asian *Homo erectus* specimens and the Dali cranium consistently overlap with recent modern human ranges of relative facial size.

Second, all fossil specimens that fall well outside of the recent modern human scaling pattern because their faces are relatively large also have (or are presumed to have) body proportions and other features conducive for arboreality, whereas fossil specimens that fall within the modern human scaling pattern have (or are presumed to have) body proportions and other features conducive for running bipedally on the ground. For example, all Neandertal (La Chapelle aux Saints, Gibraltar 1, Tabun 1, La Ferrassie, Shanidar 1, Saccopostre 1, Guattari 1, Amud 1, Spy 1, Monte Circe, La Quina 5) and Pleistocene *Homo sapiens* specimens (Skhūl 5,

Jebel Irhoud 5) as well as other fossils attributed to *Homo* (Kabwe, Steinheim, Petralona, Sima de los Huesos 5, Dali, and Harbin) including *Homo erectus sensu lato* (Sangiran 17, Zhoukoudian 11, Ngawi 1, KNM-ER 3733, KNM-WT 15000) specimens scale within or extremely close to the range of recent modern human faces, and all of these species possess (or are widely assumed to possess) body proportions similar to modern humans (Aiello and Dean, 1990; Hunt, 1994; Aiello and Wells, 2002; Antón, 2003; Lieberman, 2011; Kubo et al., 2013; Bastir and Rosas, 2016; Figures 16–31). Perhaps *Homo floresiensis* is an island-dwarfed descendant of Asian *Homo erectus* (Kaifu et al., 2011a; van den Bergh et al., 2016), however, the atavisms required to re-evolve postcranial and cranial form so immaculately strain the limits of credulity. Evolution from a Dmanisi-like or African early *Homo*-like (not including *Homo erectus*) ancestor appear as far better alternatives based on current evidence (Dennell and Roebroecks, 2005; Larson et al., 2007; Tocheri et al., 2007; Argue et al., 2009; Gordon et al., 2008; Jungers et al., 2009a,b; Baab and McNulty, 2009; Dembo et al., 2015, 2016; Zhu et al., 2018; Scardia et al., 2021), including the facial scaling results of this study (Figures 13–76).

Table 1. Univariate comparisons of raw and size-adjusted measurements between LB 1 and recent modern humans

Measurement	Brown et al. (2004) measurements[1]	p value[2]	Kaifu et al. (2011a) measurements[1]	p value[2]	Recent modern human range	Bootstrapped 95% lower and upper confidence intervals of the recent modern human mean	
GOL	143	< **0.001**	139	< **0.001**	151.0–206.0	178.8	179.5
GOL'	1.43	0.387	1.43	0.311	1.30–1.60	1.47	1.47
GOL"	1.27	0.157	1.24	0.488	1.09–1.38	1.21	1.22
GOL"'	1.33	0.713	1.33	0.689	1.18–1.44	1.32	1.32
XCB	113	**0.001**	114	**0.002**	116.0–167.0	136.6	137.1
XCB'	1.13	0.838	1.17	0.349	0.97–1.31	1.12	1.12
XCB"	1.00	0.034	1.02	**0.011**	0.82–1.07	0.93	0.93
XCB"'	1.05	0.331	1.09	0.076	0.87–1.19	1.00	1.01
ASB	97	0.084	92	**0.009**	88.0–128.0	106.6	107.1
ASB'	0.97	**0.007**	0.94	0.053	0.74–1.01	0.87	0.88
ASB"	0.86	< **0.001**	0.82	**0.002**	0.59–0.84	0.72	0.73
ASB"'	0.90	< **0.001**	0.88	**0.001**	0.69–0.89	0.78	0.79
BBH	89	< **0.001**	89	< **0.001**	107–155	131.4	131.9
BBH'	0.89	< **0.001**	0.91	< **0.001**	0.93–1.21	1.08	1.08
BBH"	0.79	< **0.001**	0.79	< **0.001**	0.82–1.07	0.93	0.93
BBH"'	0.83	< **0.001**	0.85	**0.001**	0.85–1.06	0.97	0.97
BNL	81	**0.002**	78	< **0.001**	83.0–120.0	98.9	99.3
BNL'	0.81	0.997	0.80	0.658	0.72–0.90	0.81	0.81
BNL"	0.72	0.088	0.70	0.369	0.57–0.78	0.67	0.67
BNL"'	0.76	0.349	0.75	0.514	0.61–0.82	0.73	0.73
BPL	88	0.125	85	0.045	80.0–123.0	97.5	98.0
BPL'	0.88	0.031	0.87	0.056	0.67–0.93	0.80	0.80
BPL"	0.78	**0.003**	0.76	0.016	0.52–0.80	0.66	0.66
BPL"'	0.82	**0.013**	0.81	0.020	0.58–0.87	0.72	0.72

NPH	–	–	54	0.031	48.0–82.0	65.8	66.2
NPH'	0.54	0.983	0.55	0.703	0.40–0.66	0.54	0.54
NPH''	0.48	0.294	0.48	0.250	0.33–0.55	0.45	0.45
NPH'''	0.50	0.585	0.52	0.340	0.36–0.60	0.48	0.49
ZYB	–	–	114	0.031	105.0–158.0	130.5	131.1
ZYB'	1.14	0.089	1.17	**0.018**	0.92–1.21	1.07	1.07
ZYB''	1.01	**0.001**	1.02	**< 0.001**	0.77–1.01	0.88	0.89
ZYB'''	1.06	**0.011**	1.09	**0.001**	0.83–1.10	0.96	0.96
ZMB	–	–	77	**0.002**	79.0–120.0	94.7	95.2
ZMB'	0.77	0.862	0.79	0.755	0.65–0.93	0.78	0.78
ZMB''	0.68	0.246	0.69	0.196	0.53–0.77	0.64	0.65
ZMB'''	0.72	0.604	0.74	0.293	0.59–0.84	0.70	0.67
MAB	–	–	52	**0.004**	52.0–78.0	63.4	63.7
MAB'	0.52	0.988	0.53	0.615	0.44–0.61	0.52	0.52
MAB''	0.46	0.183	0.46	0.143	0.36–0.52	0.43	0.43
MAB'''	0.48	0.480	0.50	0.213	0.39–0.56	0.47	0.47
BOB	–	–	76	**< 0.001**	83.0–113.0	97.2	97.5
BOB'	0.76	0.189	0.78	0.520	0.71–0.90	0.80	0.80
BOB''	0.67	0.591	0.68	0.479	0.58–0.76	0.66	0.66
BOB'''	0.71	0.781	0.73	0.665	0.64–0.81	0.72	0.72

[1] raw measurements obtained from the indicated reference, size-adjusted measurements (', '', ''') calculated for this study

[2] values in bold are statistically significant from the recent modern human mean at 0.05 using a sequential Bonferroni correction for multiple comparisons

Table 2. The MA regression slopes and 95% confidence intervals (CIs), intercepts, and coefficients of determination (R^2) for the bivariate empirical scaling analyses

Regression	Sample	Slope	95% CIs	Intercept	R^2
lnNPH–lnGM1	recent modern humans	3.07	2.92–3.23	-10.55	0.365
lnNPH–lnGM2	recent modern humans	3.13	2.98–3.30	-11.47	0.366
	extant great apes	3.06	2.74–3.45	-9.80	0.456
lnNPH–lnGM3	recent modern humans	3.14	2.98–3.33	-11.26	0.324
lnNPH–lnGOL	recent modern humans	3.06	2.84–3.32	-11.69	0.199
	extant great apes	1.46	1.31–1.63	-2.69	0.474
lnZYB–lnGM1	recent modern humans	1.67	1.62–1.73	-3.17	0.580
lnZYB–lnGM2	recent modern humans	1.75	1.68–1.81	-3.85	0.532
	extant great apes	1.97	1.74–2.24	-4.31	0.689
lnZYB–lnGM3	recent modern humans	1.68	1.62–1.74	-3.37	0.520
lnZYB–lnGOL	recent modern humans	1.48	1.40–1.57	-2.81	0.308
	extant great apes	0.93	0.81–1.07	0.31	0.633
lnZMB–lnGM1	recent modern humans	1.98	1.87–2.09	-4.95	0.325
lnZMB–lnGM2	recent modern humans	1.75	1.68–1.81	-3.85	0.267
	extant great apes	3.11	2.47–4.14	-10.02	0.206
lnZMB–lnGM3	recent modern humans	2.07	1.94–2.21	-5.60	0.256
lnZMB–lnGOL	recent modern humans	1.75	1.60–1.92	-4.52	0.157
	extant great apes	2.05	1.66–2.62	-5.59	0.248
lnMAB–lnGM1	recent modern humans	2.04	1.94–2.15	-5.65	0.376
lnMAB–lnGM2	recent modern humans	2.23	2.11–2.37	-6.99	0.308
	extant great apes	3.96	2.63–7.56	-14.34	0.066
lnMAB–lnGM3	recent modern humans	2.10	1.99–2.23	-6.17	0.314
lnMAB–lnGOL	recent modern humans	1.80	1.67–1.95	-5.21	0.209
	extant great apes	2.09	1.45–3.38	-6.13	0.093
lnBOB–lnGM1	recent modern humans	1.14	1.09–1.19	-0.87	0.440
lnBOB–lnGM2	recent modern humans	1.20	1.13–1.27	-1.40	0.313
lnBOB–lnGM3	recent modern humans	1.12	1.06–1.18	-0.91	0.350
lnBOB–lnGOL	recent modern humans	0.85	0.81–0.90	0.15	0.344

(back to text)

Table 3. Raw and squared residuals from fitted scaling lines between craniofacial variables and GM1 for recent modern humans[1]

Taxon / Specimen	lnNPH		lnZYB		lnZMB		lnMAB		lnBOB	
	raw	squared	raw	squared	raw	squared	raw	squared	raw	squared
Homo floresiensis										
LB 1	**0.153**	**0.023**	**0.123**	**0.015**	**0.107**	**0.011**	**0.114** | 0.093	**0.013** | 0.009	0.006	0.000
Early *Homo*										
KNM-ER 1813	**0.162** | **0.159**	**0.026** | **0.025**	**0.089**	0.008	**0.127** | **0.113**	**0.016** | **0.013**	**0.162**	**0.026**	0.045	0.002
OH 24	**0.211**	**0.044**	–	–	**0.202**	**0.041**	**0.217**	**0.047**	**0.125**	0.016
KNM-ER 1470	–	–	–	–	–	–	–	–	–	–
STW 53	–	–	–	–	–	–	–	–	–	–
Homo erectus s.l.										
Africa										
KNM-ER 3733	0.032 | 0.023	0.001 | 0.001	-0.008	0.000	0.012 | -0.011	0.000 | 0.000	-0.021	0.000	0.012	0.000
KNM-ER 3883	–	–	–	–	–	–	–	–	–	–
KNM-WT 15000	–	–	–	–	–	–	–	–	–	–
KNM-ER 42700	–	–	–	–	–	–	–	–	–	–
OH 9	–	–	–	–	–	–	–	–	–	–
Dmanisi										
D2700	0.103	0.011	0.019	0.000	0.093	0.009	0.087	0.008	–	–
D2282	–	–	–	–	–	–	–	–	–	–
D3444	–	–	–	–	–	–	–	–	–	–
D4500	–	–	–	–	–	–	–	–	–	–
D2280	–	–	–	–	–	–	–	–	–	–
Asia										
Sangiran 17	-0.042	0.002	-0.028	0.001	0.017 | -0.020	0.000 | 0.000	–	–	0.024	0.001
Zhoukoudian 11	0.006	0.000	0.025	0.001	-0.026	0.001	0.009	0.000	0.053	0.003
Ngawi	–	–	–	–	–	–	–	–	–	–
Sangiran IX	–	–	–	–	–	–	–	–	–	–
Australopiths										
MRD-VP-1/1	–	–	–	–	–	–	–	–	–	–
A.L. 444-2	–	–	–	–	–	–	–	–	–	–
A.L. 888-1	–	–	–	–	–	–	–	–	–	–
STW 573	–	–		–	–	–	–	–	–	–
STS 5	**0.129**	**0.017**	0.054	0.003	**0.126**	**0.016**	0.093	0.009	-0.041	0.002
STS 71	–	–	–	–	–	–	–	–	–	–
OH 5	**0.167** | **0.163**	**0.028** | **0.027**	**0.131** | **0.142**	**0.017** | **0.020**	**0.116**	**0.013**	**0.115**	**0.013**	-0.007 | 0.016	0.000 | 0.000
KNM-ER 406	–	–	**0.174**	**0.030**	**0.169**	**0.028**	**0.109**	**0.012**	0.029	0.001

KNM-WT 17000	–	–	–	–	–	–	–	–	–	–
SK 48	–	–	–	–	–	–	–	–	–	–
DNH 7	–	–	–	–	–	–	–	–	–	–
Other *Homo*										
LES 1	–	–	–	–	–	–	–	–	–	–
Sima de los Huesos 5	0.008	0.000	-0.014	0.000	0.033	0.001	0.012	0.000	0.043	0.002
Sima de los Huesos 6	–	–	–	–	–	–	–	–	–	–
Kabwe	0.006	0.000	-0.038	0.001	-0.035	0.001	-0.012	0.000	0.053	0.003
Steinheim	0.058	0.003	0.023	0.001	0.038	0.001	0.049	0.002	0.072	0.005
Petralona	–	–	–	–	–	–	–	–	–	–
Dali	-0.039	0.001	-0.022	0.000	-0.002	0.000	-0.008	0.000	0.059	0.003
Harbin	**-0.121**	**0.015**	-0.039	0.002	-0.075	0.006	-0.060	0.004	0.065	0.004
Neandertals										
La Chapelle aux Saints	-0.069	0.005	-0.056	0.003	-0.076	0.006	-0.094	0.009	-0.027	0.001
Gibraltar 1	-0.002	0.000	-0.038	0.001	-0.016	0.000	-0.010	0.000	-0.013	0.000
Tabun 1	0.030	0.001	-0.026	0.001	–	–	0.014	0.000	–	–
La Ferrassie	-0.059	0.003	-0.069	0.005	–	–	-0.067	0.005	–	–
Shanidar 1	-0.034	0.001	-0.070	0.005	-0.068	0.005	-0.058	0.003	–	–
Saccopostre 1	0.061	0.004	–	–	–	–	0.023	0.001	0.021	0.000
Guattari 1	–	–	–	–	–	–	–	–	–	–
Amud 1	–	–	–	–	–	–	–	–	–	–
Spy 1	–	–	–	–	–	–	–	–	–	–
Monte Circe	–	–	–	–	–	–	–	–	–	–
La Quina 5	–	–	–	–	–	–	–	–	–	–
Homo sapiens										
Skhul V	-0.029	0.001	-0.001	0.000	0.010	0.000	-0.017	0.000	–	–
Jebel Irhoud 1	–	–	–	–	–	–	–	–	–	–
Recent[1]	0.000 (-0.104–0.108)	0.001 (0.000–0.012)	0.000 (-0.101–0.068)	0.001 (0.000–0.010)	0.000 (-0.101–0.099)	0.001 (0.000–0.011)	0.000 (-0.100–0.103)	0.000 (0.000–0.011)	0.000 (-0.082–0.081)	0.000 (0.000–0.007)
Extant great apes[2]	–	–	–	–	–	–	–	–	–	–

Values in **bold** are outside the entire range for recent modern humans

[1] Howells (1996), N = 2,524

[2] missing ASB thus GM1 cannot be calculated

(back to text)

Table 4. Sum of squared residuals from fitted scaling lines between craniofacial variables and GM1 for recent modern humans[1]

Taxon / Specimen	Face				Neurocranium
	NPH, ZYB, ZMB, BOB, & MAB	NPH, ZYB, ZMB, & BOB	NPH, ZMB, & MAB	NPH & ZYB	GOL, XCB, ASB, BBH, BNL, & BPL
Homo floresiensis					
LB 1	**0.063**	**0.050**	**0.048**	**0.039**	**0.045** | **0.042**
Early *Homo*					
KNM-ER 1813	**0.079**	**0.052**	**0.069**	**0.034**	**0.046** | **0.030**
OH 24	–	–	**0.133**	–	**0.051**
KNM-ER 1470	–	–	–	–	–
STW 53	–	–	–	–	–
Homo erectus s.l.					
Africa					
KNM-ER 3733	0.002	0.001	0.002	0.001	**0.027** | **0.020**
KNM-ER 3883	–	–	–	–	–
KNM-WT 15000	–	–	–	–	–
KNM-ER 42700	–	–	–	–	–
OH 9	–	–	–	–	–
Dmanisi					
D2700	–	–	**0.027**	0.011	**0.021**
D2282	–	–	–	–	–
D3444	–	–	–	–	–
D4500	–	–	–	–	–
D2280	–	–	–	–	–
Asia					
Sangiran 17	–	0.003	–	0.003	**0.035** | **0.041** | **0.045**
Zhoukoudian 11	0.004	0.004	0.001	0.001	0.014
Ngawi	–	–	–	–	–
Sangiran IX	–	–	–	–	–
Australopiths					
MRD-VP-1/1	–	–	–	–	–
A.L. 444-2	–	–	–	–	–
A.L. 888-1	–	–	–	–	–
STW 573	–	–	–	–	–
STS 5	**0.046**	**0.037**	**0.041**	**0.020**	**0.054** | **0.057**
STS 71	–	–	–	–	–
OH 5	**0.072**	**0.059**	**0.055**	**0.045** | **0.047**	**0.065** | **0.055**
KNM-ER 406	–	–	–	–	**0.050** | **0.052**
KNM-WT 17000	–	–	–	–	–
SK 48	–	–	–	–	–

DNH 7	–	–	–	–	–
Other *Homo*					
LES 1	–	–	–	–	–
Sima de los Huesos 5	0.003	0.003	0.001	0.000	0.012
Sima de los Huesos 6	–	–	–	–	–
Kabwe	0.006	0.005	0.001	0.001	**0.018**
Steinheim	0.013	0.011	0.007	0.004	0.014
Petralona	–	–	–	–	–
Dali	0.006	0.005	0.002	0.002	**0.022**
Harbin	0.029	**0.026**	0.024	**0.016**	**0.029**
Neandertals					
La Chapelle aux Saints	0.023	0.014	0.019	0.008	**0.025** | **0.022**
Gibraltar 1	0.002	0.002	0.000	0.001	0.008
Tabun 1	–	–	–	0.002	0.012
La Ferrassie	–	–	–	0.008	**0.021** | **0.017**
Shanidar 1	–	–	0.009	0.006	0.014 | 0.013
Saccopostre 1	–	–	–	–	**0.019**
Guattari 1	–	–	–	–	–
Amud 1	–	–	–	–	–
Spy 1	–	–	–	–	–
Monte Circe	–	–	–	–	–
La Quina 5	–	–	–	–	–
Homo sapiens					
Skhul V	–	–	0.001	0.001	0.009
Jebel Irhoud 1	–	–	–	–	–
Recent[1]	0.004 (0.000–0.030)	0.003 (0.000–0.022)	0.003 (0.000-0.024)	0.001 (0.000–0.014)	0.003 (0.000–0.017)
Extant great apes[2]	–	–	–	–	–

Values in **bold** are outside the entire range for recent modern humans

[1] Howells (1996), N = 2,524

[2] missing ASB thus GM1 cannot be calculated

(back to text)

Table 5. Sum of standardized squared residuals from fitted scaling lines between craniofacial variables and GM1 for recent modern humans[1]

Taxon / Specimen	Face				Neurocranium
	NPH, ZYB, ZMB, BOB, & MAB	NPH, ZYB, ZMB, & BOB	NPH, ZMB, & MAB	NPH & ZYB	GOL, XCB, ASB, BBH, BNL, & BPL
Homo floresiensis					
LB 1	**98.91**	**67.07**	**53.08**	**54.50**	**56.05 | 53.80**
Early *Homo*					
KNM-ER 1813	**124.73**	**64.64**	**77.23**	**43.33**	**53.29 | 32.50**
OH 24	–	–	**148.86**	–	**62.66**
KNM-ER 1470	–	–	–	–	–
STW 53	–	–	–	–	–
Homo erectus s.l.					
Africa					
KNM-ER 3733	10.82	1.64	1.76	1.21	**62.60 | 49.38**
KNM-ER 3883	–	–	–	–	–
KNM-WT 15000	–	–	–	–	–
KNM-ER 42700	–	–	–	–	–
OH 9	–	–	–	–	–
Dmanisi					
D2700	–	–	**29.67**	11.96	31.37
D2282	–	–	–	–	–
D3444	–	–	–	–	–
D4500	–	–	–	–	–
D2280	–	–	–	–	–
Asia					
Sangiran 17	–	4.76	–	3.47	**91.36 | 106.25 | 112.78**
Zhoukoudian 11	6.51	6.88	0.85	1.28	**34.37**
Ngawi	–	–	–	–	–
Sangiran IX	–	–	–	–	–
Australopiths					
MRD-VP-1/1	–	–	–	–	–
A.L. 444-2	–	–	–	–	–
A.L. 888-1	–	–	–	–	–
STW 573	–	–	–	–	–
STS 5	**106.26**	**43.95**	**45.65**	**23.64**	**67.72 | 66.60**
STS 71	–	–	–	–	
OH 5	**122.19**	**78.18**	**60.43**	**63.39 | 67.85**	**112.12 | 88.90**
KNM-ER 406	–	–	–	–	**78.90 | 87.73**
KNM-WT 17000	–	–	–	–	–

SK 48	–	–	–	–	–
DNH 7	–	–	–	–	–
Other *Homo*					
LES 1	–	–	–	–	–
Sima de los Huesos 5	10.60	4.86	1.49	0.45	27.79
Sima de los Huesos 6	–	–	–	–	–
Kabwe	7.75	8.95	1.59	2.79	**41.17**
Steinheim	24.73	15.19	8.05	4.68	26.33
Petralona	–	–	–	–	–
Dali	8.75	8.51	1.68	2.55	**55.41**
Harbin	32.25	31.79	26.02	18.54	**66.47**
Neandertals					
La Chapelle aux Saints	23.42	18.69	21.92	11.16	**60.80** | **50.87**
Gibraltar 1	3.25	3.39	0.41	2.80	20.09
Tabun 1	–	–	–	2.32	28.55
La Ferrassie	–	–	–	12.92	**47.94** | **33.43**
Shanidar 1	–	–	10.26	10.63	30.97 | 28.00
Saccopostre 1	–	–	–	–	**43.58**
Guattari 1	–	–	–	–	–
Amud 1	–	–	–	–	–
Spy 1	–	–	–	–	–
Monte Circe	–	–	–	–	–
La Quina 5	–	–	–	–	–
Homo sapiens					
Skhul V	–	–	1.34	0.88	19.47
Jebel Irhoud 1	–	–	–	–	–
Recent[1]	5.08 (0.14–39.84)	4.00 (0.04–34.53)	3.00 (0.01–26.93)	2.00 (0.00–22.74)	5.68 (0.11–32.90)
Extant great apes[2]	–	–	–	–	–

Values in **bold** are outside the entire range for recent modern humans

[1] Howells (1996), N = 2,524

[2] missing ASB thus GM1 cannot be calculated

(back to text)

Table 6. Mean of the absolute value of the standardized residuals from fitted scaling lines between craniofacial variables and GM1 for recent modern humans[1]

Taxon / Specimen	Face				Neurocranium
	NPH, ZYB, ZMB, BOB, & MAB	NPH, ZYB, ZMB, & BOB	NPH, ZMB, & MAB	NPH & ZYB	GOL, XCB, ASB, BBH, BNL, & BPL
Homo floresiensis					
LB 1	**3.63**	**3.55**	**4.16**	**5.22**	**3.04** | **3.06**
Early *Homo*					
KNM-ER 1813	**4.18**	**3.83**	**5.04**	**4.60**	**2.91** | **2.26**
OH 24	–	–	**7.04**	–	**2.84**
KNM-ER 1470	–	–	–	–	–
STW 53	–	–	–	–	–
Homo erectus s.l.					
Africa					
KNM-ER 3733	0.61	0.58	0.72	0.70	**2.14** | 1.76
KNM-ER 3883	–	–	–	–	–
KNM-WT 15000	–	–	–	–	–
KNM-ER 42700	–	–	–	–	–
OH 9	–	–	–	–	–
Dmanisi					
D2700	–	–	**3.14**	2.09	**2.28**
D2282	–	–	–	–	–
D3444	–	–	–	–	–
D4500	–	–	–	–	–
D2280	–	–	–	–	–
Asia					
Sangiran 17	–	1.05	–	1.32	1.97 | **2.21** | **2.43**
Zhoukoudien 11	0.93	1.09	0.45	0.65	1.21
Ngawi	–	–	–	–	–
Sangiran IX	–	–	–	–	–
Australopiths					
MRD-VP-1/1	–	–	–	–	–
A.L. 444-2	–	–	–	–	–
A.L. 888-1	–	–	–	–	–
STW 573	–	–	–	–	–
STS 5	**3.15**	**3.13**	**3.87**	**3.31**	**3.38** | **3.29**
STS 71	–	–	–	–	–
OH 5	**3.87**	**3.84**	**4.43**	**5.63** | **5.81**	**3.79** | **3.48**
KNM-ER 406	–	–	–	–	**3.42** | **3.57**

KNM-WT 17000	–	–	–	–	–
SK 48	–	–	–	–	–
DNH 7	–	–	–	–	–
Other *Homo*					
LES 1	–	–	–	–	–
Sima de los Huesos 5	0.84	0.94	0.60	0.44	1.56
Sima de los Huesos 6	–	–	–	–	–
Kabwe	1.12	1.30	0.59	0.92	1.82
Steinheim	1.77	1.79	1.62	1.46	1.73
Petralona	–	–	–	–	–
Dali	1.00	1.19	0.53	1.12	1.79
Harbin	2.58	2.70	2.83	2.83	**2.33**
Neandertals					
La Chapelle aux Saints	2.32	2.08	2.67	2.36	2.06 | 1.67
Gibraltar 1	0.64	0.71	0.32	0.87	1.07
Tabun 1	–	–	–	1.07	1.35
La Ferrassie	–	–	–	2.48	2.02 | 1.87
Shanidar 1	–	–	1.78	2.09	1.55 | 1.55
Saccopostre 1	–	–	–	–	1.55
Guattari 1	–	–	–	–	–
Amud 1	–	–	–	–	–
Spy 1	–	–	–	–	–
Monte Circe	–	–	–	–	–
La Quina 5	–	–	–	–	–
Homo sapiens					
Skhul V	–	–	0.62	0.50	1.52
Jebel Irhoud 1	–	–	–	–	–
Recent[1]	0.80 (0.12–2.76)	0.80 (0.06–2.74)	0.80 (0.04–2.97)	0.80 (0.01–3.10)	0.80 (0.12–2.11)
Extant great apes[2]	–	–	–	–	–

Values in **bold** are outside the entire range for recent modern humans

[1] Howells (1996), N = 2,524

[2] missing ASB thus GM1 cannot be calculated

(back to text)

Table 7. Raw and squared residuals from fitted scaling lines between craniofacial variables and GM2 for recent modern humans[1]

Taxon / Specimen	lnNPH		lnZYB		lnZMB		lnMAB		lnBOB	
	raw	squared	raw	squared	raw	squared	raw	squared	raw	squared
Homo floresiensis										
LB 1	**0.202**	**0.041**	**0.171**	**0.029**	**0.162**	**0.026**	**0.169 | 0.163**	**0.029 | 0.027**	0.053	0.003
Early *Homo*										
KNM-ER 1813	**0.240 | 0.212**	**0.058 | 0.045**	**0.163**	**0.027**	**0.206 | 0.169**	**0.042 | 0.029**	**0.239 | 0.245**	**0.057 | 0.061**	**0.114 | 0.135**	**0.013 | 0.018**
OH 24	**0.238**	**0.057**	–	–	**0.231**	**0.053**	**0.245**	**0.060**	**0.151 | 0.135**	**0.023 | 0.018**
KNM-ER 1470	–	–	–	–	–	–	–	–	–	–
STW 53	**0.113 | 0.172**	**0.013 | 0.030**	**0.138**	**0.019**	0.077 | **0.160**	0.006 | **0.026**	**–**	**–**	**–**	**–**
Homo erectus s.l.										
Africa										
KNM-ER 3733	**0.116 | 0.100**	0.010	0.069	0.005	0.090 | 0.061	0.008 | 0.004	0.059	0.004	0.079 | 0.074	0.006 | 0.006
KNM-ER 3883	–	–	**0.138**	**0.019**	**0.111**	**0.012**	–	–	**0.129 | 0.126**	**0.017 | 0.016**
KNM-WT 15000	**0.137**	**0.013**	–	–	**0.107**	0.011	–	–	0.063 | 0.076	0.004 | 0.006
KNM-ER 42700	–	–	–	–	–	–	–	–	0.093	0.009
OH 9	–	–	–	–	–	–	–	–	0.092 | **0.143**	0.009 | **0.021**
Dmanisi										
D2700	**0.170 | 0.169**	**0.029 | 0.029**	**0.083 | 0.107**	0.007 | **0.011**	**0.157**	**0.025**	**0.152**	**0.023**	0.083	0.007
D2282	**0.258**	**0.067**	**0.176**	**0.031**	–	–	–	–	**0.103**	**0.011**
D3444	**0.118**	**0.014**	**0.105**	**0.011**	**0.117**	**0.014**	**–**	**–**	–	–
D4500	**0.243**	**0.059**	**0.258**	**0.066**	**–**	**–**	**–**	**–**	–	–
D2280	–	–	–	–	–	–	–	–	0.098	0.010
Asia										
Sangiran 17	0.027 | -0.013	0.001 | 0.000	0.032	0.001	0.075 | 0.034	0.006 | 0.001	–	–	0.075 | 0.066	0.006 | 0.004
Zhoukoudian 11	0.049	0.002	0.064	0.004	0.015	0.000	0.047	0.002	0.086	0.007
Ngawi	–	–	–	–	–	–	–	–	0.023	0.001
Sangiran IX	–	–	–	–	–	–	–	–	–	–
Australopiths										
MRD-VP-1/1	**0.312**	**0.097**	**0.160**	**0.026**	**0.190**	**0.036**	–	–	0.068	0.005
A.L. 444-2	–	–	–	–	–	–	–	–	–	–
A.L. 888-1	–	–	–	–	–	–	–	–	–	–
STW 573	**0.282**	**0.080**	**0.178**	**0.032**	**–**	**–**	**–**	**–**	**–**	**–**
STS 5	**0.262**	**0.069**	**0.178**	**0.032**	**0.251**	**0.063**	**0.222**	**0.049**	0.071	0.005
STS 71	–	–	–	–	–	–	–	–	–	–
OH 5	**0.258 | 0.242**	**0.067 | 0.059**	**0.213 | 0.213**	**0.045 | 0.045**	**0.198**	**0.039**	**0.197**	**0.039**	0.069 | 0.082	0.005 | 0.007
KNM-ER 406	–	–	**0.267**	**0.071**	**0.260**	**0.068**	**0.205**	**0.042**	**0.115**	**0.013**

KNM-WT 17000	**0.392**	**0.154**	**0.351**	**0.123**	–	–	–	–	–	–
SK 48	**0.353**	**0.124**	**0.319**	**0.102**	**0.334**	**0.111**	**0.258**	**0.067**	–	–
DNH 7	–	–	–	–	–	–	–	–	–	–
Other *Homo*										
LES 1	**0.281**	**0.079**	**0.172**	**0.030**	–	–	**0.275**	**0.076**	–	–
Sima de los Huesos 5	0.063	0.004	0.035	0.001	0.079	0.006	0.059	0.003	0.084	0.007
Sima de los Huesos 6	–	–	–	–	-0.015	0.000	–	–	0.012	0.000
Kabwe	0.050	0.003	0.002	0.000	0.003	0.000	0.025	0.001	0.085 | 0.067	0.007 | 0.004
Steinheim	**0.110**	**0.012**	0.071	0.005	0.087	0.008	0.097	0.009	**0.113**	**0.013**
Petralona	0.025	0.001	0.027	0.001	0.007	0.000	0.057	0.003	–	–
Dali	-0.018	0.000	-0.005	0.000	0.012	0.000	0.007	0.000	0.071	0.005
Harbin	-0.083	0.007	-0.008	0.000	-0.045	0.002	-0.032	0.001	0.087	0.008
Neandertals										
La Chapelle aux Saints	-0.007 | -0.002	0.000 | 0.000	-0.002 | 0.002	0.000 | 0.000	-0.022 | -0.018	0.001 | 0.000	-0.039 | -0.034	0.002 | 0.001	0.019 | 0.023	0.000 | 0.001
Gibraltar 1	0.021	0.000	-0.017	0.000	0.003	0.000	0.009	0.000	0.004	0.000
Tabun 1	0.081	0.007	0.021	0.000	–	–	0.061	0.004	–	–
La Ferrassie	-0.013	0.000	-0.028	0.001	–	–	-0.029	0.001	–	–
Shanidar 1	-0.006	0.000	-0.045	0.002	-0.045	0.002	-0.035	0.001	–	–
Saccopostre 1	**0.124 | 0.124**	0.016 | 0.015	–	–	–	–	0.081 | 0.082	0.007 | 0.007	0.071	0.005
Guattari 1	0.027	0.001	–	–	0.0255	0.0007	-0.052	0.003	–	–
Amud 1	–	–	–	–	–	–	–	–	–	–
Spy 1	–	–	–	–	–	–	–	–	–	–
Monte Circe	–	–	–	–	–	–	–	–	–	–
La Quina 5	–	–	–	–	–	–	–	–	–	–
Homo sapiens										
Skhul V	0.001	0.000	0.024	0.001	0.0332	0.001	0.0080	0.000	–	–
Jebel Irhoud 1	–	–	–	–	–	–	–	–	–	–
Recent[1]	0.000 (-0.106–0.096)	0.0010 (0.000–0.011)	0.0000 (-0.086–0.070)	0.0010 (0.000–0.007)	0.000 (-0.111–0.098)	0.0010 (0.000–0.012)	0.0000 (-0.096–0.098)	0.0010 (0.000–0.010)	0.000 (-0.087–0.095)	0.001 (0.000–0.009)

Extant great apes										
Pan[2]	**0.401 (0.318–0.487)**	**0.162 (0.101–0.237)**	–	–	**0.273 (0.208–0.348)**	**0.076 (0.043–0.121)**	**0.291 (0.204–0.372)**	**0.086 (0.042–0.138)**	–	–
Pan, *Gorilla*, & *Pongo*[3]	**0.398 (0.285–0.523)**	**0.161 (0.081–0.274)**	**0.284 (0.220–0.426)**	**0.083 (0.049–0.181)**	–	–	–	–	–	–
Pan, Gorilla, & Pongo[4]	**0.400 (0.285–0.523)**	**0.161 (0.081–0.274)**	–	–	–	–	–	–	–	–
Pan & *Pongo*[3]	**0.413 (0.326–0.523)**	**0.172 (0.106–0.274)**	**0.281 (0.231–0.347)**	**0.079 (0.053–0.120)**	–	–	–	–	–	–
Pan & *Pongo*[4]	**0.404 (0.318–0.523)**	**0.165 (0.101–0.274)**	–	–	–	–	–	–	–	–

Values in **bold** are outside the entire range for recent modern humans

[1] Howells (1996), N = 2,524

[2] Weaver and Stringer (2015), N = 237

[3] Perez-Claros and Palmqvist (2022), N = 117 total, 88 without *Gorilla*

[4] Weaver and Stringer (2015) and Perez-Claros and Palmqvist (2022), N = 354 total, 325 without *Gorilla*

Table 8. Sum of squared residuals from fitted scaling lines between craniofacial variables and GM2 for recent modern humans[1] and for extant great apes[2, 3, 4]

	Face								Neurocranium				
	recent modern humans[1]				*Pan, Gorilla* & *Pongo*[4]		*Pan* & *Pongo*[4]		recent modern humans[1]	*Pan, Gorilla* & *Pongo*[4]		*Pan* & *Pongo*[4]	
Taxon / Specimen	NPH, ZYB, ZMB, BOB, & MAB	NPH, ZYB, ZMB, & BOB	NPH, ZMB, & MAB	NPH & ZYB	NPH, ZYB, ZMB, & MAB	NPH, ZYB, & ZMB	NPH, ZYB, ZMB, & MAB	NPH, ZYB, & ZMB	GOL, XCB, ASB, BBH, BNL, & BPL	GOL, XCB, BBH, BNL, & BPL	GOL, XCB, BBH, & BPL	GOL, XCB, BBH, BNL, & BPL	GOL, XCB, BBH, & BPL
Homo floresiensis													
LB 1	**0.128**	**0.099**	**0.096**	**0.070**	**0.072**	**0.062**	**0.045**	**0.035**	**0.104 | 0.116**	**0.091 | 0.082**	**0.058 | 0.054**	**0.061 | 0.056**	**0.028 | 0.028**
Early *Homo*													
KNM-ER 1813	**0.197**	**0.139**	**0.157**	**0.084**	**0.050**	**0.045**	**0.039**	**0.034**	**0.120**	**0.063 | 0.093**	**0.036 | 0.056**	**0.050 | 0.071**	**0.023 | 0.034**
OH 24	–	–	**0.170**	–	–	–	–	–	**0.081**	**0.133**	**0.067**	**0.103**	**0.038**
KNM-ER 1470	–	–	–	–	–	–	–	–	**–**	**–**	**–**	**–**	**–**
STW 53	–	–	**–**	**0.049**	–	0.092	–	–	–	**–**	**0.080**	**–**	**0.075**
Homo erectus s.l.													
Africa													
KNM-ER 3733	**0.036**	**0.032**	**0.025**	**0.018**	0.246	0.178	0.283	0.214	**0.041**	0.190	0.134 | 0.142	0.176	0.120 | 0.126
KNM-ER 3883	–	–	–	–	–	–	–	–	**–**	–	–	–	–
KNM-WT 15000	–	–	–	–	–	–	–	–	**–**	–	–	–	–
KNM-ER 42700	–	–	–	–	–	–	–	–	**–**	–	–	–	–
OH 9	–	–	–	–	–	–	–	–	**–**	–	–	–	–
Dmanisi													
D2700	–	–	**0.077**	**0.036**	**0.136**	0.111	**0.126**	**0.102**	**0.064**	**0.128**	**0.091**	**0.101**	**0.063**
D2282	–	–	–	**0.098**	–	–	–	–	**–**	**–**	**0.047**	**–**	**–**
D3444	–	–	–	**0.025**	–	0.143			–	–	**0.098**		
D4500	–	–	–	**0.125**	–	–	–	–	**–**	**–**	**0.020**	**–**	**–**
D2280	–	–	–	**–**	–	–	–	–	**–**	**–**	**–**	**–**	**–**
Asia													
Sangiran 17	–	0.013	–	0.002	–	0.274	–	0.338	**0.035**	0.286 | 0.306	0.214 | 0.232	0.281 | 0.275	0.207 | 0.202
Zhoukoudian 11	0.016	0.014	0.005	0.006	0.342	0.259	0.385	0.302	0.013	0.245	0.175	0.229	0.159
Ngawi	–	–	–	–	–	–	–	–	–	–	–	–	–
Sangiran IX	–	–	–	–	–	–	–	–	–	–	–	–	–
Australopiths													
MRD-VP-1/1	–	**0.163**	–	**0.123**	–	**0.032**	–	**0.039**	–	–	**0.024**	–	**0.017**
A.L. 444-2	–	–	–	–	–	–	–	–	–	–	–	–	–
A.L. 888-1	**–**	**–**	**–**	**–**	–	**–**	**–**	**–**	**–**	**–**	**–**	**–**	**–**
STW 573	–	–	–	**0.049**	–	–	–	–	–			–	**0.031**
STS 5	**0.218**	**0.169**	**0.181**	**0.100**	**0.041**	**0.033**	**0.043**	**0.035**	**0.158**	**0.031**	**0.020**	**0.029**	**0.018**
STS 71	–	–	–	–	–	–	–	–	–	–	–	–	–
OH 5	**0.195**	**0.156**	**0.145**	**0.112 | 0.104**	**0.066**	**0.042**	**0.116**	**0.092**	**0.087**	**0.111 | 0.129**	**0.090**	**0.099 | 0.113**	**0.079 | 0.083**
KNM-ER 406	–	–	–	–	–	–	–	–	**0.088 | 0.072**	**0.083 | 0.131**	**0.064 | 0.103**	**0.077 | 0.112**	**0.058 | 0.084**
KNM-WT 17000	–	–	–	**0.277**	–	–	–	–	–	–		–	**0.003**
SK 48	–	–	**0.302**	**0.226**	**0.006**	**0.004**			–	–	**0.019**		
DNH 7	–	–	–	–	–	–	–	–	–	–	–	–	–

Other *Homo*													
LES 1	–	–	–	**0.108**	–	–	–	–	–	–	**0.035**	–	0.018
Sima de los Huesos 5	0.022	0.018	0.014	0.005	0.324	0.241	0.382	0.298	0.008	0.245	0.176	0.232	0.163
Sima de los Huesos 6	–	–	–	–	–	–	–	–	–	–	–	–	–
Kabwe	0.010	0.010	0.003	0.003	0.416	0.307	0.502	0.394	0.010	0.299	0.214	0.298	0.213
Steinheim	**0.047**	**0.037**	**0.029**	0.017	**0.229**	0.177	0.245	0.193	**0.028**	0.168	0.111	0.161	0.104
Petralona	–	–	0.004	0.001	0.412	0.313	0.501	0.403	–	–	0.225	–	0.219
Dali	0.006	0.006	0.001	0.000	0.474	0.360	0.525	0.411	0.019	0.349	0.256	0.324	0.231
Harbin	0.018	0.017	0.010	0.007	0.621	0.466	0.709	0.555	0.015	0.385	0.278	0.384	0.277
Neandertals													
La Chapelle aux Saints	0.002	0.001	0.002 | 0.001	0.000	0.516 | 0.503	0.372 | 0.362	0.603 | 0.588	0.459 | 0.448	0.009	0.288 | 0.301	0.222 | 0.233	0.298 | 0.290	0.230 | 0.219
Gibraltar 1	0.001	0.001	0.001	0.001	0.439	0.332	0.482	0.375	0.006	0.293	0.223	0.267	0.197
Tabun 1	–	–	–	0.007	–	–	–	–	0.019	0.235	0.182	0.205	0.151
La Ferrassie	–	–	–	0.001	–	–	–	–	0.010	0.327 | 0.366	0.251 | 0.282	0.321 | 0.354	0.245 | 0.270
Shanidar 1	–	–	0.003	0.002	0.550	0.408	0.626	0.484	0.006	0.336 | 0.343	0.236 | 0.250	0.326 | 0.334	0.239 | 0.244
Saccopostre 1	–	–	–	–	–	–	–	–	**0.029**	0.207	0.139 | 0.147	0.187	0.127 | 0.122
Guattari 1	–	–	0.004	–	–	–	–	–	–	–	–	–	–
Amud 1	–	–	–	–	–	–	–	–	–	–	–	–	–
Spy 1	–	–	–	–	–	–	–	–	–	–	–	–	–
Monte Circe	–	–	–	–	–	–	–	–	–	–	–	–	–
La Quina 5	–	–	–	–	–	–	–	–	–	–	–	–	–
Homo sapiens													
Skhul V	–	–	0.001	0.001	0.419	0.313	0.461	0.355	0.005	0.302	0.193	0.291	0.182
Jebel Irhoud 1	–	–	–	–	–	–	–	–	–	–	–	–	–
Recent[1]	0.004 (0.000–0.033)	0.003 (0.000–0.030)	0.003 (0.000–0.024)	0.001 (0.000–0.018)	0.438 (0.239–0.720)	0.243 (0.090–0.530)	0.447 (0.201–0.762)	0.345 (0.160–0.599)	0.004 (0.000–0.026)	0.306 (0.162–0.508)	0.217 (0.107–0.367)	0.270 (0.147–0.442)	0.180 (0.092–0.289)
Extant great apes													
Pan[2]	–	–	**0.323 (0.203–0.474)**	–	–	–	–	–	–	**0.002 (0.000–0.011)**	–	**0.002 (0.000–0.008)**	–
Pan, *Gorilla*, & *Pongo*[3]	–	–	–	**0.243 (0.142–0.455)**	–	–	–	–	–	–	–	–	–
Pan, Gorilla, & Pongo[4]	–	–	–	–	–	–	–	–	–	–	**0.003 (0.000–0.021)**	–	**0.004 (0.000–0.066)**
Pan & *Pongo*[3]	–	–	–	**0.258 (0.160–0.455)**	–	–	–	–	–	–	**0.002 (0.000–0.021)**	–	–
Pan & *Pongo*[4]	–	–	–	–	–	–	–	–	–	–	–	–	**0.002 (0.000–0.019)**

Values in **bold** are outside the entire range for recent modern humans

[1] Howells (1996), N = 2,524

[2] Weaver and Stringer (2015), N = 237

[3] Perez-Claros and Palmqvist (2022), N = 117 total, 88 without *Gorilla*

[4] Weaver and Stringer (2015) and Perez-Claros and Palmqvist (2022), N = 354 total, 325 without *Gorilla*

(back to text)

Table 9. Sum of standardized squared residuals from fitted scaling lines between craniofacial variables and GM2 for recent modern humans[1] and for extant great apes[2,3,4]

	Face				Neurocranium				
	recent modern humans[1]				recent modern humans[1]	*Pan, Gorilla* & *Pongo*[4]		*Pan* & *Pongo*[4]	
Taxon / Specimen	NPH, ZYB, ZMB, BOB, & MAB	NPH, ZYB, ZMB, & BOB	NPH, ZMB, & MAB	NPH & ZYB	GOL, XCB, ASB, BBH, BNL, & BPL	GOL, XCB, BBH, BNL, & BPL	GOL, XCB, BBH, & BPL	GOL, XCB, BBH, BNL, & BPL	GOL, XCB, BBH, & BPL
Homo floresiensis									
LB 1	**157.89**	**126.99**	**102.71**	**96.60**	**131.96 | 148.40**	**195.89 | 172.55**	**61.13 | 55.16**	**145.13 | 128.30**	**42.64 | 38.62**
Early *Homo*									
KNM-ER 1813	**232.43**	**170.98**	**168.34**	**110.67**	**145.14 | 98.06**	**140.62 | 195.95**	**58.36 | 38.11**	**118.37 | 156.60**	**31.80**
OH 24	–	–	**181.19**	–	**98.43**	**313.14**	**75.77**	**259.00**	**59.63**
KNM-ER 1470	–	–	–	–	–	–	–	–	–
STW 53	–	–	–	66.203	–	–	**76.22**	–	**95.03**
Homo erectus s.l.									
Africa									
KNM-ER 3733	**43.44**	**39.66**	**26.81**	23.10	**59.98 | 46.56**	426.40 | 421.60	173.13 | 164.42	381.81 | 375.05	166.74 | 175.18
KNM-ER 3883	–	–	–	–	–	–	–	–	–
KNM-WT 15000	–	–	–	–	–	–	–	–	–
KNM-ER 42700	–	–	–	–	–	–	–	–	–
OH 9	–	–	–	–	–	–	–	–	–
Dmanisi									
D2700	–	–	**82.15**	**43.97 | 51.71**	**81.21**	**276.49**	**105.16 | 68.43**	**218.66**	**88.63 | 59.58**
D2282	–	–	–	**128.26**	–	–	**49.46**	–	**51.40**
D3444	–	–	–	**34.68**	–	–	**105.46**	–	**97.94**
D4500	–	–	–	**182.22**	–	–	**21.06**	–	**36.29**
D2280	–	–	–	–	–	–	–	–	–
Asia									
Sangiran 17	–	15.86	–	2.66	**73.45 | 53.89**	682.90 | 647.31	282.43 | 267.26	611.35 | 596.80	290.72 | 284.63
Zhoukoudian 11	22.31	19.89	5.36	9.81	26.26	523.73	205.79	480.80	216.12
Ngawi	–	–	–	–	–	–	–	–	–
Sangiran IX	–	–	–	–	–	–	–	–	–
Australopiths									
MRD-VP-1/1	–	**195.41**	–	**152.57**	–	–	**41.45**	–	**69.29**
A.L. 444-2	–	–	–	–	–	–	–	–	–
A.L. 888-1	–	–	–	–	–	–	–	–	–
STW 573	–	–	–	**143.86**	–	–	**41.11**	–	**42.47**
STS 5	**255.68**	**202.76**	**193.38**	**131.82**	**189.29 | 176.99**	**68.611**	**26.30**	**62.07**	**26.44**
STS 71	–	–	–	–	–	–	–	–	–
OH 5	**241.99**	**200.01**	**155.71**	**153.78 | 144.84**	**119.70 | 118.11**	**274.92** | 322.87	136.55 | 122.46	**234.51 | 268.74**	122.56 | 131.11
KNM-ER 406	–	–	–	–	**108.41 | 92.91**	**198.49** | 334.41	150.52 | **87.27**	**170.93 | 267.20**	**86.18 | 140.11**
KNM-WT 17000	–	–	–	387.74	–	–	**0.61**	–	**8.69**
SK 48	–	–	322.99	316.92	–	–	**17.21**	–	**11.25**
DNH 7	–	–	–	–	–	–	–	–	–

Other *Homo*									
LES 1	–	–	–	139.27	–	–	**31.89**	–	**20.93**
Sima de los Huesos 5	25.85	22.08	14.39	6.44	11.80	535.34	224.62	486.35	231.30
Sima de los Huesos 6	–	–	–	–	–	–	–	–	–
Kabwe	13.04	12.37	3.48	2.81	20.55	606.38	240.99	613.09	292.65
Steinheim	**57.16**	**46.95**	**31.21**	22.22	**40.45**	338.76	115.43	338.32	139.21
Petralona	–	–	4.23	2.01	–	–	265.77	–	300.20
Dali	7.35	7.3	0.57	0.42	**46.38**	736.99	292.05	681.96	311.51
Harbin	21.03	19.3	10.77	7.69	**35.40**	825.98	338.26	800.58	382.57
Neandertals									
La Chapelle aux Saints	2.66 | 2.30	1.04 | 1.03	2.17 | 1.59	0.06 | 0.02	20.92 | 22.32	632.45 | 603.62	287.39 | 261.27	605.23 | 595.72	320.70 | 303.46
Gibraltar 1	1.11	1.03	0.59	1.00	13.47	608.79	264.81	542.86	269.71
Tabun 1	–	–	–	8.11	30.82	480.56	209.08	413.25	204.16
La Ferrassie	–	–	–	1.60	16.07 | 17.11	691.21 | 767.37	313.36 | 351.79	654.17 | 719.34	343.98 | 381.51
Shanidar 1	–	–	3.41	3.65	14.98 | 14.51	702.40 | 717.19	306.36 | 299.90	667.60 | 683.43	331.12 | 339.25
Saccopostre 1	–	–	–	–	**43.99**	456.24	176.17 | 169.26	402.77	174.94 | 169.64
Guattari 1	–	–	4.39	–	–	683.53	276.73	633.73	295.02
Amud 1	–	–	–	–	–	–	–	–	–
Spy 1	–	–	–	–	–	–	–	–	–
Monte Circe	–	–	–	–	–	–	–	–	–
La Quina 5	–	–	–	–	–	–	–	–	–
Homo sapiens									
Skhul V	–	–	1.19	1.03	9.09	653.54	232.76	621.75	253.76
Jebel Irhoud 1	–	–	–	–	–	–	–	–	–
Recent[1]	5.00 (0.03–41.64)	4.00 (0.01–37.80)	3.00 (0.01–24.97)	1.99 (0.00–24.45)	6.00 (0.16–34.97)	634.80 (322.23–1081.96)	257.97 (113.81–467.56)	563.04 (306.68–936.76)	257.31 (122.48–421.48)

Extant great apes									
Pan[2]	–	–	**348.1 (218.96–511.22)**	–	–	**5.09 (0.159–22.14)**	–	**5.08 (0.12–20.64)**	–
Pan, *Gorilla*, & *Pongo*[3]	–	–	–	**323.01 (195.36–622.06)**	–	–	–	–	–
Pan, Gorilla, & Pongo[4]	–	–	–	–	–	–	**3.99 (0.03–36.38)**	–	9.09 (0.08–173.83)
Pan & *Pongo*[3]	–	–	–	**342.06 (211.75–622.06)**	–	–	–	–	–
Pan & *Pongo*[4]	–	–	–	–	–	–	**3.49 (0.03–36.38)**	–	**3.99 (0.08–32.92)**

Values in **bold** are outside the entire range for recent modern humans

[1] Howells (1996), N = 2,524

[2] Weaver and Stringer (2015), N = 237

[3] Perez-Claros and Palmqvist (2022), N = 117 total, 88 without *Gorilla*

[4] Weaver and Stringer (2015) and Perez-Claros and Palmqvist (2022), N = 354 total, 325 without *Gorilla*

(back to text)

Table 10. Mean of the absolute value of the standardized residuals from fitted scaling lines between craniofacial variables and GM2 for recent modern humans[1] and for extant great apes[2,3,4]

	Face				Neurocranium				
	recent modern humans[1]				recent modern humans[1]	*Pan, Gorilla* & *Pongo*[4]		*Pan* & *Pongo*[4]	
Taxon / Specimen	NPH, ZYB, ZMB, BOB, & MAB	NPH, ZYB, ZMB, & BOB	NPH, ZMB, & MAB	NPH & ZYB	GOL, XCB, ASB, BBH, BNL, & BPL	GOL, XCB, BBH, BNL, & BPL	GOL, XCB, BBH, & BPL	GOL, XCB, BBH, BNL, & BPL	GOL, XCB, BBH, & BPL
Homo floresiensis									
LB 1	**5.31**	**5.25**	**5.81**	**6.95**	**3.51 | 3.59**	**5.17 | 5.53**	**3.24 | 3.46**	**4.69 | 4.33**	**3.03 | 2.76**
Early *Homo*									
KNM-ER 1813	**6.68**	**6.39**	**7.46**	**7.42**	**3.42 | 3.04**	**4.68 | 5.16**	**2.80 | 3.09**	**3.98 | 4.39**	**2.38 | 2.59**
OH 24	–	–	**7.77**	–	**3.05**	**6.96**	**4.05**	**6.07**	**3.64**
KNM-ER 1470	–	–	–	–	–	–	–	–	–
STW 53	–	–	–	**5.75**	–	–	**3.11**	–	**4.03**
Homo erectus s.l.									
Africa									
KNM-ER 3733	**2.89**	**3.12**	**2.89**	3.36	**2.47** | 2.02	8.72 | 8.62	6.05 | 6.10	7.54 | 7.44	5.37 | 5.41
KNM-ER 3883	–	–	–	–	–	–	–	–	–
KNM-WT 15000	–	–	–	–	–	–	–	–	–
KNM-ER 42700	–	–	–	–	–	–	–	–	–
OH 9	–	–	–	–	–	–	–	–	–
Dmanisi									
D2700	–	–	**5.22**	**4.56 | 5.05**	**2.54**	**6.79**	4.62 | **3.47**	**5.83**	**4.11 | 3.08**
D2282	–	–	–	**7.98**	–	–	**3.11**	–	**2.52**
D3444	–	–	–	**4.16**	–	–	**4.20**	–	**4.13**
D4500	–	–	–	**9.45**	–	–	**1.79**	–	**2.73**
D2280	–	–	–	–	–	–	–	–	–
Asia									
Sangiran 17	–	1.85	–	1.13	**2.83 | 2.16**	11.23 | 10.94	8.07 | 7.85	9.63 | 9.45	7.15 | 6.99
Zhoukoudian 11	1.9	1.98	1.23	2.15	1.57	9.45	6.53	8.53	6.15
Ngawi	–	–	–	–	–	–	–	–	–
Sangiran IX	–	–	–	–	–	–	–	–	–
Australopiths									
MRD-VP-1/1	–	**6.41**	–	**8.54**	–	–	**2.69**	–	**3.24**
A.L. 444-2	–	–	–	–	–	–	–	–	–
A.L. 888-1	–	–	–	–	–	–	–	–	–

STW 573	–	–	–	**8.42**	–	–	**2.53**	–	**2.82**
STS 5	**6.81**	**6.70**	**8.01**	**8.09**	**3.57 | 3.47**	**3.26**	**2.18**	**3.09**	**2.21**
STS 71	–	–	–	–	–	–	–	–	–
OH5	**6.57**	**6.59**	**7.13**	**8.77 | 8.50**	**3.15 | 2.74**	7.24 | 7.81	5.46 | 5.72	6.33 | 6.92	5.08 | 5.39
KNM-ER 406	–	–	–	–	**2.65 | 2.53**	**6.06** | 7.89	4.46 | 5.92	**5.34 | 7.06**	4.14 | 5.69
KNM-WT 17000	–	–	–	**13.90**	–	–	**0.35**	–	**1.34**
SK 48	–	–	**10.29**	**12.56**	–	–	**1.12**	–	**1.24**
DNH 7	–	–	–	–	–	–	–	–	–
Other *Homo*									
LES 1	–	–	–	**8.28**	–	–	**1.89**	–	**1.64**
Sima de los Huesos 5	2.21	2.27	2.18	1.77	0.99	9.26	6.48	8.78	6.54
Sima de los Huesos 6	–	–	–	–	–	–	–	–	–
Kabwe	1.16	1.24	0.86	0.88	1.73	9.57	6.50	10.07	7.60
Steinheim	**3.34**	**3.38**	**3.20**	3.32	1.88	7.03	4.48	7.22	5.08
Petralona	–	–	0.97	0.99	–	–	7.19	–	7.56
Dali	0.81	0.95	0.41	0.41	2.01	11.31	7.88	10.04	7.25
Harbin	1.76	1.93	1.75	1.55	1.81	11.80	8.26	11.35	8.51
Neandertals									
La Chapelle aux Saints	0.597 | 0.540	0.428 | 0.393	0.74 | 0.59	0.16 | 0.09	1.21 | 1.18	10.20 | 10.00	7.47 | 7.14	9.99 | 9.93	7.84 | 7.68
Gibraltar 1	0.393	0.418	0.37	0.71	1.042	9.96	7.10	9.25	6.99
Tabun 1	–	–	–	1.80	1.687	8.90	6.38	7.93	5.93
La Ferrassie	–	–	–	0.81	1.01 | 1.27	10.60 | 10.93	7.68 | 7.89	10.40 | 10.93	8.13 | 8.59
Shanidar 1	–	–	0.93	1.05	1.15 | 2.13	10.56 | 10.59	7.44 | 7.44	10.47 | 10.61	7.99 | 8.11
Saccopostre 1	–	–	–	–	**2.13**	8.94	6.19 / 6.10	7.70	5.45 | 5.41
Guattari 1	–	–	1.14	–	–	10.73	7.49	9.93	7.31
Amud 1	–	–	–	–	–	–	–	–	–
Spy 1	–	–	–	–	–	–	–	–	–
Monte Circe	–	–	–	–	–	–	–	–	–
La Quina 5	–	–	–	–	–	–	–	–	–
Homo sapiens									
Skhul V	–	–	0.45	0.53	1.221	9.76	6.31	9.90	7.02
Jebel Irhoud 1	–	–	–	–	–	–	–	–	–
Recent[1]	0.80 (0.07–2.82)	0.81 (0.06–3.03)	0.80 (0.045–2.85)	0.81 (0.02–3.49)	0.72 (0.11–2.05)	9.61 (6.39–13.11)	6.54 (4.02–9.05)	9.30 (6.80–11.89)	6.83 (4.37–8.84)

Extant great apes									
Pan[2]	–	–	**10.54 (8.34–12.48)**	–	–	**0.80 (0.15–1.90)**	–	**0.80 (0.12–1.77)**	–
Pan, *Gorilla*, & *Pongo*[3]	–	–	–	**12.58 (9.88–17.63)**	–	–	–	–	–
Pan, Gorilla, & *Pongo*[4]	–	–	–	–	–	–	**0.75 (0.07–2.65)**	–	0.97 (0.12–6.18)
Pan & *Pongo*[3]	–	–	–	**12.96 (10.27–17.63)**	–	–	–	–	–
Pan & *Pongo*[4]	–	–	–	–	–	–	**0.75 (0.07–2.65)**	–	**0.77 (0.12–2.54)**

Values in **bold** are outside the entire range for recent modern humans

[1] Howells (1996), N = 2,524

[2] Weaver and Stringer (2015), N = 237

[3] Perez-Claros and Palmqvist (2022), N = 117 total, 88 without *Gorilla*

[4] Weaver and Stringer (2015) and Perez-Claros and Palmqvist (2022), N = 354 total, 325 without *Gorilla*

(back to text)

Table 11. Raw and squared residuals from fitted scaling lines between craniofacial variables and GM3 for recent modern humans[1]

Taxon / Specimen	lnNPH		lnZYB		lnZMB		lnMAB		lnBOB	
	raw	squared	raw	squared	raw	squared	raw	squared	raw	squared
Homo floresiensis										
LB 1	**0.192**	**0.037**	**0.157**	**0.025**	**0.147**	**0.022**	**0.153 | 0.128**	**0.023 | 0.016**	0.032	0.001
Early *Homo*										
KNM-ER 1813	**0.234 | 0.196**	**0.055**	**0.154**	**0.024**	**0.197 | 0.150**	**0.039 | 0.023**	**0.231 | 0.239**	**0.053 | 0.057**	**0.100 | 0.113**	**0.009 | 0.013**
OH 24	**0.251**	**0.063**	–	–	**0.241**	**0.058**	**0.256**	**0.065**	**0.154 | 0.118**	**0.024 | 0.014**
KNM-ER 1470	–	–	–	–	–	–	–	–	–	–
STW 53	–	–	–	–	–	–	–	–	–	–
Homo erectus s.l.										
Africa										
KNM-ER 3733	0.080 | 0.077	0.006 | 0.006	0.037	0.001	0.057 | 0.041	0.003 | 0.002	0.026	0.001	0.052 | 0.048	0.003 | 0.002
KNM-ER 3883	–	–	**0.109**	**0.012**	**0.209**	**0.044**	–	–	**0.102 | 0.100**	**0.010 | 0.010**
KNM-WT 15000	**0.125**	**0.016**	–	–	0.097	0.009	–	–	0.052 | **0.086**	0.003 | **0.007**
KNM-ER 42700	–	–	–	–	–	–	–	–	**0.073**	**0.005**
OH 9	–	–	–	–	–	–	–	–	**0.078 | 0.131**	**0.006 | 0.017**
Dmanisi										
D2700	**0.149 | 0.128**	**0.022 | 0.016**	0.061 | 0.066	0.004 | 0.004	**0.137**	**0.019**	**0.131**	**0.017**	0.062	0.004
D2282	**0.224**	**0.050**	0.143	0.020	–	–	–	–	– | 0.090	– | 0.008
D3444	**0.090**	**0.008**	0.078	0.006	**0.089**	**0.008**	–	–	–	–
D4500	**0.218**	**0.048**	0.236	0.056	–	–	–	–	–	–
D2280	–	–	–	–	–	–	–	–	0.103	0.011
Asia										
Sangiran 17	-0.003	0.000	0.008	0.000	0.051 | 0.042	0.003 | 0.001	–	–	0.057 | 0.048	0.003 | 0.002
Zhoukoudian 11	0.050	0.002	0.066	0.004	0.016	0.000	0.050	0.003	0.090	0.008
Ngawi	–	–	–	–	–	–	–	–	0.024	0.001
Sangiran IX	–	–	–	–	–	–	–	–	–	–
Australopiths										
MRD-VP-1/1	–	–	–	–	–	–	–	–	–	–
A.L. 444-2	–	–	–	–	–	–	–	–	–	–
A.L. 888-1	–	–	–	–	–	–	–	–	–	–
STW 573	–	–	–	–	–	–	–	–	–	–
STS 5	**0.227**	**0.051**	**0.143**	**0.020**	**0.217**	**0.047**	**0.186**	**0.035**	0.034	0.001
STS 71	–	–	–	–	–	–	–	–	–	–
OH 5	**0.323 | 0.031**	**0.104 | 0.095**	**0.275 | 0.276**	**0.076 | 0.076**	**0.263**	**0.069**	**0.264**	**0.070**	0.118 | 0.132	0.014 | 0.017
KNM-ER 406	–	–	**0.295**	**0.087**	**0.290**	**0.084**	**0.234**	**0.055**	**0.134**	**0.018**
KNM-WT 17000	–	–	–	–	–	–	–	–	–	–
SK 48	–	–	–	–	–	–	–	–	–	–
DNH 7	–	–	–	–	–	–	–	–	–	–

Other *Homo*										
LES 1	–	–	–	–	–	–	–	–	–	–
Sima de los Huesos 5	0.055	0.003	0.030	0.001	0.076	0.006	0.057	0.003	0.083	0.007
Sima de los Huesos 6	–	–	–	–	-0.046	0.002	–	–	-0.012	0.000
Kabwe	0.002	0.000	-0.038	0.001	-0.039	0.002	-0.015	0.000	0.054 | 0.035	0.003 | 0.001
Steinheim	0.083 | 0.080	0.007 | 0.006	0.046 | 0.044	0.002 | 0.002	0.062	0.004	0.073 | 0.070	0.005 | 0.005	**0.093**	**0.009**
Petralona	0.021	0.000	0.028	0.001	0.006	0.000	0.061	0.004	–	–
Dali	-0.017	0.000	-0.001	0.000	0.017	0.000	0.012	0.000	0.079	0.006
Harbin	-0.098	0.010	-0.018	0.000	-0.056	0.003	-0.040	0.002	**0.086**	**0.007**
Neandertals										
La Chapelle aux Saints	-0.029 | 0.001	0.001 0.000	-0.018 | 0.009	0.000 | 0.000	-0.040 | -0.011	0.002 | 0.000	-0.056 | -0.028	0.003 | 0.001	0.008 | 0.031	0.000 | 0.001
Gibraltar 1	0.039	0.001	0.000	0.000	0.022	0.000	0.028	0.001	0.020	0.000
Tabun 1	0.054	0.003	-0.004	0.000	–	–	0.036	0.001	–	–
La Ferrassie	-0.017	0.000	-0.029	0.001	–	–	-0.028	0.001	–	–
Shanidar 1	-0.006	0.000	-0.043	0.002	-0.042	0.002	-0.031	0.001	–	–
Saccopostre 1	**0.107 | 0.109**	0.011 | 0. 012	–	–	–	–	0.067 | 0.070	0.004 | 0.005	0.058	0.003
Guattari 1	–	–	–	–	–	–	–	–	–	–
Amud 1	–	–	–	–	–	–	–	–	–	–
Spy 1	–	–	–	–	–	–	–	–	–	–
Monte Circe	–	–	–	–	–	–	–	–	–	–
La Quina 5	–	–	–	–	–	–	–	–	–	–
Homo sapiens										
Skhul V	-0.027	0.001	0.001	0.000	0.009	0.000	-0.016	0.000	–	–
Jebel Irhoud 1	–	–	–	–	–	–	–	–	–	–
Recent[1]	0.000 (-0.113–0.095)	0.001 (0.000–0.013)	0.000 (-0.082–0.086)	0.000 (0.000–0.007)	0.000 (-0.099–0.126)	0.000 (0.000–0.016)	0.000 (-0.111–0.098)	0.000 (0.000–0.012)	0.000 (-0.080–0.085)	0.000 (0.000–0.007)
Extant great apes[2]	–	–	–	–	–	–	–	–	–	–

Values in **bold** are outside the entire range for recent modern humans

[1] Howells (1996), N = 2,524

[2] missing ASB thus GM3 cannot be calculated

Table 12. Sum of squared residuals from fitted scaling lines between craniofacial variables and GM3 for recent modern humans[1]

Taxon / Specimen	Face				Neurocranium
	NPH, ZYB, ZMB, BOB, & MAB	NPH, ZYB, ZMB, & BOB	NPH, ZMB, & MAB	NPH & ZYB	GOL, XCB, ASB, BBH, BNL, & BPL
Homo floresiensis					
LB 1	**0.107**	**0.084**	**0.082**	**0.061**	**0.096 | 0.088**
Early *Homo*					
KNM-ER 1813	**0.180**	**0.127**	**0.147**	**0.078**	**0.114 | 0.070**
OH 24	–	–	**0.186**	–	**0.095**
KNM-ER 1470	–	–	–	–	–
STW 53	–	–	–	–	–
Homo erectus s.l.					
Africa					
KNM-ER 3733	0.014	0.014	0.010	0.008	0.031 | 0.034
KNM-ER 3883	–	–	–	–	–
KNM-WT 15000	–	–	–	–	–
KNM-ER 42700	–	–	–	–	–
OH 9	–	–	–	–	–
Dmanisi					
D2700	–	–	**0.058**	**0.026 | 0.021**	**0.055**
D2282	–	–	–	**0.070**	–
D3444	–	–	–	0.014	–
D4500	–	–	–	**0.103**	–
D2280	–	–	–	–	–
Asia					
Sangiran 17	–	0.006	–	0.000	0.030 | **0.039** | **0.042**
Zhoukoudian 11	0.018	0.015	0.005	0.007	0.021
Ngawi	–	–	–	–	–
Sangiran IX	–	–	–	–	–
Australopiths					
MRD-VP-1/1	–	–	–	–	–
A.L. 444-2	–	–	–	–	–
A.L. 888-1	–	–	–	–	–
STW 573	–	–	–	–	–
STS 5	**0.155**	**0.120**	**0.133**	**0.072**	**0.115 | 0.132**
STS 71	–	–	–	–	–
OH 5	**0.332**	**0.263**	**0.243**	**0.180 | 0.171**	**0.148 | 0.133**
KNM-ER 406	–	–	–	–	**0.115 | 0.124**
KNM-WT 17000	–	–	–	–	–
SK 48	–	–	–	–	–
DNH 7	–	–	–	–	–

Other *Homo*					
LES 1	–	–	–	–	–
Sima de los Huesos 5	0.020	0.017	0.012	0.004	0.014
Sima de los Huesos 6	–	–	–	–	–
Kabwe	0.006	0.006	0.002	0.001	0.022
Steinheim	0.027	0.021	0.016	0.009 | 0.008	0.027
Petralona	–	–	0.004	0.001	–
Dali	0.007	0.007	0.001	0.000	0.024
Harbin	0.022	0.020	0.014	0.010	0.019
Neandertals					
La Chapelle aux Saints	0.006 | 0.002	0.003 | 0.001	0.006 | 0.001	0.001 | 0.000	0.017 | 0.016
Gibraltar 1	0.003	0.002	0.003	0.001	0.016
Tabun 1	–	–	–	0.003	0.024
La Ferrassie	–	–	–	0.001	0.012
Shanidar 1	–	–	0.003	0.002	0.011 | 0.010
Saccopostre 1	–	–	–	–	0.030
Guattari 1	–	–	–	–	–
Amud 1	–	–	–	–	–
Spy 1	–	–	–	–	–
Monte Circe	–	–	–	–	–
La Quina 5	–	–	–	–	–
Homo sapiens					
Skhul V	–	–	0.001	0.001	0.006
Jebel Irhoud 1	–	–	–	–	–
Mala	0.032	**0.031**	**0.031**	**0.028**	**0.044**
Recent[1]	(0.000-0.034)	(0.000–0.029)	(0.000–0.026)	(0.000–0.016)	(0.003–0.037)
Extant great apes[2]	–	–	–	–	–

Values in **bold** are outside the entire range for recent modern humans

[1] Howells (1996), N = 2,524

[2] missing ASB thus GM3 cannot be calculated

(back to text)

Table 13. Sum of standardized squared residuals from fitted scaling lines between craniofacial variables and GM3 for recent modern humans[1]

Taxon / Specimen	Face				Neurocranium
	NPH, ZYB, ZMB, BOB, & MAB	NPH, ZYB, ZMB, & BOB	NPH, ZMB, & MAB	NPH & ZYB	GOL, XCB, ASB, BBH, BNL, & BPL
Homo floresiensis					
LB 1	**121.22**	**97.25**	**79.76**	**75.56**	**174.84 | 168.73**
Early *Homo*					
KNM-ER 1813	**196.36**	**141.54**	**144.26**	**91.15**	**184.45 | 129.31**
OH 24	–	–	**182.61**	–	**136.38**
KNM-ER 1470	–	–	–	–	–
STW 53	–	–	–	–	–
Homo erectus s.l.					
Africa					
KNM-ER 3733	15.96	15.27	10.00	8.40	68.97 | 66.91
KNM-ER 3883	–	–	–	–	–
KNM-WT 15000	–	–	–	–	–
KNM-ER 42700	–	–	–	–	–
OH 9	–	–	–	–	–
Dmanisi					
D2700	–	–	**56.91**	**27.51 | 22.94**	**109.62**
D2282	–	–	–	**81.37**	–
D3444	–	–	–	17.69	–
D4500	–	–	–	**136.00**	–
D2280	–	–	–	–	–
Asia					
Sangiran 17	–	7.11	–	0.12	64.10 | 84.80 | **90.00**
Zhoukoudian 11	23.47	20.87	5.26	9.47	51.40
Ngawi	–	–	–	–	–
Sangiran IX	–	–	–	–	–
Australopiths					
MRD-VP-1/1	–	–	–	–	–
A.L. 444-2	–	–	–	–	–
A.L. 888-1	–	–	–	–	–
STW 573	–	–	–	–	–
STS 5	**164.58**	**128.88**	**129.85**	**82.78**	**185.91 | 209.99**
STS 71	–	–	–	–	–
OH 5	**379.10**	**307.69**	**237.30**	**223.55 | 215.22**	**236.07 | 194.63**
KNM-ER 406	–	–	–	–	**179.64 | 178.98**
KNM-WT 17000	–	–	–	–	–
SK 48	–	–	–	–	–
DNH 7	–	–	–	–	–

Other *Homo*					
LES 1	–	–	–	–	–
Sima de los Huesos 5	22.53	19.25	11.63	4.43	32.39
Sima de los Huesos 6	–	–	–	–	–
Kabwe	8.13	7.89	1.68	2.38	43.85
Steinheim	31.10	25.66	15.68	10.17 | 9.34	66.04
Petralona	–	–	4.25	1.67	–
Dali	9.24	9.09	0.69	0.27	58.98
Harbin	24.65	22.96	13.92	9.78	37.52
Neandertals					
La Chapelle aux Saints	6.19 | 2.38	2.94 | 1.58	5.56 | 0.92	1.37 | 0.12	43.94 | 44.07
Gibraltar 1	3.26	2.45	2.71	1.44	49.70
Tabun 1	–	–	–	2.82	67.39
La Ferrassie	–	–	–	1.68	33.92 | 32.10
Shanidar 1	–	–	2.70	3.00	30.64 | 28.78
Saccopostre 1	–	–	–	–	62.29
Guattari 1	–	–	–	–	–
Amud 1	–	–	–	–	–
Spy 1	–	–	–	–	–
Monte Circe	–	–	–	–	–
La Quina 5	–	–	–	–	–
Homo sapiens					
Skhul V	–	–	1.07	0.71	13.69
Jebel Irhoud 1	–	–	–	–	–
Recent[1]	5.00 (0.06–40.01)	4.00 (0.06–34.24)	3.00 (0.00–25.52)	2.00 (0.00–18.15)	35.44 (8.04–86.59)
Extant great apes[2]	–	–	–	–	–

Values in **bold** are outside the entire range for recent modern humans

[1] Howells (1996), N = 2,524

[2] missing ASB thus GM3 cannot be calculated

(back to text)

Table 14. Mean of the absolute value of the standardized residuals from fitted scaling lines between craniofacial variables and GM3 for recent modern humans[1]

Taxon / Specimen	Face				Neurocranium
	NPH, ZYB, ZMB, BOB, & MAB	NPH, ZYB, ZMB, & BOB	NPH, ZMB, & MAB	NPH & ZYB	GOL, XCB, ASB, BBH, BNL, & BPL
Homo floresiensis					
LB 1	**4.58**	**4.50**	**5.12**	**6.14**	**4.56 | 4.55**
Early *Homo*					
KNM-ER 1813	**6.13**	**5.81**	**6.91**	**6.73**	**4.82 | 3.84**
OH 24	–	–	**7.80**	–	**4.33**
KNM-ER 1470	–	–	–	–	–
STW 53	–	–	–	–	–
Homo erectus s.l.					
Africa					
KNM-ER 3733	1.70	1.92	1.70	1.99	**3.00 | 2.94**
KNM-ER 3883	–	–	–	–	–
KNM-WT 15000	–	–	–	–	–
KNM-ER 42700	–	–	–	–	–
OH 9	–	–	–	–	–
Dmanisi					
D2700	–	–	**4.35**	**3.54 | 3.32**	**3.60**
D2282	–	–	–	**6.35**	–
D3444	–	–	–	2.97	–
D4500	–	–	–	**8.13**	–
D2280	–	–	–	–	–
Asia					
Sangiran 17	–	1.03	–	0.21	2.87 | 2.91 | 2.93
Zhoukoudian 11	1.93	2.01	1.22	2.10	2.59
Ngawi	–	–	–	–	–
Sangiran IX	–	–	–	–	–
Australopiths					
MRD-VP-1/1	–	–	–	–	–
A.L. 444-2	–	–	–	–	–
A.L. 888-1	–	–	–	–	–
STW 573	–	–	–	–	–
STS 5	**5.34**	**5.19**	**6.56**	**6.40**	**4.19 | 4.69**
STS 71	–	–	–	–	–
OH5	**8.40**	**8.39**	**8.85**	**10.56 | 10.35**	**5.37 | 4.86**
KNM-ER 406	–	–	–	–	**4.49 | 4.62**
KNM-WT 17000	–	–	–	–	–
SK 48	–	–	–	–	–
DNH 7	–	–	–	–	–

Other *Homo*					
LES 1	–	–	–	–	–
Sima de los Huesos 5	2.03	2.08	1.95	1.47	1.79
Sima de los Huesos 6	–	–	–	–	–
Kabwe	1.06	1.21	0.59	0.81	2.27
Steinheim	2.43	2.45	2.27	2.23 | 2.13	2.77
Petralona	–	–	0.93	0.89	–
Dali	0.88	1.00	0.48	0.28	2.52
Harbin	1.99	2.17	2.02	1.88	1.87
Neandertals					
La Chapelle aux Saints	0.99 | 0.55	0.79 | 0.47	1.31 | 0.42	0.83 | 0.18	1.95 | 2.09
Gibraltar 1	0.71	0.66	0.92	0.60	2.06
Tabun 1	–	–	–	0.91	2.47
La Ferrassie	–	–	–	0.86	1.57 | 1.71
Shanidar 1	–	–	0.82	0.95	1.66 | 1.66
Saccopostre 1	–	–	–	–	**2.96**
Guattari 1	–	–	–	–	–
Amud 1	–	–	–	–	–
Spy 1	–	–	–	–	–
Monte Circe	–	–	–	–	–
La Quina 5	–	–	–	–	–
Homo sapiens					
Skhul V	–	–	0.55	0.44	1.19
Jebel Irhoud 1	–	–	–	–	–
Recent[1]	0.80 (0.10–2.77)	0.80 (0.11–2.87)	0.80 (0.04–2.85)	0.80 (0.01–2.98)	1.57 (0.76–2.93)
Extant great apes[2]	–	–	–	–	–

Values in **bold** are outside the entire range for recent modern humans

[1] Howells (1996), N = 2,524

[2] missing ASB thus GM3 cannot be calculated

(back to text)

Table 15. Raw and squared residuals from fitted scaling lines between craniofacial variables and GOL for recent modern humans[1]

Taxon / Specimen	lnNPH		lnZYB		lnZMB		lnMAB		lnBOB	
	raw	squared	raw	squared	raw	squared	raw	squared	raw	squared
Homo floresiensis										
LB 1	**0.179**	**0.032**	**0.134**	**0.018**	0.116	0.013	0.125 | 0.100	0.016 | 0.010	-0.023	0.001
Early *Homo*										
KNM-ER 1813	**0.175 | 0.192**	**0.031 | 0.037**	0.091	0.008	**0.133 | 0.134**	**0.018 | 0.018**	**0.172 | 0.196**	**0.030 | 0.038**	0.026 | 0.061	0.001 | 0.004
OH 24	**0.206**	**0.042**	–	–	**0.194**	**0.038**	**0.211**	**0.044**	0.094 | 0.086	0.009 | 0.007
KNM-ER 1470	**0.169 | 0.158**	**0.029 | 0.025**	–	–	**0.152 | 0.138** | 0.071	**0.023 | 0.019** | 0.005	**0.178**	**0.032**	0.078 | **0.118**	0.006 | **0.014**
STW 53	0.085 | **0.215**	0.007 | **0.046**	0.055	0.003	**0.161** | 0.045 | 0.077	**0.026** | 0.002 | 0.006	–	–	–	–
Homo erectus s.l.										
Africa										
KNM-ER 3733	0.056 | 0.049	0.003 | 0.003	0.017	0.000	0.041 | 0.017	0.002 | 0.000	0.005	0.000	0.040	0.002
KNM-ER 3883	–	–	0.064	0.004	**0.179**	**0.032**	–	–	0.069	0.005
KNM-WT 15000	0.070	0.005	–	–	0.046	0.002	–	–	0.005 | 0.051	0.000 | 0.003
KNM-ER 42700	–	–	–	–	–	–	–	–	0.022	0.000
OH 9	–	–	–	–	–	–	–	–	0.039 | 0.087	0.002 | 0.008
Dmanisi										
D2700	**0.152** | 0.076	**0.023** | 0.015	0.053	0.003	0.136	0.019	0.130	0.017	0.043	0.002
D2282	**0.154**	**0.024**	0.075	0.006	–	–	–	–	0.011	0.000
D3444	**0.076**	**0.006**	0.061	0.004	0.072	0.005	–	–	–	–
D4500	**0.110**	**0.012**	0.141	0.020	–	–	–	–	–	–
D2280	–	–	–	–	–	–	–	–	0.051	0.003
Asia										
Sangiran 17	-0.065 | -0.097	0.004 | 0.009	-0.039	0.002	0.011 | -0.026	0.000 | 0.000	–	–	0.036	0.001
Zhoukoudian 11	-0.018	0.000	0.012	0.000	-0.045	0.002	-0.007	0.000	0.055	0.003
Ngawi	–	–	–	–	–	–	–	–	-0.020	0.000
Sangiran IX	–	–	-0.021	0.000	–	–	-0.029	0.001	–	–
Australopiths										
MRD-VP-1/1	**0.274**	**0.075**	0.113	0.013	0.143	0.020	–	–	-0.004	0.000
A.L. 444-2	**0.196**	**0.038**	**0.104 | 0.168**	**0.011 | 0.028**	**0.152**	**0.023**	**0.185**	**0.034**	–	–
A.L. 888-1	–	–	**0.270**	**0.073**	**0.261**	**0.068**	–	–	–	–
STW 573	**0.249**	**0.062**	**0.139**	**0.019**	–	–	–	–	–	–

STS 5	**0.243**	**0.059**	**0.149 | 0.148**	**0.022 | 0.022**	**0.232 | 0.222**	**0.054 | 0.49**	**0.197 | 0.206**	**0.039 | 0.042**	0.012	0.000
STS 71	**0.335**	**0.112**	**0.252 | 0.218**	**0.063 | 0.048**	**0.290 | 0.309**	**0.084 | 0.096**	**0.380 | 0.375**	**0.145 | 0.140**	0.074	0.005
OH 5	**0.198 | 0.211**	**0.039 | 0.045**	**0.169 | 0.196**	**0.029 | 0.038**	**0.155**	**0.024**	**0.154 | 0.148**	**0.024 | 0.022**	0.012 | 0.049	0.000 | 0.002
KNM-ER 406	–	–	**0.254 | 0.262**	**0.065 | 0.069**	**0.253 | 0.258**	**0.064 | 0.067**	**0.188 | 0.193**	**0.035 | 0.037**	0.082	0.007
KNM-WT 17000	**0.305**	**0.093**	**0.276**	**0.076**	–	–	–	–	–	–
SK 48	**0.292**	**0.085**	**0.260**	**0.068**	**0.275**	**0.076**	**0.185**	**0.034**	–	–
DNH 7	**0.268**	**0.072**	**0.141**	**0.020**	0.116	0.014	**0.165**	**0.027**	–	–
Other *Homo*										
LES 1	**0.224**	**0.050**	0.103	0.011	–	–	**0.216**	**0.046**	–	–
Sima de los Huesos 5	0.048	0.002	0.027	0.001	0.082	0.007	0.059	0.003	0.093	0.009
Sima de los Huesos 6	–	–	–	–	-0.043	0.002	–	–	-0.004	0.000
Kabwe	-0.037	0.001	-0.066	0.004	-0.065	0.004	-0.040	0.002	0.056 | 0.049	0.003 | 0.002
Steinheim	0.007	0.000	-0.021	0.000	-0.007	0.000	0.005	0.000	0.044	0.002
Petralona	-0.045	0.002	-0.021	0.000	-0.043	0.002	0.016	0.000	–	–
Dali	-0.121	0.015	-0.087	0.008	-0.068	0.005	-0.075	0.006	0.029	0.001
Harbin	**-0.155**	**0.024**	-0.054	0.003	-0.094	0.009	-0.078	0.006	0.088	0.008
Neandertals										
La Chapelle aux Saints	-0.059 | -0.064	0.004 | 0.004	-0.036 | -0.040	0.001 | 0.002	-0.057 | -0.061	0.003 | 0.004	-0.077 | -0.081	0.006 | 0.007	0.010 | 0.007	0.000 | 0.000
Gibraltar 1	-0.017 | 0.001	0.000 | 0.000	-0.048 | -0.035	0.002 | 0.001	-0.024 | -0.011	0.001 | 0.000	-0.018 | -0.004	0.000 | 0.000	-0.013 | -0.003	0.000 | 0.000
Tabun 1	0.036 | 0.073	0.001 | 0.005	-0.021	0.000	–	–	0.024	0.001	–	–
La Ferrassie	-0.050	0.003	-0.050	0.003	–	–	-0.048	0.002	–	–
Shanidar 1	-0.055	0.003	-0.081	0.007	-0.080	0.006	-0.069	0.005	–	–
Saccopostre 1	0.070 | 0.071	0.005 | 0.005	–	–	–	–	0.036 | 0.38	0.001 | 0.001	0.035	0.001
Guattari 1	-0.037	0.001	–	–	-0.018	0.000	-0.110	0.012	–	–
Amud 1	-0.091	0.008	-0.078	0.006	-0.068	0.005	-0.066	0.004	–	–
Spy 1	-0.053	0.003	–	–	–	–	–	–	–	–
Monte Circe	-0.032	0.001	-0.042	0.002	-0.026	0.001	-0.088	0.008	–	–
La Quina 5	–	–	-0.124	0.015	–	–	-0.016	0.000	–	–

Homo sapiens										
Skhul V	-0.034	0.001	0.001	0.000	0.013	0.000	-0.017	0.000	–	–
Jebel Irhoud 1	-0.026	0.001	–	–	-0.026	0.001	-0.021	0.000	0.054	0.003
Recent[1]	0.000 (-0.132–0.140)	0.002 (0.000–0.019)	0.000 (-0.106–0.120)	0.001 (0.000–0.014)	0.000 (-0.145–0.148)	0.002 (0.000–0.022)	0.000 (-0.125–0.141)	0.002 (0.000–0.020)	0.000 (-0.101–0.100)	0.001 (0.000–0.010)
Extant great apes										
Pan[2]	**0.357 (0.264–0.441)**	**0.129 (0.070–0.195)**	–	–	0.213 (0.134–0.300)	0.047 (0.018–0.090)	0.233 (0.132–0.316)	0.056 (0.018–0.100)	–	–
Pan, *Gorilla*, & *Pongo*[3]	0.340 (0.007–0.543)	0.127 (0.000–0.295)	0.221 (0.009–0.458)	0.055 (0.000–0.210)	–	–	–	–	–	–
Pan, Gorilla, & *Pongo*[4]	0.351 (0.007–0.543)	0.128 (0.00–0.295)	–	–	–	–	–	–	–	–
Pan & *Pongo*[3]	**0.387 (0.273–0.543)**	**0.153 0.075–0.295)**	**0.230 (0.172–0.302)**	**0.054 (0.030–0.091)**	–	–	–	–	–	–
Pan & *Pongo*[4]	**0.365 (0.264–0.543)**	**0.135 (0.070–0.295)**	–	–	–	–	–	–	–	–

Values in **bold** are outside the entire range for recent modern humans

[1] Howells (1996), N = 2,524

[2] Weaver and Stringer (2015), N = 237

[3] Perez-Claros and Palmqvist (2022), N = 117 total, 88 without *Gorilla*

[4] Weaver and Stringer (2015) and Perez-Claros and Palmqvist (2022), N = 354 total, 325 without *Gorilla*

(back to text)

Table 16. Sum of squared residuals from fitted scaling lines between craniofacial variables and GOL for recent modern humans[1] and for extant great apes[2, 3, 4]

	Face								Neurocranium				
	recent modern humans[1]				*Pan, Gorilla* & *Pongo*[4]		*Pan* & *Pongo*[4]		recent modern humans[1]	*Pan, Gorilla* & *Pongo*[4]		*Pan* & *Pongo*[4]	
Taxon / Specimen	NPH, ZYB, ZMB, BOB, & MAB	NPH, ZYB, ZMB, & BOB	NPH, ZMB, & MAB	NPH & ZYB	NPH, ZYB, ZMB, & MAB	NPH, ZYB, & ZMB	NPH, ZYB, ZMB, & MAB	NPH, ZYB, & ZMB	XCB, ASB, BBH, BNL, & BPL	XCB, BBH, BNL, & BPL	XCB, BBH, & BPL	XCB, BBH, BNL, & BPL	XCB, BBH, & BPL
Homo floresiensis													
LB 1	**0.080**	**0.064**	**0.061**	**0.050**	0.117	0.106	**0.047**	**0.036**	0.048 | 0.046	**0.117** | **0.117**	**0.108** | **0.111**	**0.075** | **0.078**	**0.041** | **0.044**
Early *Homo*													
KNM-ER 1813	**0.087**	**0.057**	**0.078**	**0.039**	**0.088**	0.083	**0.064**	**0.059**	0.051 | 0.040	**0.098** | **0.072**	**0.093** | **0.067**	**0.076** | **0.075**	**0.038** | **0.040**
OH 24	–	–	–	–	–	–	–	–	0.042	**0.116**	**0.116**	**0.129**	**0.052**
KNM-ER 1470	–	–	**0.084**	–	–	–	–	–	–	–	–	–	–
STW 53	–	–	–	0.010	–	0.131	–	0.151	–	–	**0.149**	–	**0.104**
Homo erectus s.l.													
Africa													
KNM-ER 3733	0.007	0.007	0.005	0.003	0.194	0.136	0.291	0.232	0.032 | 0.025	0.194 | 0.182	0.189 | 0.180	0.174 | 0.166	0.124 | 0.126
KNM-ER 3883	–	–	–	–	–	–	–	–	–	–	–	–	–
KNM-WT 15000	–	–	–	–	–	–	–	–	–	–	–	–	–
KNM-ER 42700	–	–	–	–	–	–	–	–	–	–	–	–	–
OH 9	–	–	–	–	–	–	–	–	–	–	–	–	–
Dmanisi													
D2700	–	–	**0.059**	0.026	0.110	0.098	0.097	**0.085**	0.041	**0.138**	**0.131** | **0.106**	**0.094**	**0.066**
D2282	–	–	–	**0.029**	–	–	–	–	–	–	**0.092**	–	**0.092**
D3444	–	–	–	0.009	–	0.157	–	0.157	–	–	**0.152**	–	**0.152**
D4500	–	–	–	**0.032**	–	–	–	–	–	–	**0.045**	–	**0.045**
D2280	–	–	–	–	–	–	–	–	–	–	–	–	–
Asia													
Sangiran 17	–	0.007	–	0.006	–	0.232	–	0.415	**0.053** | 0.043	0.321 | 0.281	0.318 | 0.280	0.309 | 0.277	0.236 | 0.211
Zhoukoudian 11	0.006	0.005	0.002	0.000	0.291	0.224	0.407	0.340	0.020	0.242	0.240	0.231	0.168
Ngawi	–	–	–	–	–	–	–	–	–	–	–	–	–
Sangiran IX	–	–	–	–	–	–	–	–	–	–	–	–	–

Australopiths													
MRD-VP-1/1	–	**0.108**	–	**0.088**	–	0.022	–	**0.038**	–	–	**0.050**	–	**0.058**
A.L. 444-2	–	–	–	**0.049**	–	–	–	–	–	–	–	–	–
A.L. 888-1	–	–	–	–	–	–	–	–	–	–	–	–	–
STW 573	–	–	–	**0.081**	–	–	–	–	–	–	**0.056**	–	**0.056**
STS 5	**0.174**	**0.135**	**0.152**	**0.081**	**0.025**	0.023	**0.029**	**0.027**	**0.135 | 0.128**	**0.038**	**0.026**	**0.020**	**0.015**
STS 71	**0.41**	**0.235**	**0.341**	**0.176**	**0.029**	0.011	**0.024**	**0.005**	–	–	–	–	–
OH 5	**0.116**	**0.092**	**0.087**	**0.068**	**0.022**	0.011	**0.105**	0.094	**0.085 | 0.077**	**0.134 | 0.126**	**0.124 | 0.116**	**0.099 | 0.095**	**0.083 | 0.0757**
KNM-ER 406	–	–	–	–	–	–	–	–	**0.087 | 0.095**	**0.090 | 0.141**	**0.079 | 0.130**	**0.090** | 0.141	**0.079** | 0.130
KNM-WT 17000	–	–	–	**0.169**	–	–	–	–	–	–	**0.000**	–	**0.009**
SK 48	–	–	**0.195**	**0.153**	**0.014**	0.011	0.014	**0.011**	–	–	**0.054**	–	**0.054**
DNH 7	–	–	**0.113**	**0.092**	**0.026**	0.020	0.026	**0.020**	–	–	–	–	–
Other *Homo*													
LES 1	–	–	–	**0.061**	–	–	–	–	–	–	**0.084**	–	**0.035**
Sima de los Huesos 5	0.022	0.018	0.012	0.003	0.156	0.118	0.269	0.231	0.012	0.228	0.226	0.178	0.137
Sima de los Huesos 6	–	–	–	–	–	–	–	–	–	–	–	–	–
Kabwe	0.015	0.013	0.007	0.006	0.324	0.234	0.552	0.463	0.035	0.298	0.296	0.314	0.234
Steinheim	0.003	0.003	0.000	0.001	0.276	0.218	0.353	0.294	0.026	0.179	0.176	0.216	0.144
Petralona	–	–	0.004	0.003	0.279	0.218	0.493	0.431	–	–	0.299	–	0.220
Dali	0.033	0.028	0.025	0.022	0.467	0.357	0.642	0.532	**0.066**	0.369	0.367	0.374	0.276
Harbin	0.05	0.044	**0.039**	0.027	0.489	0.373	0.713	0.597	0.040	0.361	0.361	0.355	0.268
Neandertals													
La Chapelle aux Saints	0.014 | 0.016	0.008 | 0.009	0.013 | 0.014	0.005 | 0.006	0.358 | 0.368	0.249 | 0.255	0.561 | 0.574	0.451 | 0.462	0.029 | 0.018	0.306 | 0.284	0.301 | 0.285	0.255 | 0.267	0.212 | 0.212
Gibraltar 1	0.004 | 0.001	0.003 | 0.001	0.001 | 0.000	0.003 | 0.001	0.311 | 0.280	0.238 | 0.214	0.426 | 0.388	0.353 | 0.322	0.011	0.304	0.300	0.237	0.189
Tabun 1	–	–	–	0.002 | 0.006	–	–	–	–	0.014	0.297	0.257	0.198	0.159
La Ferrassie	–	–	–	0.005	–	–	–	–	0.012 | 0.011	0.366 | 0.409	0.322 | 0.364	0.260 | 0.280	0.216 | 0.234
Shanidar 1	–	–	0.014	0.010	0.388	0.284	0.579	0.474	0.017 | 0.017	0.389 | 0.395	0.328 | 0.333	0.287 | 0.288	0.224 | 0.226
Saccopostre 1	–	–	–	–	–	–	–	–	0.02246152	0.253	0.200 | 0.185	0.185	0.132 | 0.123
Guattari 1	–	–	0.014	–	–	–	–	–	–	0.388	0.314	0.294	0.219
Amud 1	–	–	0.017	0.014	0.400	0.294	0.629	0.522	–	–	–	–	–
Spy 1	–	–	–	–	–	–	–	–	–	–	–	–	–
Monte Circe	–	–	0.009	0.003	0.330	0.216	0.521	0.406	–				
La Quina 5	–	–	–	–	–	–	–	–	–	–	–	–	–

Homo sapiens													
Skhul V	–	–	0.002	0.001	0.298	0.226	0.399	0.327	0.011	0.344	0.256	0.255	0.167
Jebel Irhoud 1	–	–	0.002	–	–	–	–	–	–	–	–	–	–
Recent[1]	0.006 (0.00–0.068)	0.005 (0.00–0.056)	0.005 (0.000–0.050)	0.003 (0.000–0.0273)	0.304 (0.101–0.620)	0.336 (0.005–0.530)	0.331 (0.100–0.622)	0.270 (0.080–0.501)	0.006 (0.000–0.052)	0.303 (0.162–0.496)	0.301 (0.161–0.496)	0.226 (0.129–0.367)	0.170 (0.095–0.268)
Extant great apes													
Pan[2]	–	–	0.231 (0.111–0.366)	–	–	–	–	–	–	0.028 (0.016–0.045)	–	0.002 (0.000–0.008)	–
Pan, *Gorilla*, & *Pongo*[3]	–	–	–	0.182 (0.000–0.505)	–	–	–	–	–	–	–	–	–
Pan, Gorilla, & Pongo[4]	–	–	–		–	–	–	–	–	–	0.005 (0.000–0.108)	–	0.004 (0.000–0.066)
Pan & *Pongo*[3]	–	–	–	0.220 (0.104–0.505)	–	–	–	–	–	–	–	–	–
Pan & *Pongo*[4]	–	–	–	–	–	–	–	–	–	–	0.005 (0.000–0.108)	–	0.002 (0.000–0.019)

Values in **bold** are outside the entire range for recent modern humans

[1] Howells (1996), N = 2,524

[2] Weaver and Stringer (2015), N = 237

[3] Perez-Claros and Palmqvist (2022), N = 117 total, 88 without *Gorilla*

[4] Weaver and Stringer (2015) and Perez-Claros and Palmqvist (2022), N = 354 total, 325 without *Gorilla*

(back to text)

Table 17. Sum of standardized squared residuals from fitted scaling lines between craniofacial variables and GOL for recent modern humans[1] and for extant great apes[2, 3, 4]

	Face				Neurocranium				
	recent modern humans[1]				recent modern humans[1]	*Pan, Gorilla* & *Pongo*[4]		*Pan* & *Pongo*[4]	
Taxon / Specimen	NPH, ZYB, ZMB, BOB, & MAB	NPH, ZYB, ZMB, & BOB	NPH, ZMB, & MAB	NPH & ZYB	XCB, ASB, BBH, BNL, & BPL	XCB, BBH, BNL, & BPL	XCB, BBH, & BPL	XCB, BBH, BNL, & BPL	XCB, BBH, & BPL
Homo floresiensis									
	–	–	–	–					
LB 1	**52.83**	**42.56**	**37.50**	**33.66**	38.01 | 37.16	**211.55 | 207.46**	**51.90 | 49.33**	**128.05 | 128.39**	**31.51 | 30.28**
Early *Homo*									
KNM-ER 1813	56.14	36.58	**48.62**	**24.95**	**42.68** | 33.07	**195.98 | 149.62**	**58.36 | 38.11**	**127.20 | 125.04**	24.35 | 26.48
OH 24	–	–	77.41	–	32.38	310.04	**59.55**	235.66	**41.05**
KNM-ER 1470	–	–	52.10	–	–	–	**–**	–	**–**
STW 53	–	–	–	6.79	–	–	**61.60**	–	**64.93**
Homo erectus s.l.									
Africa									
KNM-ER 3733	5.05	5.03	2.92	2.13	26.29 | 20.38	330.51 | 318.79	111.97 | 107.65	259.51 | 240.08	82.90 | 84.04
KNM-ER 3883	**–**	**–**	–	–	–	–	–	–	–
KNM-WT 15000	**–**	**–**	–	–	–	–	–	–	–
KNM-ER 42700	**–**	**–**	–	–	–	–	–	–	–
OH 9	**–**	**–**	–	–	–	–	–	–	–
Dmanisi									
D2700	–	–	**36.13**	**15.92** | 11.33	34.68	**222.48**	**71.50 | 50.28**	**145.79**	**48.94 | 35.54**
D2282	**–**	**–**	–	**18.60**	–	–	**42.54**	**–**	**44.20**
D3444	**–**	**–**	–	6.42	–	–	**73.29**	**–**	**52.60**
D4500	**–**	**–**	–	**23.55**	–	–	**19.73**	**–**	**39.86**
D2280	**–**	**–**	–	–	–	–	–	**–**	–
Asia									
Sangiran 17	–	5.35	–	3.74	**43.17** | 34.42	550.82 | 488.11	189.34 | 174.05	440.50 | 397.55	155.28 | 139.73
Zhoukoudian 11	5.08	5.05	1.43	0.30	16.30	430.51	134.20	336.99	106.50
Ngawi	–	–	–	–	–	–	–	–	–
Sangiran IX	–	–	–	–	–	–	–	–	–
Australopiths									
MRD-VP-1/1	–	67.49	–	**54.94**	–	–	35.89	–	72.98
A.L. 444-2	–	–	–	**31.69**	–	–	–	–	–
A.L. 888-1	–	–	–	**–**	–	–	–	–	–
STW 573	–	–	–	**52.29**	–	–	26.94	–	19.64
STS 5	**111.89**	**82.2**	**93.50**	**53.04**	**124.23 | 118.76**	42.03	15.84	30.22	10.09
STS 71	**217.76**	**176.37**	**213.43**	**118.40**	–	–	–	–	–
OH 5	**77.15**	**61.47**	**53.43**	**46.65**	**74.64 | 66.96**	**196.59 | 178.83**	90.21 | 81.88	**139.89 | 146.11**	62.88 | 65.37
KNM-ER 406	–	–	–	–	**84.73 | 80.07**	**183.28 | 120.12**	99.28 | **56.13**	**86.70 | 127.23**	**38.80** | 71.44
KNM-WT 17000	–	–	**–**	**117.20**	–	–	**0.18**	**–**	**8.25**
SK 48	–	–	**119.40**	**105.83**	–	–	**21.32**	**–**	**13.86**
DNH 7	–	–	**68.73**	**58.86**	–	–	–	–	–

Other *Homo*									
LES 1	–	–	–	**38.40**	–	–	**33.89**	**–**	**20.66**
Sima de los Huesos 5	18.39	16.12	7.73	2.00	10.29	354.66	137.76	255.69	93.34
Sima de los Huesos 6	–	–	–	–	–	–	–	–	–
Kabwe	11.69	10.66	4.43	4.40	26.83	532.17	153.33	446.52	139.04
Steinheim	2.71	2.7	0.08	0.40	19.85	372.50	82.31	322.43	85.12
Petralona	–	–	2.54	1.59	**–**	–	167.53	–	135.86
Dali	22.39	18.7	15.15	14.87	**55.64**	666.73	197.76	537.78	170.51
Harbin	35.08	31.07	23.60	16.61	32.62	626.30	211.43	506.72	167.73
Neandertals									
La Chapelle aux Saints	9.10 | 10.36	5.22 | 6.04	7.94 | 9.01	3.14 | 3.72	13.73 | 21.68	456.61 | 454.21	162.10 | 177.55	345.82 | 368.43	134.08 | 130.84
Gibraltar 1	2.19 | 1.09	2.62 | 1.08	0.74 | 0.08	2.05 | 1.00	9.00	464.11	167.98	329.82	122.23
Tabun 1	–	–	–	1.12 | 3.50	11.82	399.23	137.94	275.70	101.96
La Ferrassie	–	–	–	3.57	9.72 | 8.35	525.15 | 478.36	213.88 | 191.97	354.60 | 377.28	138.67 | 150.35
Shanidar 1	–	–	8.88	7.23	13.42 | 12.85	530.00 | 525.11	188.70 | 185.75	400.04 | 402.34	140.45 | 141.26
Saccopostre 1	–	–	–	–	18.043	361.67	115.94 | 110.38	276.34	88.08 | 83.34
Guattari 1	–	–	9.01	–	–	543.67	177.38	422.32	138.75
Amud 1	–	–	10.60	9.89	–	–	–	–	–
Spy 1	–	–	–	–	–	–	–	–	–
Monte Circe	–	–	6.13	2.06	–	–	–	–	–
La Quina 5	–	–	–	–	–	–	–	–	–
Homo sapiens									
Skhul V	–	–	0.99	0.70	10.28	493.45	142.96	389.17	104.46
Jebel Irhoud 1	–	–	1.12	–	–	–	–	–	–
Recent[1]	5.00 (0.06–49.79)	4.00 (0.00–41.82)	3.00 (0.003–33.45)	2.00 (0.00–18.08)	5.00 (0.09–42.60)	470.07 (272.41–788.10)	159.79 (76.00–287.46)	322.46 (180.57–540.37)	108.92 (59.85–188.05)
Extant great apes									
Pan[2]	–	–	**141.50 (67.69–224.26)**	–	–	**4.03 (0.11–16.15)**	–	**4.10 (0.05–21.91)**	–
Pan, *Gorilla*, & *Pongo*[3]	–	–	–	120.53 (0.22–346.97)	–	–	–	–	–
Pan, Gorilla, & *Pongo*[4]	–	–	–	–	–	–	**2.99 (0.02–49.69)**	–	**7.98 (0.02–205.03)**

Pan & *Pongo*[3]	–	–	–	145.36 (68.46–346.97)	–	–	–	–	–
Pan & *Pongo*[4]	–	–	–	–	–	–	**2.82 (0.02–49.69)**	–	**2.99 (0.02–51.52)**

Values in **bold** are outside the entire range for recent modern humans

[1] Howells (1996), N = 2,524

[2] Weaver and Stringer (2015), N = 237

[3] Perez-Claros and Palmqvist (2022), N = 117 total, 88 without *Gorilla*

[4] Weaver and Stringer (2015) and Perez-Claros and Palmqvist (2022), N = 354 total, 325 without *Gorilla*

(back to text)

Table 18. Mean of the absolute value of the standardized residuals from fitted scaling lines between craniofacial variables and GOL for recent modern humans[1] and for extant great apes[2,3,4]

	Face				Neurocranium				
	recent modern humans[1]				recent modern humans[1]	*Pan, Gorilla* & *Pongo*[4]		*Pan* & *Pongo*[4]	
Taxon / Specimen	NPH, ZYB, ZMB, BOB, & MAB	NPH, ZYB, ZMB, & BOB	NPH, ZMB, & MAB	NPH & ZYB	XCB, ASB, BBH, BNL, & BPL	XCB, BBH, BNL, & BPL	XCB, BBH, & BPL	XCB, BBH, BNL, & BPL	XCB, BBH, & BPL
Homo floresiensis									
LB 1	3.01	2.97	**3.48**	**4.09**	2.55 | 2.57	**6.12 | 6.07**	2.58 | 2.55	**4.86 | 4.86**	2.12 | 2.09
Early *Homo*									
KNM-ER 1813	3.09	2.76	**4.00**	**3.43**	2.36 | 2.14	**6.03 | 5.51**	2.56 | 2.16	**4.73 | 4.61**	1.88 | 1.86
OH 24	–	–	**5.07**	–	2.29	**7.55**	**2.91**	**6.44**	**2.53**
KNM-ER 1470	–	–	**4.15**	–	–	**–**	**–**	**–**	**–**
STW 53	–	–	**–**	1.826	–	**–**	**2.74**	**–**	**2.68**
Homo erectus s.l.									
Africa									
KNM-ER 3733	0.87	1.06	0.83	0.93	1.84 | 1.72	8.18 | 8.17	3.90 | 4.10	6.90 | 6.50	3.29 | 3.19
KNM-ER 3883	–	–	–	–	–	–	–	–	–
KNM-WT 15000	–	–	–	–	–	–	–	–	–
KNM-ER 42700	–	–	–	–	–	–	–	–	–
OH 9	–	–	–	–	–	–	–	–	–
Dmanisi									
D2700	–	–	**3.47**	**2.61 | 2.26**	2.47	**6.73**	**3.28** | 2.71	**5.13**	**2.47 | 1.88**
D2282	–	–	–	**2.95**	–	**–**	**2.51**	**–**	**2.24**
D3444	–	–	–	**1.79**	–	**–**	**3.41**	**–**	**2.34**
D4500	–	–	–	**3.36**	–	**–**	**1.70**	**–**	**2.49**
D2280	–	–	–	–	–	–	–	–	–
Asia									
Sangiran 17	–	1.05	–	1.35	2.04 | 1.68	10.22 | 9.84	4.89 | 4.83	9.24 | 8.68	4.69 | 4.37
Zhoukoudian 11	0.78	0.94	0.57	0.39	1.23	9.45	4.53	7.49	3.45
Ngawi	–	–	–	–	–	–	–	–	–
Sangiran IX	–	–	–	–	–	–	–	–	–

Australopiths									
MRD-VP-1/1	–	3.4	–	**4.95**	–	–	2.04	–	2.87
A.L. 444-2	–	–	–	**3.88**	–	–	–	–	–
A.L. 888-1	–	–	–	–	–	–	–	–	–
STW 573	–	–	–	**5.01**	–	–	2.16	–	1.46
STS 5	**4.28**	**4.08**	**5.57**	**5.08**	**3.77 | 5.51**	**3.19**	1.70	**2.55**	1.29
STS 71	**6.97**	**6.27**	**8.37**	**7.68**	–	–	–	–	–
OH 5	**3.57**	**3.48**	**4.20**	**4.83 | 5.38**	**3.48 | 3.25**	**6.00 | 5.78**	**3.20 | 3.12**	**5.56 | 5.56**	**3.22 | 3.13**
KNM-ER 406	–	–	–	–	**3.34 | 3.09**	**5.74 | 4.93**	**3.43 | 2.75**	**4.06 | 4.87**	**2.26 | 3.00**
KNM-WT 17000	–	–	–	**7.65**	–	–	0.16	–	1.17
SK 48	–	–	**6.22**	**7.27**	–	–	1.20	–	1.19
DNH 7	–	–	**4.54**	**5.28**	–	–	–	–	–
Other *Homo*									
LES 1	–	–	–	4.20	–	–	1.75	–	1.22
Sima de los Huesos 5	1.73	1.79	1.57	0.98	1.24	9.08	4.88	7.02	3.61
Sima de los Huesos 6	–	–	–	–	–	–	–	–	–
Kabwe	1.47	1.58	1.17	1.40	1.96	10.67	5.08	7.80	3.27
Steinheim	0.52	0.62	0.16	0.39	1.63	8.33	**3.44**	6.65	**2.55**
Petralona	–	–	0.86	0.86	–	–	5.26	–	3.57
Dali	2.01	2.03	2.18	2.72	**2.92**	11.39	5.26	9.59	4.47
Harbin	2.53	2.66	2.70	2.66	2.17	11.72	5.87	8.90	4.10
Neandertals									
La Chapelle aux Saints	1.24 | 1.30	1.05 | 1.11	1.61 | 1.71	1.24 | 1.35	1.13 | 1.55	10.09 | 10.07	5.47 | 5.29	7.50 | 7.47	3.84 | 3.55
Gibraltar 1	0.66 | 0.30	0.70 | 0.35	0.49 | 0.14	0.89 | 0.51	1.00	10.08	5.30	7.49	3.77
Tabun 1	–	–	–	0.73 | 1.18	1.46	9.10	4.68	6.65	3.29
La Ferrassie	–	–	–	1.33	1.16 | 1.01	11.03 | 10.46	5.75 | 5.05	8.16 | 7.85	3.55 | 4.10
Shanidar 1	–	–	1.70	1.83	1.42 | 1.40	10.98 | 10.88	5.74 | 5.66	8.13 | 8.23	3.94 | 4.01
Saccopostre 1	–	–	–	–	1.43	8.59	4.11 | 4.00	7.04	3.33 | 3.26
Guattari 1	–	–	1.39	–	–	10.77	5.31	8.25	3.83
Amud 1	–	–	1.86	2.22	–	–	–	–	–
Spy 1	–	–	–	–	–	–	–	–	–
Monte Circe	–	–	1.23	0.99	–	–	–	–	–
La Quina 5	–	–	–	–	–	–	–	–	–

Homo sapiens									
Skhul V	–	–	–	–	1.27	10.56	5.05	8.16	3.55
Jebel Irhoud 1	–	–	0.61	–	–	–	–	–	–
Recent[1]	0.8 (0.09–3.13)	0.8 (0.05–3.20)	0.80 (0.03–3.33)	0.81 (0.02–3.00)	0.78 (0.13–2.90)	10.31 (7.70–13.45)	5.35 (3.54–7.15)	7.82 (5.66–10.32)	3.87 (2.25–5.60)
Extant great apes									
Pan[2]	–	–	**6.66 (4.48–8.53)**	–	–	**0.79 (0.15–1.95)**	–	**0.80 (0.11–2.31)**	–
Pan, *Gorilla*, & *Pongo*[3]	–	–	–	7.30 (0.30–13.17)	–	–	–	–	–
Pan, Gorilla, & *Pongo*[4]	–	–	–	–	–	–	**0.55 (0.05–2.73)**	–	**0.74 (0.05–5.90)**
Pan & *Pongo*[3]	–	–	–	8.30 (5.79–13.17)	–	–	–	–	–
Pan & *Pongo*[4]	–	–	–	–	–	–	**0.53 (0.05–2.73)**	–	**0.56 (0.05–3.05)**

Values in **bold** are outside the entire range for recent modern humans

[1] Howells (1996), N = 2,524

[2] Weaver and Stringer (2015), N = 237

[3] Perez-Claros and Palmqvist (2022), N = 117 total, 88 without *Gorilla*

[4] Weaver and Stringer (2015) and Perez-Claros and Palmqvist (2022), N = 354 total, 325 without *Gorilla*

(back to text)

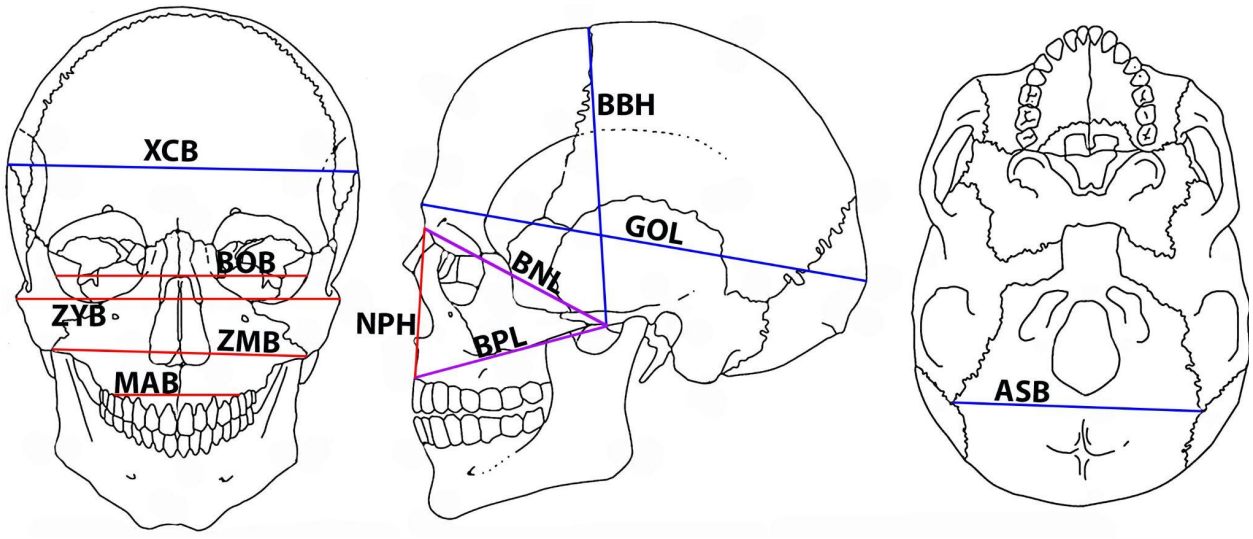

Figure 1. Illustration of a modern human cranium depicting the 11 cranial measurements used in this study. The five measures of the face are shown in red (NPH, nasion-prosthion height; BOB, bi-orbital breadth; ZYB, zygomatic breadth; ZMB, zygomaxillary breadth; MAB, maxillary breadth), the four measures of the neurocranium are shown in blue (GOL, glabella-opisthocranion length; BBH, basion-bregma height; XCB, supramastoid breadth; ASB, asterionic breadth), and the two measures of facial projection relative to the neurocranium are shown in purple (BNL, basion-nasion length ; BPL, basion-prosthion length). Geometric means were calculated using various combinations of the neurocranium and facial projection measurements (see text for details). Modified from Howells (1973). (back to text)

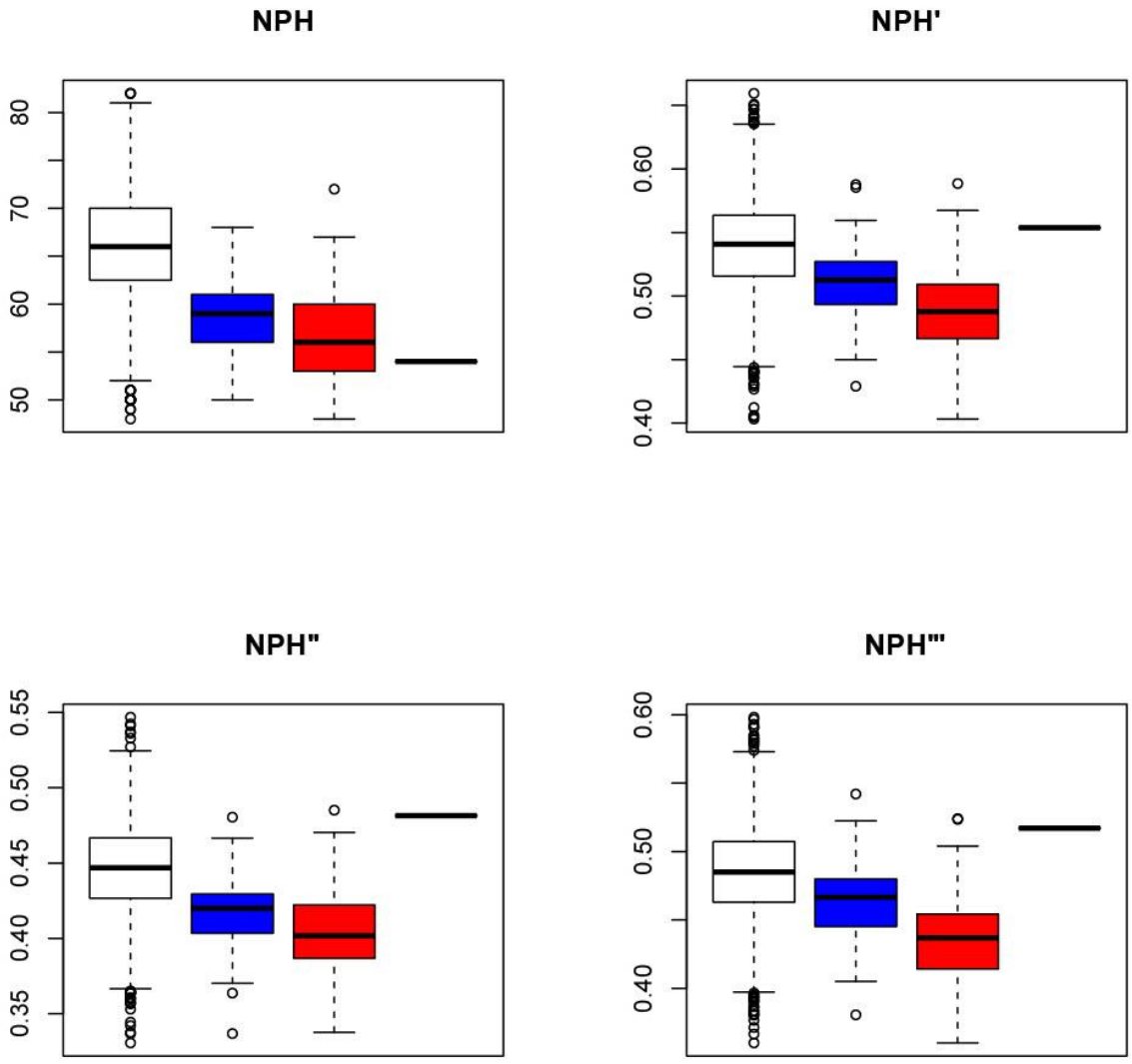

Figure 2. Box and whisker plots for absolute and size-adjusted facial heights (NPH) for the total recent modern human sample (white) with Andaman Islanders only shown in blue and San only shown in red. LB 1 is shown as the black bar on the right. NPH′, NPH″, and NPH‴ were calculated by dividing NPH by GM1, GM2, and GM3, respectively (see text for details). (back to text)

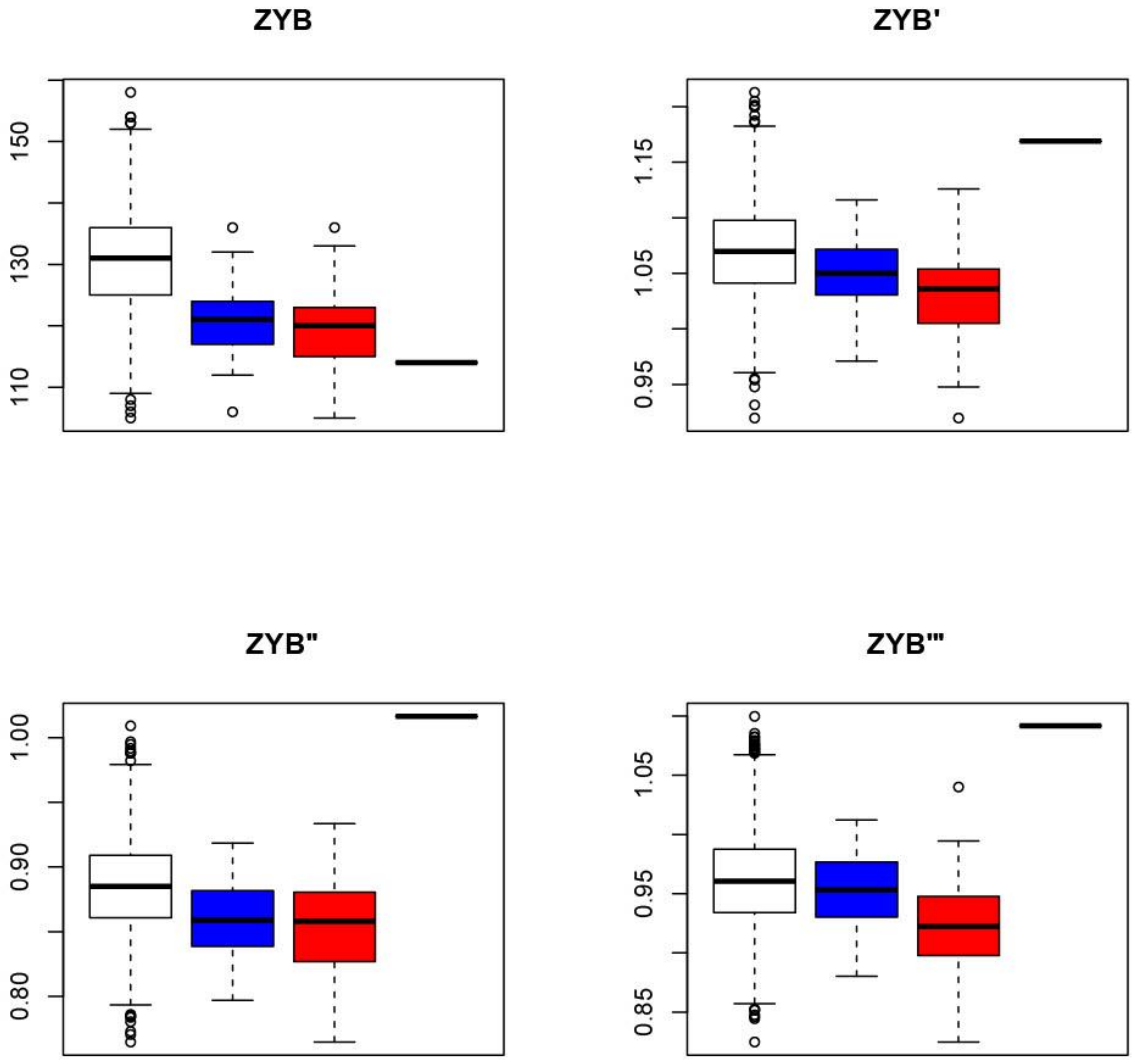

Figure 3. Box and whisker plots for absolute and size-adjusted zygomatic breadths (ZYB) for the total recent modern human sample (white) with Andaman Islanders only shown in blue and San only shown in red. LB 1 is shown as the black bar on the right. ZYB′, ZYB″, and ZYB‴ were calculated by dividing ZYB by GM1, GM2, and GM3, respectively (see text for details). (back to text)

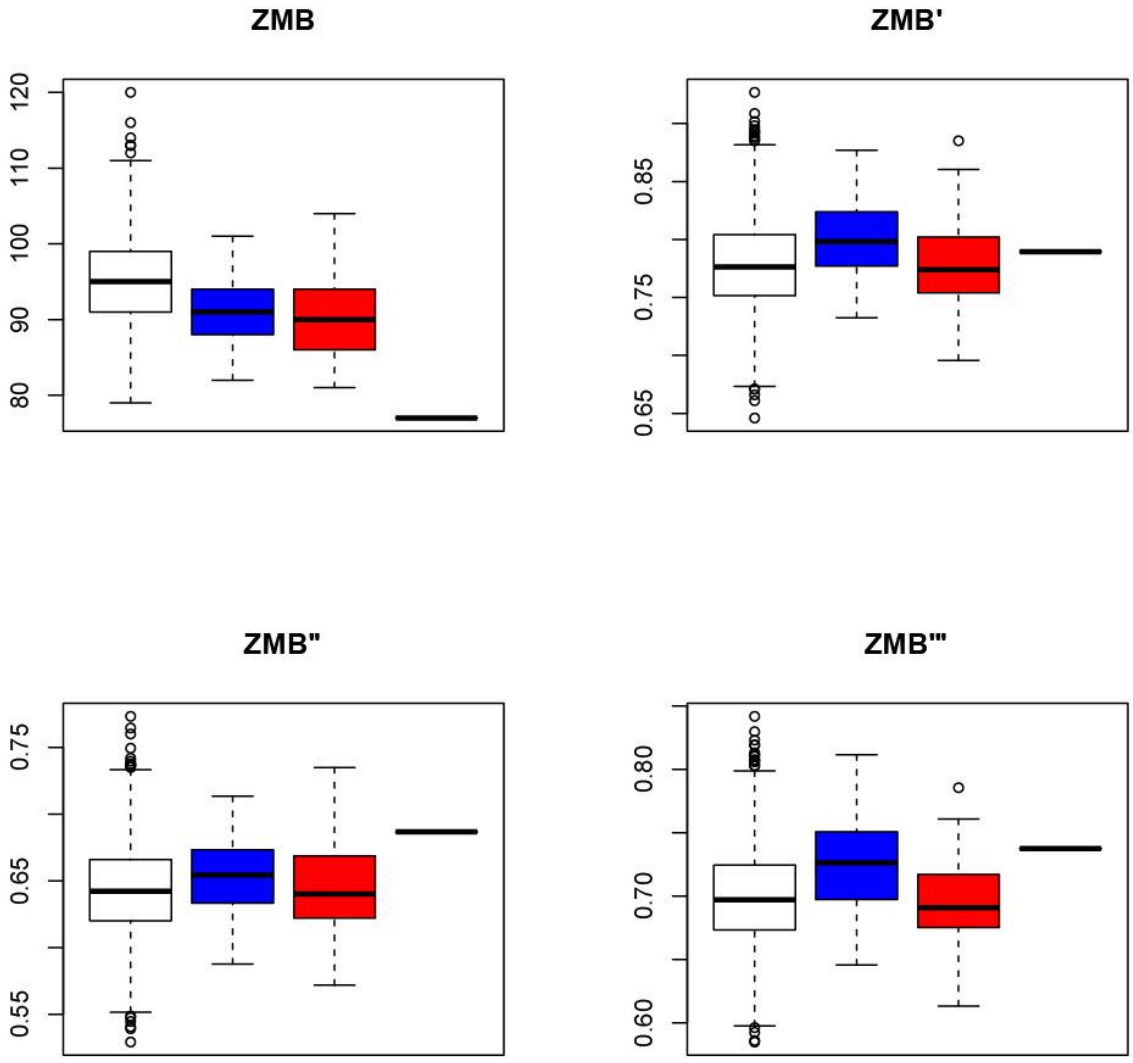

Figure 4. Box and whisker plots for absolute and size-adjusted zygomaxillary breadths (ZMB) for the total recent modern human sample (white) with Andaman Islanders only shown in blue and San only shown in red. LB 1 is shown as the black bar on the right. ZMB′, ZMB″, and ZMB‴ were calculated by dividing ZMB by GM1, GM2, and GM3, respectively (see text for details). (back to text)

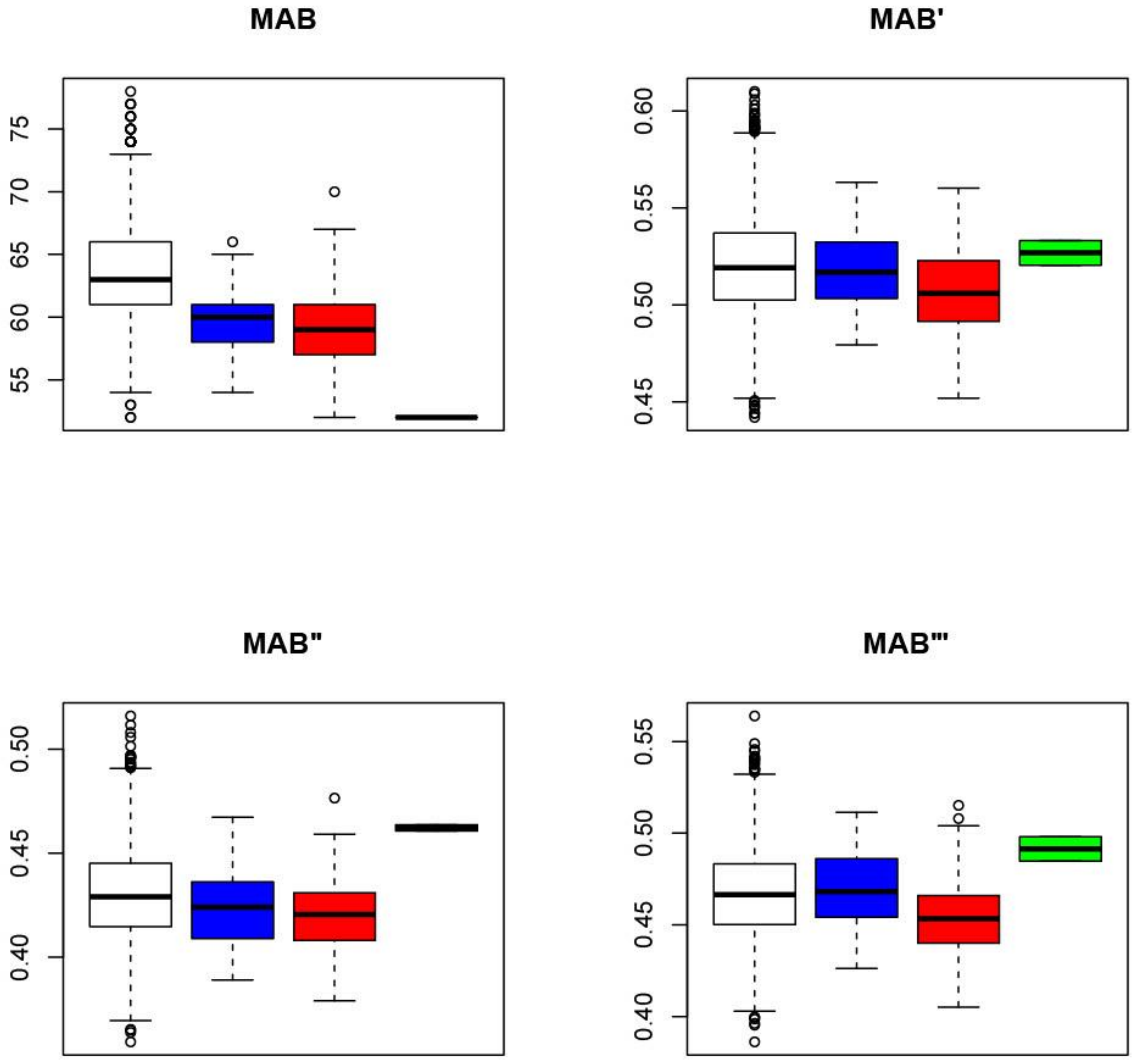

Figure 5. Box and whisker plots for absolute and size-adjusted maxillary breadths (MAB) for the total recent modern human sample (white) with Andaman Islanders only shown in blue and San only shown in red. LB 1 is shown as the black bar or green box on the right. MAB′, MAB″, and MAB‴ were calculated by dividing MAB by GM1, GM2, and GM3, respectively (see text for details). (back to text)

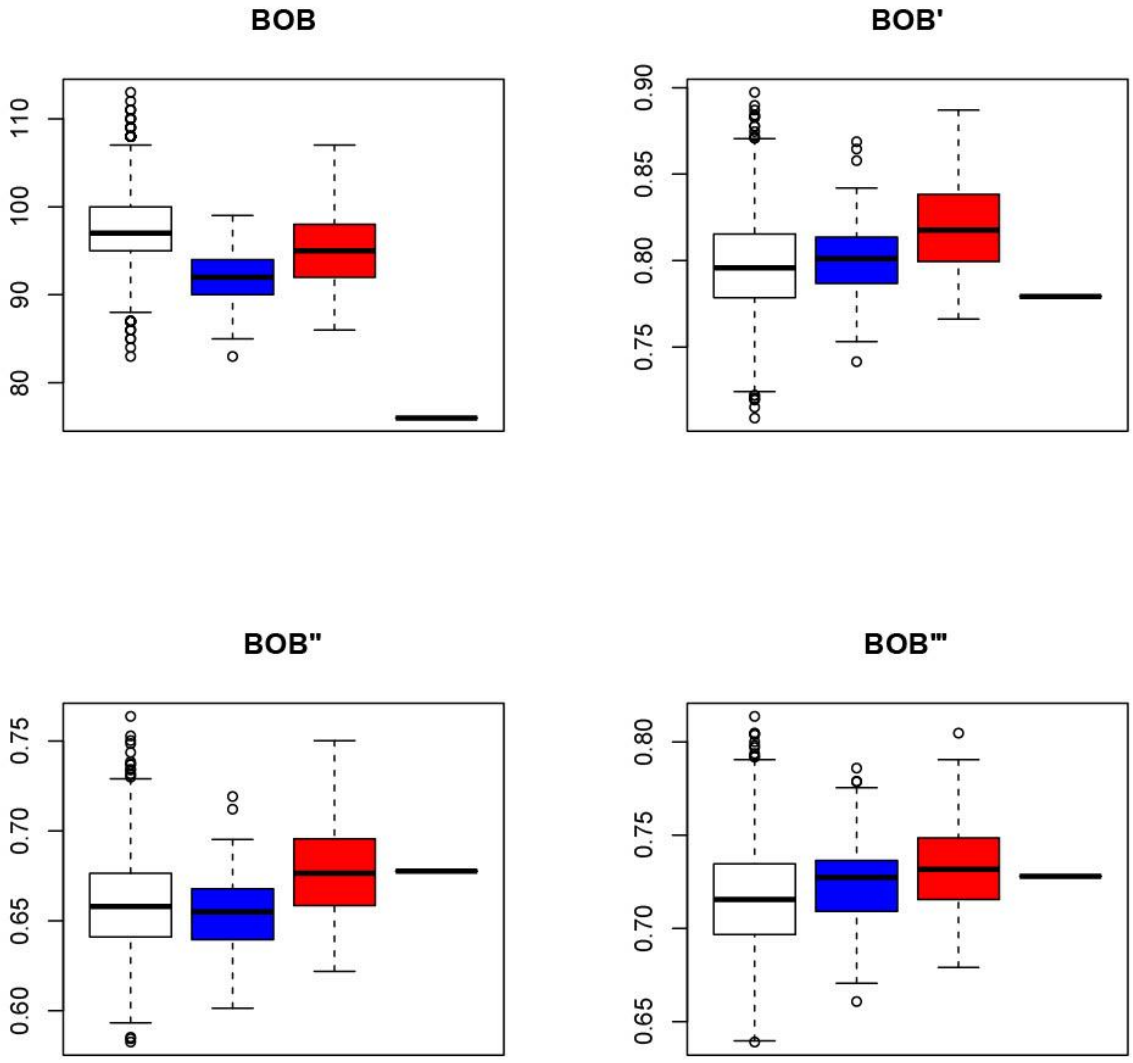

Figure 6. Box and whisker plots for absolute and size-adjusted bi-orbital outer breadths (BOB) for the total recent modern human sample (white) with Andaman Islanders only shown in blue and San only shown in red. LB 1 is shown as the black bar on the right. BOB′, BOB″, and BOB‴ were calculated by dividing BOB by GM1, GM2, and GM3, respectively (see text for details). (back to text)

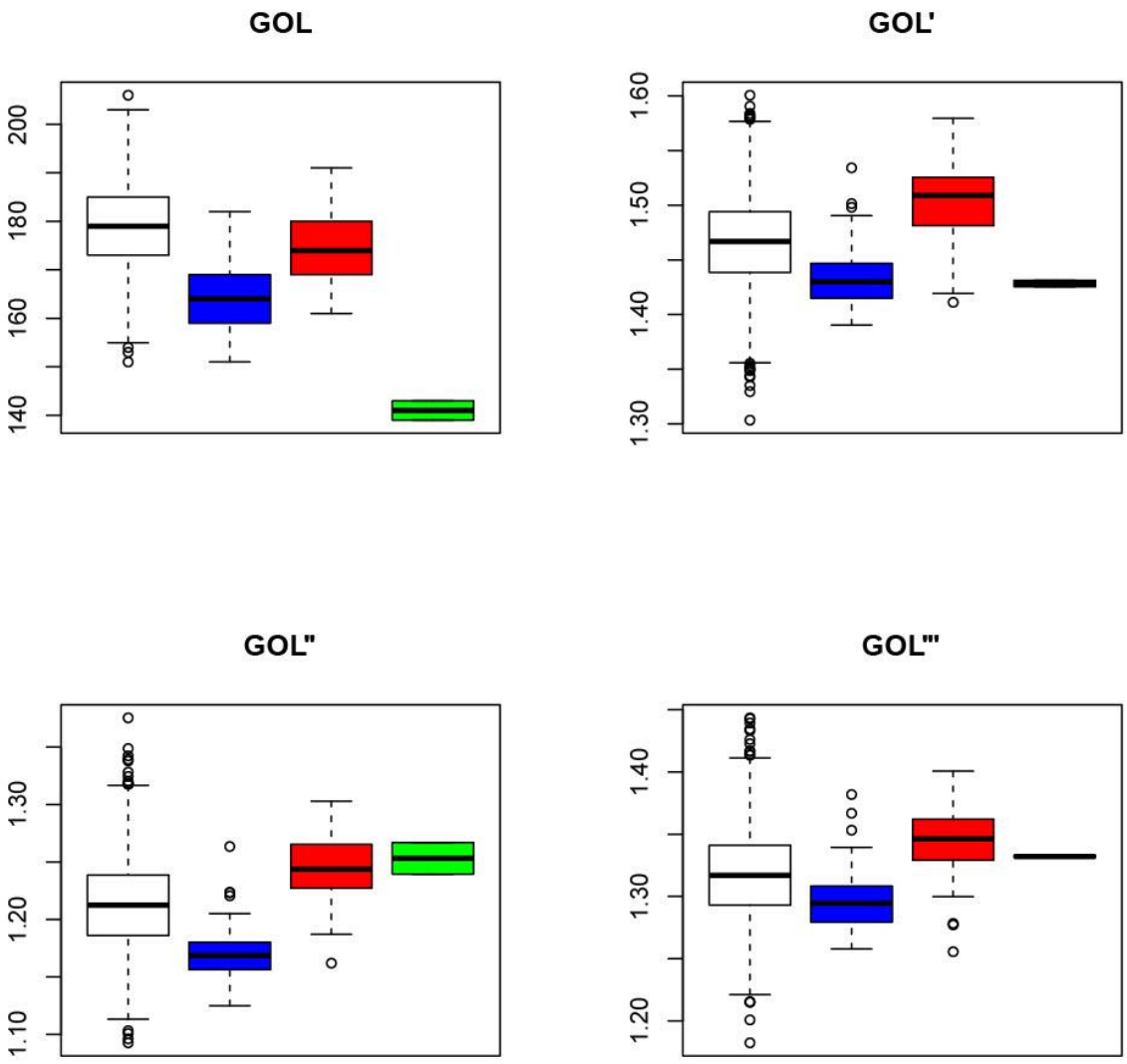

Figure 7. Box and whisker plots for absolute and size-adjusted greatest cranial length (GOL) for the total recent modern human sample (white) with Andaman Islanders only shown in blue and San only shown in red. LB 1 is shown as the green box on the right, the top and bottom of which represent slight differences in the published measurements for LB 1 (Brown et al., 2004; Kaifu et al., 2011). GOL′, GOL″, and GOL‴ were calculated by dividing GOL by GM1, GM2, and GM3, respectively (see text for details). (back to text)

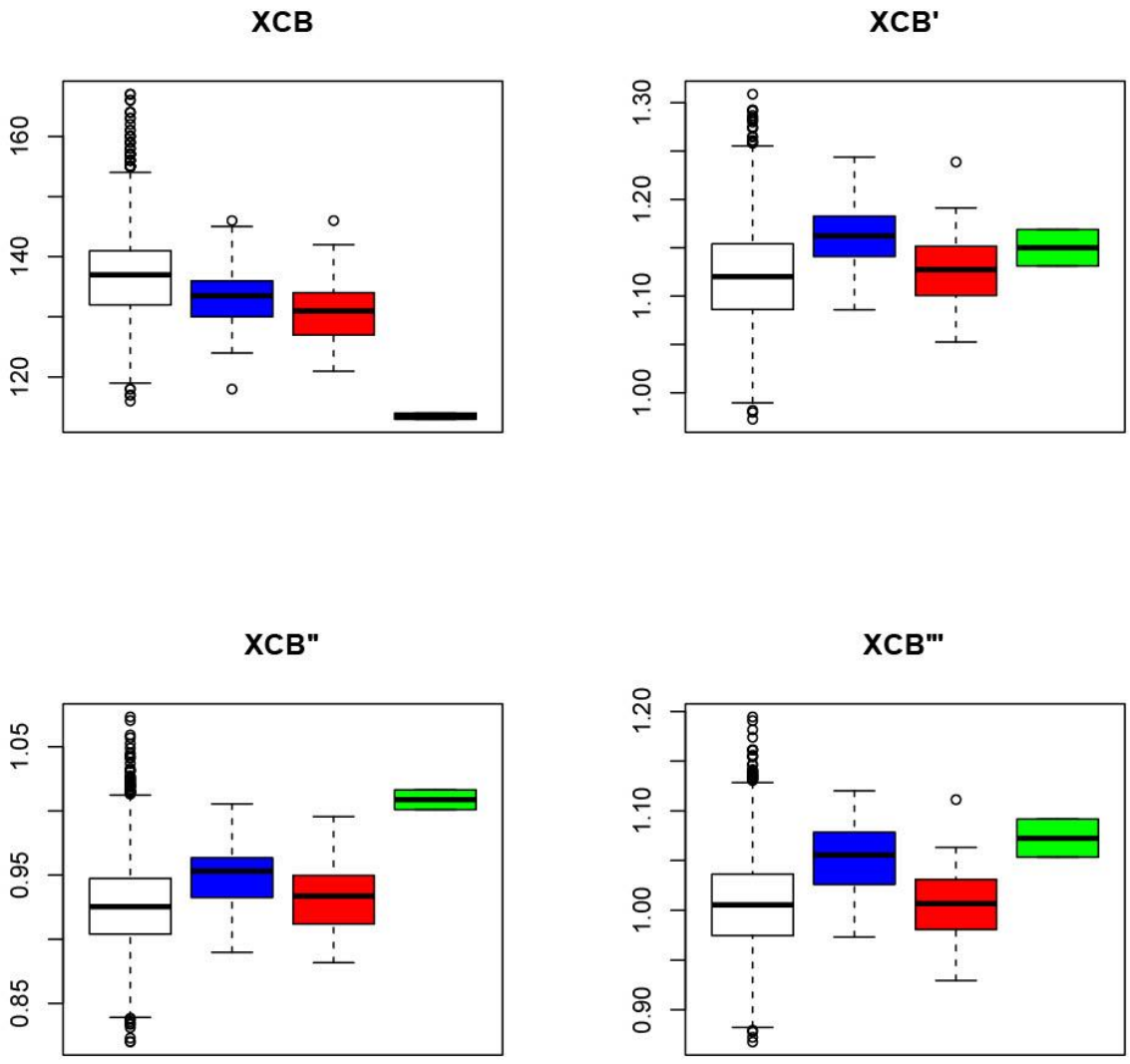

Figure 8. Box and whisker plots for absolute and size-adjusted greatest cranial breadth (XCB) for the total recent modern human sample (white) with Andaman Islanders only shown in blue and San only shown in red. LB 1 is shown as the green box on the right, the top and bottom of which represent slight differences in the published measurements for LB 1 (Brown et al., 2004; Kaifu et al., 2011). XCB′, XCB″, and XCB‴ were calculated by dividing XCB by GM1, GM2, and GM3, respectively (see text for details). (back to text)

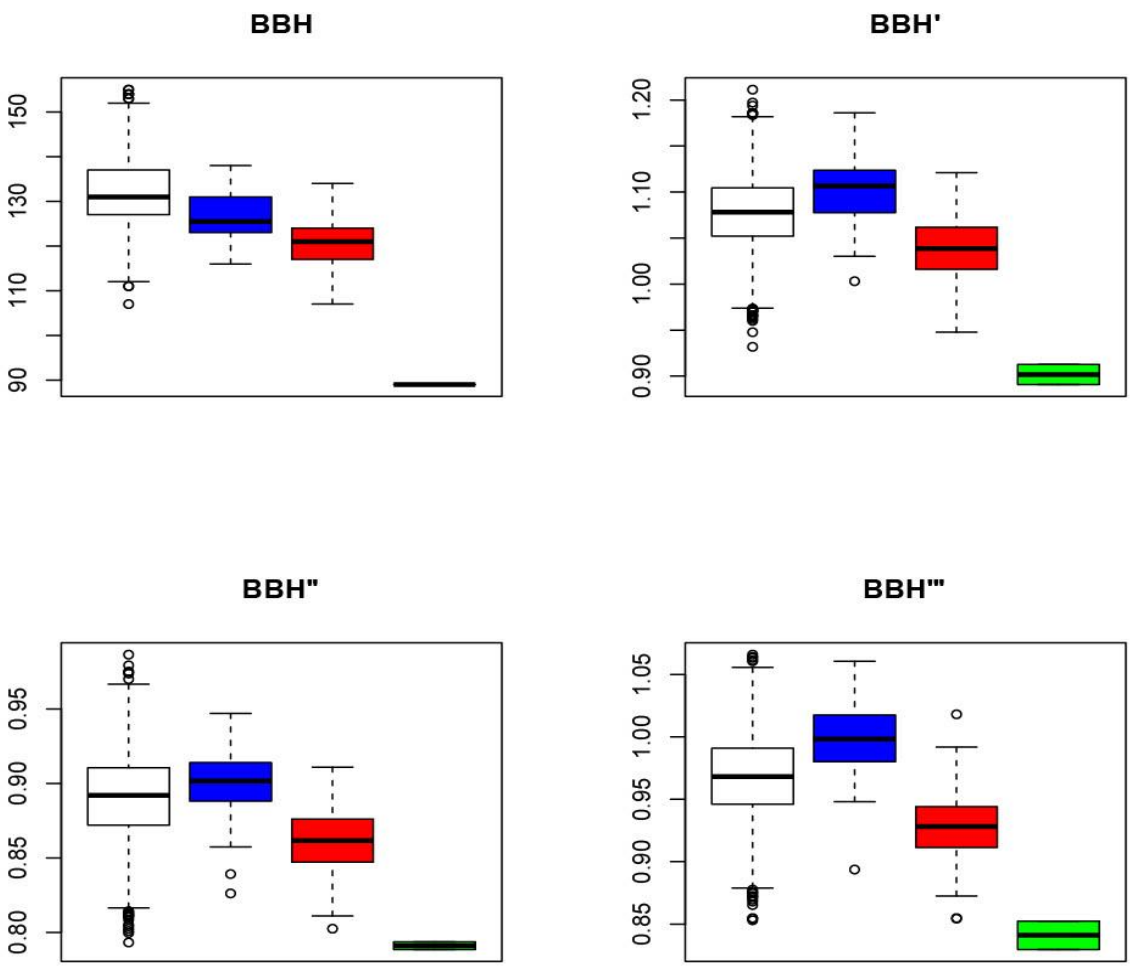

Figure 9. Box and whisker plots for absolute and size-adjusted cranial heights (BBH) for the total recent modern human sample (white) with Andaman Islanders only shown in blue and San only shown in red. LB 1 is shown as the green box on the right, the top and bottom of which represent slight differences in the published measurements for LB 1 (Brown et al., 2004; Kaifu et al., 2011). BBH′, BBH″, and BBH‴ were calculated by dividing BBH by GM1, GM2, and GM3, respectively (see text for details). (back to text)

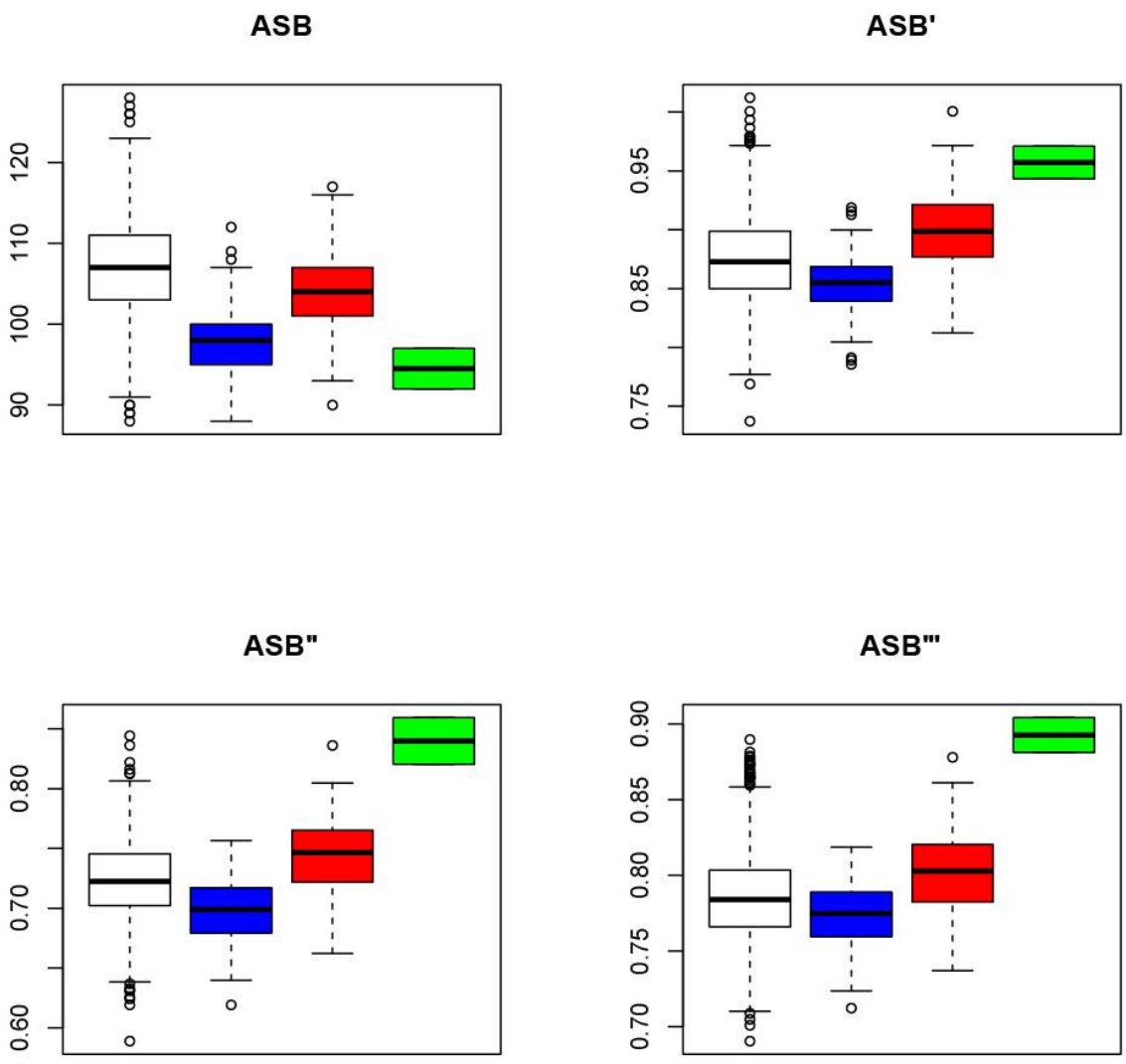

Figure 10. Box and whisker plots for absolute and size-adjusted basicranial breadths (ASB) for the total recent modern human sample (white) with Andaman Islanders only shown in blue and San only shown in red. LB 1 is shown as the green box on the right, the top and bottom of which represent slight differences in the published measurements for LB 1 (Brown et al., 2004; Kaifu et al., 2011). ASB′, ASB″, and ASB‴ were calculated by dividing ASB by GM1, GM2, and GM3, respectively (see text for details). (back to text)

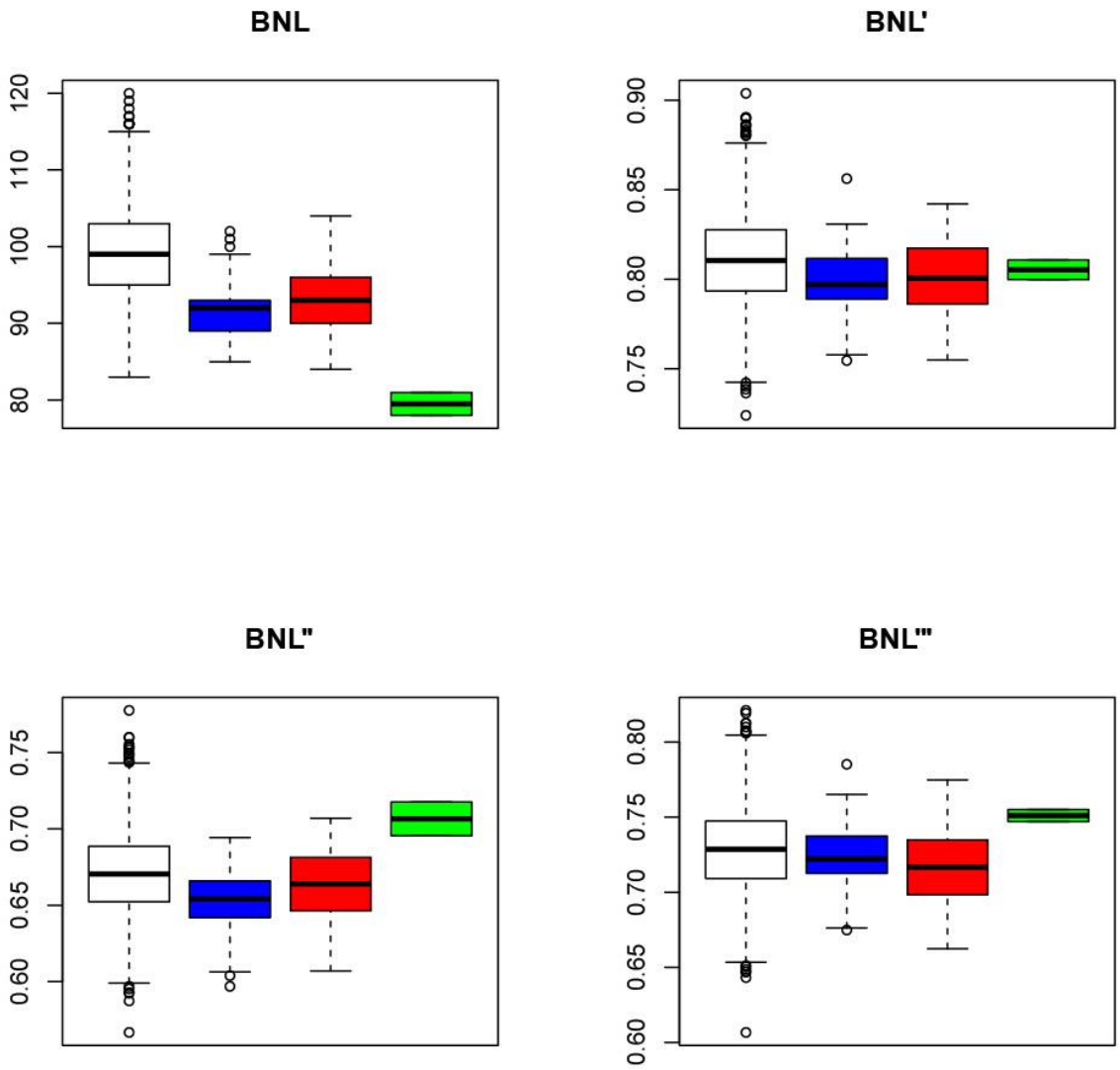

Figure 11. Box and whisker plots for absolute and size-adjusted upper facial projections (BNL) for the total recent modern human sample (white) with Andaman Islanders only shown in blue and San only shown in red. LB 1 is shown as the green box on the right, the top and bottom of which represent slight differences in the published measurements for LB 1 (Brown et al., 2004; Kaifu et al., 2011). BNL′, BNL″, and BNL‴ were calculated by dividing BNL by GM1, GM2, and GM3, respectively (see text for details). (back to text)

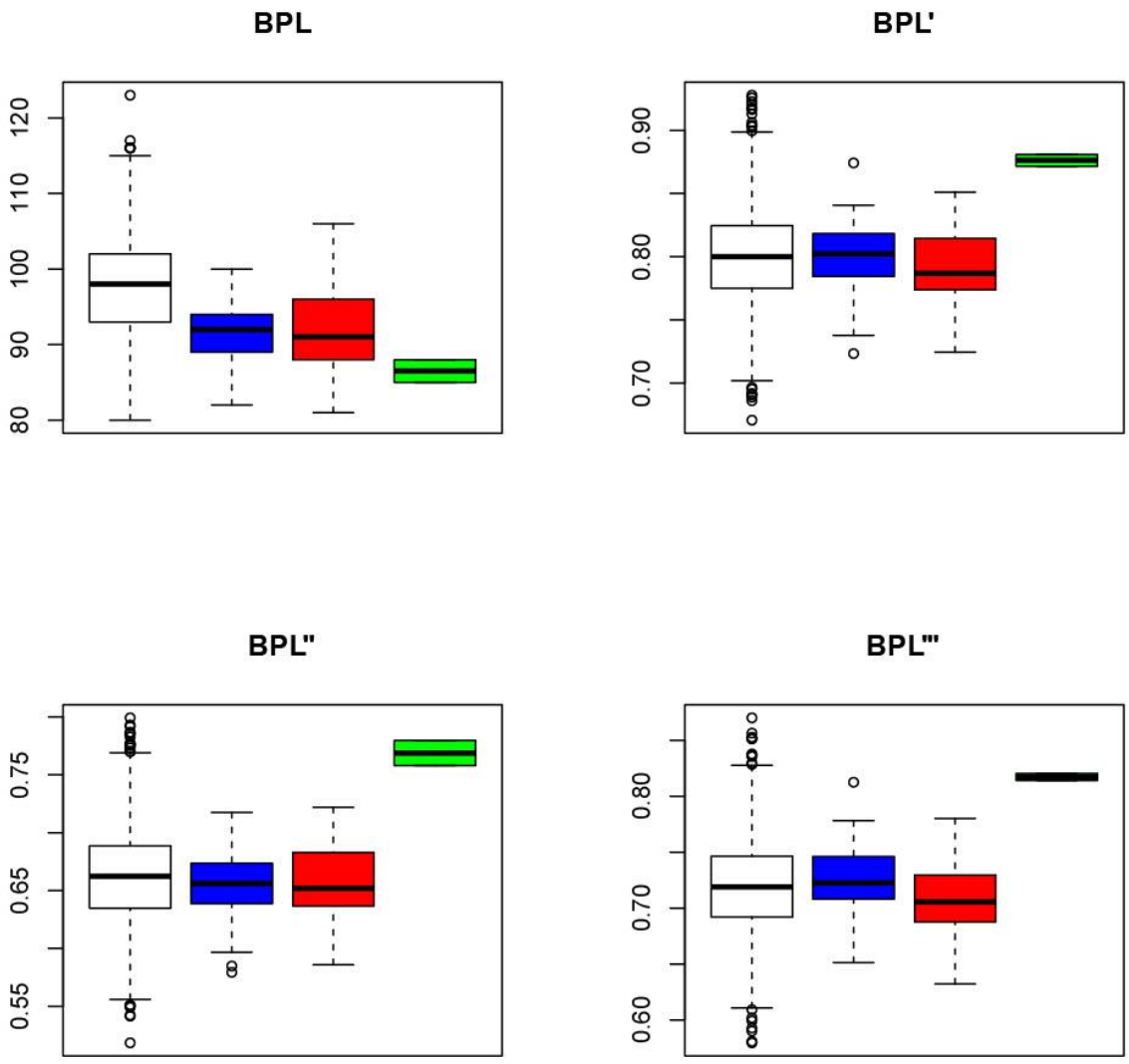

Figure 12. Box and whisker plots for absolute and size-adjusted lower facial projections (BPL) for the total recent modern human sample (white) with Andaman Islanders only shown in blue and San only shown in red. LB 1 is shown as the green box on the right, the top and bottom of which represent slight differences in the published measurements for LB 1 (Brown et al., 2004; Kaifu et al., 2011). BPL′, BPL″, and BPL‴ were calculated by dividing BPL by GM1, GM2, and GM3, respectively (see text for details). (back to text)

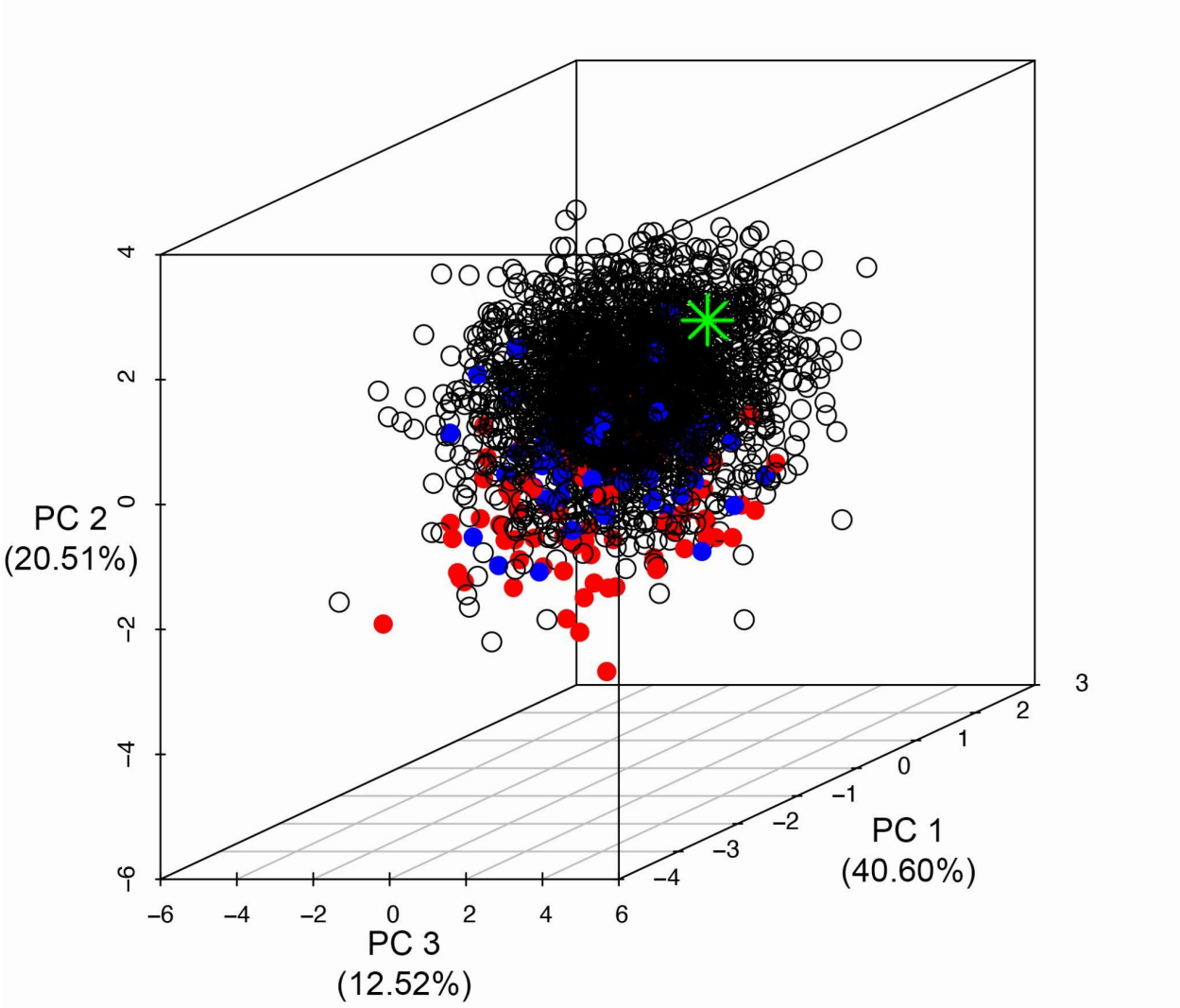

Figure 13. PCA of facial shape variables for LB 1 and recent modern humans. Red dots are Andaman Islanders; blue dots are San Bushman; green star is LB 1 . (back to text)

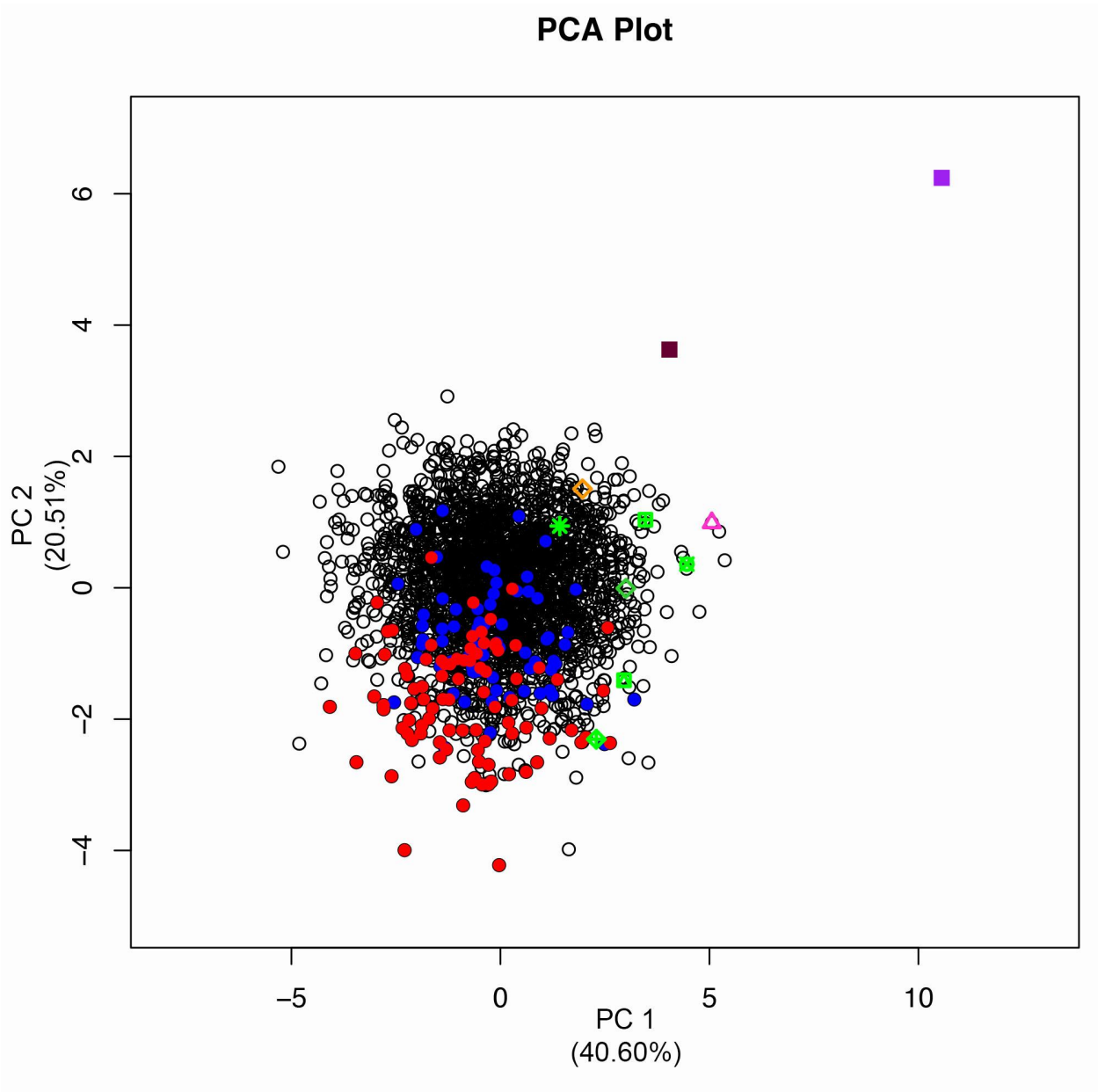

Figure 14. PCA components 1 and 2 of facial shape variables for fossils and modern humans. Symbols are the same as the previous graph with the addition of OH 5 (purple square), Sts 5 (brown square), KNM-ER 1813 (pink triangle), KNM-ER 3733 (orange diamond), Zhoukoudian 11 (green diamond), Kabwe (green square with cross), Sima de los Huesos 5 (green circle with X), Dali (green square with triangle), and Harbin (green diamond with cross). (back to text).

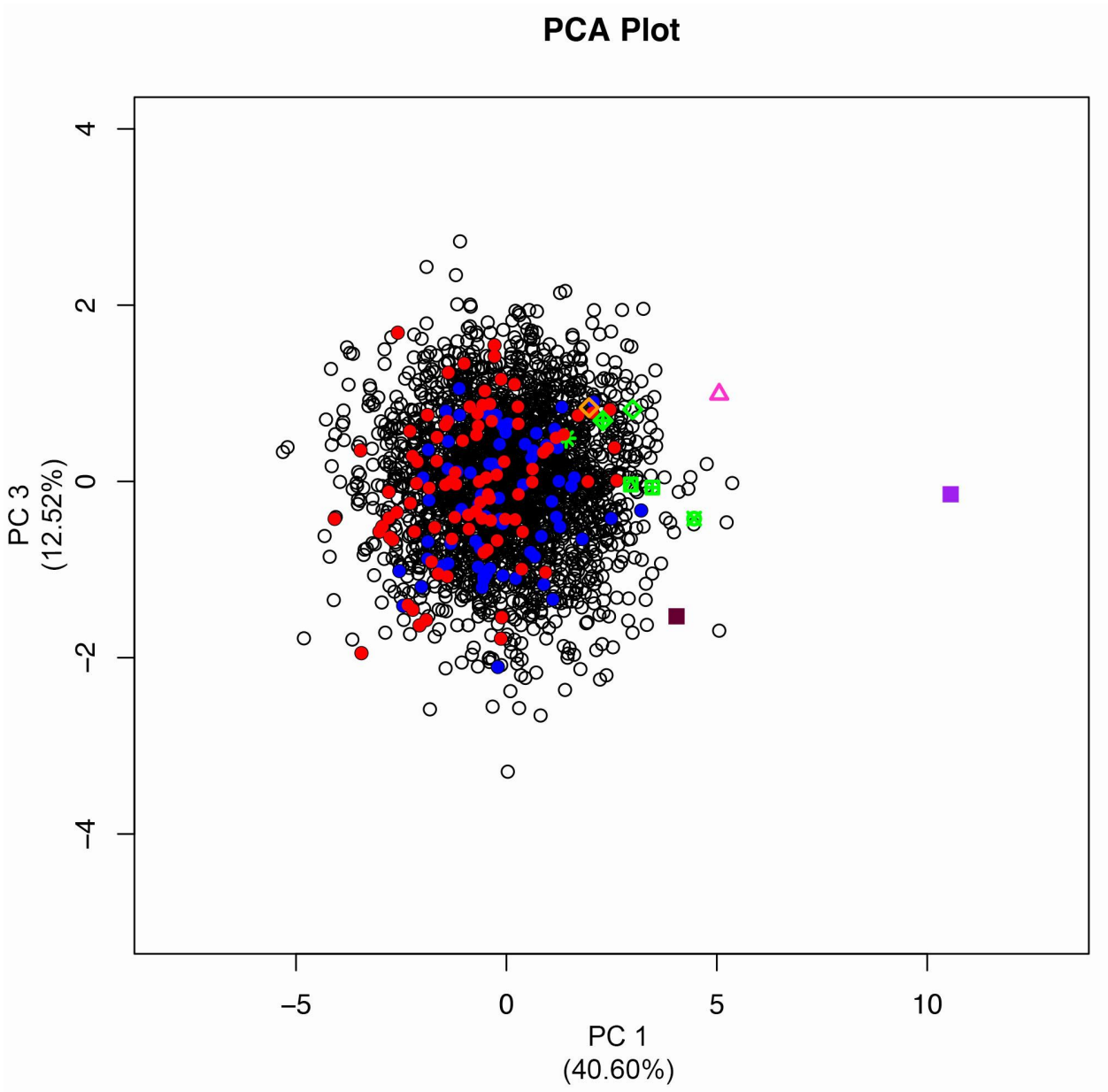

Figure 15. PCA components 1 and 3 of facial shape variables for fossils and modern humans. Symbols are the same as the previous graph with the addition of OH 5 (purple square), Sts 5 (brown square), KNM-ER 1813 (pink triangle), KNM-ER 3733 (orange diamond), Zhoukoudian 11 (green diamond), Kabwe (green square with cross), Sima de los Huesos 5 (green circle with X), Dali (green square with triangle), and Harbin (green diamond with cross). (back to text).

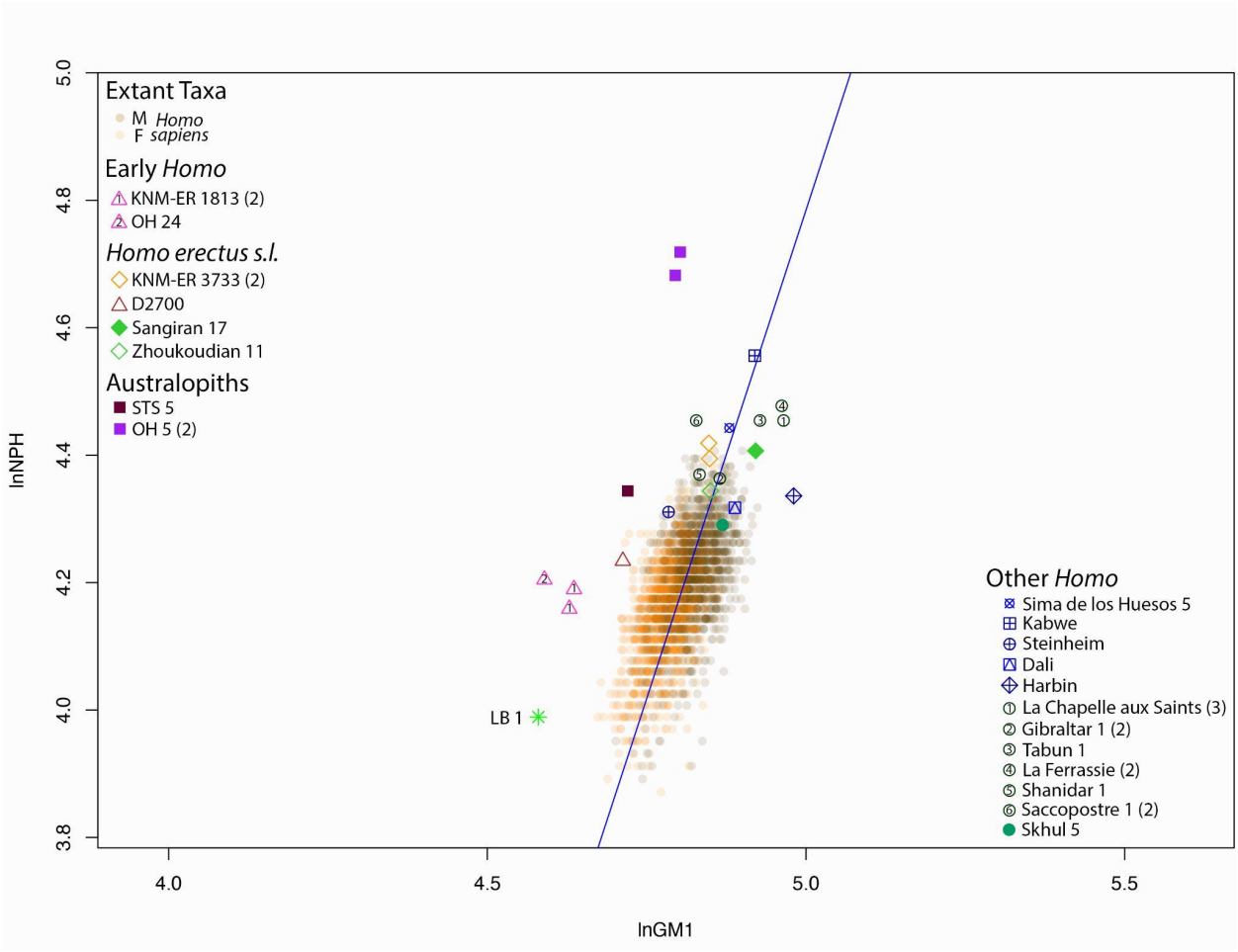

Figure 16. Bivariate scaling relationship between nasion prosthion height (lnNPH) and overall cranial size (lnGM1) in modern humans and fossil hominins. The blue line is the major axis fitted line for the modern human sample (N = 2,524). (back to text)

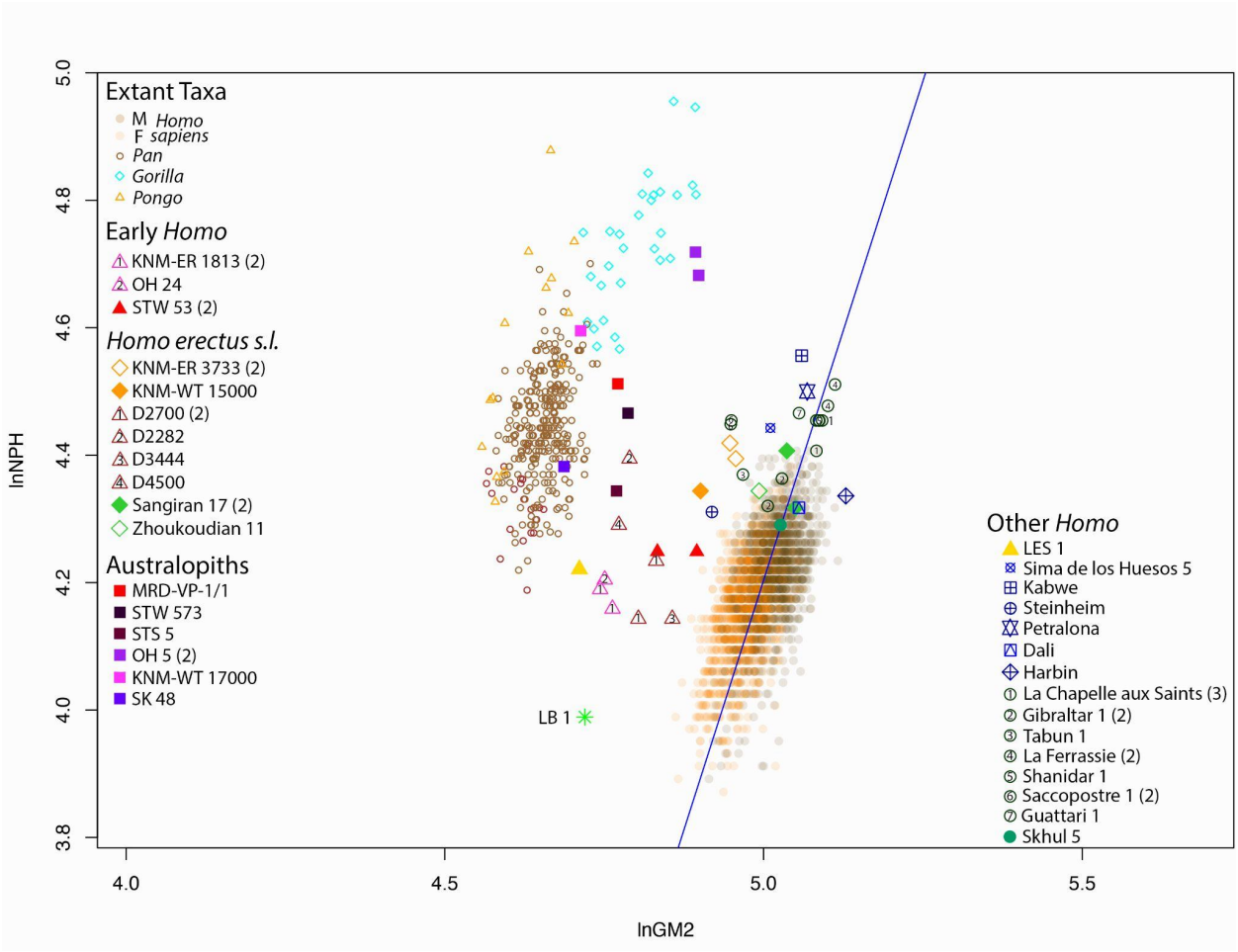

Figure 17. Bivariate scaling relationship between nasion prosthion height (lnNPH) and neurocranial size (lnGM2) as calculated using maximum cranial breadth in modern humans and fossil hominins. The blue line is the major axis fitted line for the modern human sample (N = 2,524). Numbers in parentheses indicate more than one published set of measurements were included for comparison. (back to text)

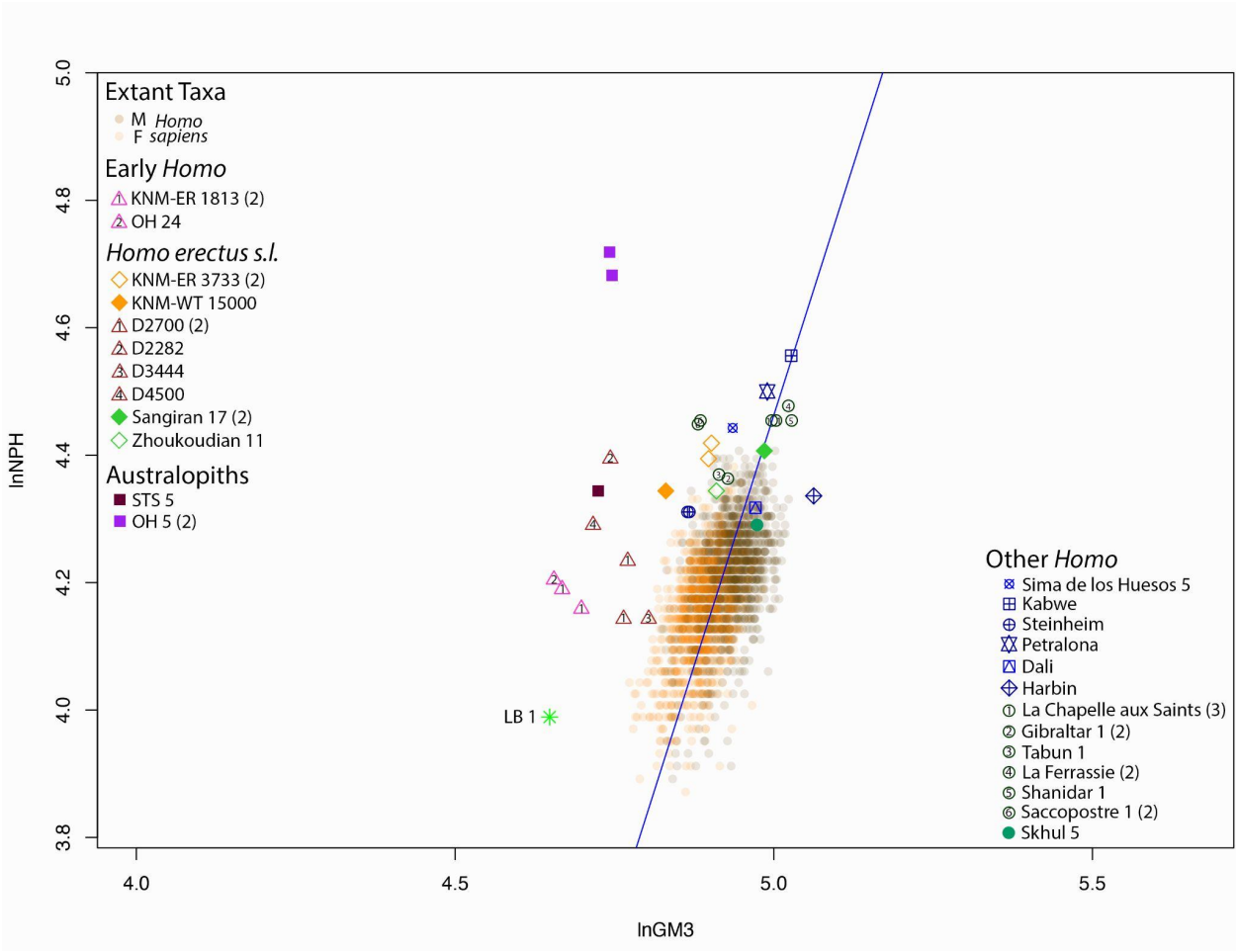

Figure 18. Bivariate scaling relationship between nasion prosthion height (lnNPH) and neurocranial size (lnGM3) as calculated using asterionic breadth in modern humans and fossil hominins. The blue line is the major axis fitted line for the modern human sample (N = 2,524). Numbers in parentheses indicate more than one published set of measurements were included for comparison. (back to text)

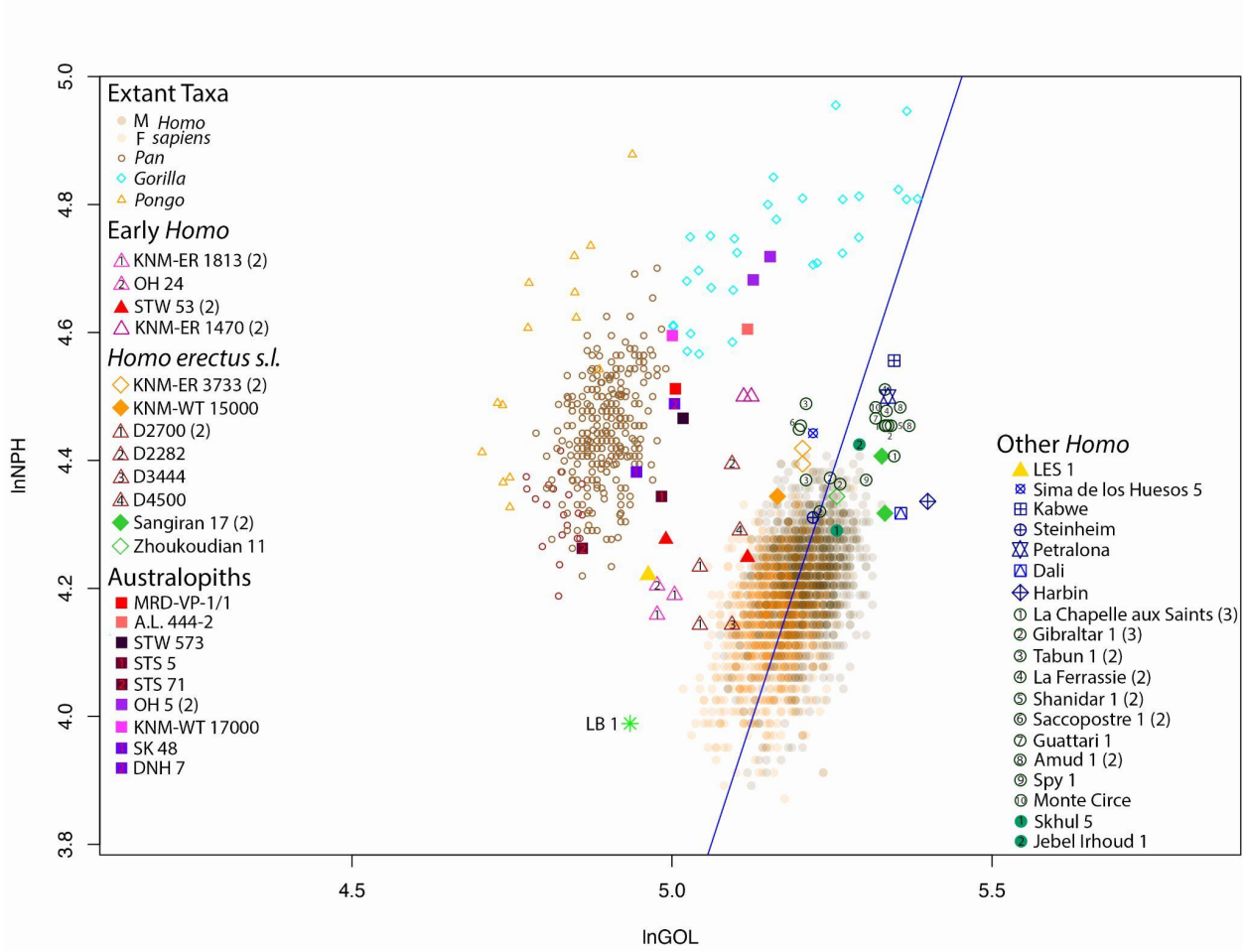

Figure 19. Bivariate scaling relationship between nasion prosthion height (lnNPH) and glabella-opisthocranion length (lnGOL) as calculated in modern humans, extant great apes, and fossil hominins. The blue line is the major axis fitted line for the modern human sample. Numbers in parentheses indicate more than one published set of measurements were included for comparison. (back to text)

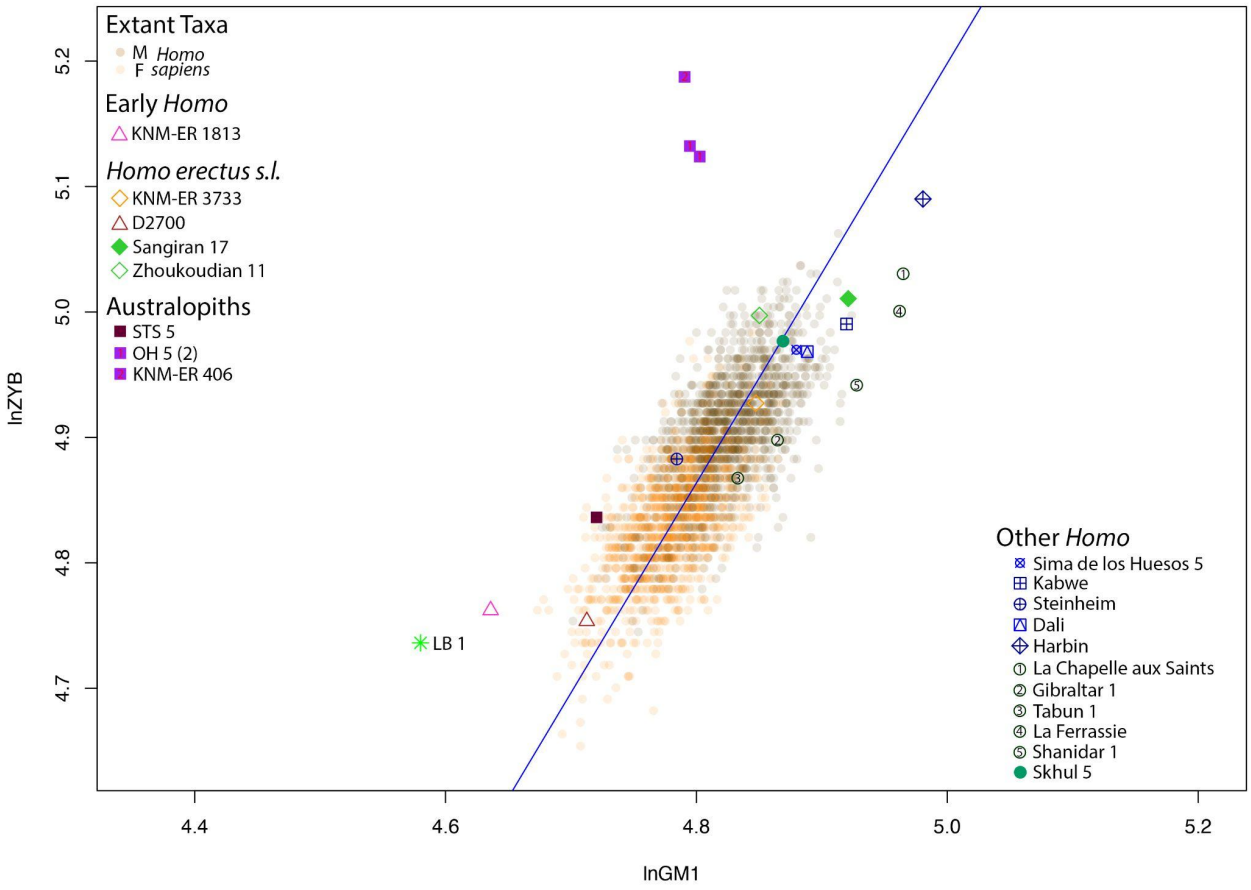

Figure 20. Bivariate scaling relationship between zygomatic breadth (lnZYB) and overall cranial size (lnGM1) in modern humans and fossil hominins. The blue line is the major axis fitted line for the modern human sample (N = 2,524). Numbers in parentheses indicate more than one published set of measurements were included for comparison. (back to text)

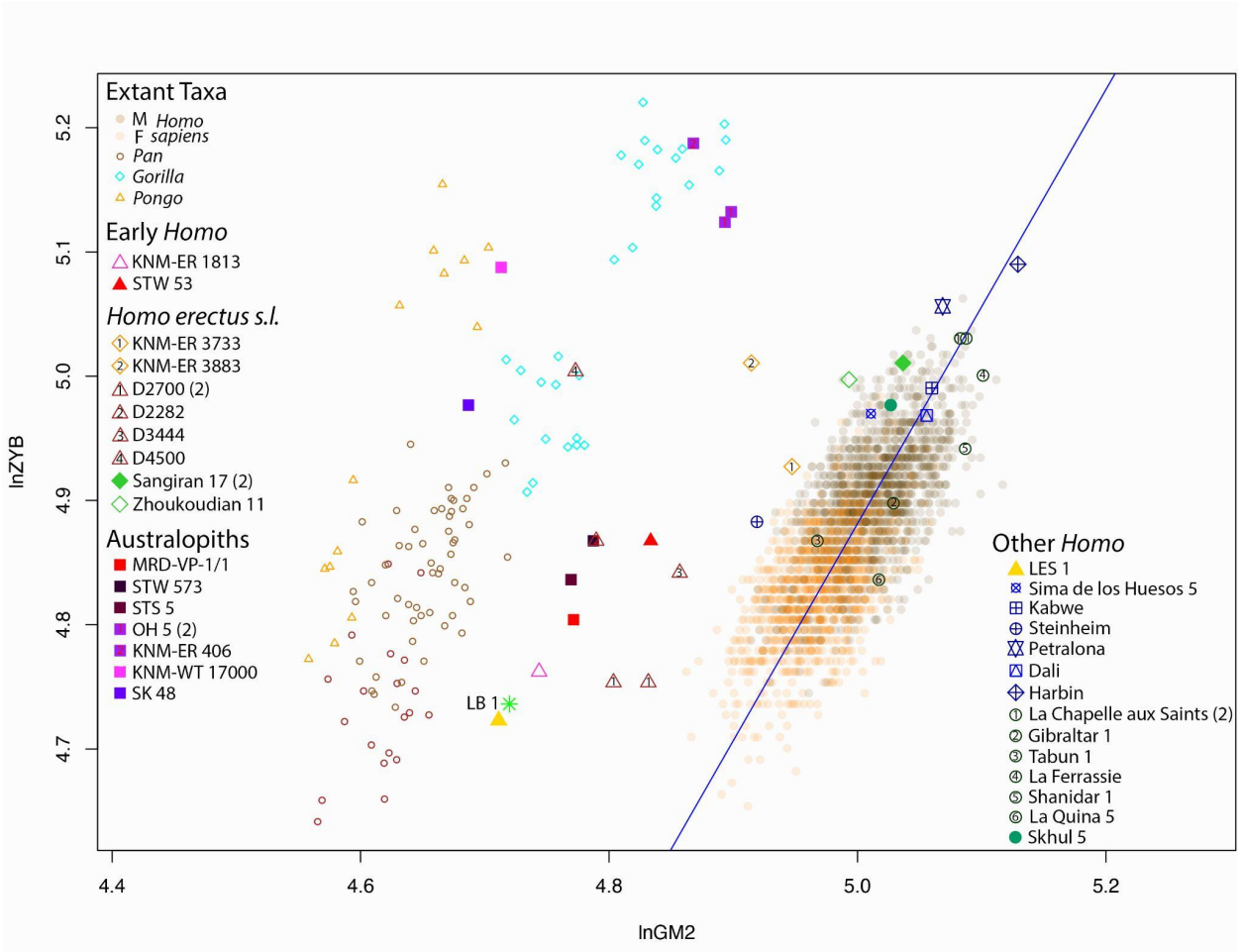

Figure 21. Bivariate scaling relationship between zygomatic breadth (lnZYB) and neurocranial size (lnGM2) as calculated using maximum cranial breadth in modern humans and fossil hominins. The blue line is the major axis fitted line for the modern human sample (N = 2,524). (back to text)

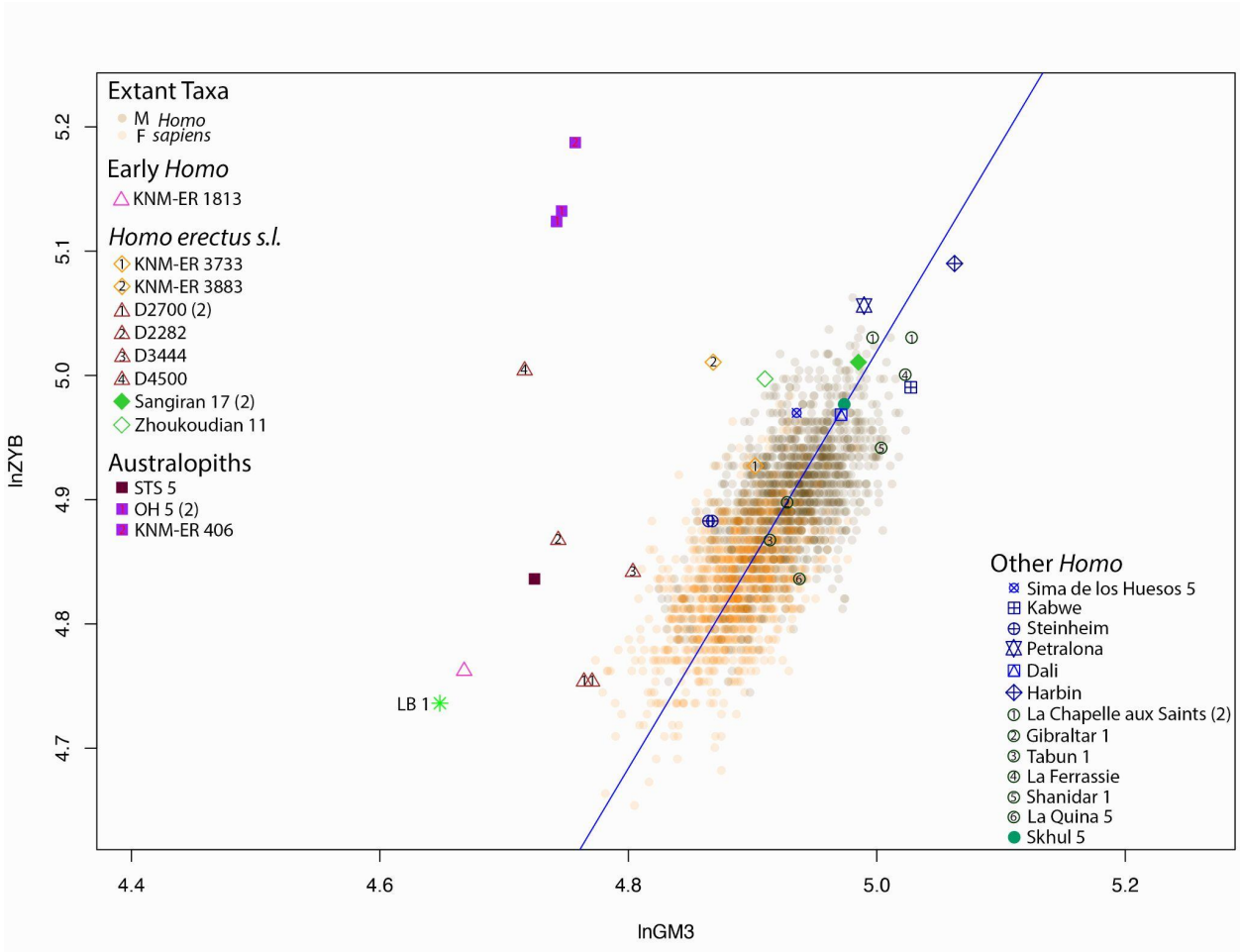

Figure 22. Bivariate scaling relationship between zygomatic breadth (lnZYB) and neurocranial size (lnGM3) as calculated using asterionic breadth in modern humans and fossil hominins. The blue line is the major axis fitted line for the modern human sample (N = 2,524). (back to text)

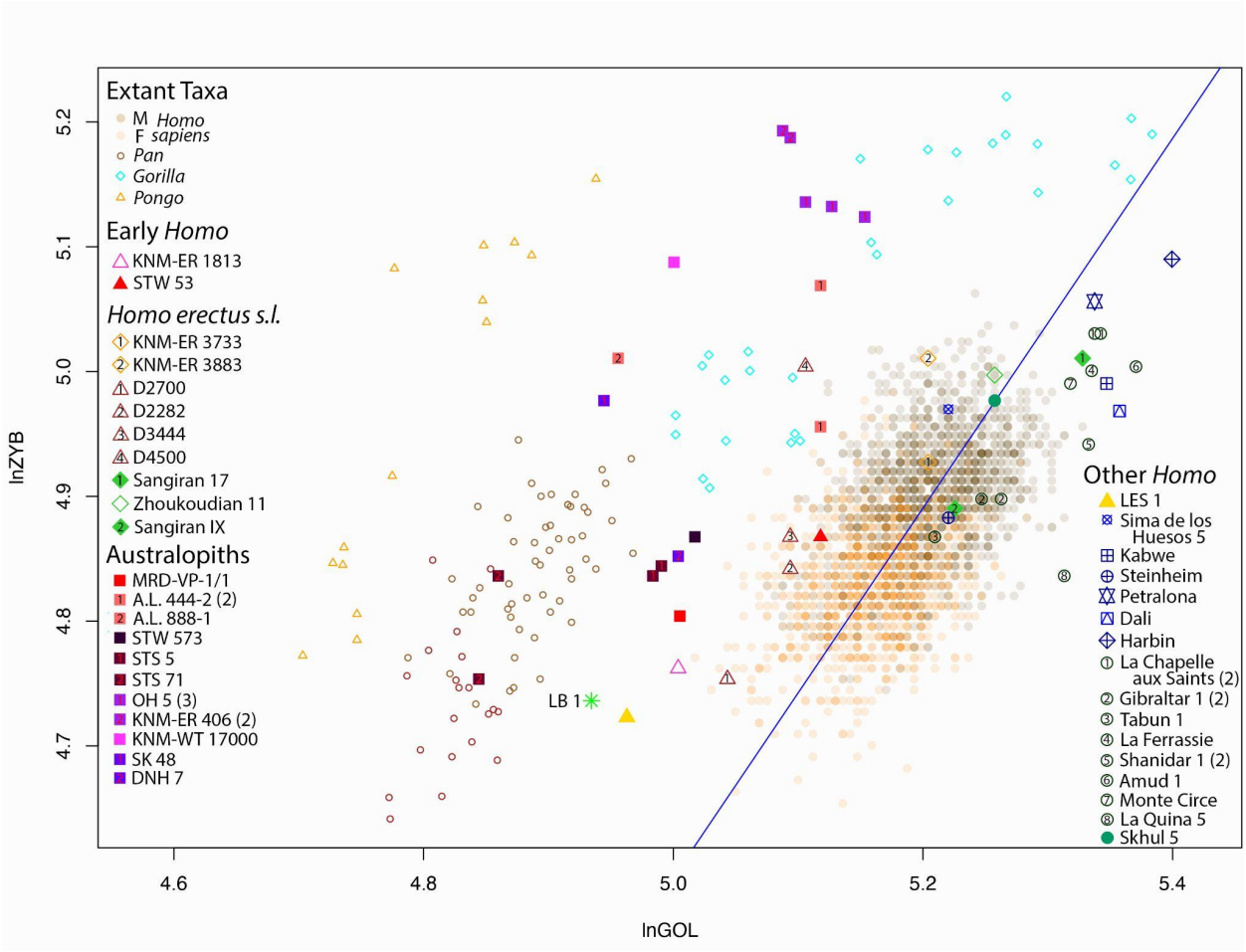

Figure 23. Bivariate scaling relationship between zygomatic breadth (lnZYB) and glabella-opisthocranion length (lnGOL) as calculated in modern humans, extant great apes, and fossil hominins. The blue line is the major axis fitted line for the modern human sample. Numbers in parentheses indicate more than one published set of measurements were included for comparison. (back to text)

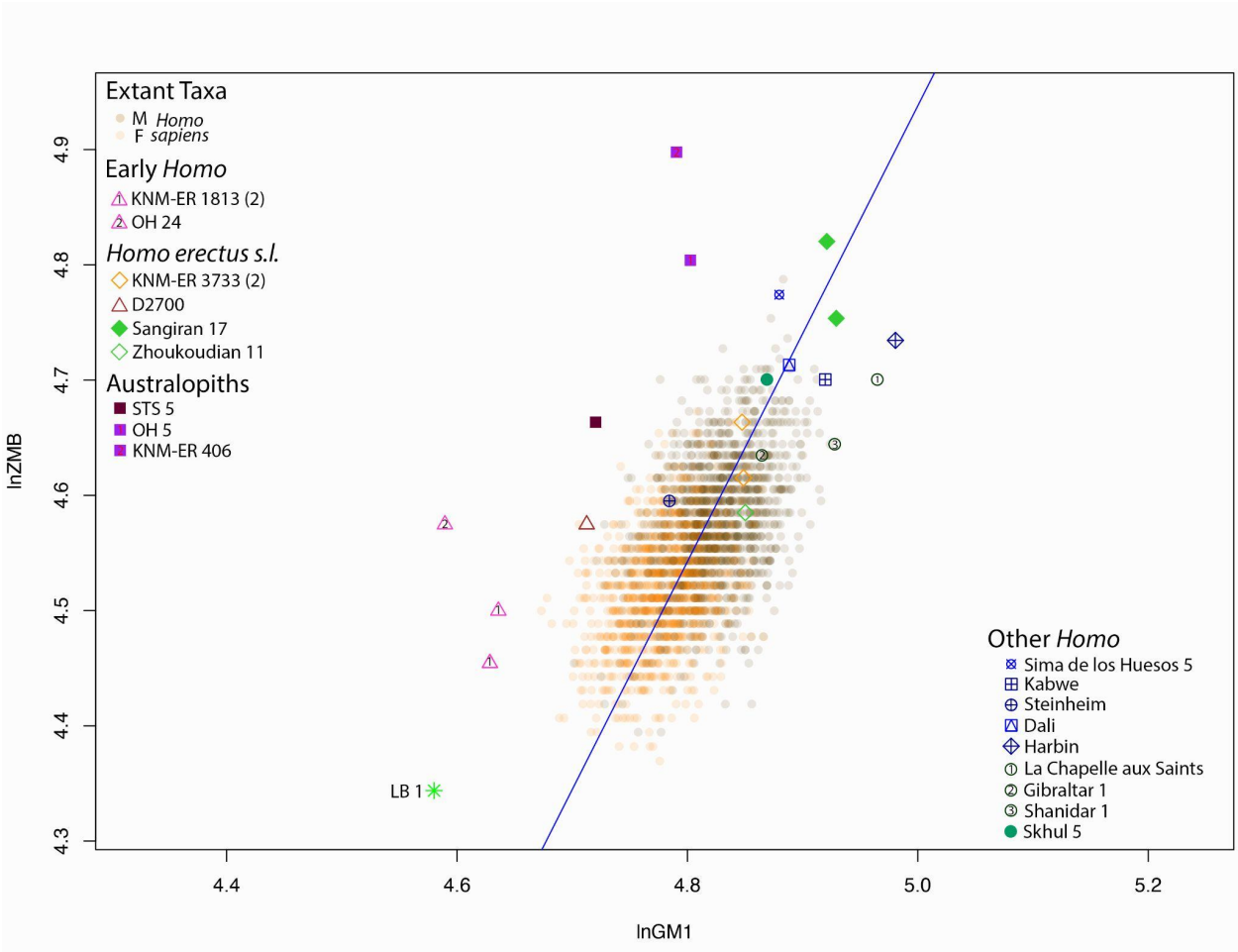

Figure 24. Bivariate scaling relationship between zygomaxillary breadth (lnZMB) and overall cranial size (lnGM) in modern humans and fossil hominins. The blue line is the major axis fitted line for the modern human sample (N = 2,524). (back to text)

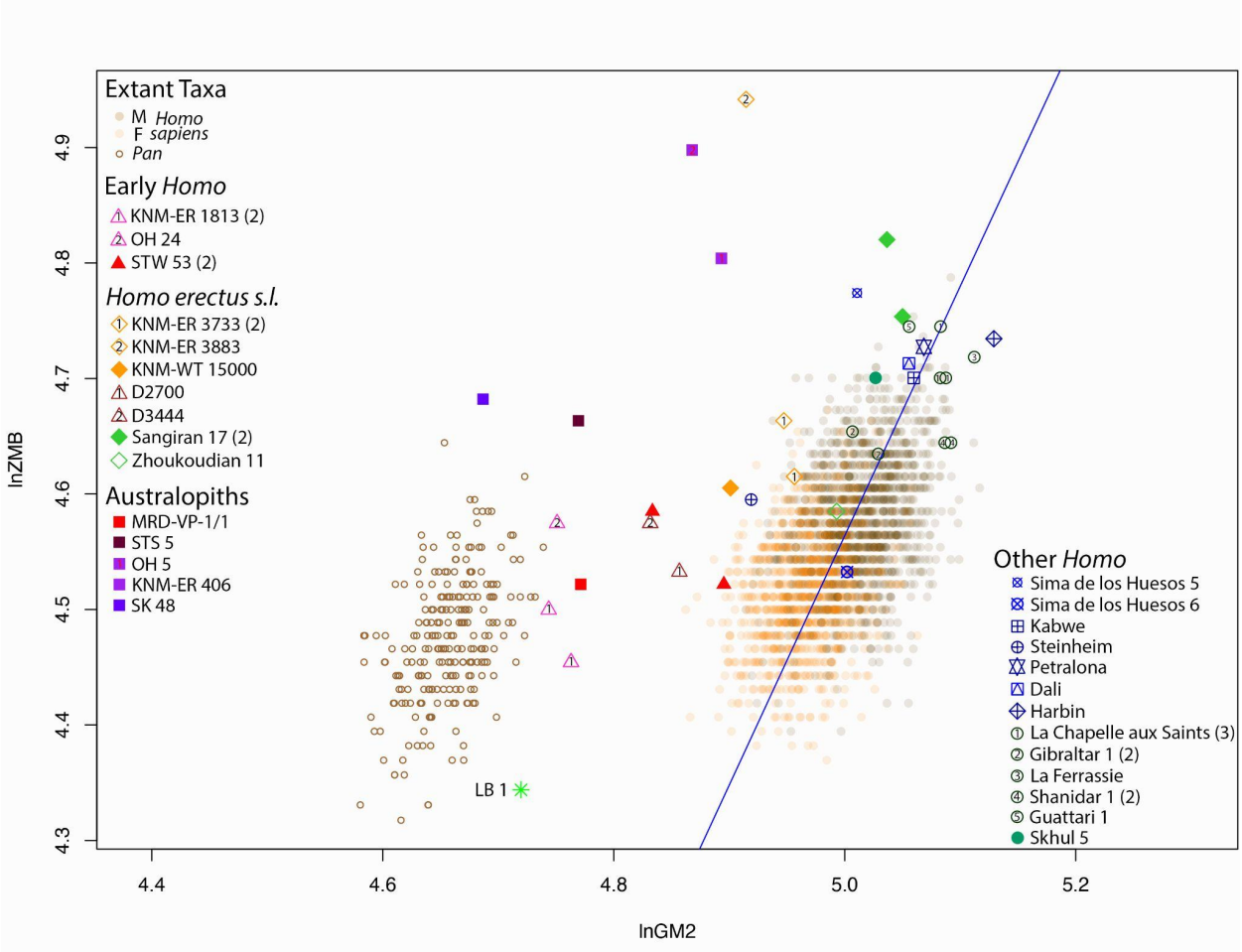

Figure 25. Bivariate scaling relationship between zygomaxillary breadth (lnZMB) and neurocranial size (lnGM2) as calculated using maximum cranial breadth in modern humans and fossil hominins. The blue line is the major axis fitted line for the modern human sample (N = 2,524). (back to text)

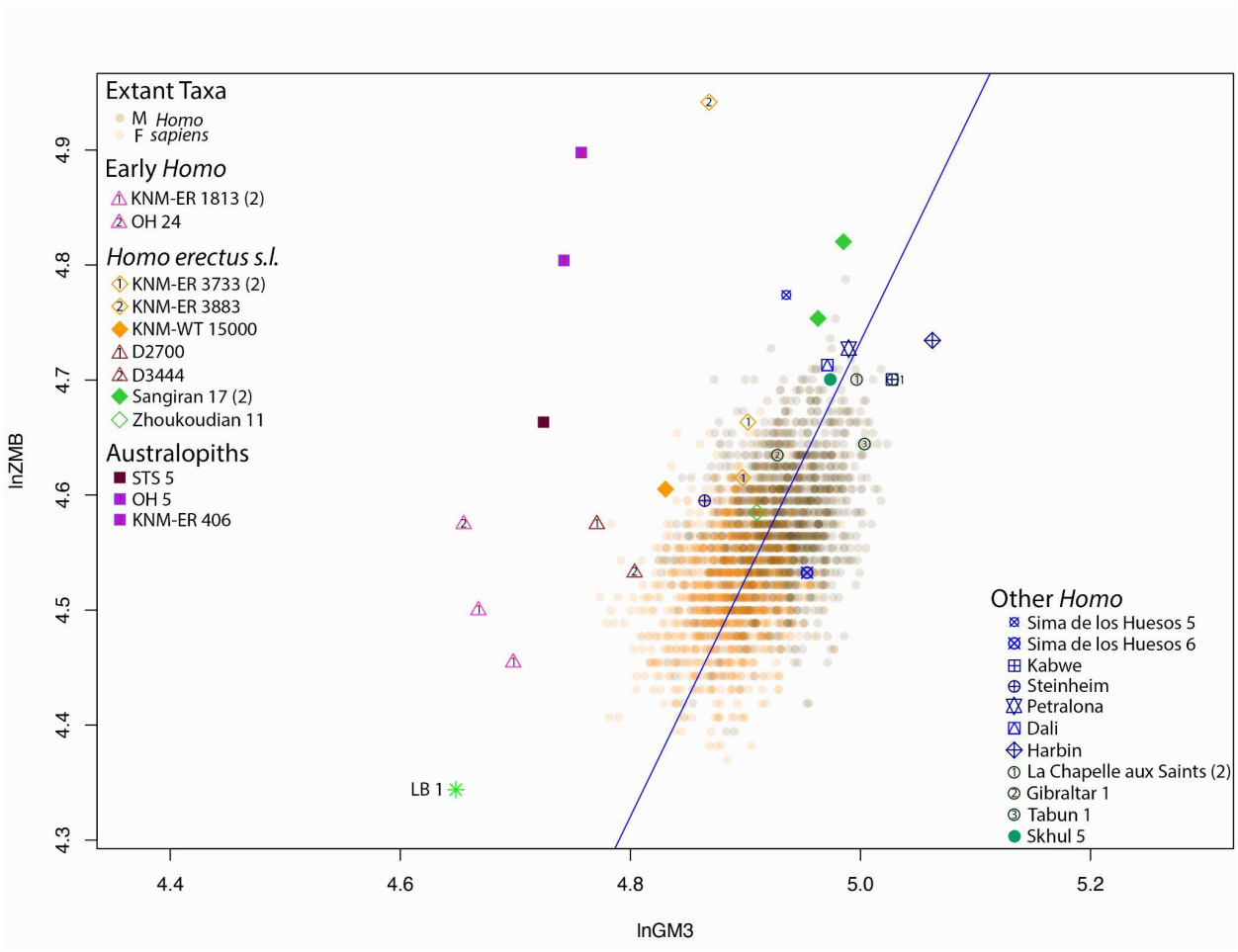

Figure 26. Bivariate scaling relationship between zygomaxillary breadth (lnZMB) and neurocranial size (lnGM3) as calculated using asterionic breadth in modern humans and fossil hominins. The blue line is the major axis fitted line for the modern human sample (N = 2,524). (back to text)

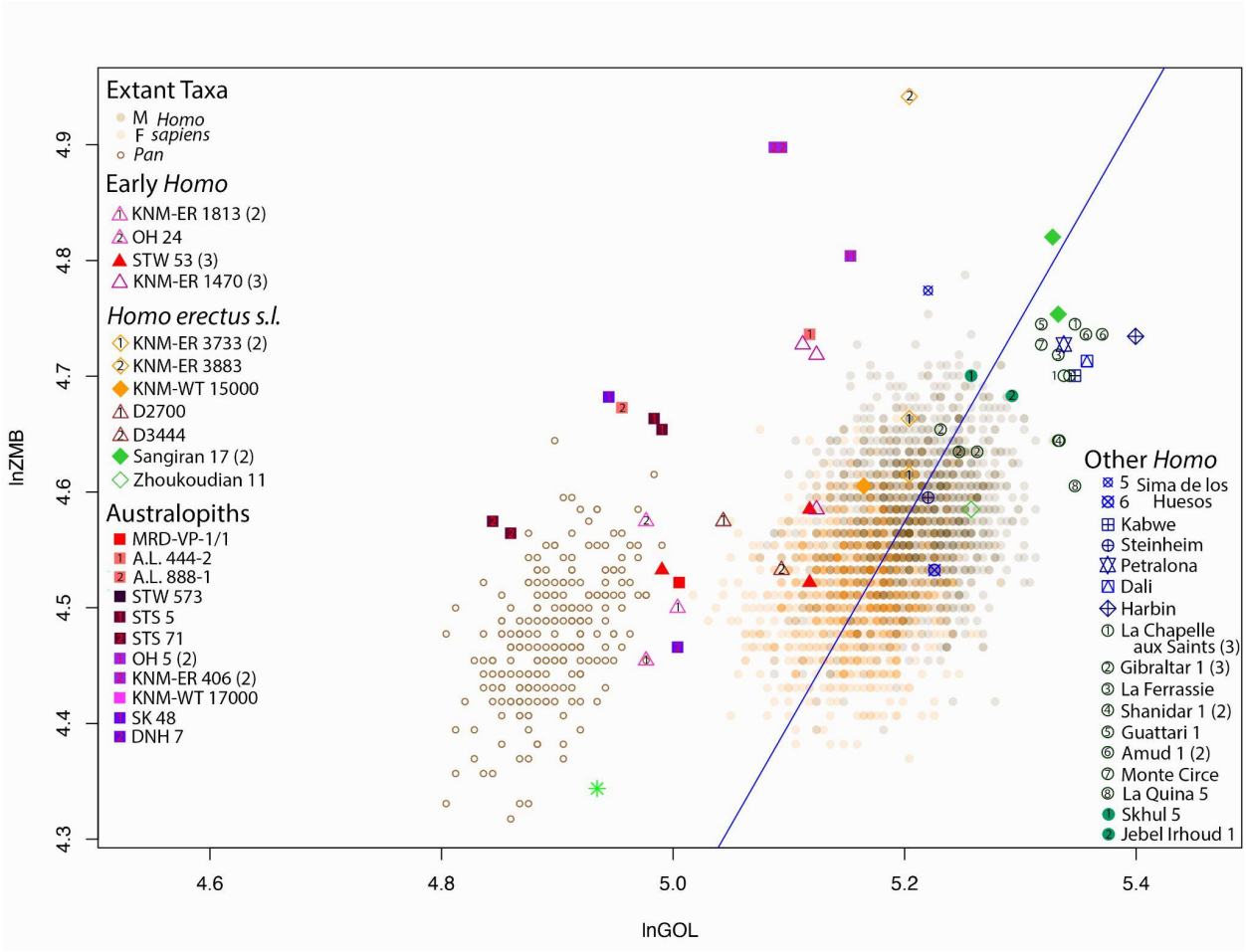

Figure 27. Bivariate scaling relationship between zygomaxillary breadth (lnZMB) and glabella-opisthocranion length (lnGOL) as calculated in modern humans, extant great apes, and fossil hominins. The blue line is the major axis fitted line for the modern human sample. Numbers in parentheses indicate more than one published set of measurements were included for comparison. Symbols are the same as in Figure 24 with additional specimens as shown. (back to text)

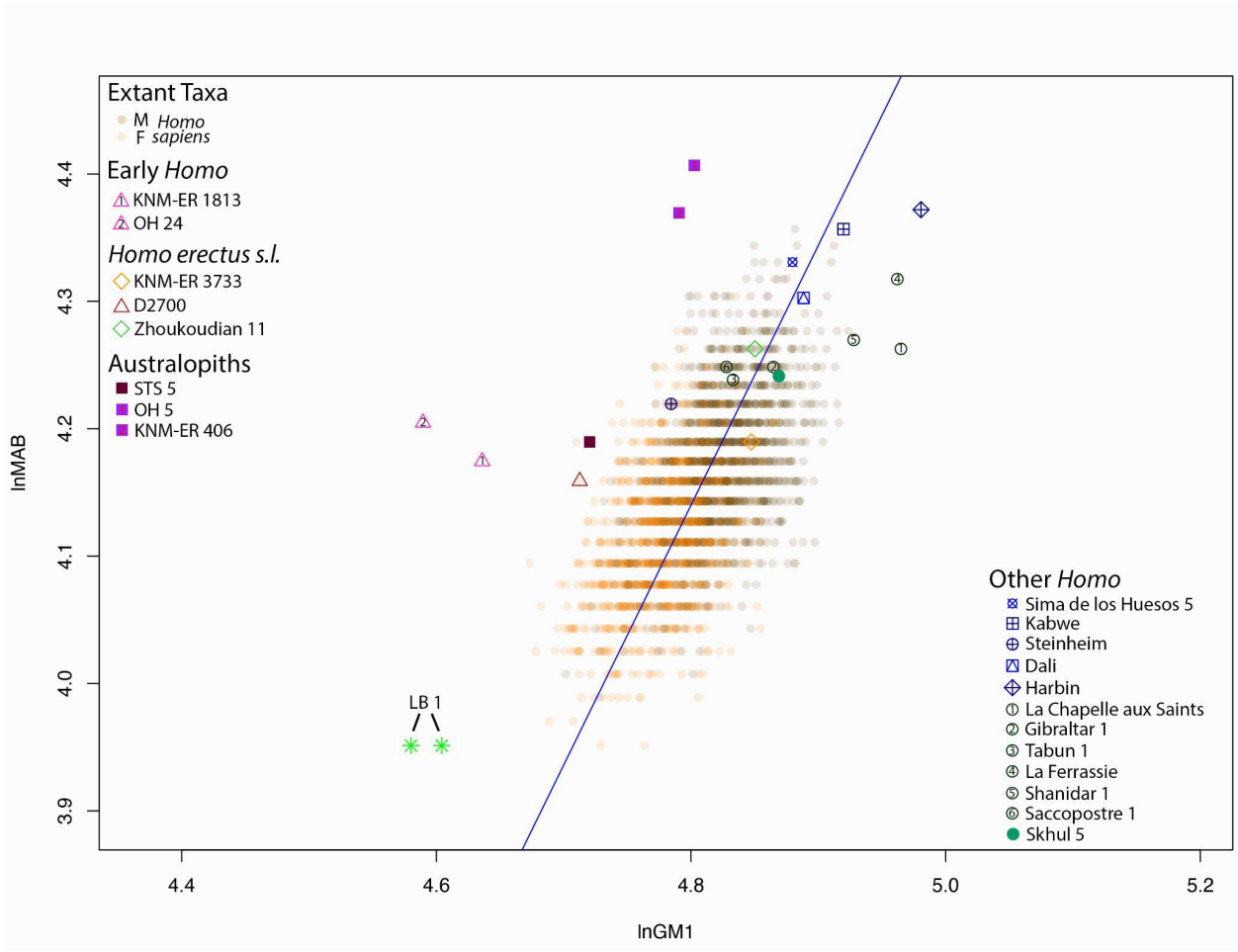

Figure 28. Bivariate scaling relationship between maxillary breadth (lnMAB) and overall cranial size (lnGM1) in modern humans and fossil hominins. The blue line is the major axis fitted line for the modern human sample (N = 2,524). (back to text)

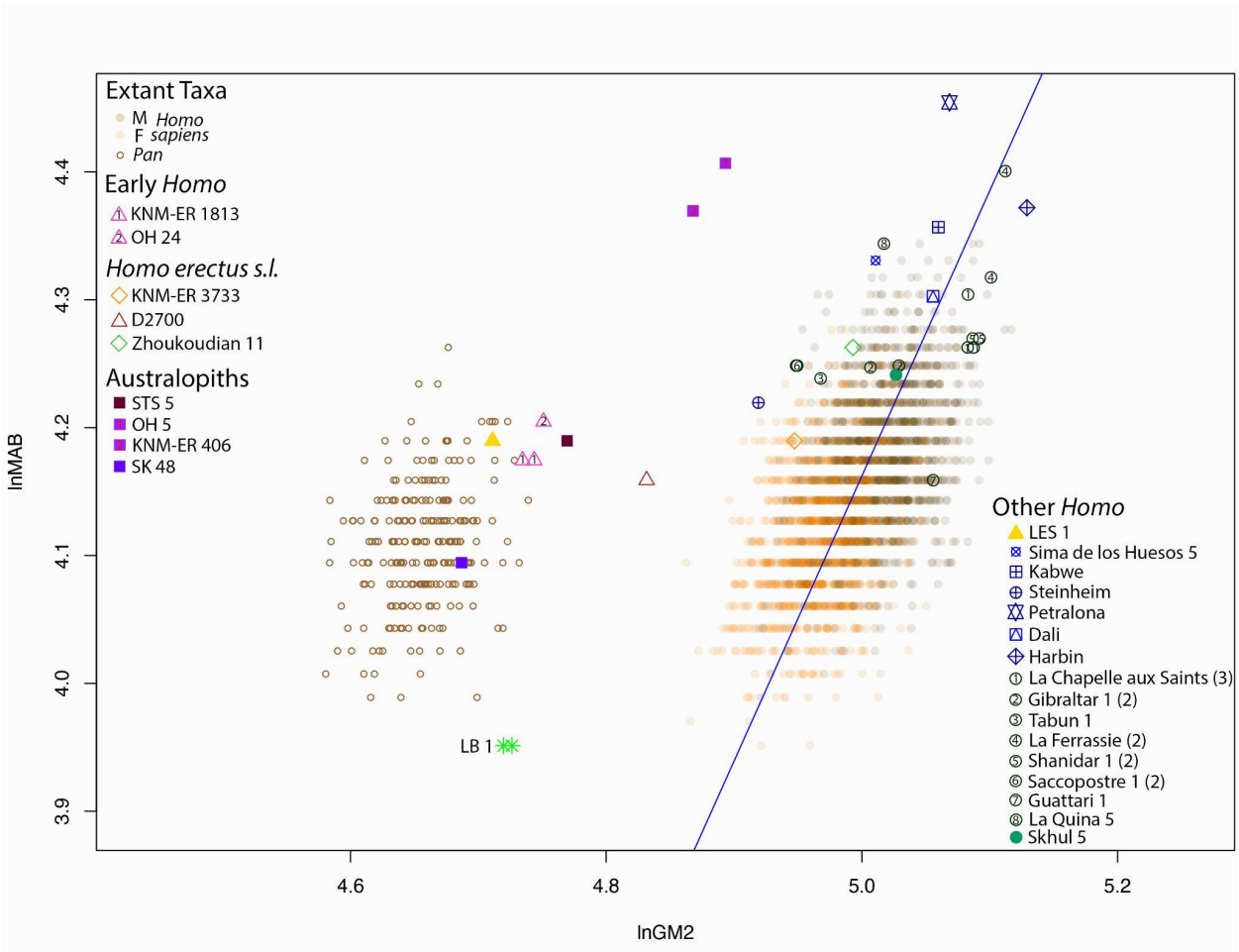

Figure 29. Bivariate scaling relationship between maxillary breadth (lnMAB) and neurocranial size (lnGM2) as calculated using maximum cranial breadth in modern humans and fossil hominins. The blue line is the major axis fitted line for the modern human sample (N = 2,524). (back to text)

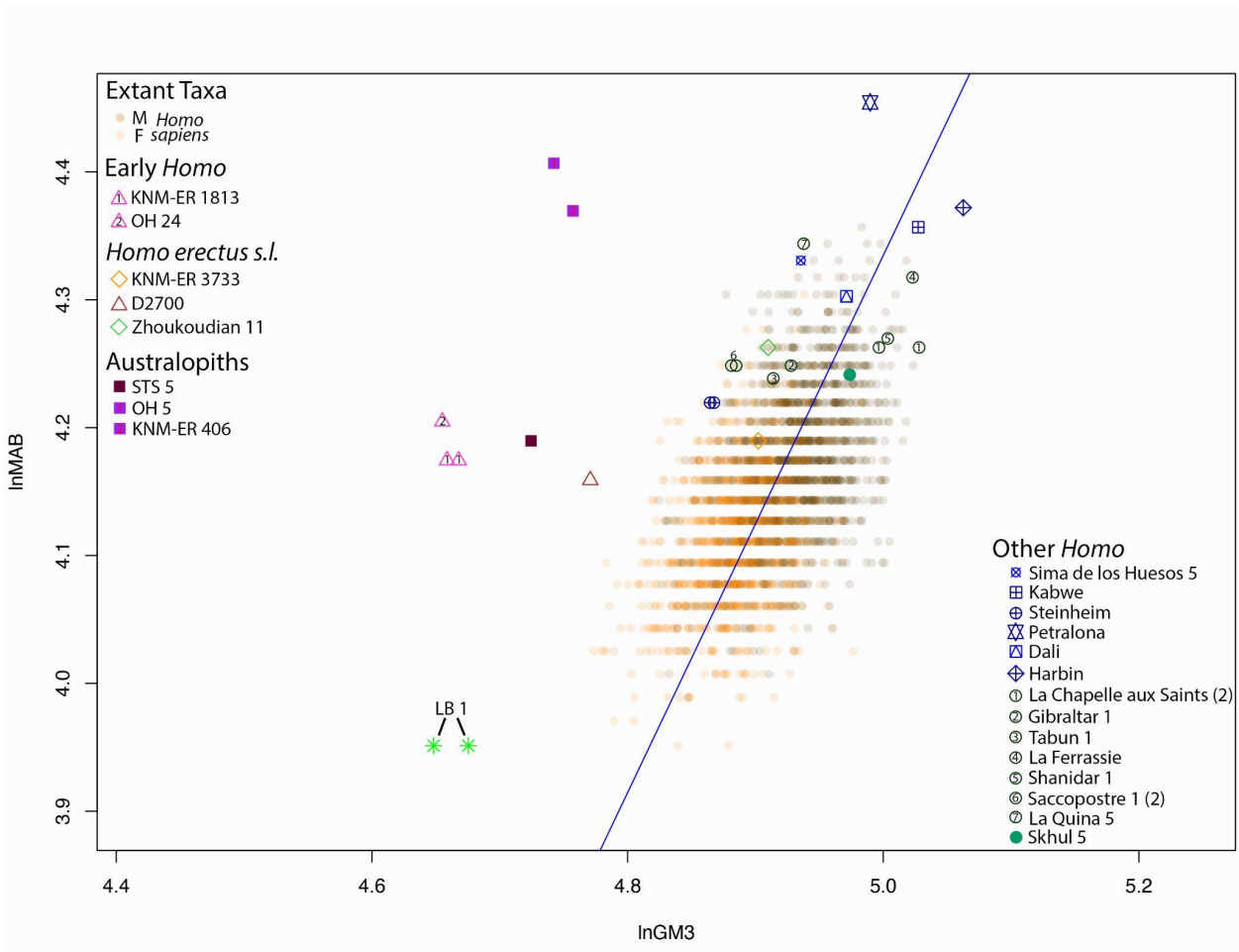

Figure 30. Bivariate scaling relationship between maxillary breadth (lnMAB) and neurocranial size (lnGM3) as calculated using asterionic breadth in modern humans and fossil hominins. The blue line is the major axis fitted line for the modern human sample (N = 2,524). (back to text)

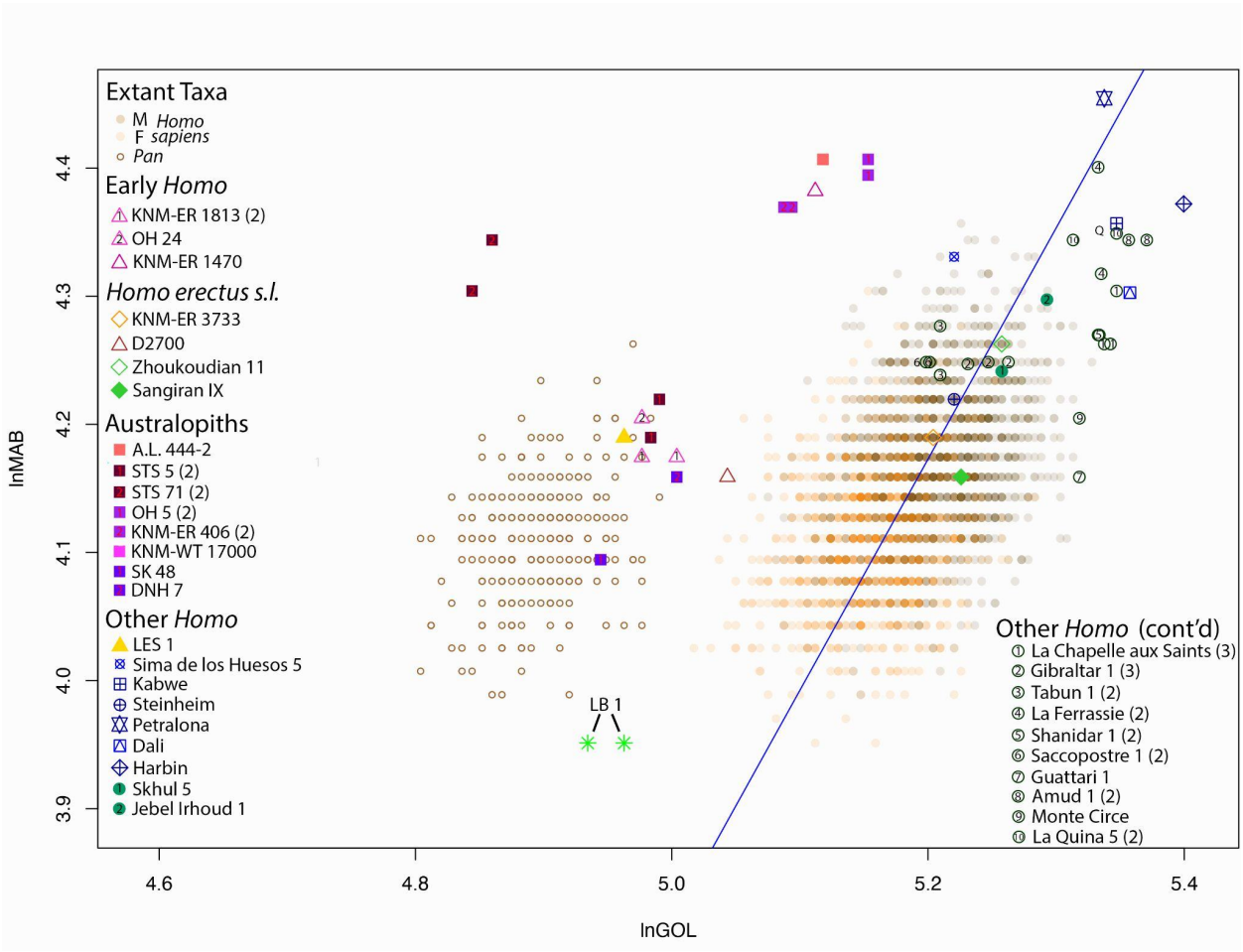

Figure 31. Bivariate scaling relationship between maxillary breadth (lnMAB) and glabella-opisthocranion length (lnGOL) as calculated in modern humans, extant great apes, and fossil hominins. The blue line is the major axis fitted line for the modern human sample. Numbers in parentheses indicate more than one published set of measurements were included for comparison. (back to text)

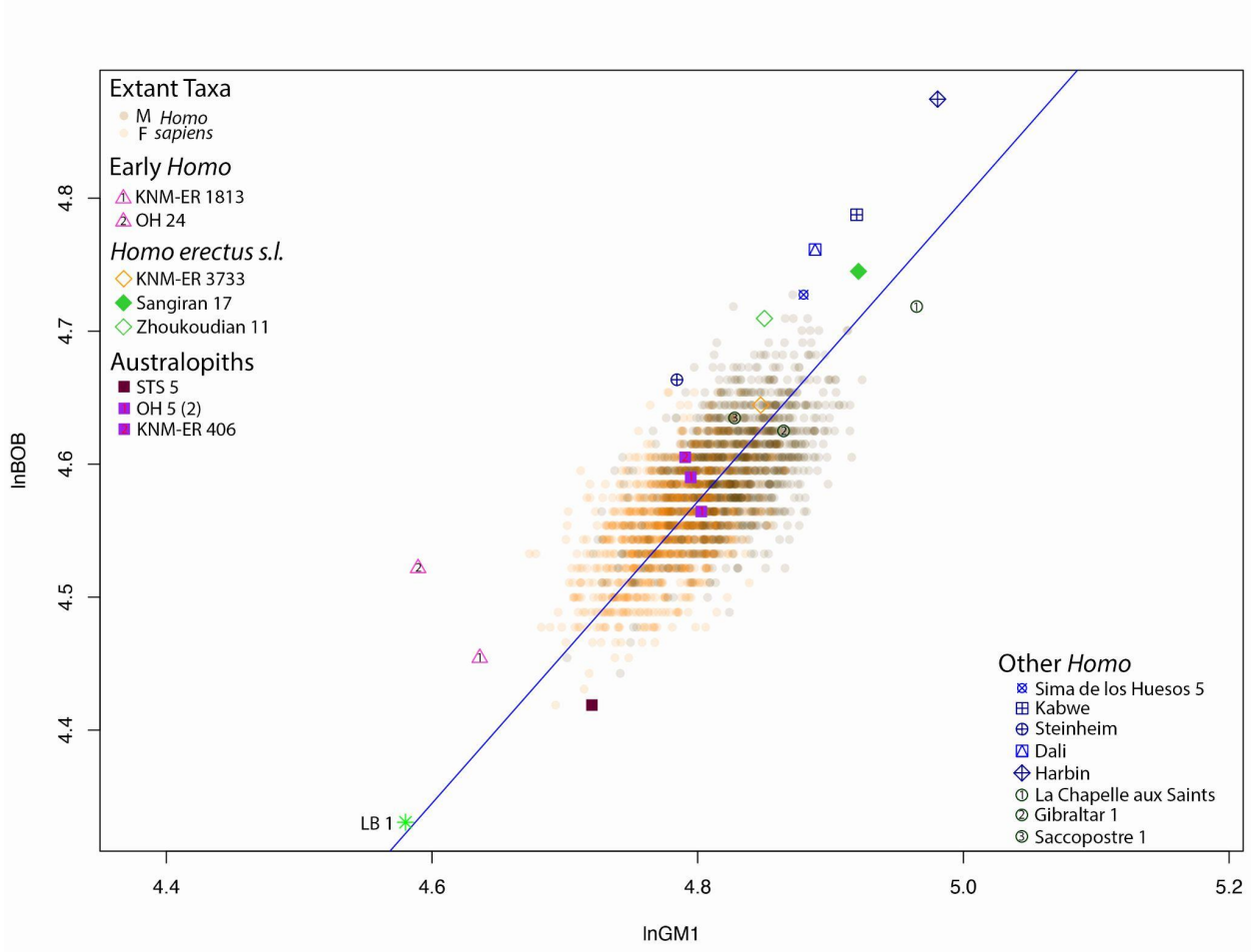

Figure 32. Bivariate scaling relationship between outer bi-orbital breadth (lnBOB) and overall cranial size (lnGM1) in modern humans and fossil hominins. The blue line is the major axis fitted line for the modern human sample (N = 2,524). (back to text).

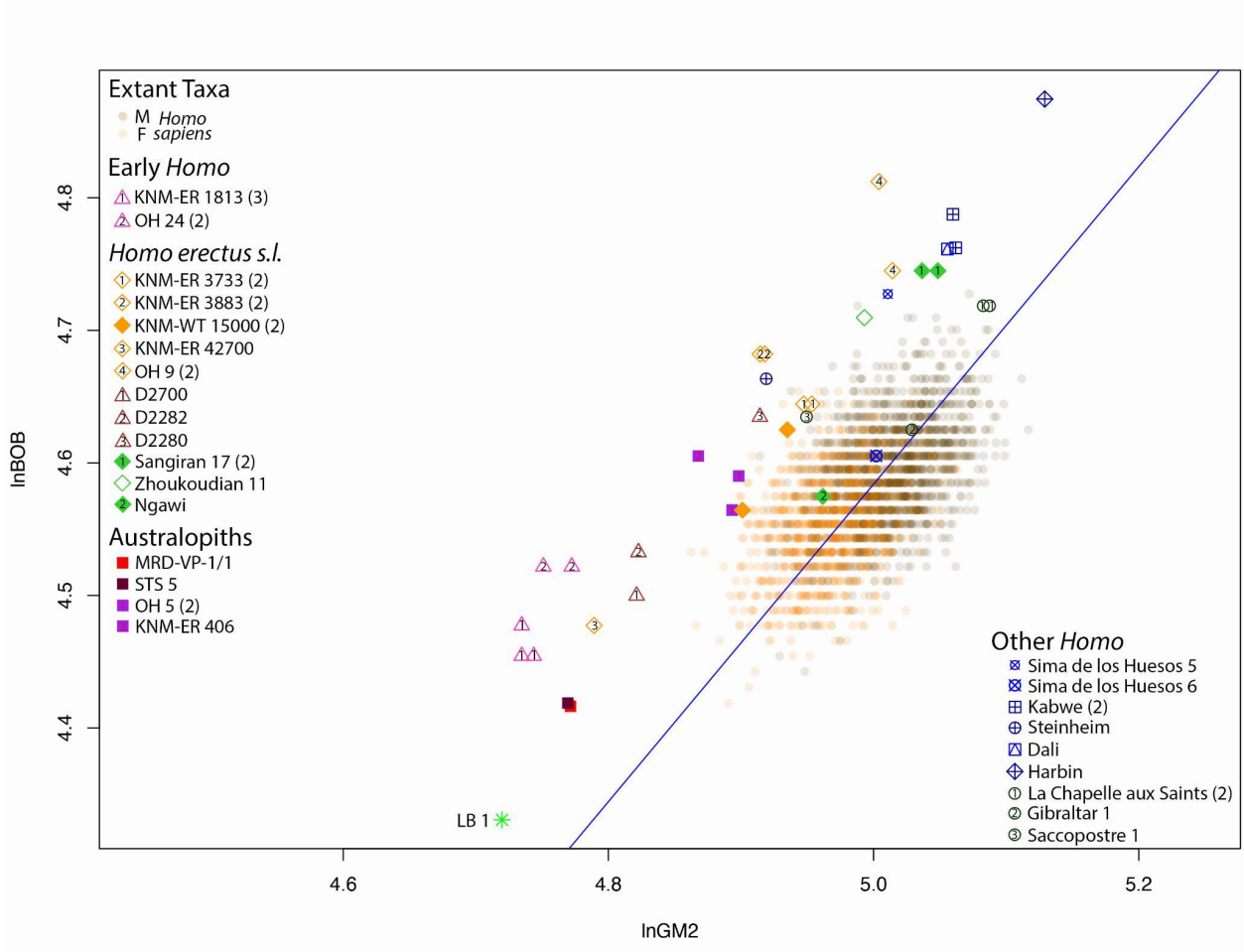

Figure 33. Bivariate scaling relationship between outer bi-orbital breadth (lnBOB) and neurocranial size (lnGM2) as calculated using maximum cranial breadth in modern humans and fossil hominins. The blue line is the major axis fitted line for the modern human sample (N = 2,524). (back to text)

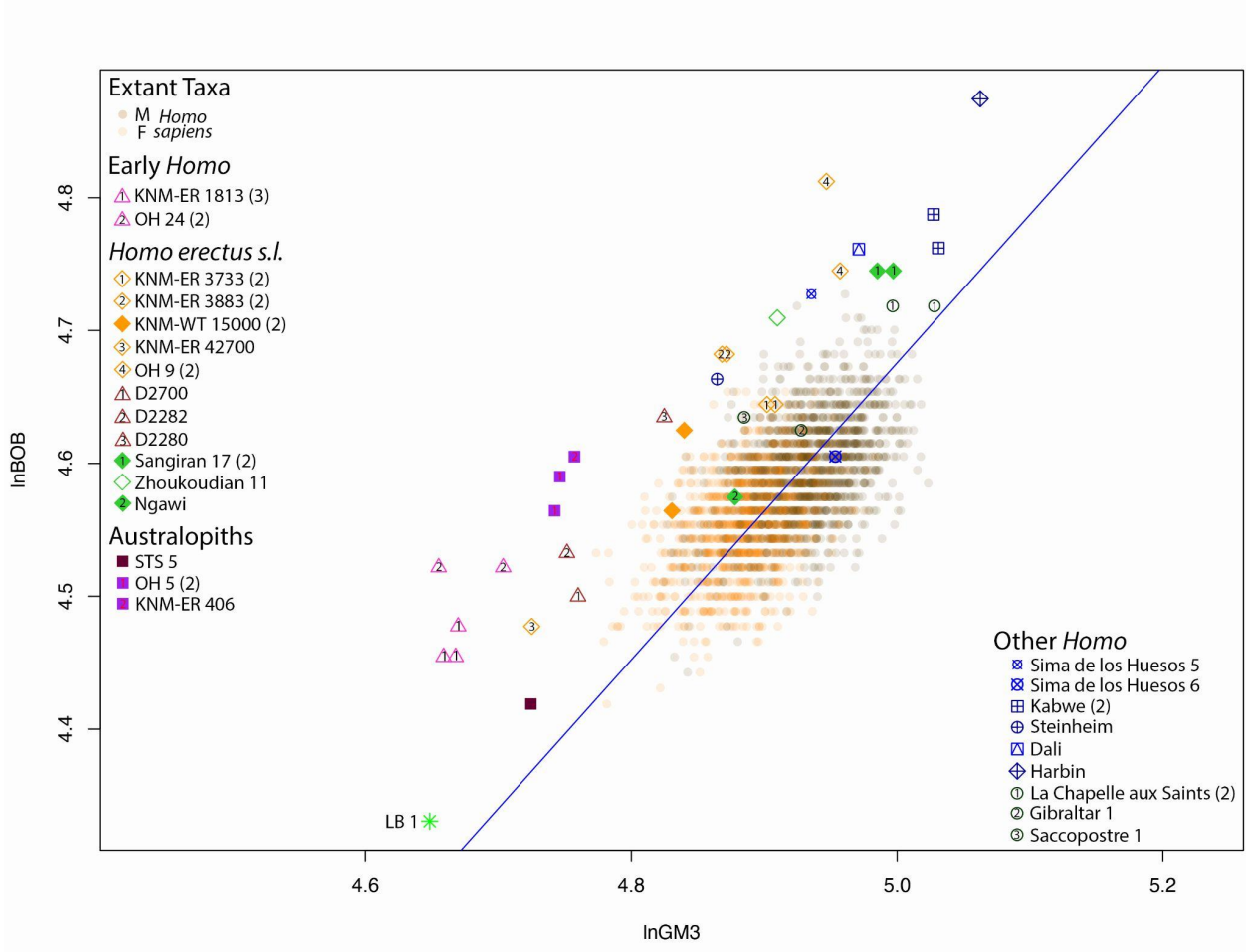

Figure 34. Bivariate scaling relationship between outer bi-orbital breadth (lnBOB) and neurocranial size (lnGM3) as calculated using asterionic breadth in modern humans and fossil hominins. The blue line is the major axis fitted line for the modern human sample (N = 2,524). (back to text)

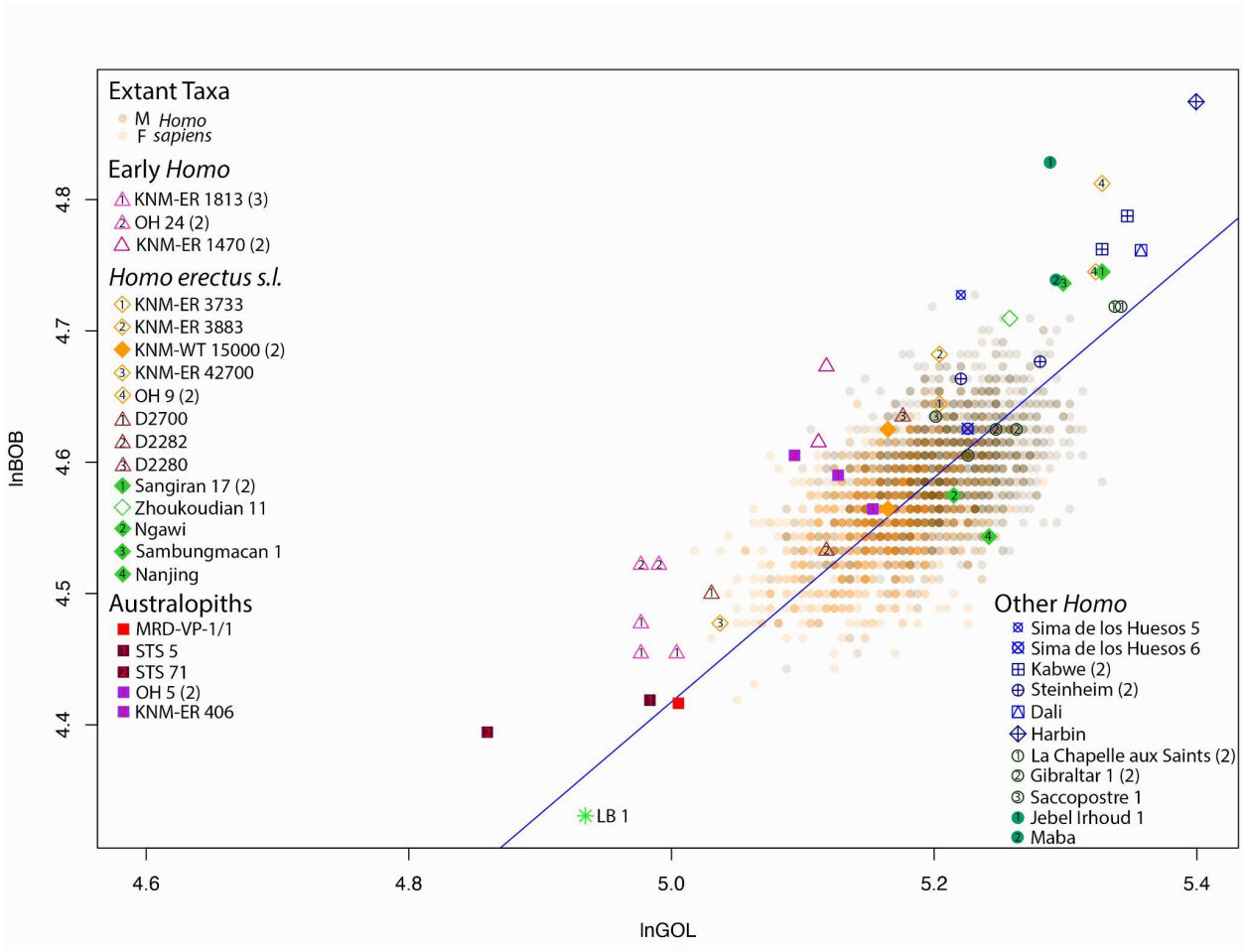

Figure 35. Bivariate scaling relationship between outer bi-orbital breadth (lnBOB) and glabella-opisthocranion length (lnGOL) as calculated in modern humans, extant great apes, and fossil hominins. The blue line is the major axis fitted line for the modern human sample. Numbers in parentheses indicate more than one published set of measurements were included for comparison. (back to text)

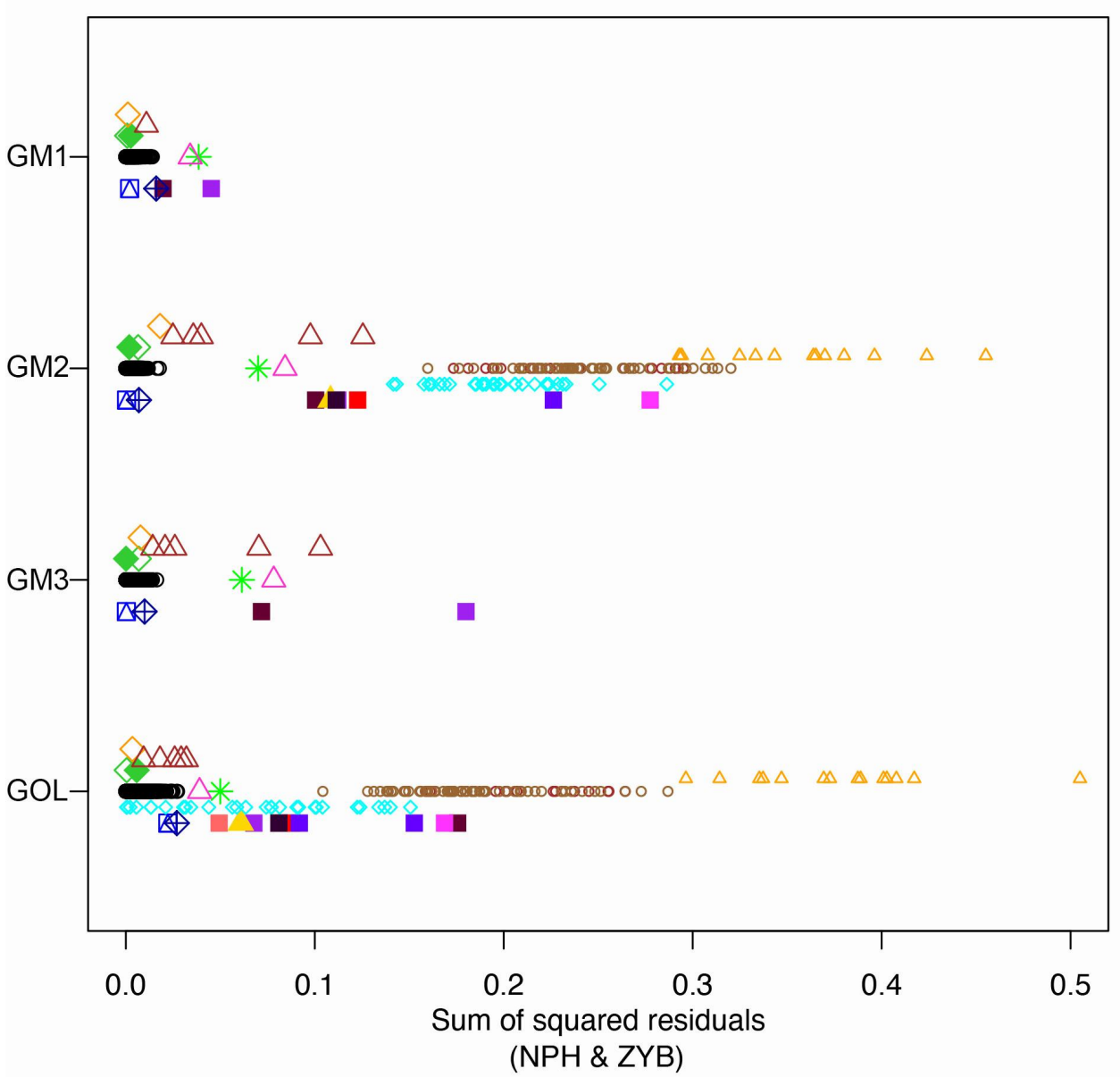

Figure 36. Visual representation of the sum of squared residuals of the NPH and ZYB for fossil and extant taxa compared when fitted against the sum of squared residuals of the NPH and ZYB for modern humans. Symbols are the same as previous figures. (back to text) (back to Discussion).

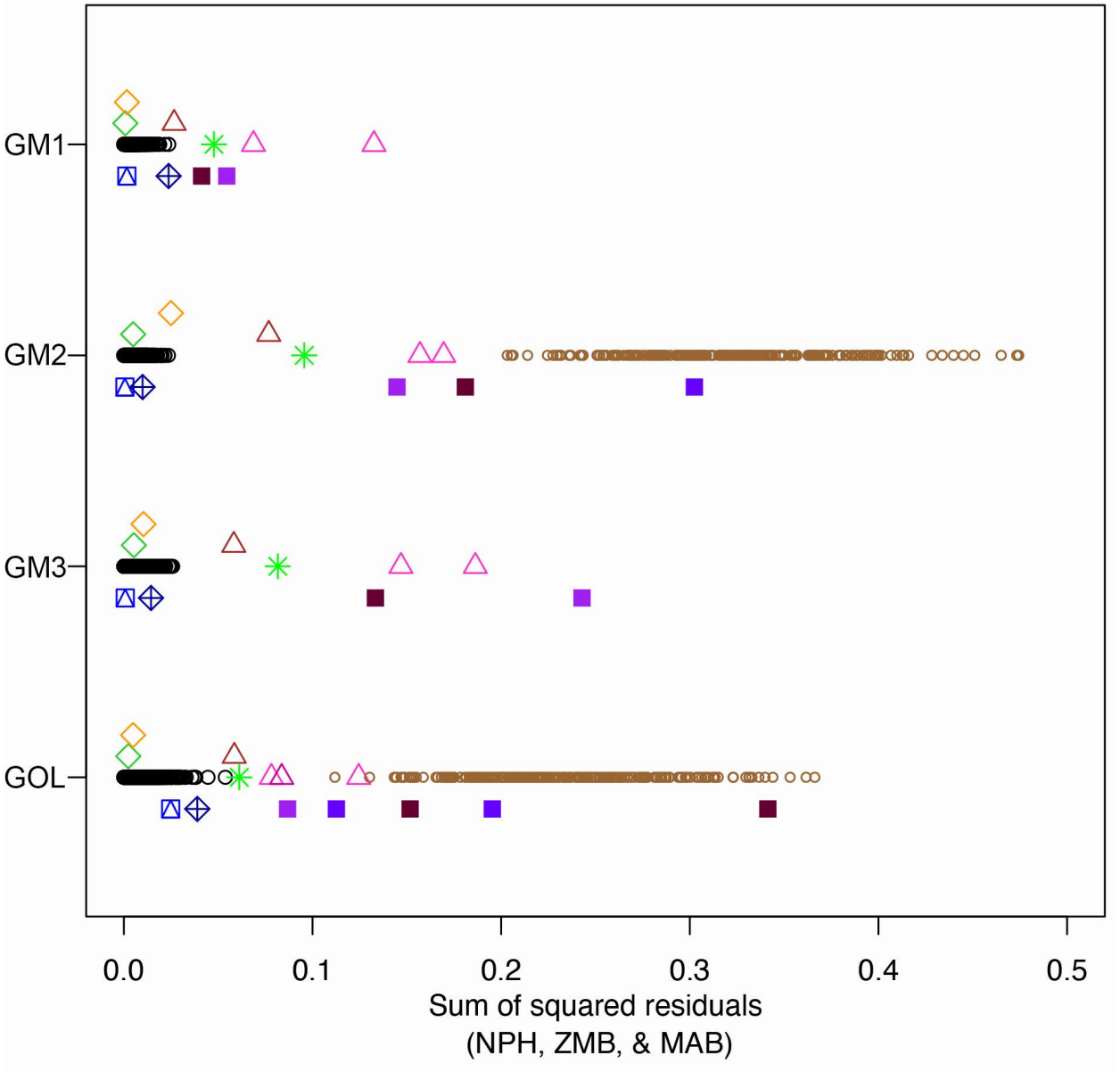

Figure 37. Visual representation of the sum of squared residuals of the NPH, ZMB, ZYB, and BOB for fossil and extant taxa compared when fitted against the sum of squared residuals of the NPH, ZMB, ZYB, and BOB, for modern humans. Symbols are the same as previous figures (back to text).

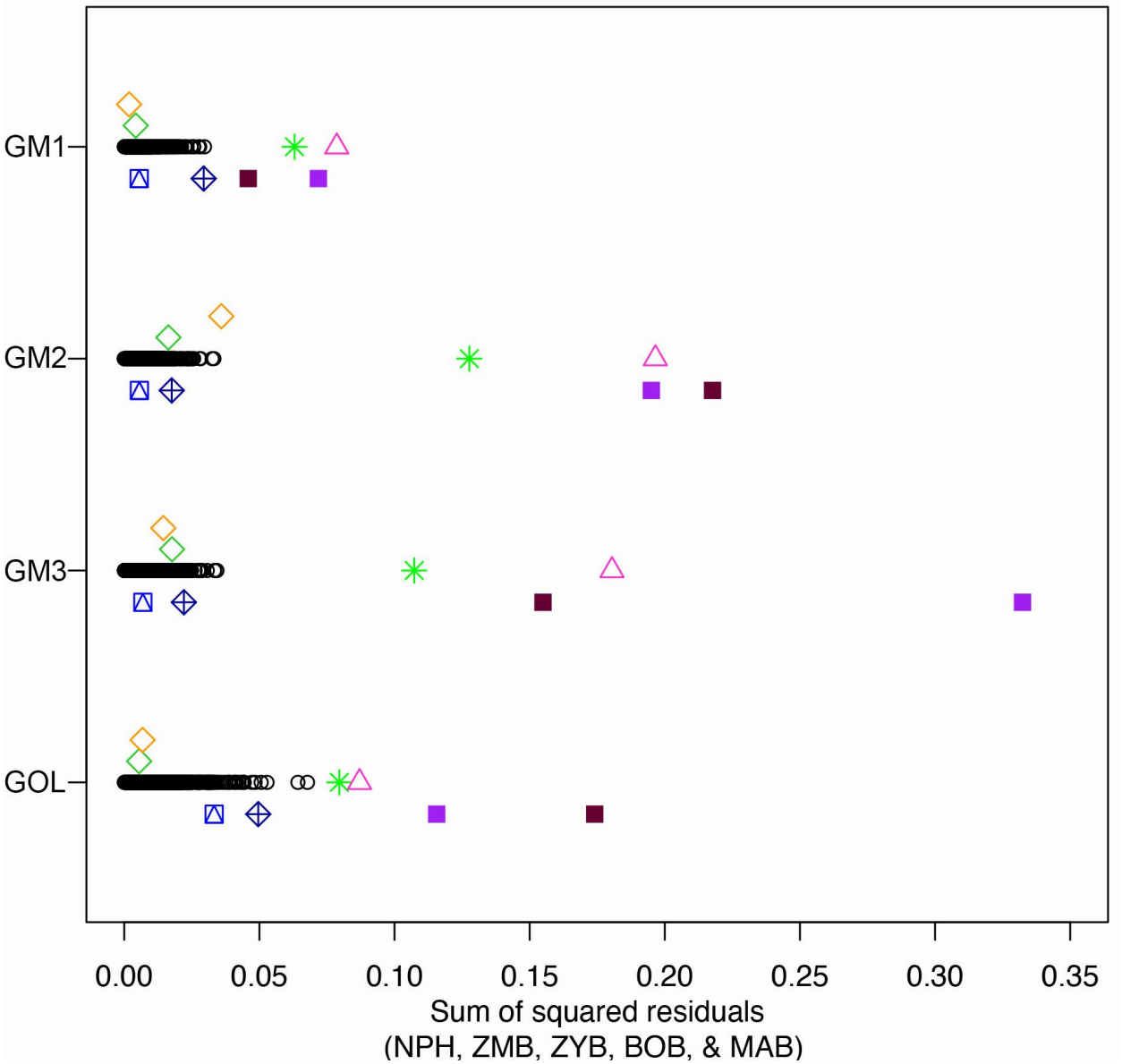

Figure 38. Visual representation of the sum of squared residuals of the NPH, ZMB, ZYB, BOB, and MAB for fossil and extant taxa compared when fitted against the sum of squared residuals of the NPH, ZMB, ZYB, BOB, and MAB for modern humans. Symbols are the same as previous figures. (back to text).

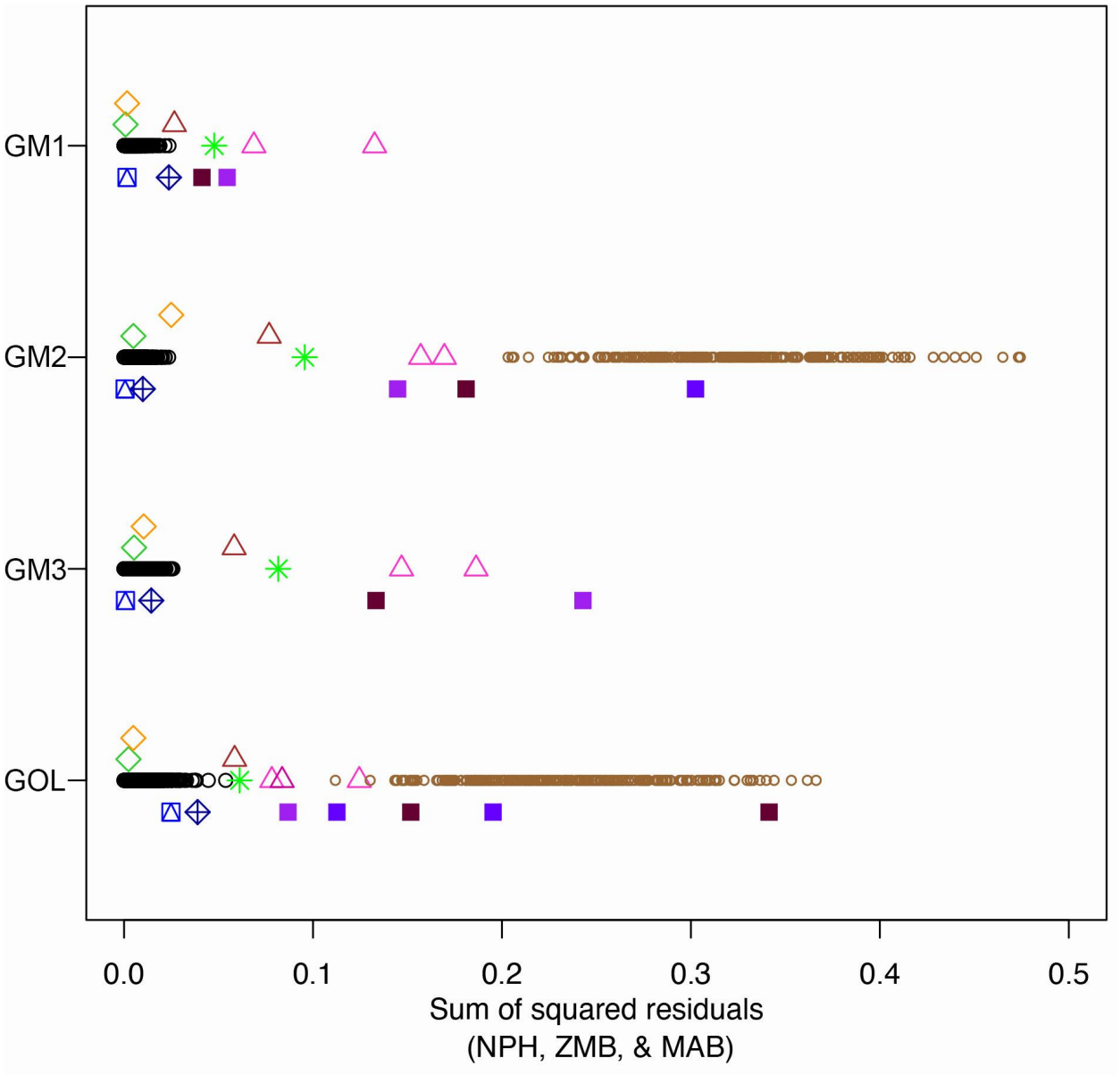

Figure 39. Visual representation of the sum of squared residuals of the NPH, ZMB, and MAB for fossil and extant taxa compared when fitted against the sum of squared residuals of the NPH, ZMB, and MAB for modern humans. Symbols are the same as previous figures. (back to text).

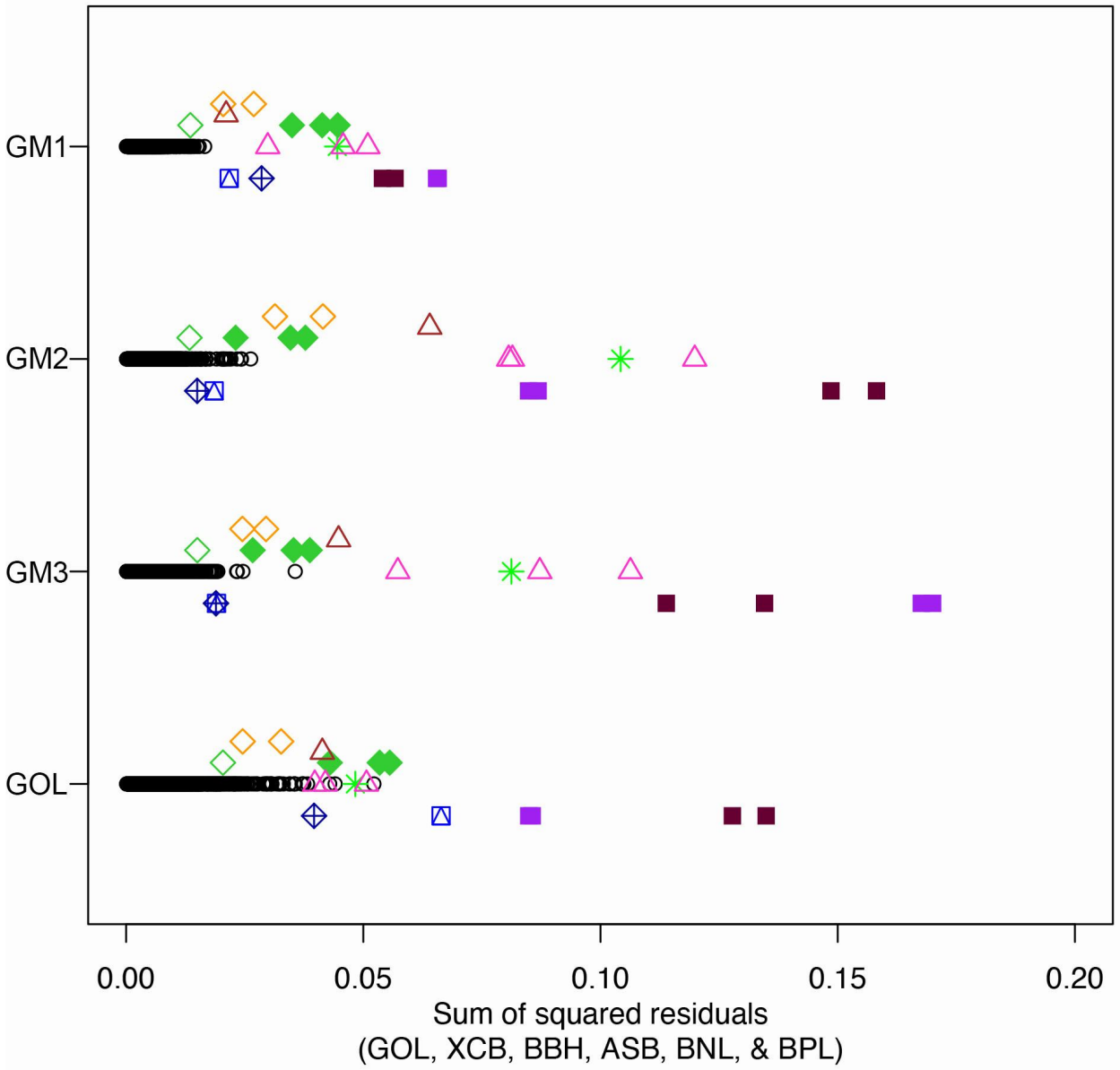

Figure 40. Visual representation of the sum of squared residuals of the GM1 neurocranial variables for fossil and extant taxa compared when fitted against the sum of squared residuals of the GM1 neurocranial variables for modern humans GM1–3. GOL sum of squared residuals axis excludes GOL. Symbols are the same as previous figures. (back to text).

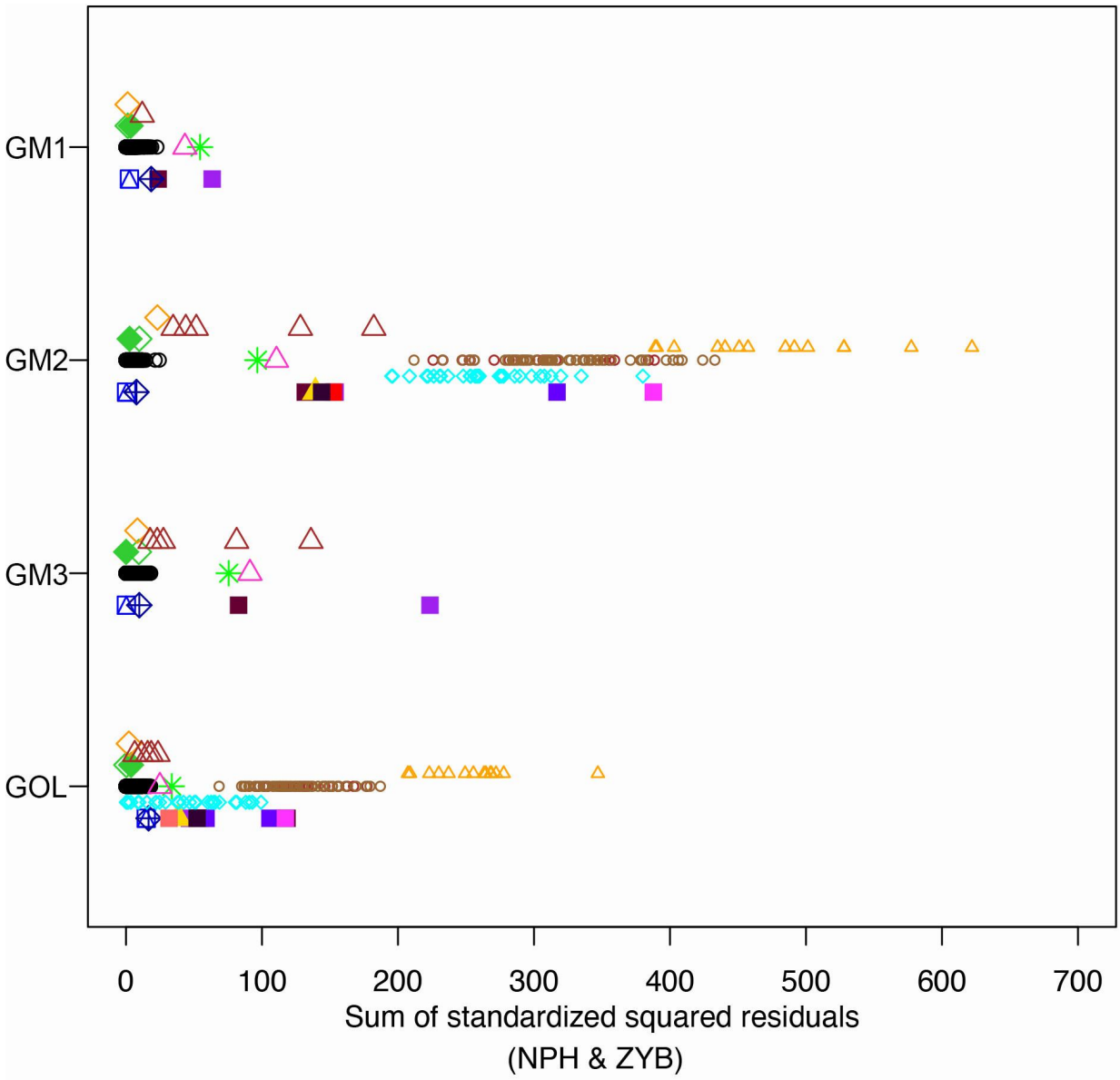

Figure 41. Visual representation of the sum of standardized squared residuals of the NPH and ZYB for fossil and extant taxa compared when fitted against the sum of standardized squared residuals of the NPH and ZYB for modern humans. Symbols are the same as previous figures. (back to text).

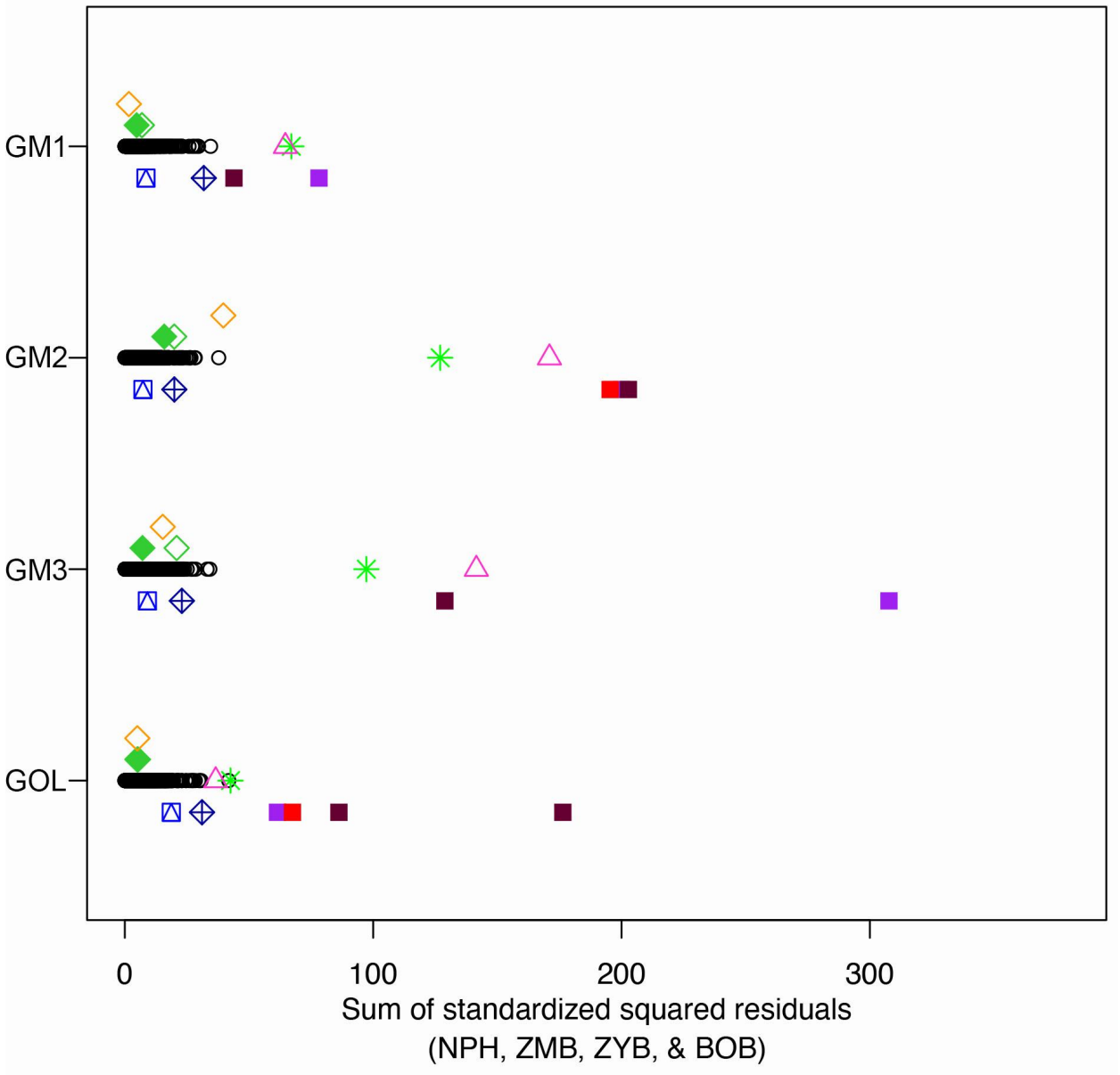

Figure 42. Visual representation of the sum of standardized squared residuals of the NPH, ZMB, ZYB, and BOB for fossil and extant taxa compared when fitted against the sum of standardized squared residuals of the NPH, ZMB, ZYB, and BOB for modern humans. Symbols are the same as previous figures. (back to text).

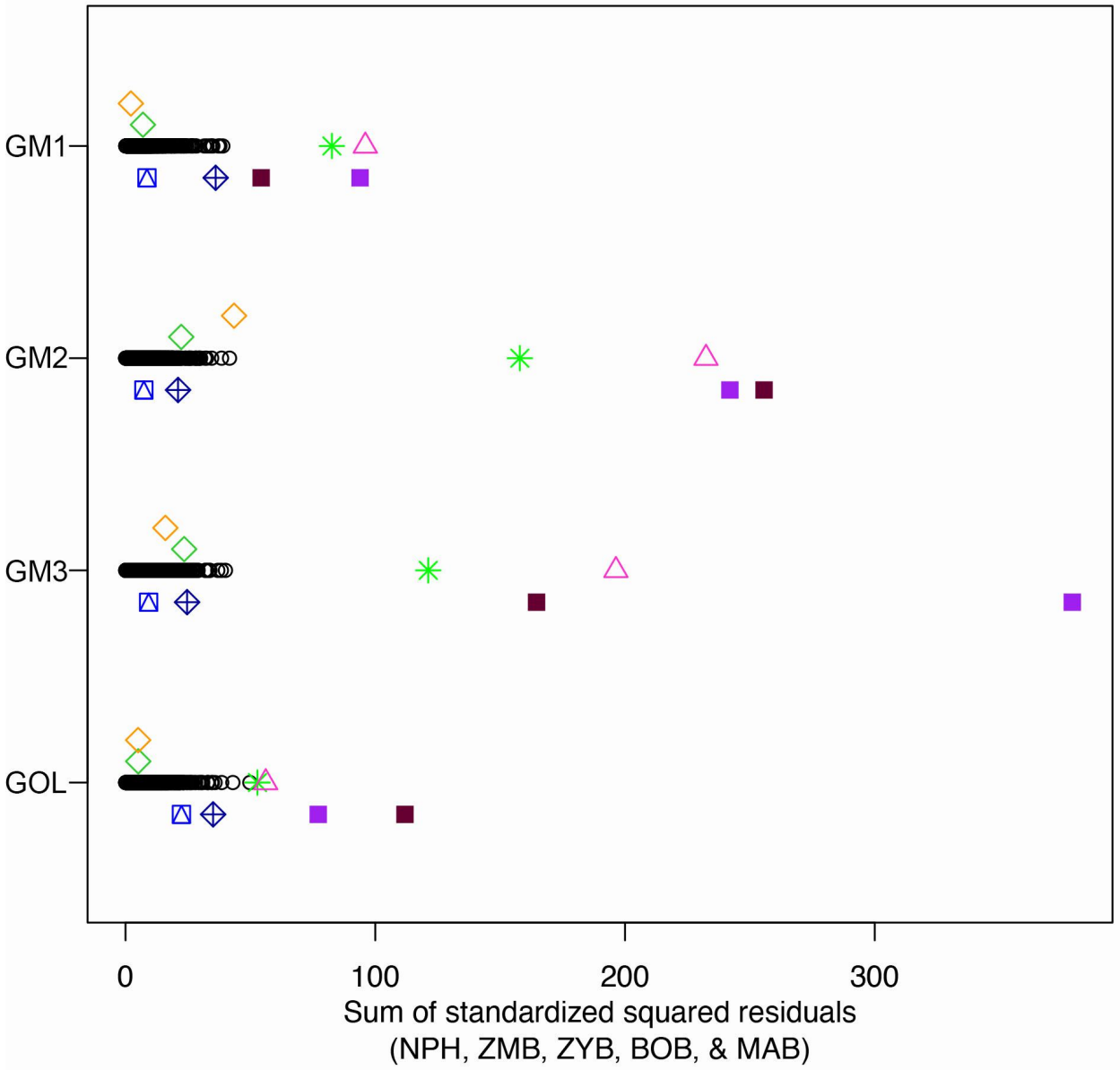

Figure 43. Visual representation of the sum of standardized squared residuals of the NPH, ZMB, ZYB, BOB, and MAB for fossil and extant taxa compared when fitted against the sum of standardized squared residuals of the NPH, ZMB, ZYB, BOB, and MAB for modern humans. Symbols are the same as previous figures. (back to text).

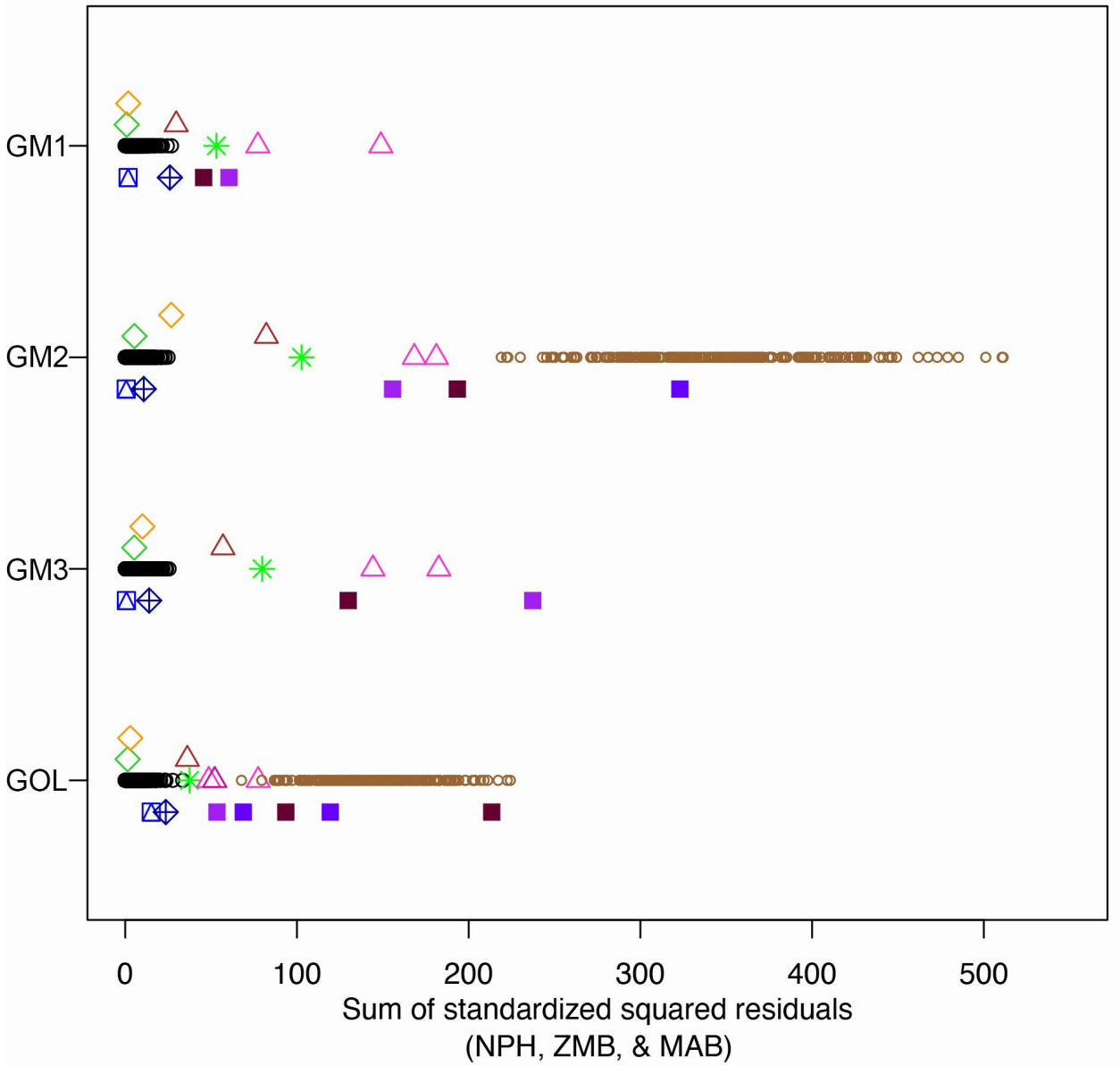

Figure 44. Visual representation of the sum of standardized squared residuals of the NPH, ZMB, and MAB for fossil and extant taxa compared when fitted against the sum of standardized squared residuals of the NPH, ZMB, and MAB for modern humans. Symbols are the same as previous figures. (back to text).

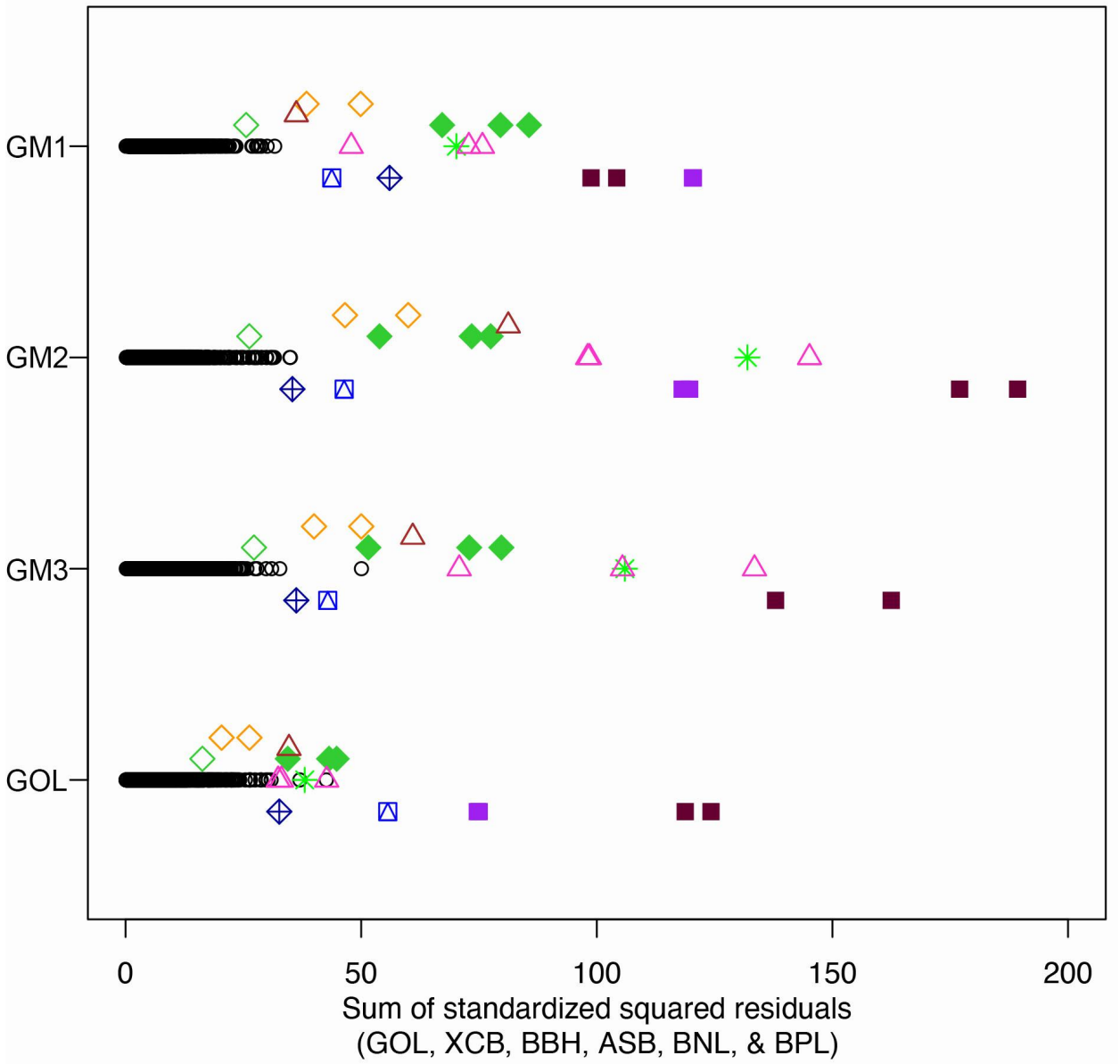

Figure 45. Visual representation of the sum of standardized squared residuals of the GM1 neurocranial variables for fossil and extant taxa compared when fitted against the sum of standardized squared residuals of the GM1 neurocranial variables for modern humans GM1–3, GOL sum of standardized squared residuals axis excludes GOL. Symbols are the same as previous figures. (back to text).

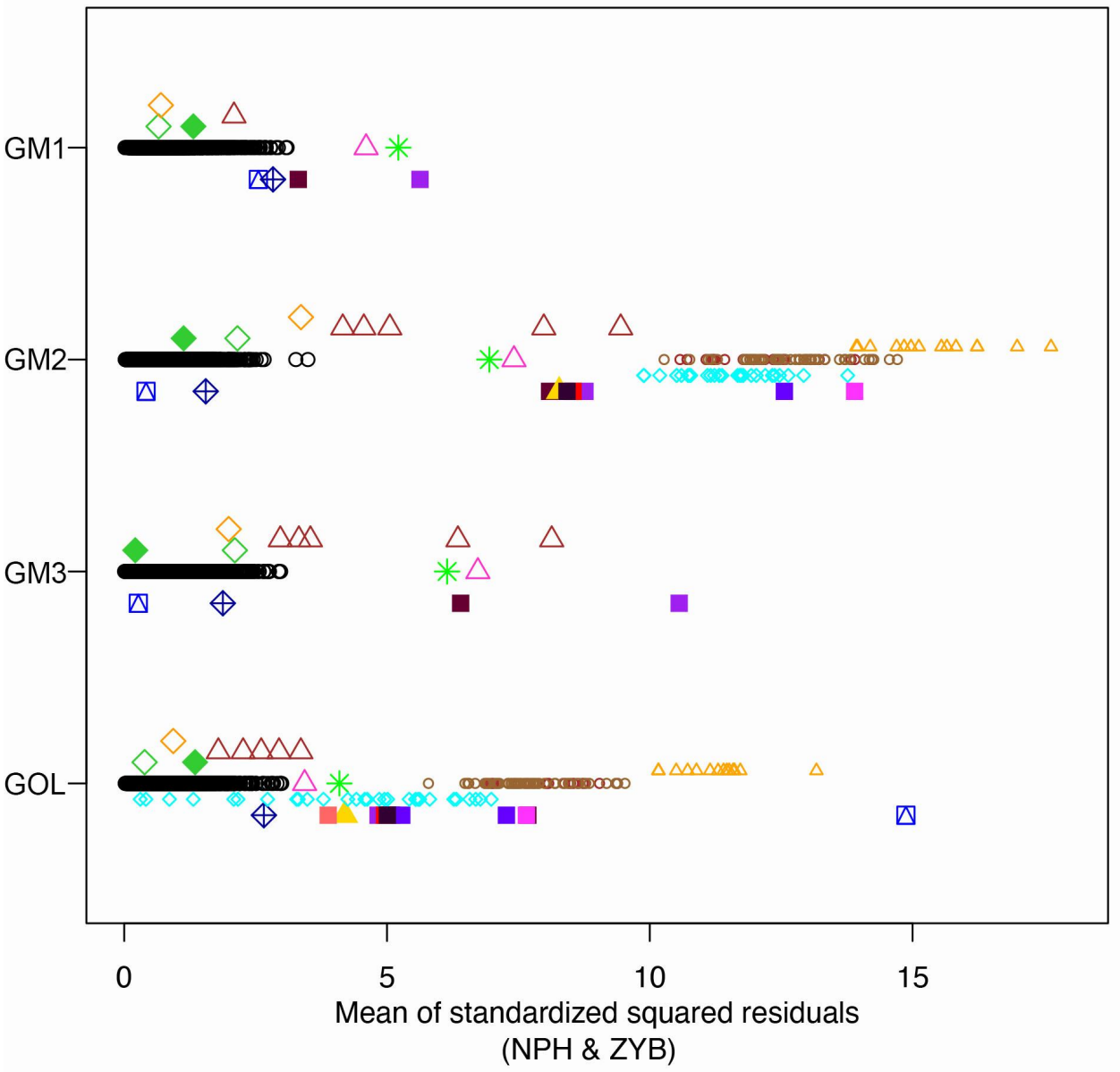

Figure 46. Visual representation of the mean of standardized squared residuals of the NPH and ZYB for fossil and extant taxa compared when fitted against the mean of standardized squared residuals of the NPH and ZYB for modern humans. Symbols are the same as previous figures. (back to text).

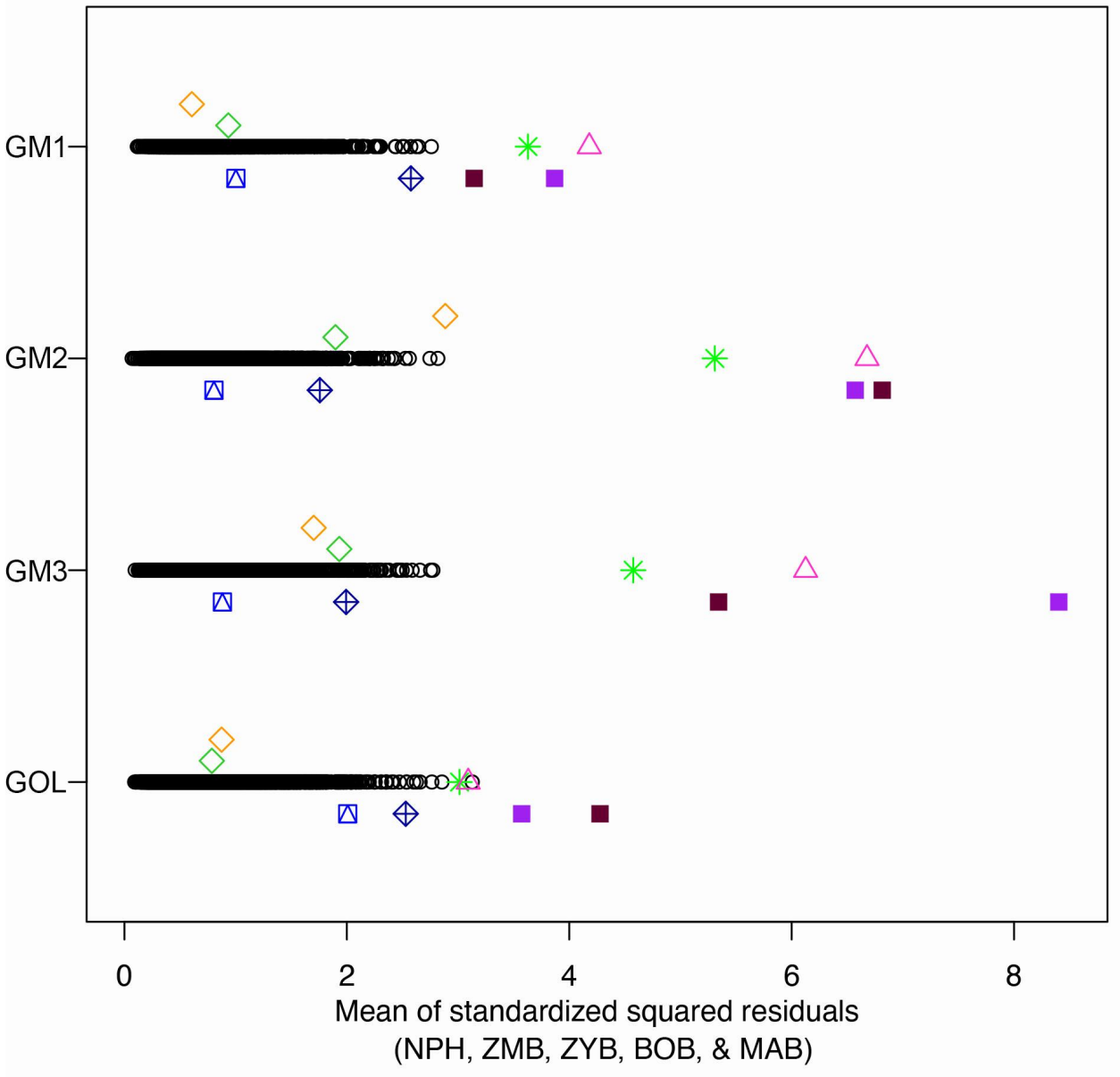

Figure 47. Visual representation of the mean of standardized squared residuals of the NPH, ZMB, ZYB, BOB, and MAB for fossil and extant taxa compared when fitted against the mean of standardized squared residuals of the NPH, ZMB, ZYB, BOB, and MAB for modern humans. Symbols are the same as previous figures. (back to text).

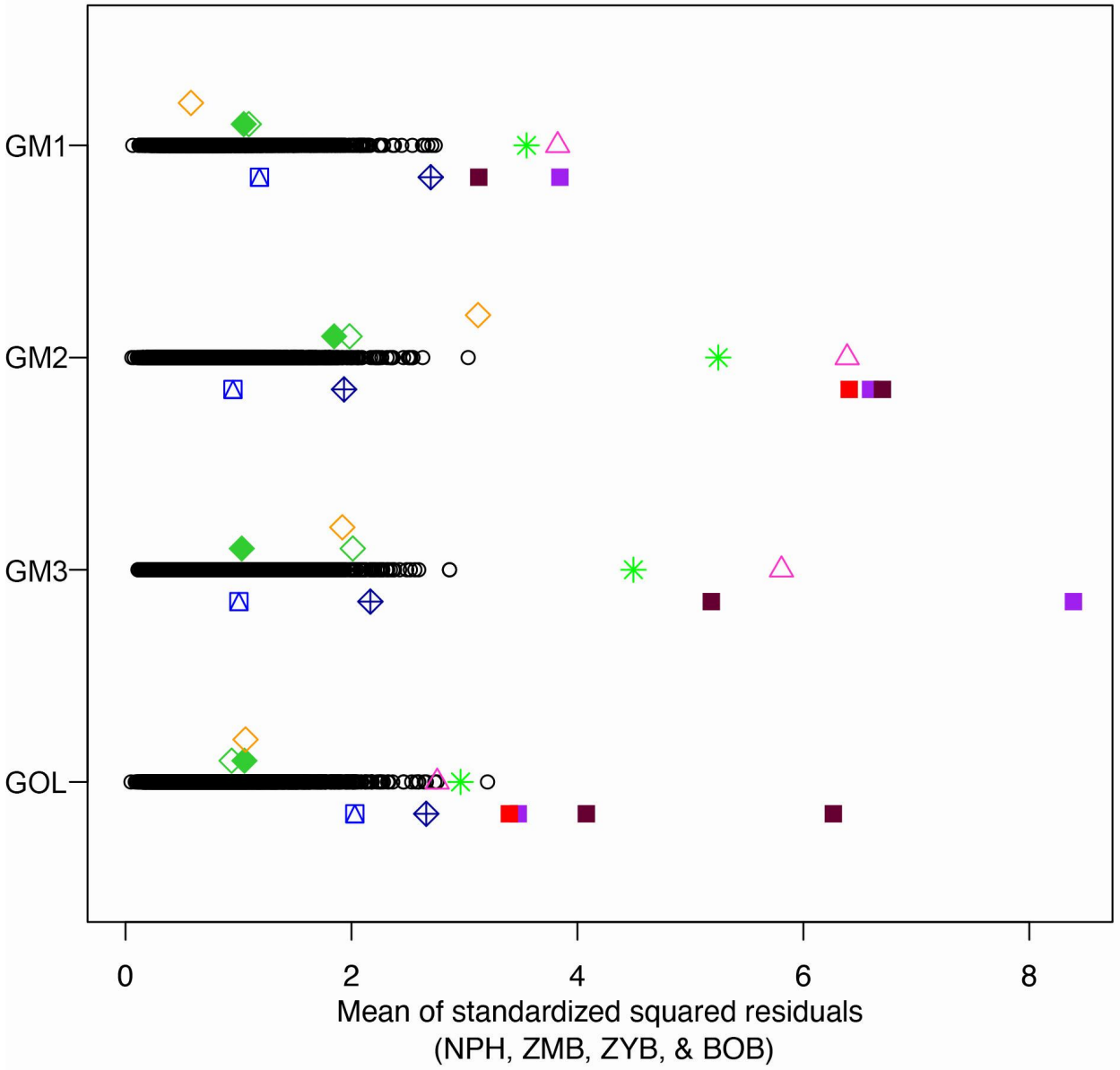

Figure 48. Visual representation of the mean of standardized squared residuals of the NPH, ZMB, ZYB, and BOB for fossil and extant taxa compared when fitted against the mean of standardized squared residuals of the NPH, ZMB, ZYB, and BOB for modern humans. Symbols are the same as previous figures. (back to text).

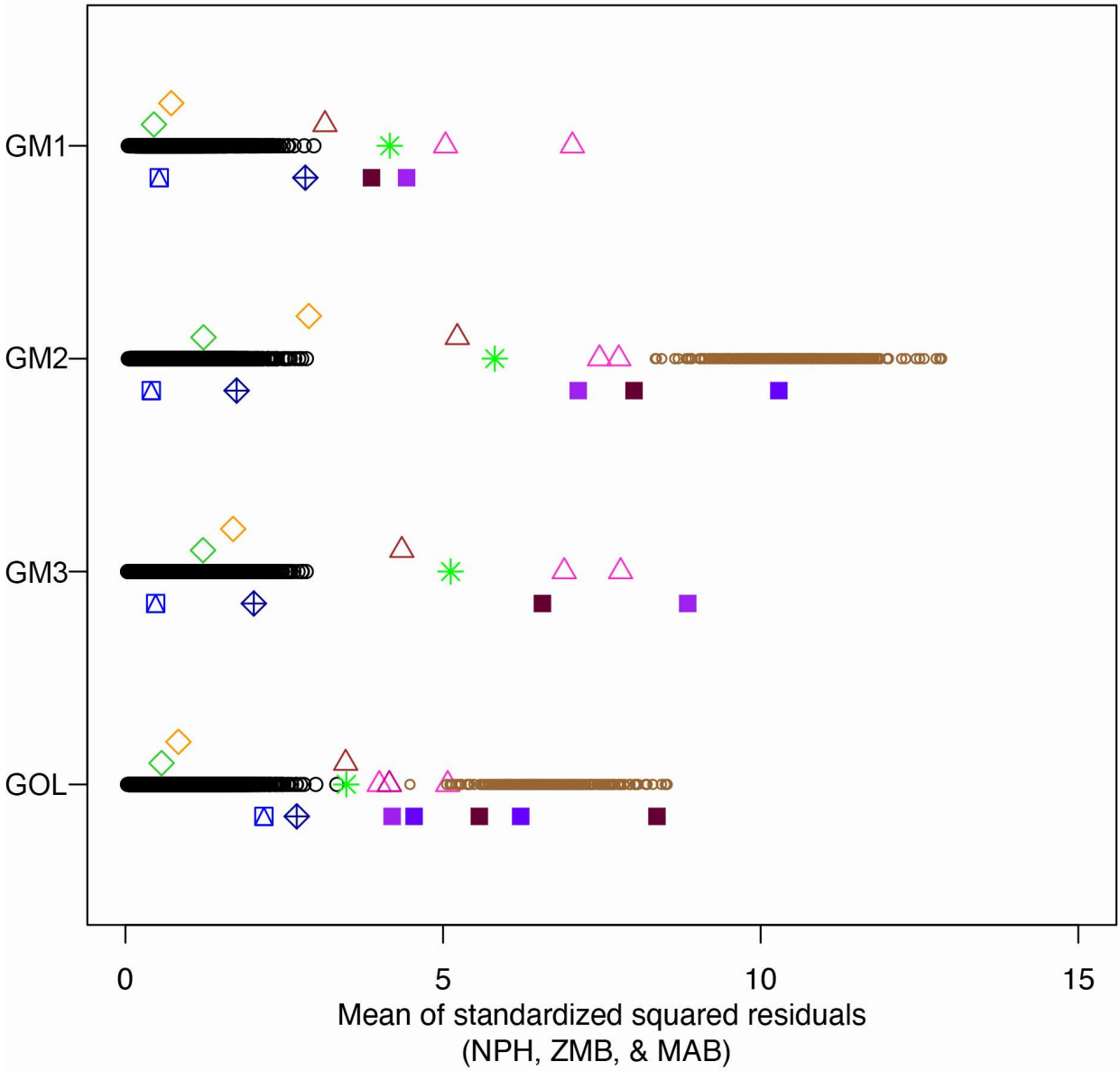

Figure 49. Visual representation of the mean of standardized squared residuals of the NPH, ZMB, and MAB for fossil and extant taxa compared when fitted against the mean of standardized squared residuals of the NPH, ZMB, and MAB for modern humans. Symbols are the same as previous figures. (back to text).

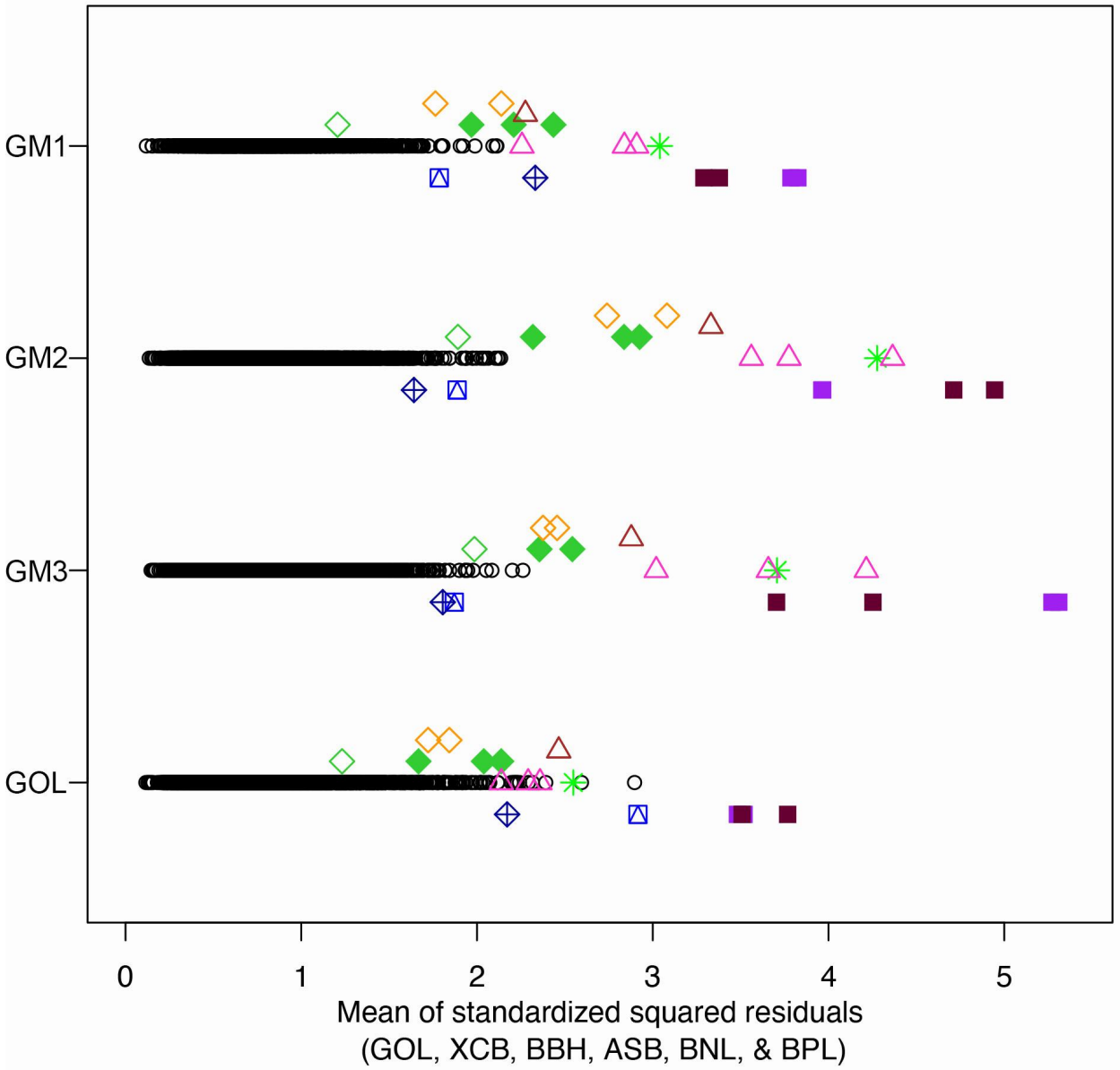

Figure 50. Visual representation of the mean of standardized squared residuals of the GM1 neurocranial variables for fossil and extant taxa compared when fitted against the mean of standardized squared residuals of the GM1 neurocranial variables for modern humans GM1–3, GOL mean of standardized squared residuals axis excludes GOL. Symbols are the same as previous figures. (back to text).

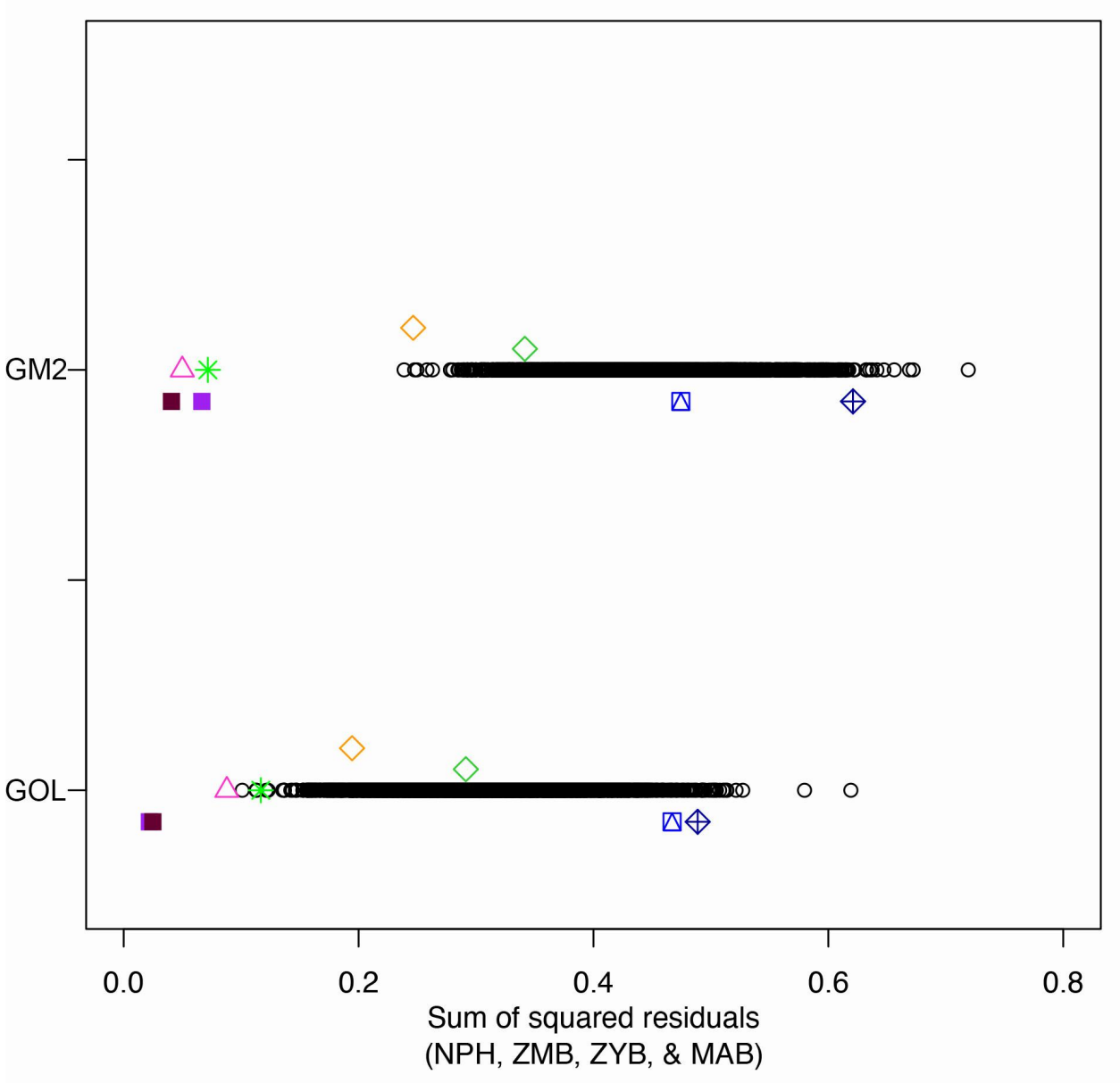

Figure 51. Visual representation of the sum of squared residuals of the NPH, ZMB, ZYB, and MAB for fossil and extant taxa compared when fitted against the sum of squared residuals of the NPH, ZMB, ZYB, and MAB for all great ape taxa. Symbols are the same as previous figures. (back to text).

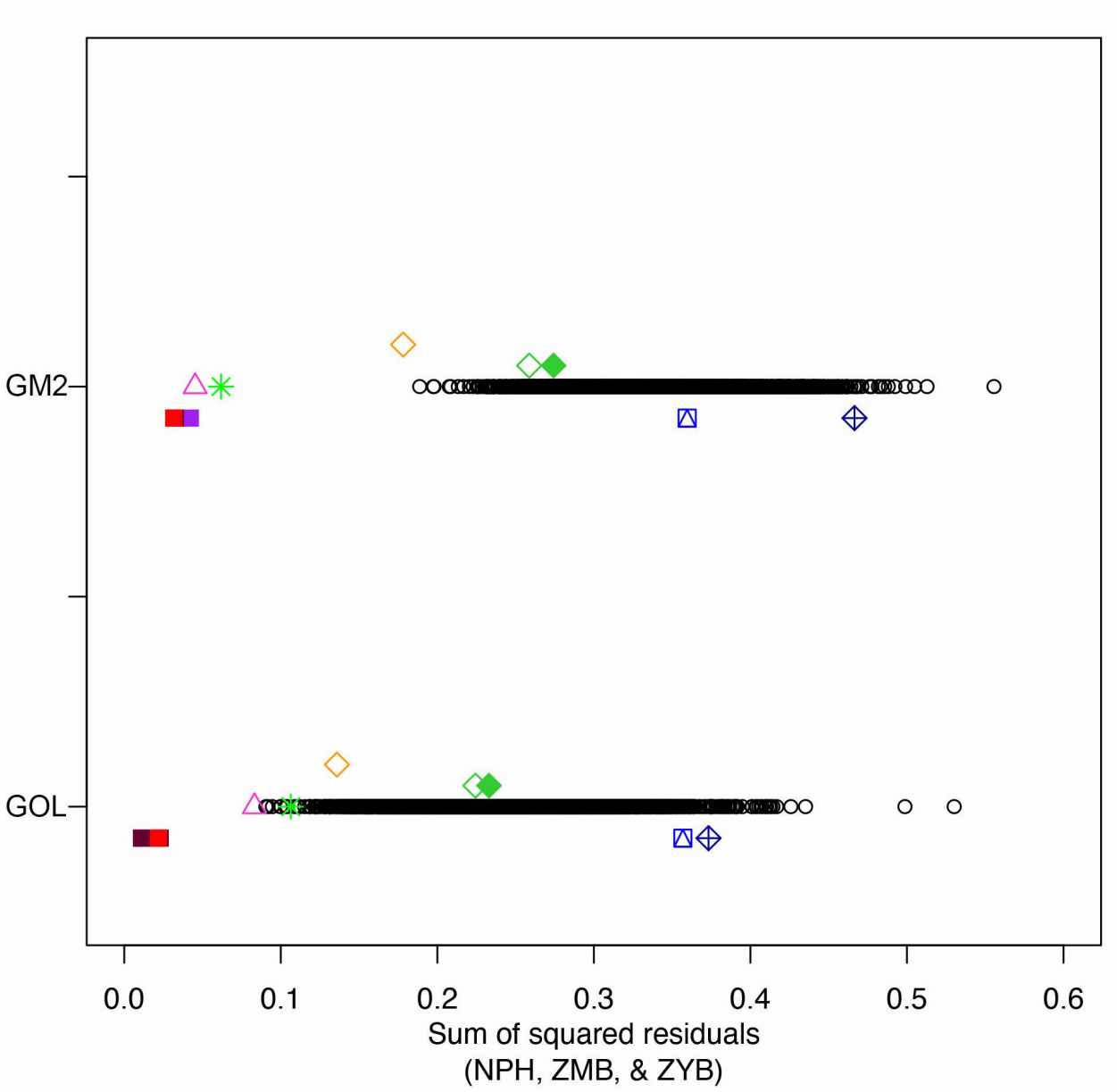

Figure 52. Visual representation of the sum of squared residuals of the NPH, ZMB, and ZYB for fossil and extant taxa compared when fitted against the sum of squared residuals of the NPH, ZMB, and ZYB for all great ape taxa. Symbols are the same as previous figures. (back to text).

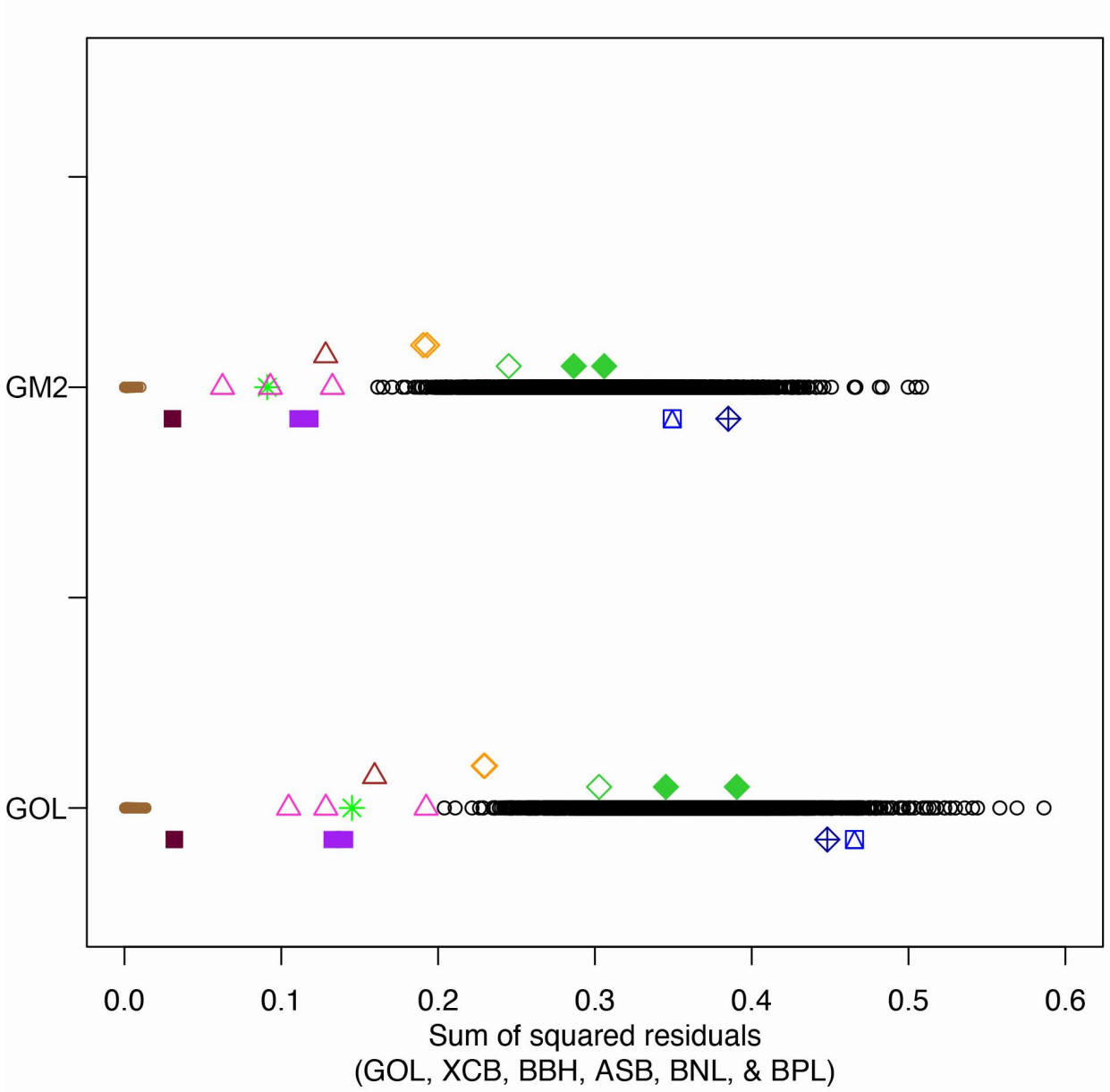

Figure 53. Visual representation of the sum of squared residuals of the GM1 neurocranial variables for fossil and extant taxa compared when fitted against the sum of squared residuals of the GM1 neurocranial variables for all great ape taxa GM2 and GOL, GOL sum of squared residuals axis excludes GOL. Symbols are the same as previous figures. (back to text).

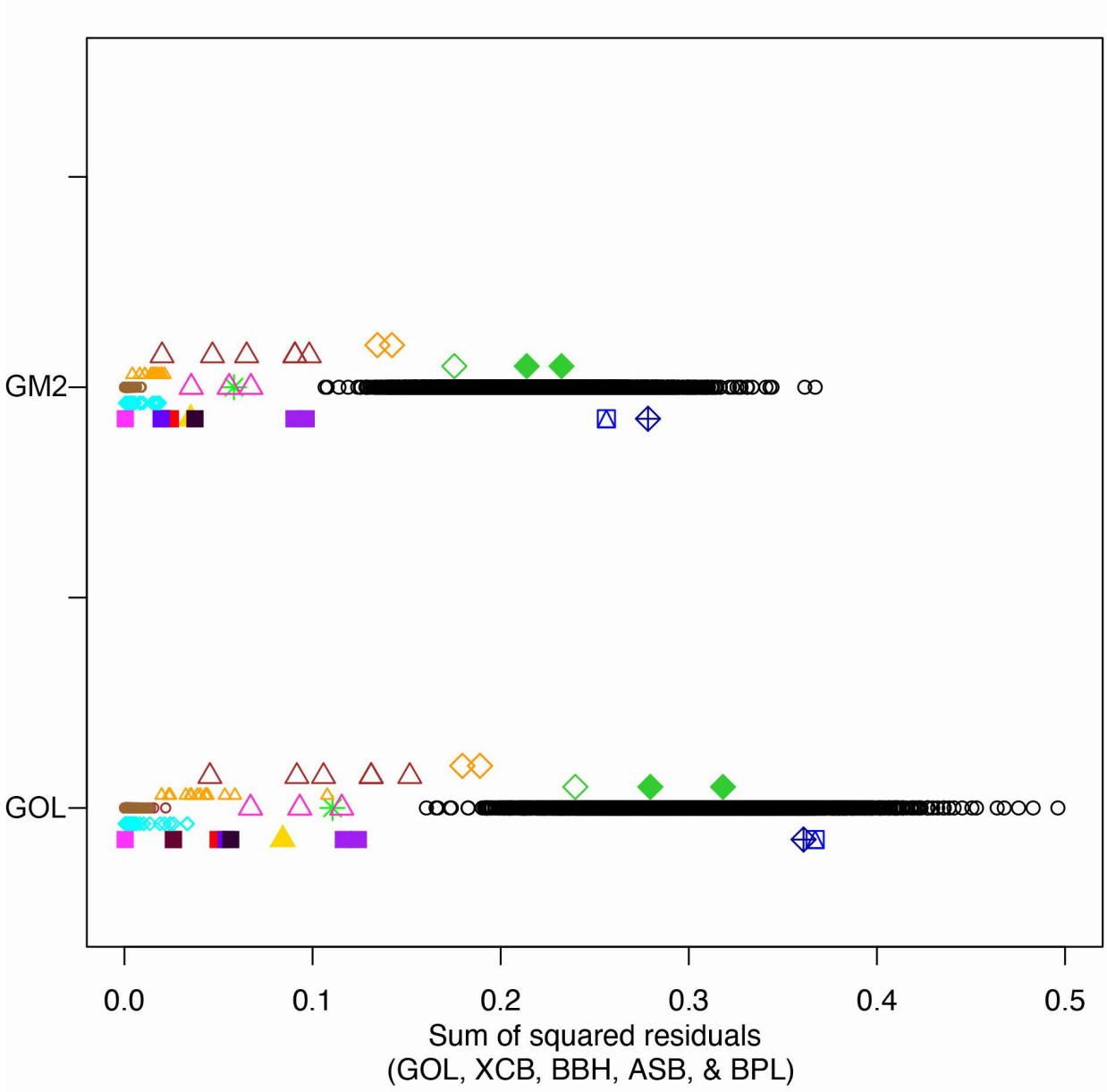

Figure 54. Visual representation of the sum of squared residuals of the GM1 neurocranial variables (BNL removed) for fossil and extant taxa compared when fitted against the sum of squared residuals of the GM1 neurocranial variables (BNL removed) for all great ape taxa GM2 and GOL, GOL sum of squared residuals axis excludes GOL. Symbols are the same as previous figures. (back to text).

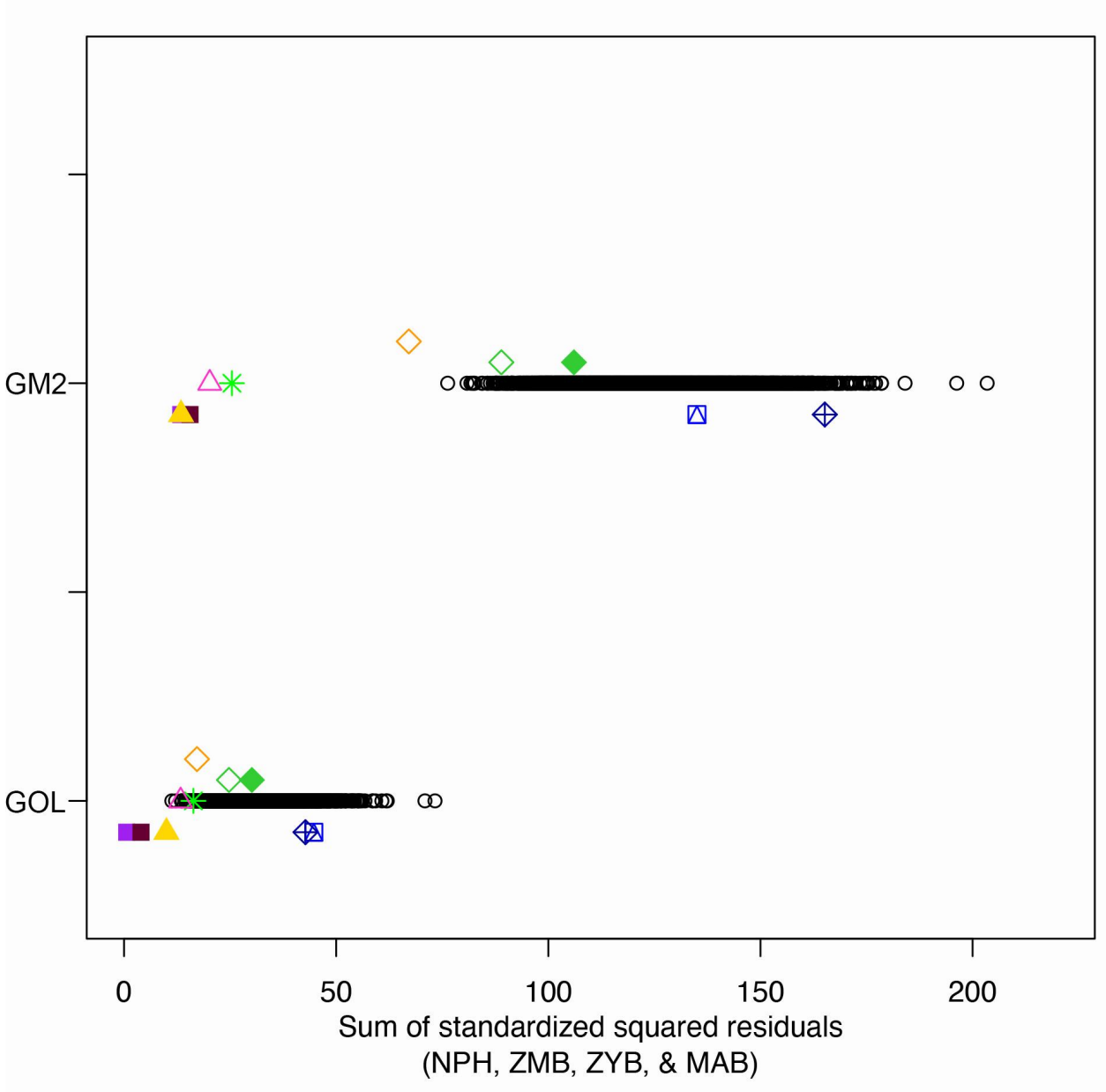

Figure 55. Visual representation of the sum of standardized squared residuals of the NPH, ZMB, ZYB, and MAB for fossil and extant taxa compared when fitted against the sum of standardized squared residuals of the NPH, ZMB, ZYB, and MAB for all great ape taxa. Symbols are the same as previous figures. (back to text).

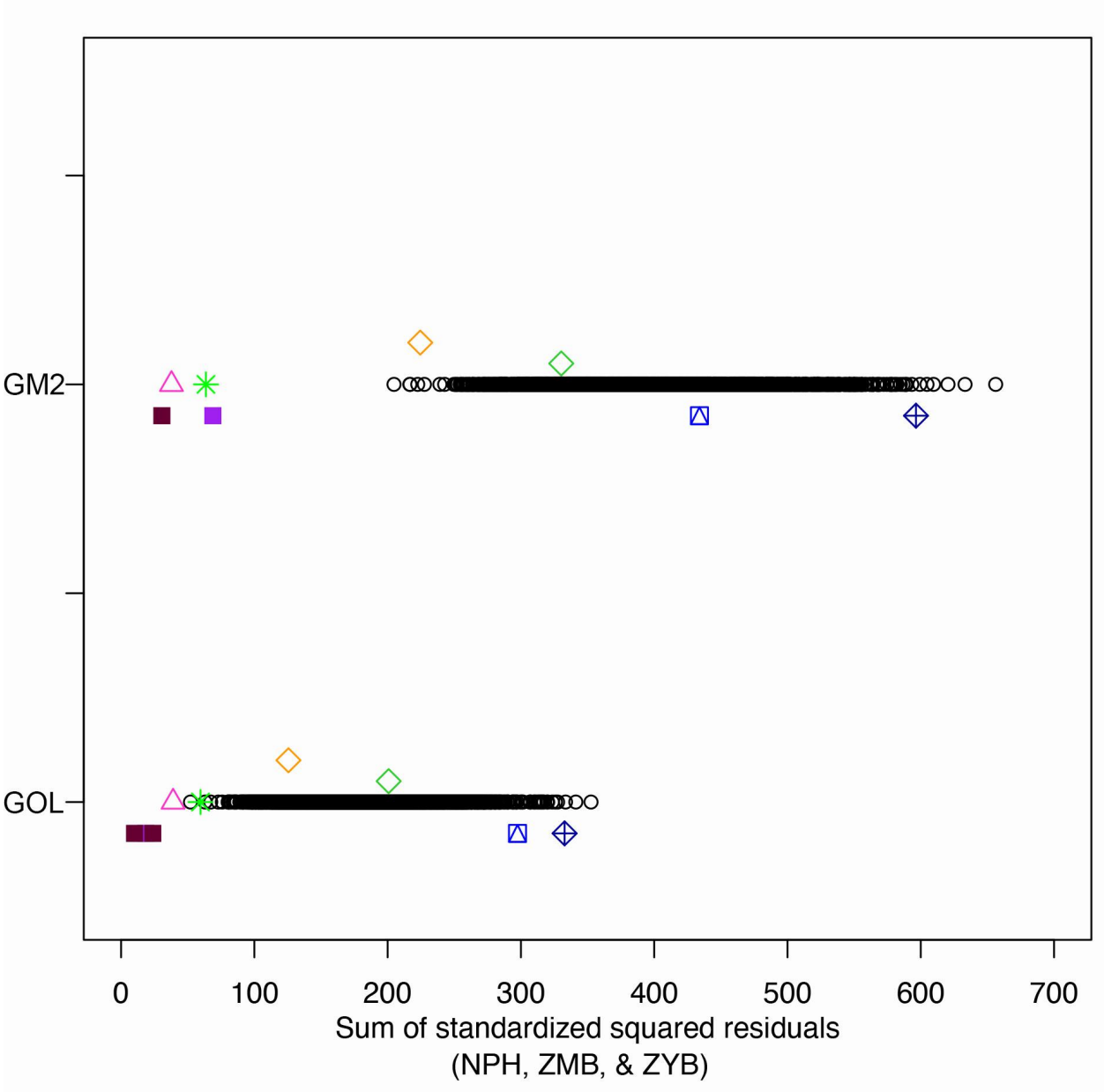

Figure 56. Visual representation of the sum of standardized squared residuals of the NPH, ZMB, and ZYB for fossil and extant taxa compared when fitted against the sum of standardized squared residuals of the NPH, ZMB, and ZYB for all great ape taxa. Symbols are the same as previous figures. (back to text).

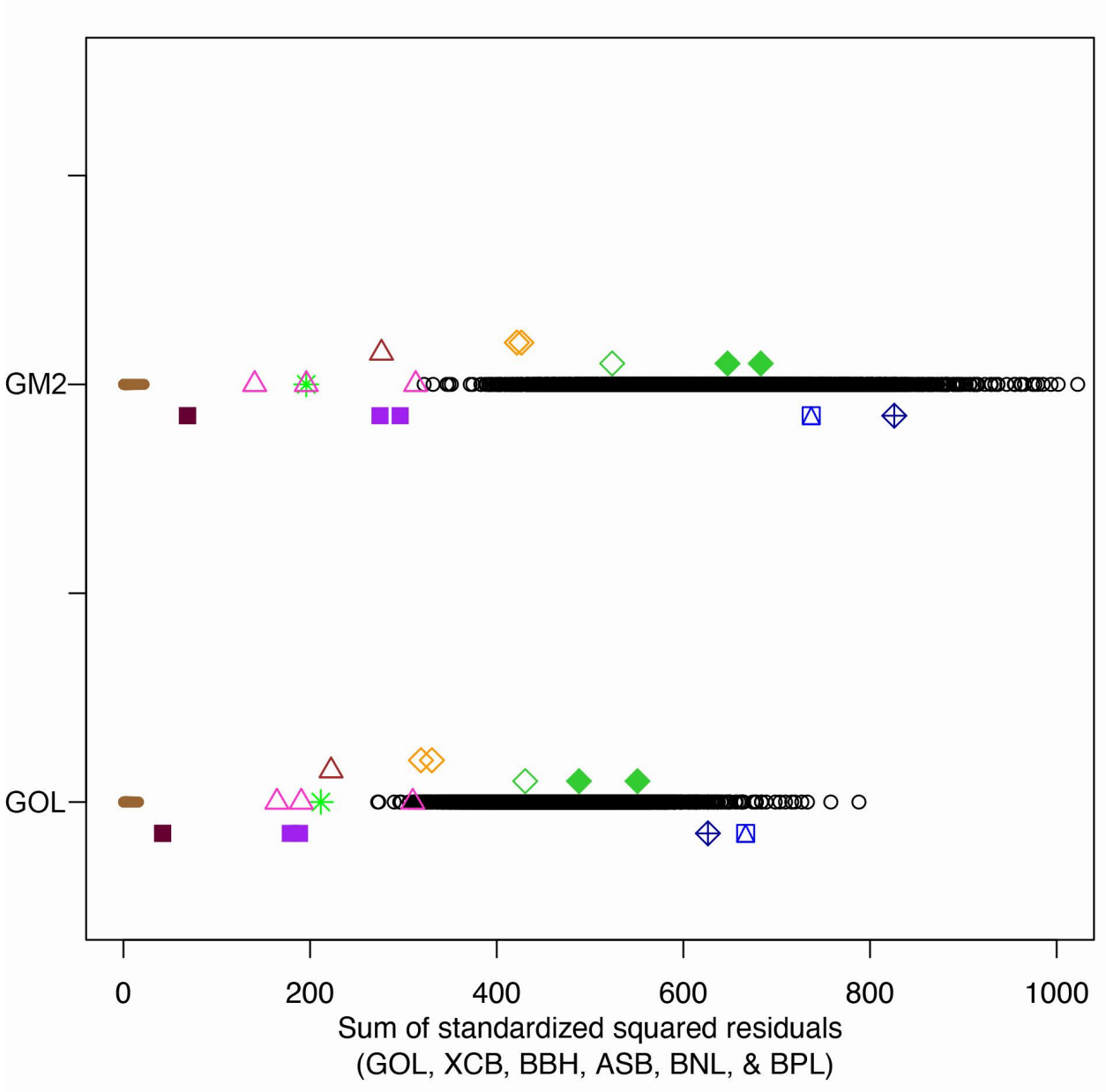

Figure 57. Visual representation of the sum of standardized squared residuals of the GM1 neurocranial variables for fossil and extant taxa compared when fitted against the sum of standardized squared residuals of the GM1 neurocranial variables for all great ape taxa GM2 and GOL, GOL sum of standardized squared residuals axis excludes GOL. Symbols are the same as previous figures. (back to text).

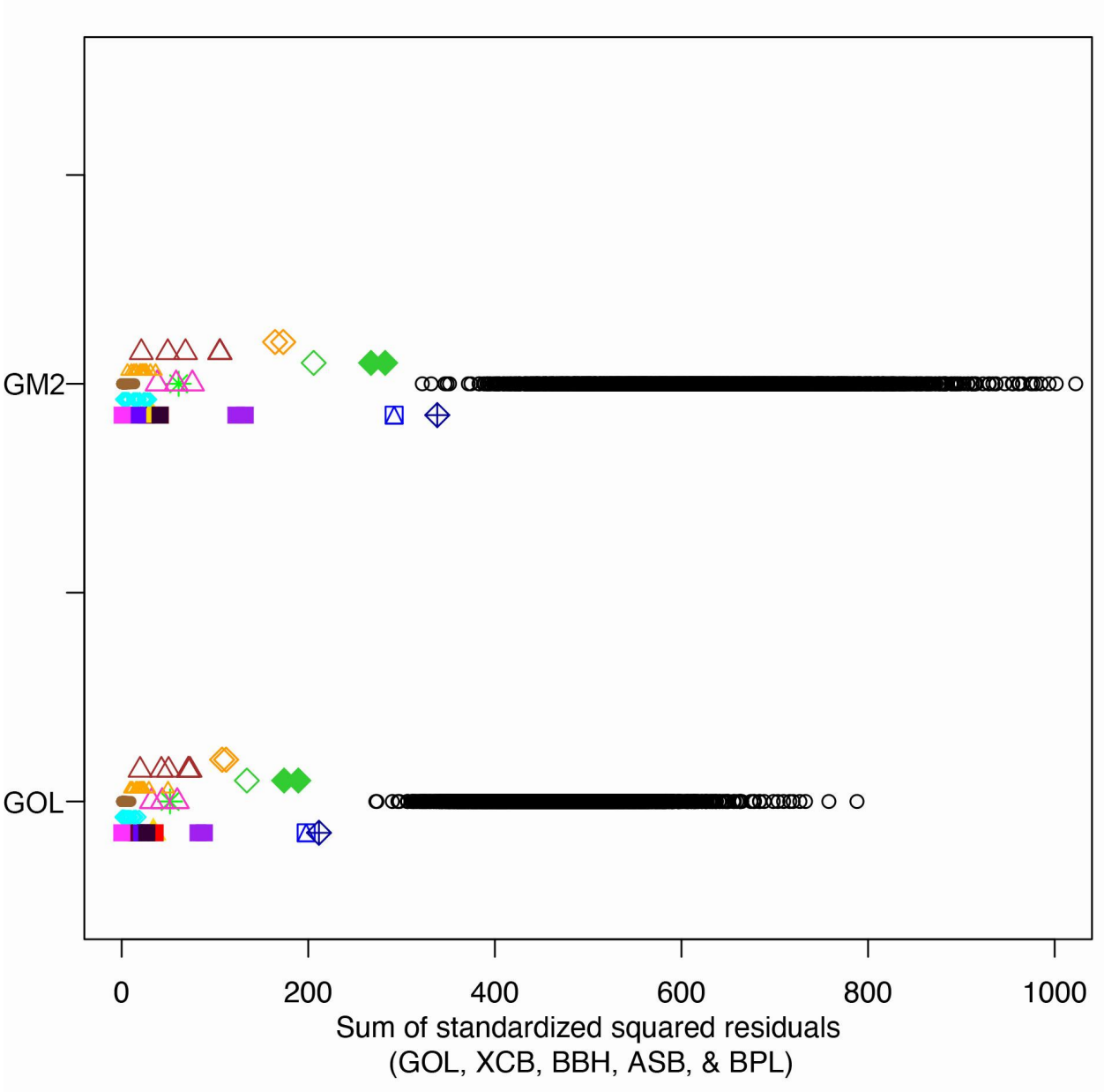

Figure 58. Visual representation of the sum of standardized squared residuals of the GM1 neurocranial variables (BNL removed) for fossil and extant taxa compared when fitted against the sum of standardized squared residuals of the GM1 neurocranial variables (BNL removed) for all great ape taxa GM2 and GOL, GOL sum of standardized squared residuals axis excludes GOL. Symbols are the same as previous figures. (back to text).

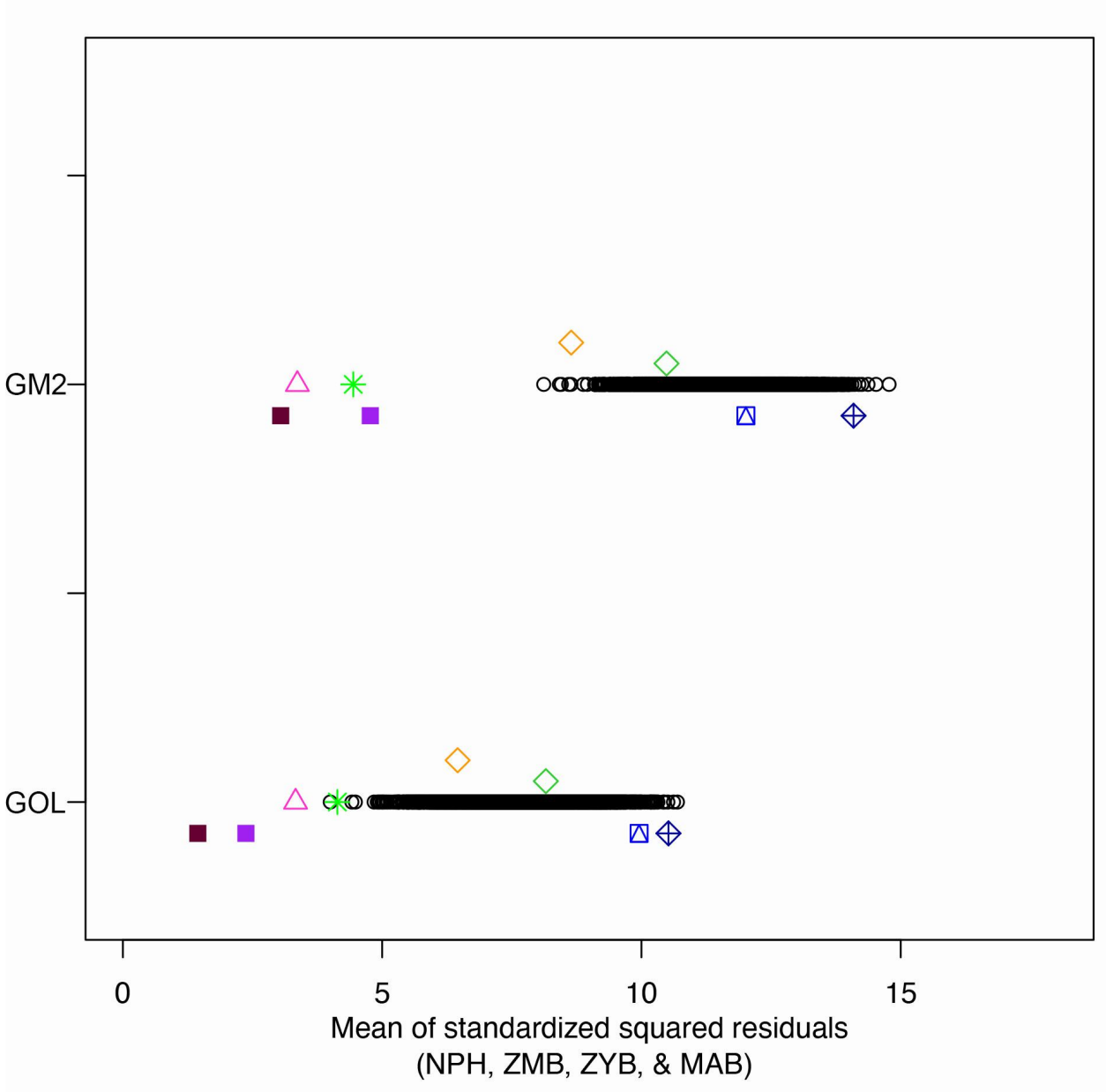

Figure 59. Visual representation of the mean of standardized squared residuals of the NPH, ZMB, ZYB, and MAB for fossil and extant taxa compared when fitted against the mean of standardized squared residuals of the NPH, ZMB, ZYB, and MAB for all great ape taxa. Symbols are the same as previous figures. (back to text).

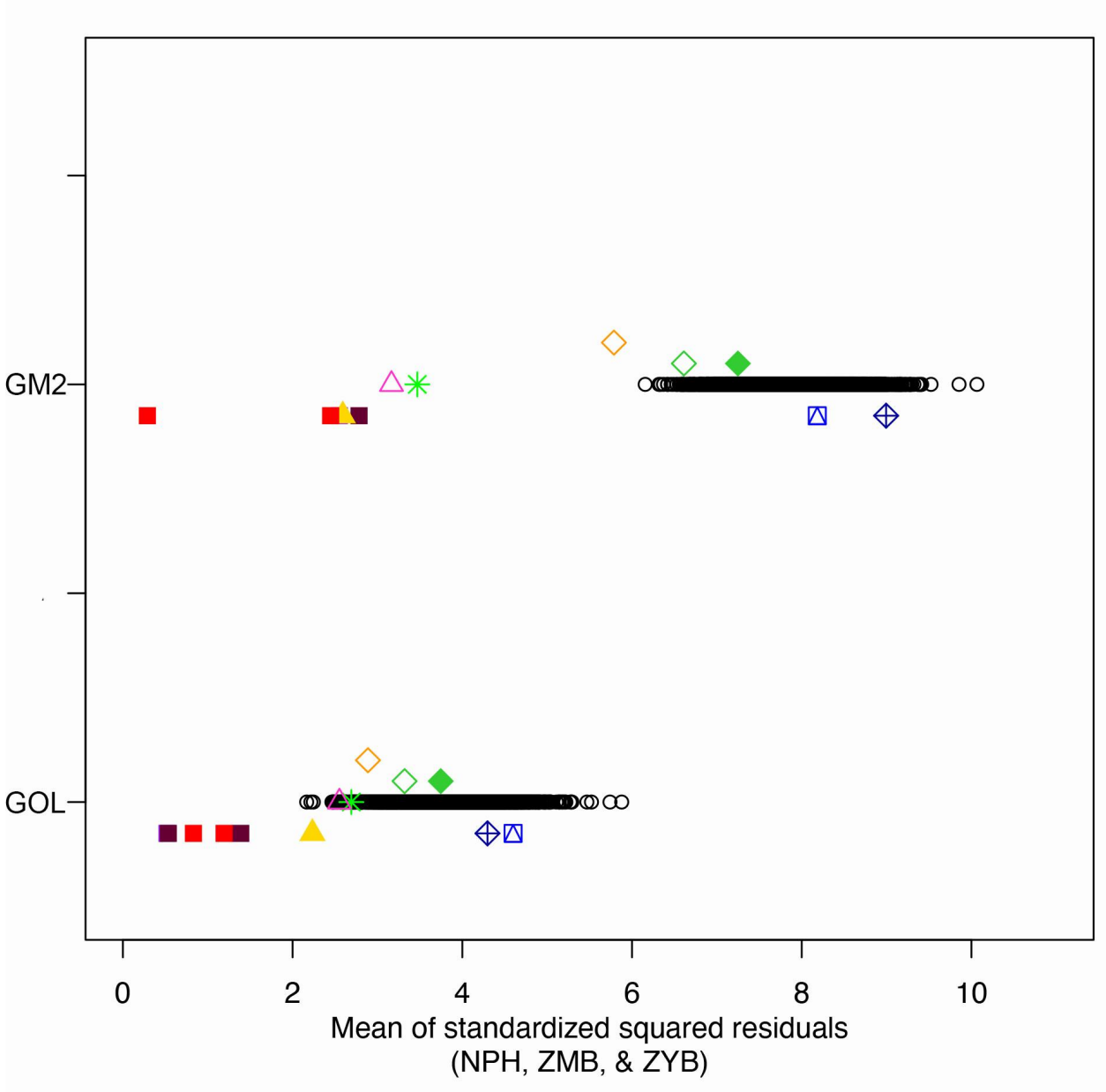

Figure 60. Visual representation of the mean of standardized squared residuals of the NPH, ZMB, and ZYB for fossil and extant taxa compared when fitted against the mean of standardized squared residuals of the NPH, ZMB, and ZYB for all great ape taxa. Symbols are the same as previous figures. (back to text).

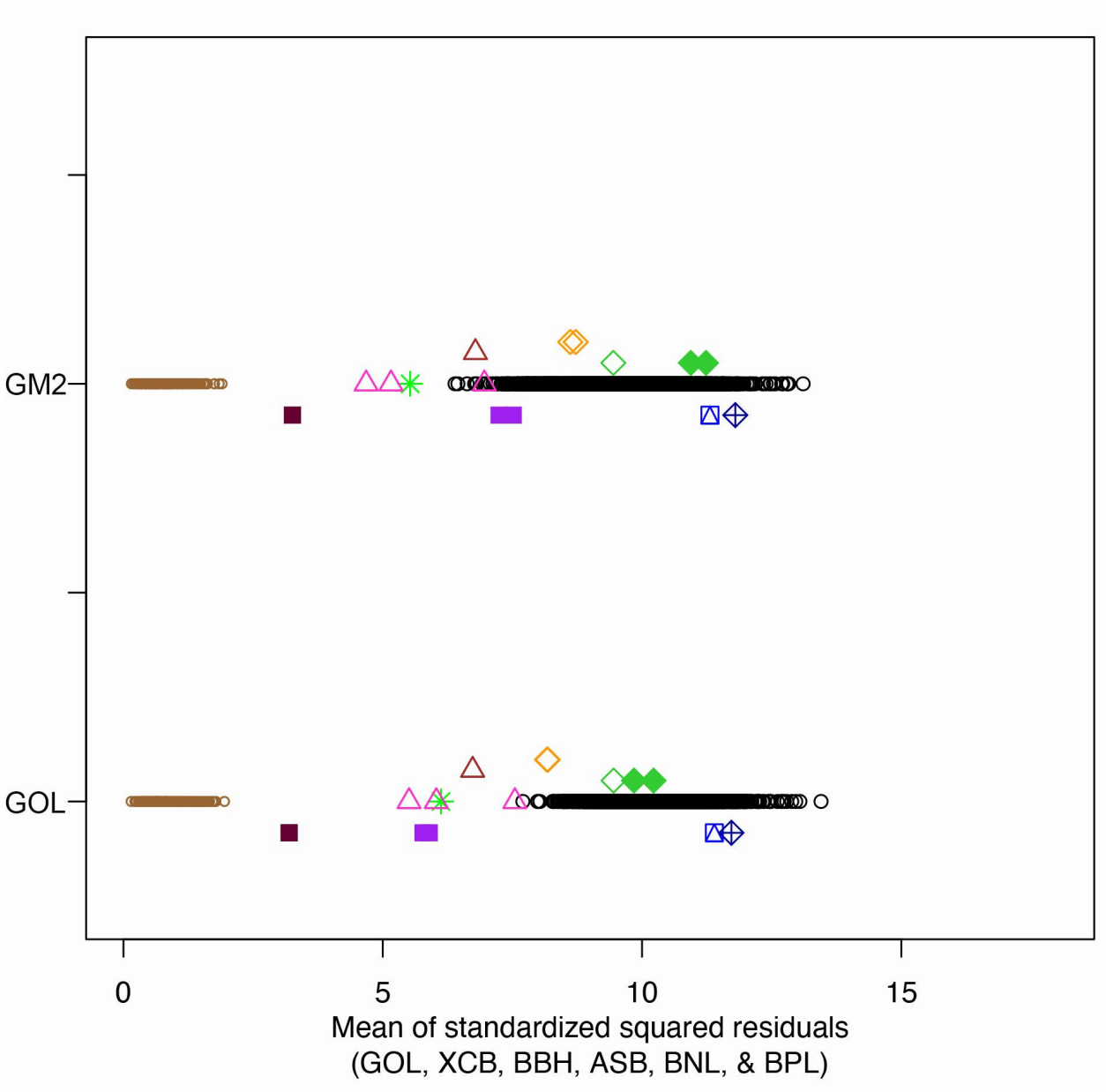

Figure 61. Visual representation of the mean of standardized squared residuals of the GM1 neurocranial variables for fossil and extant taxa compared when fitted against the mean of standardized squared residuals of the GM1 neurocranial variables for all great ape taxa GM2 and GOL, GOL mean of standardized squared residuals axis excludes GOL. Symbols are the same as previous figures. (back to text).

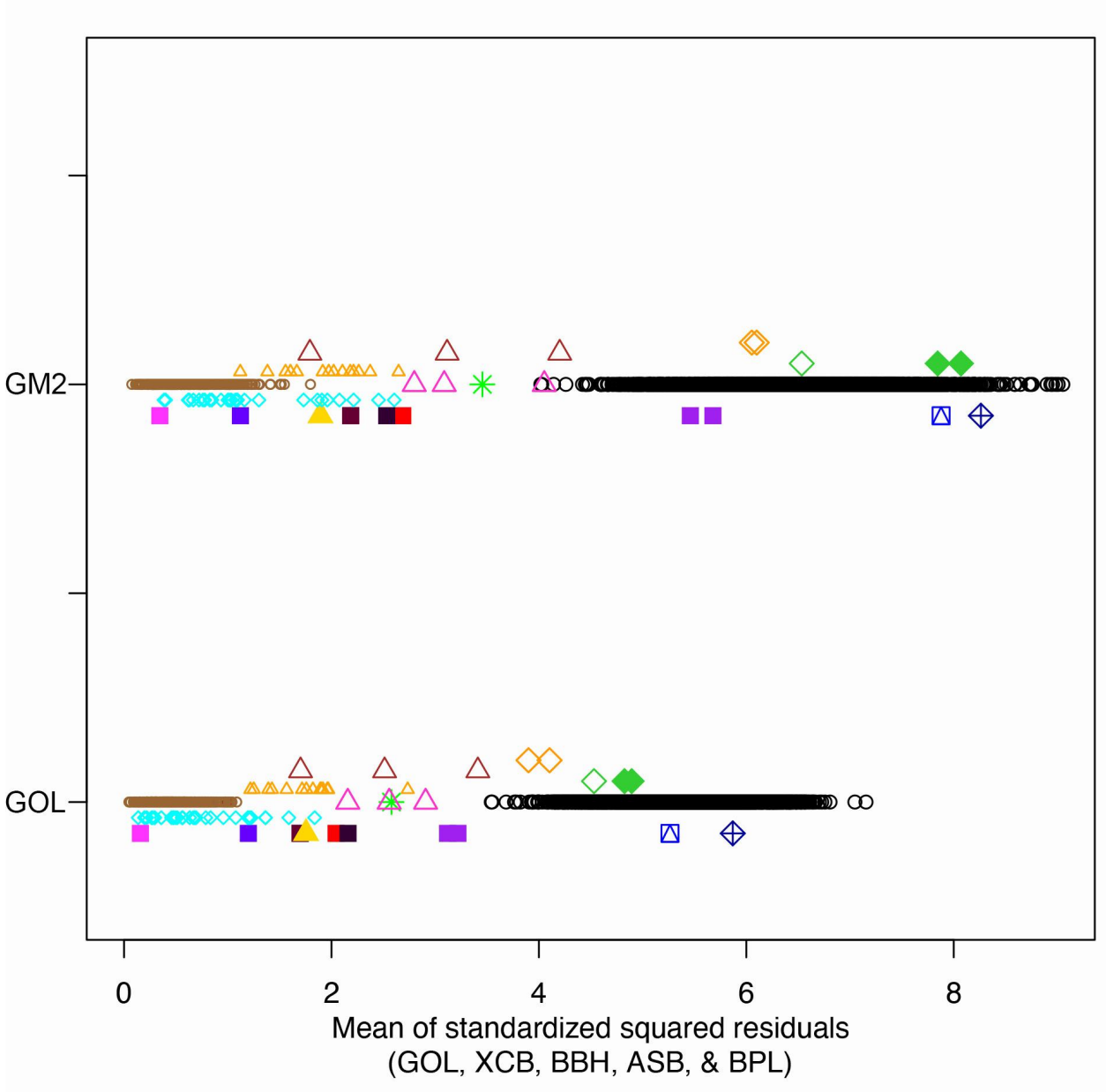

Figure 62. Visual representation of the mean of standardized squared residuals of the GM1 neurocranial variables (BNL removed) for fossil and extant taxa compared when fitted against the mean of standardized squared residuals of the GM1 neurocranial variables (BNL removed) for all great ape taxa GM2 and GOL, GOL mean of standardized squared residuals axis excludes GOL. Symbols are the same as previous figures. (back to text).

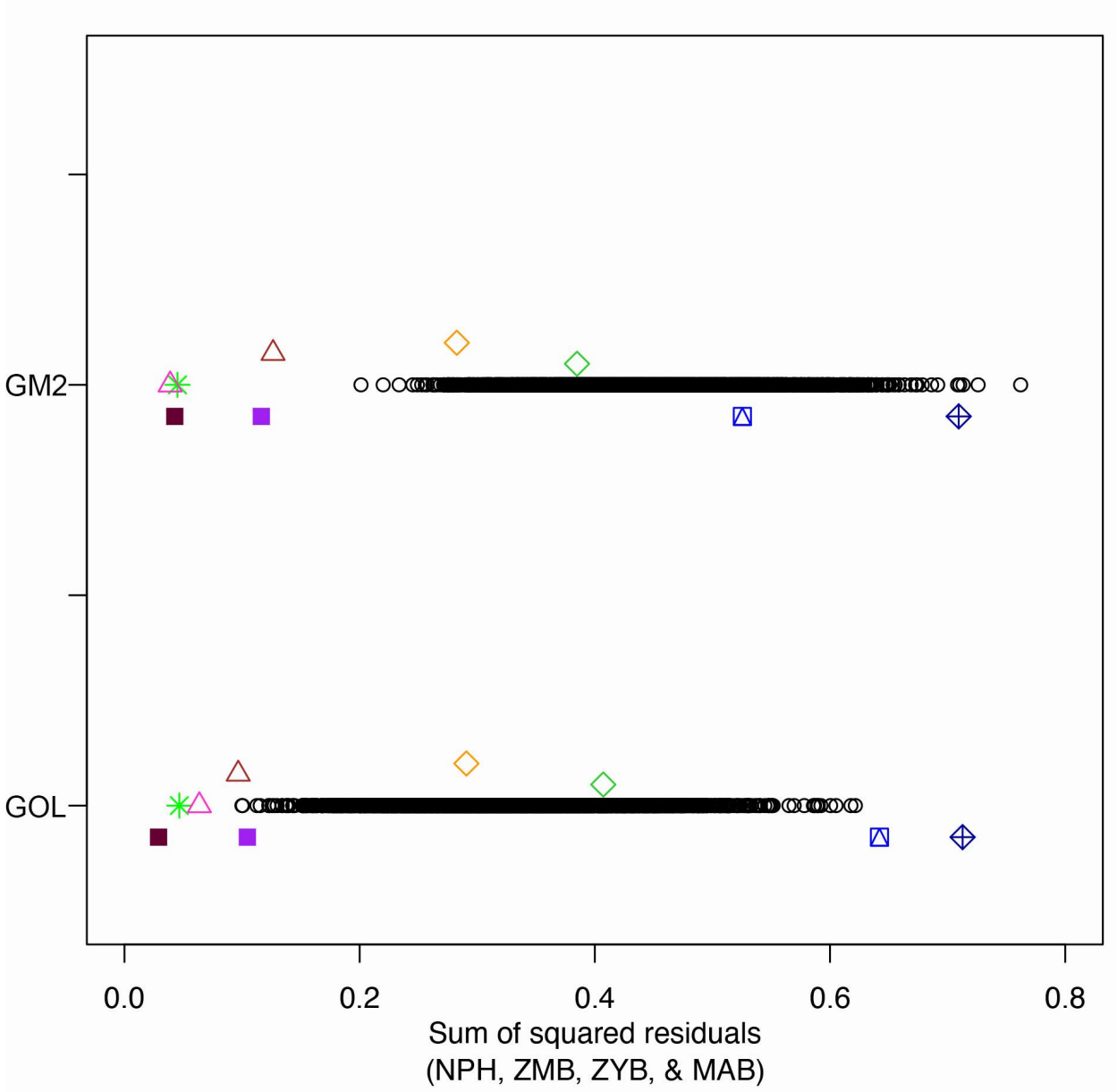

Figure 63. Visual representation of the sum of squared residuals of the NPH, ZMB, ZYB, and MAB for fossil and extant taxa compared when fitted against the sum of squared residuals of the NPH, ZMB, ZYB, and MAB for *Pan* and *Pongo*. Symbols are the same as previous figures. (back to text).

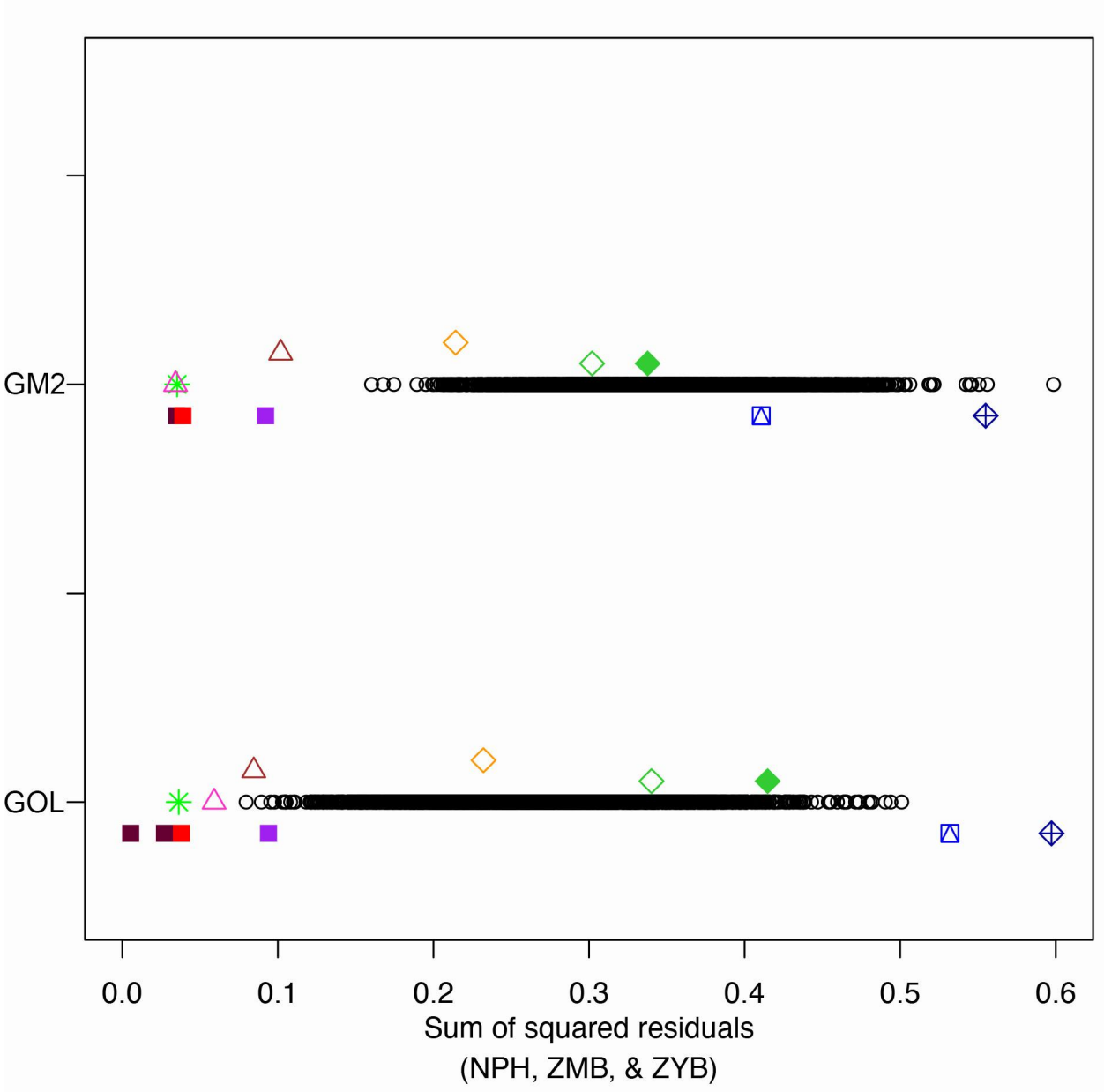

Figure 64. Visual representation of the sum of squared residuals of the NPH, ZMB, and ZYB for fossil and extant taxa compared when fitted against the sum of squared residuals of the NPH, ZMB, and ZYB for *Pan* and *Pongo*. Symbols are the same as previous figures. (back to text).

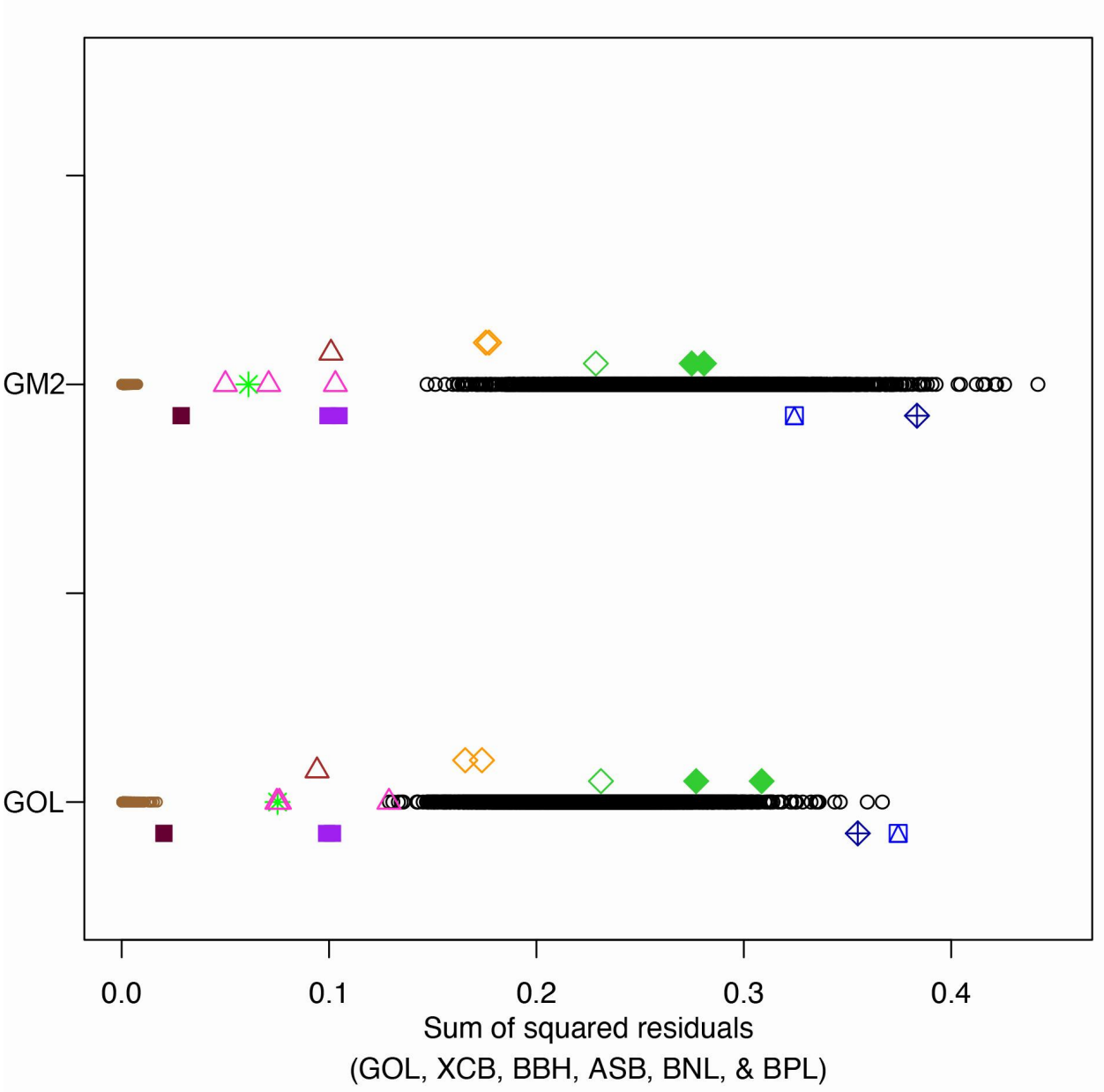

Figure 65. Visual representation of the sum of squared residuals of the GM1 neurocranial variables for fossil and extant taxa compared when fitted against the sum of squared residuals of the GM1 neurocranial variables for *Pan* and *Pongo* GM2 and GOL, GOL sum of squared residuals axis excludes GOL. Symbols are the same as previous figures. (back to text).

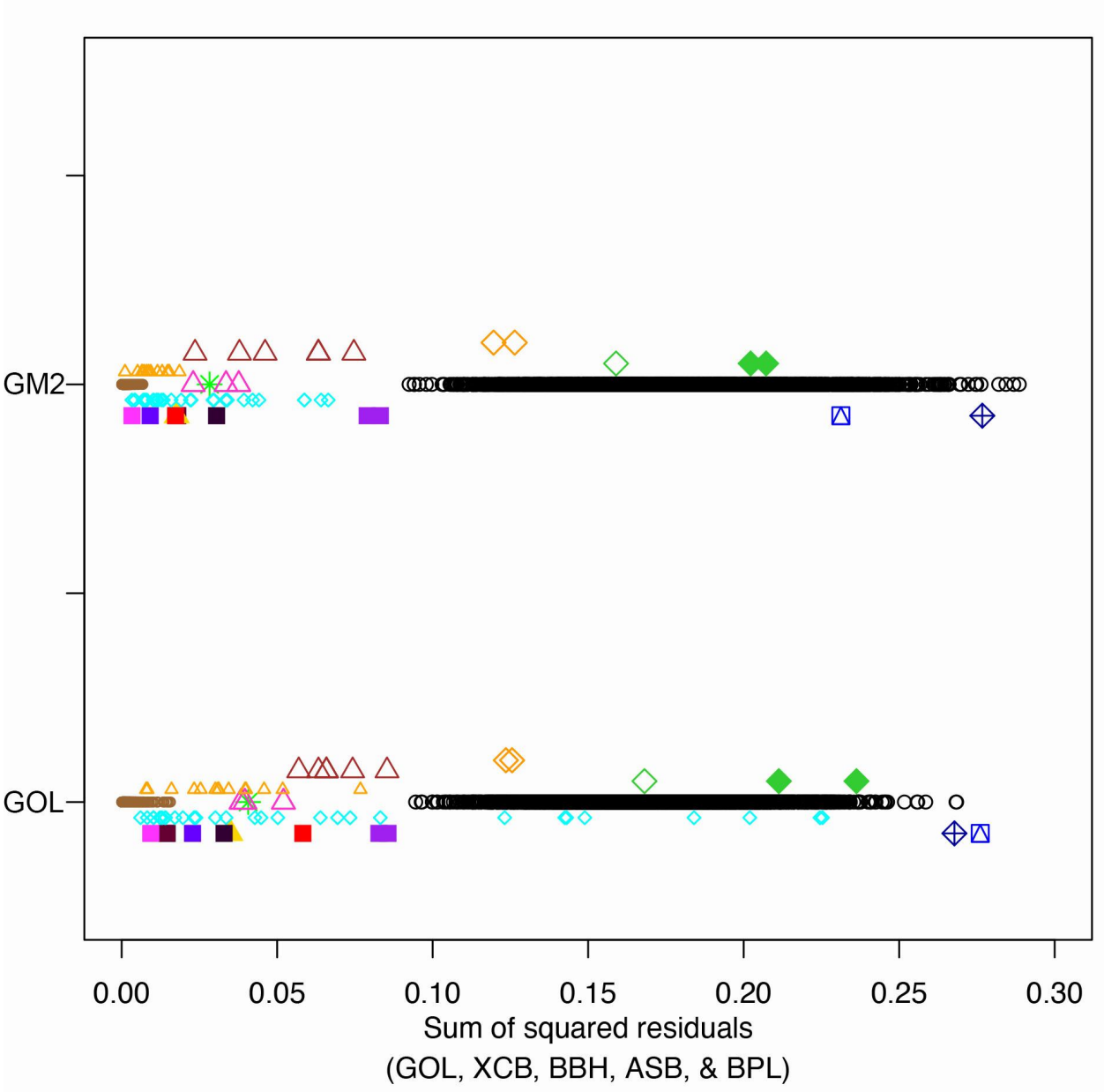

Figure 66. Visual representation of the sum of squared residuals of the GM1 neurocranial variables (BNL removed) for fossil and extant taxa compared when fitted against the sum of squared residuals of the GM1 neurocranial variables (BNL removed) for *Pan* and *Pongo* GM2 and GOL, GOL sum of squared residuals axis excludes GOL. Symbols are the same as previous figures. (back to text).

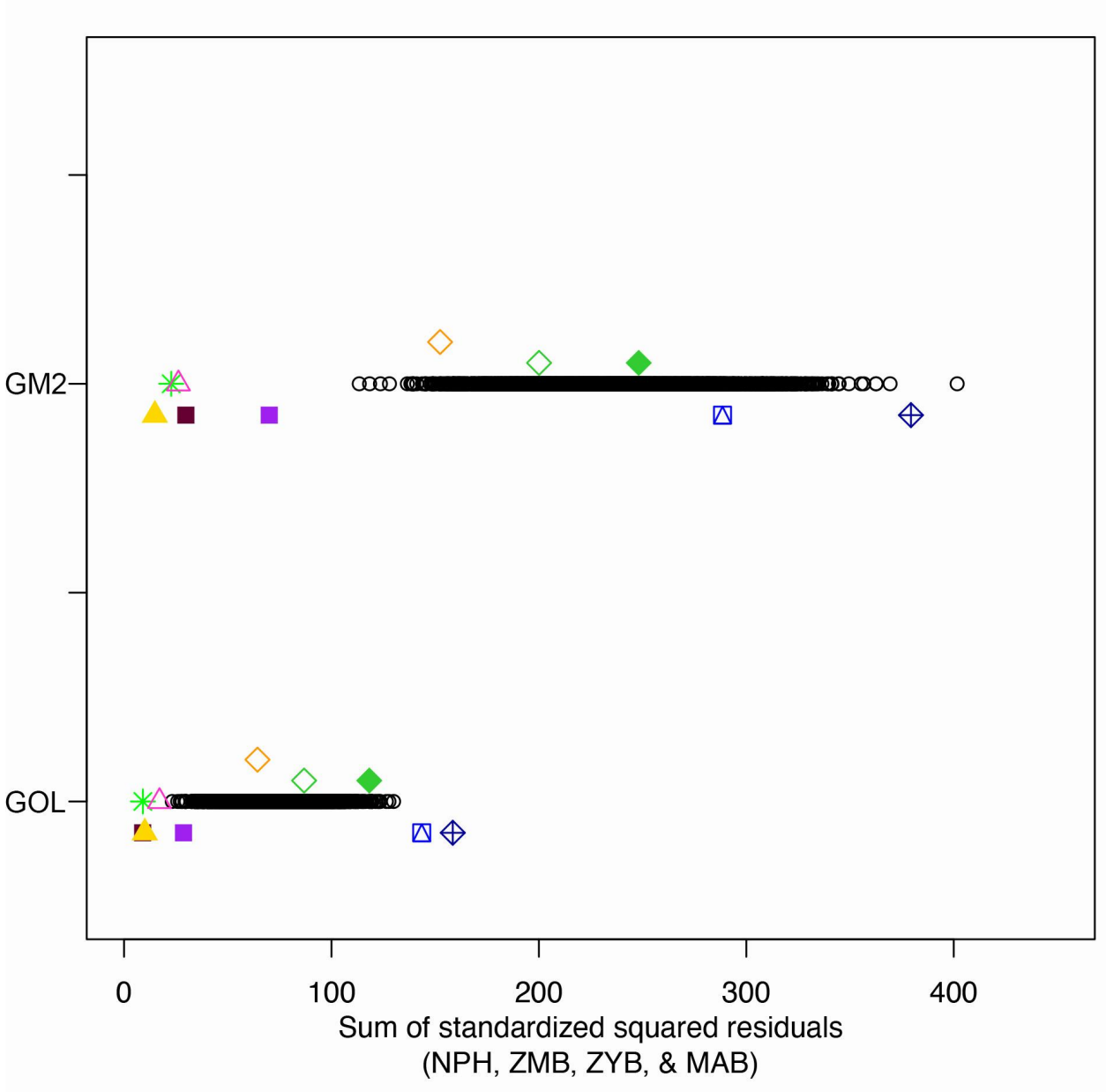

Figure 67. Visual representation of the sum of standardized squared residuals of the NPH, ZMB, ZYB, and MAB for fossil and extant taxa compared when fitted against the sum of standardized squared residuals of the NPH, ZMB, ZYB, and MAB for *Pan* and *Pongo*. Symbols are the same as previous figures. (back to text).

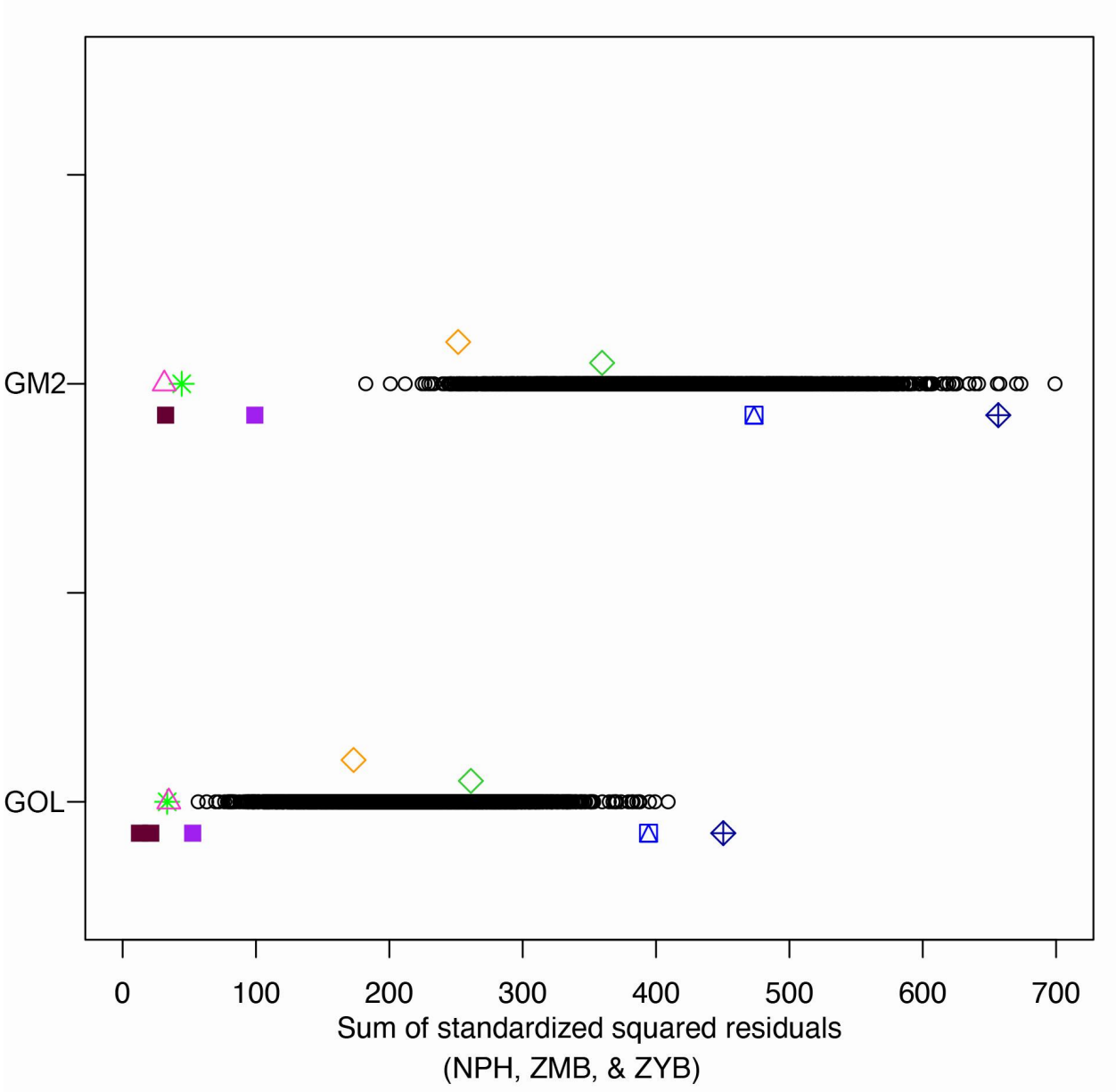

Figure 68. Visual representation of the sum of standardized squared residuals of the NPH, ZMB, and ZYBfor fossil and extant taxa compared when fitted against the sum of standardized squared residuals of the NPH, ZMB, and ZYB for *Pan* and *Pongo*. Symbols are the same as previous figures. (back to text).

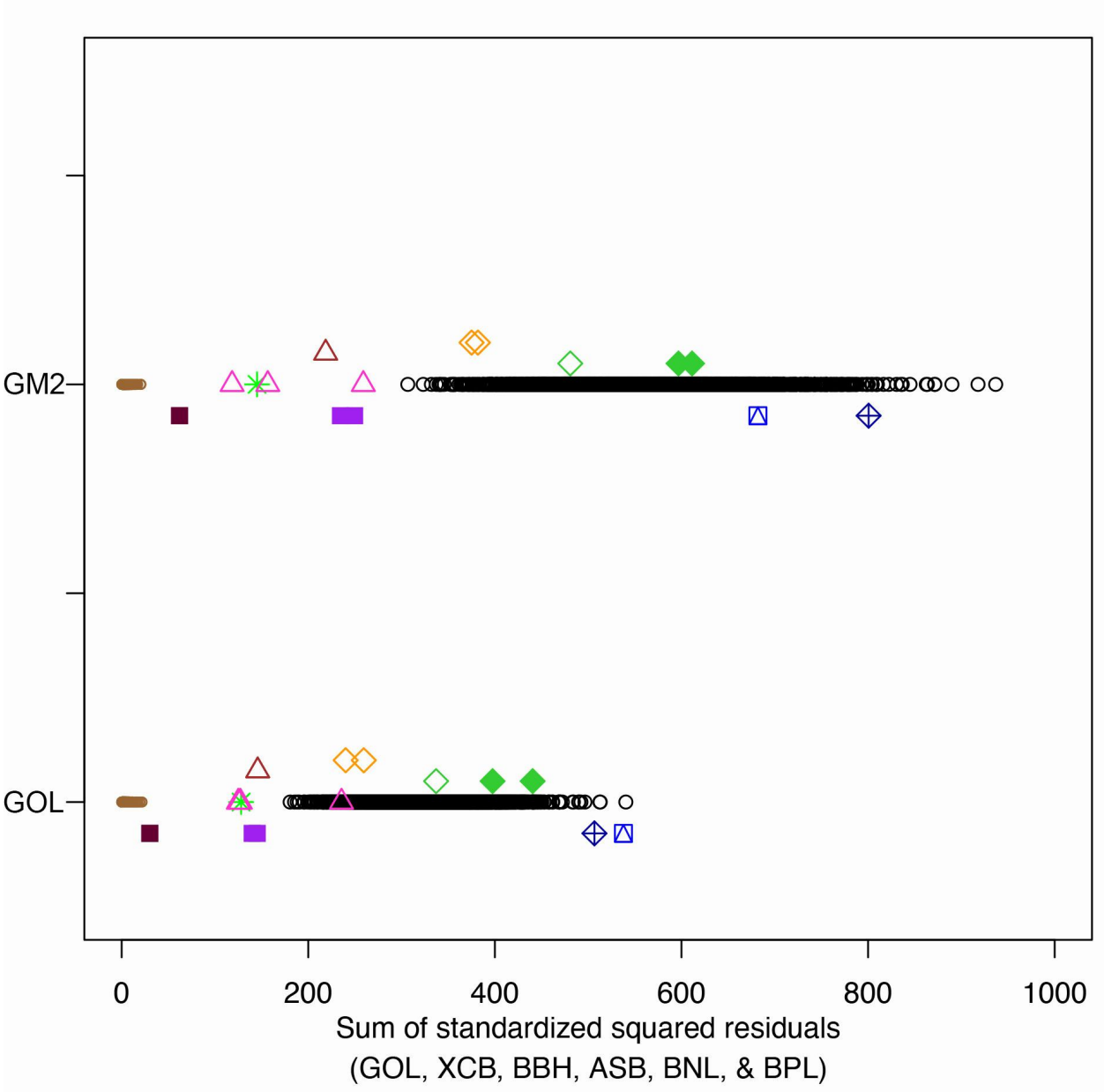

Figure 69. Visual representation of the sum of standardized squared residuals of the GM1 neurocranial variables for fossil and extant taxa compared when fitted against the sum of standardized squared residuals of the GM1 neurocranial variables for *Pan* and *Pongo* GM2 and GOL, GOL sum of standardized squared residuals axis excludes GOL. Symbols are the same as previous figures. (back to text).

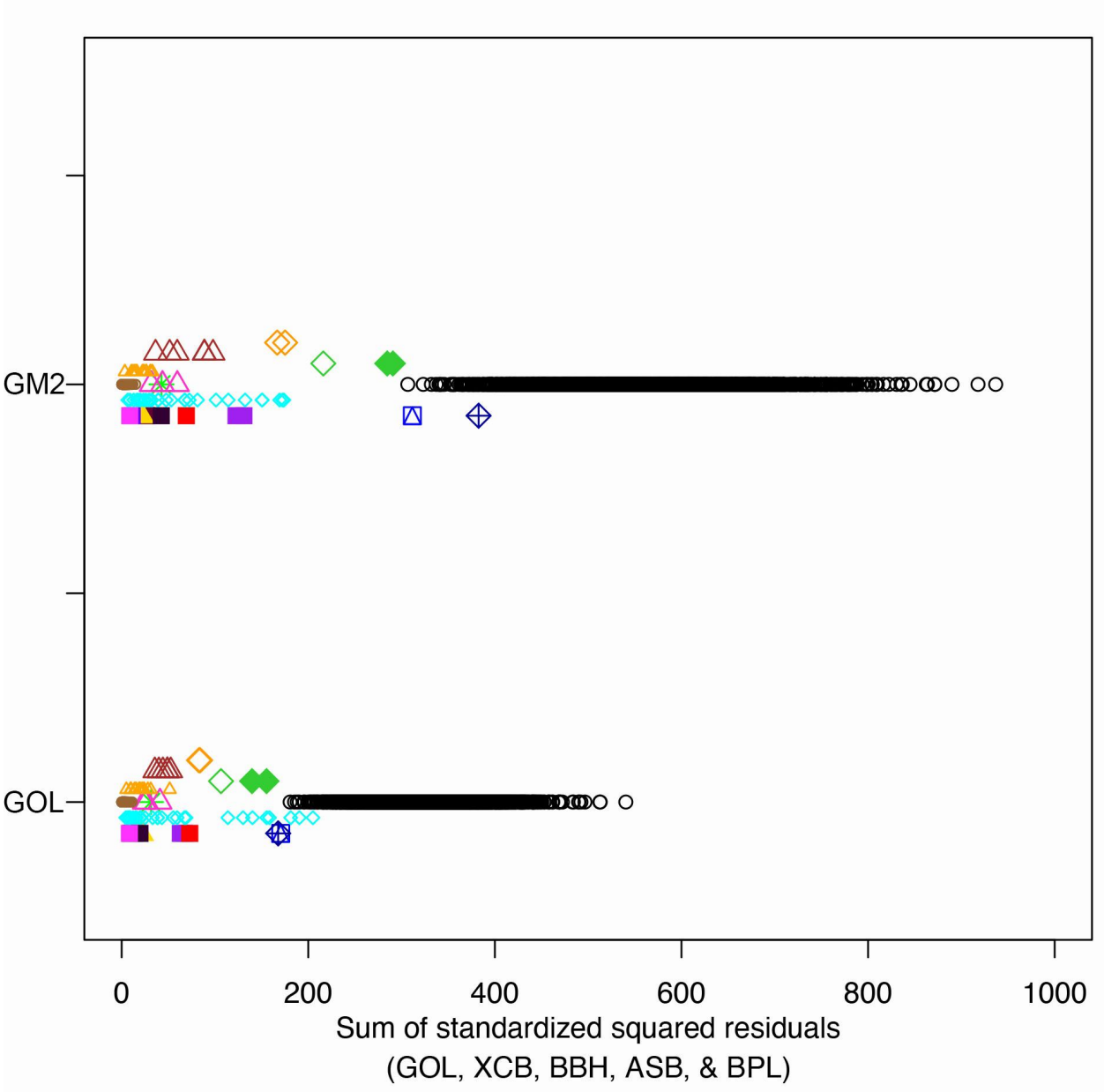

Figure 70. Visual representation of the sum of standardized squared residuals of the GM1 neurocranial variables (BNL removed) for fossil and extant taxa compared when fitted against the sum of standardized squared residuals of the GM1 neurocranial variables (BNL removed) for *Pan* and *Pongo* GM2 and GOL, GOL sum of standardized squared residuals axis excludes GOL. Symbols are the same as previous figures. (back to text).

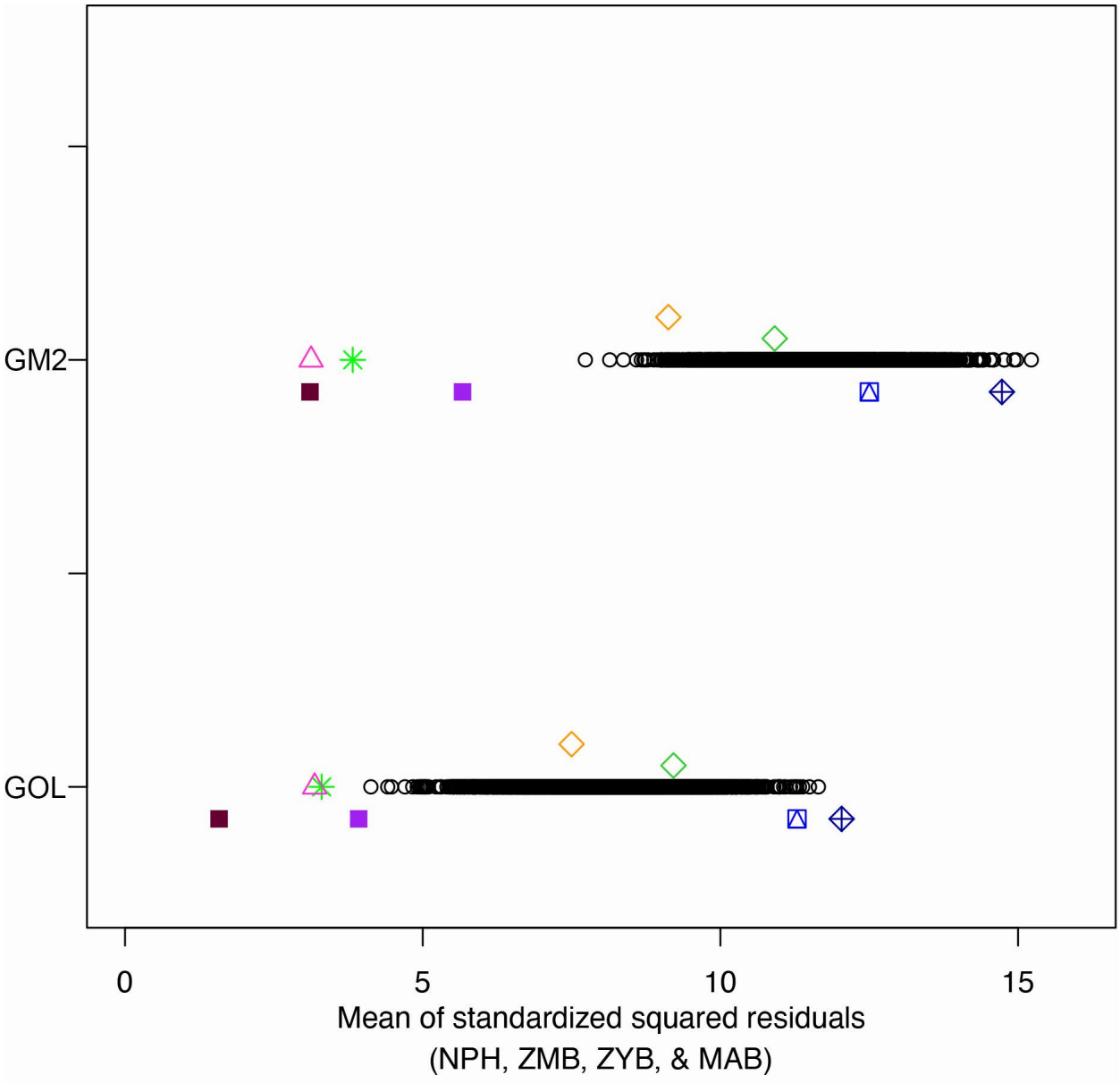

Figure 71. Visual representation of the mean of standardized squared residuals of the NPH, ZMB, ZYB, and MAB for fossil and extant taxa compared when fitted against the mean of standardized squared residuals of the NPH, ZMB, ZYB, and MAB for *Pan* and *Pongo*. Symbols are the same as previous figures. (back to text).

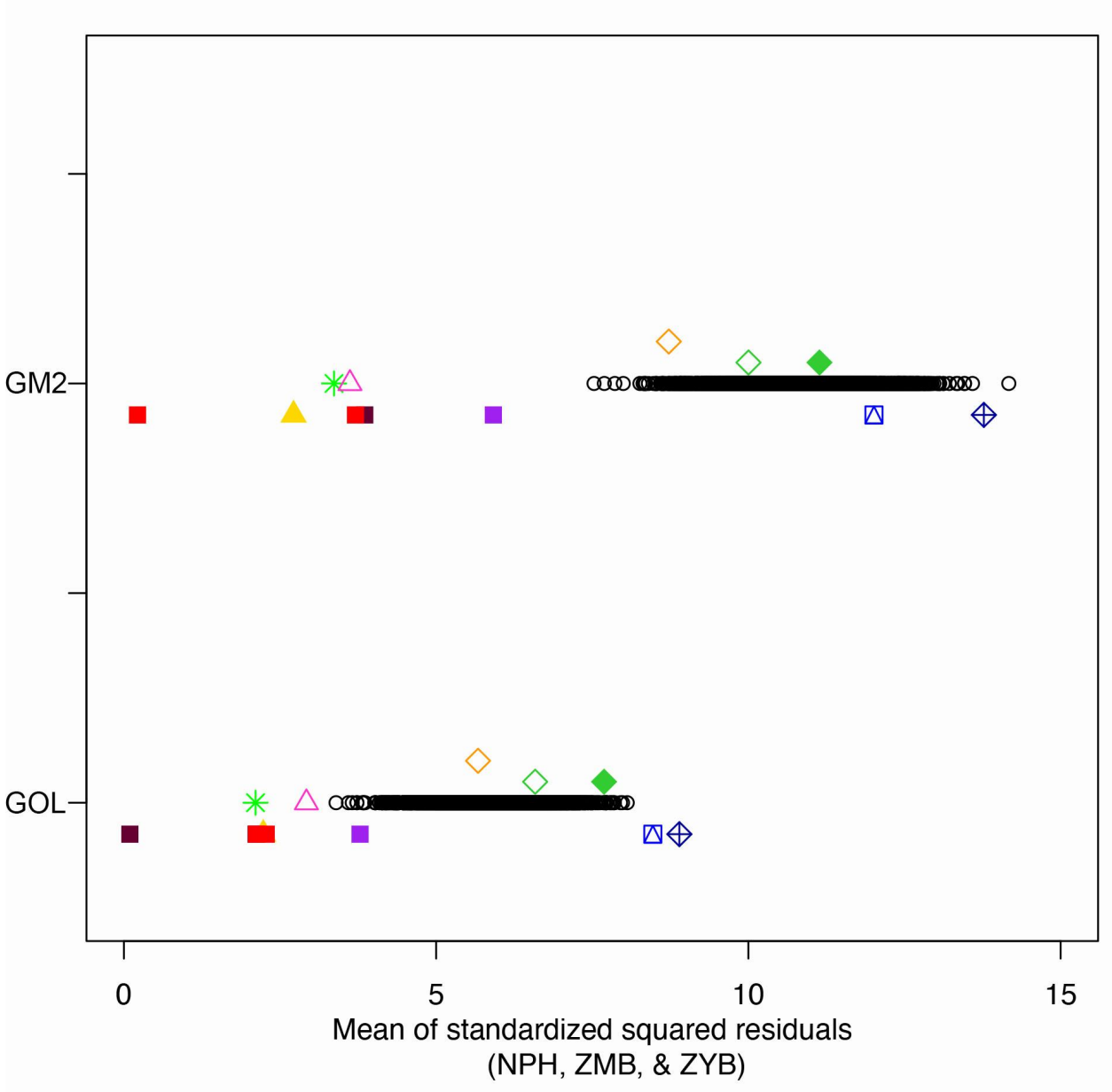

Figure 72. Visual representation of the mean of standardized squared residuals of the NPH, ZMB, and ZYB for fossil and extant taxa compared when fitted against the mean of standardized squared residuals of the NPH, ZMB, and ZYB for *Pan* and *Pongo*. Symbols are the same as previous figures. (back to text).

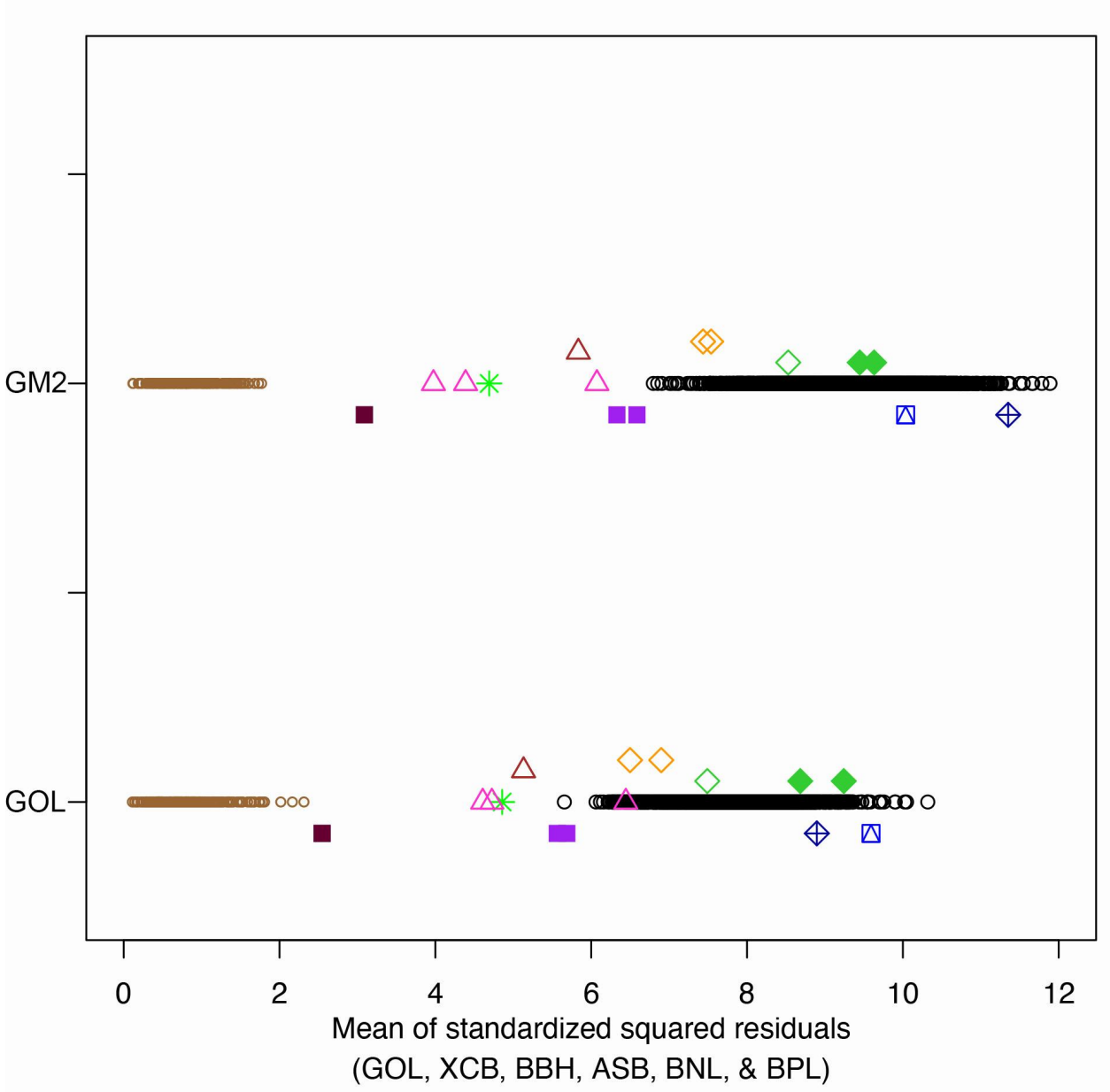

Figure 73. Visual representation of the mean of standardized squared residuals of the GM1 neurocranial variables for fossil and extant taxa compared when fitted against the mean of standardized squared residuals of the GM1 neurocranial variables for *Pan* and *Pongo* GM2 and GOL, GOL mean of standardized squared residuals axis excludes GOL. Symbols are the same as previous figures. (back to text).

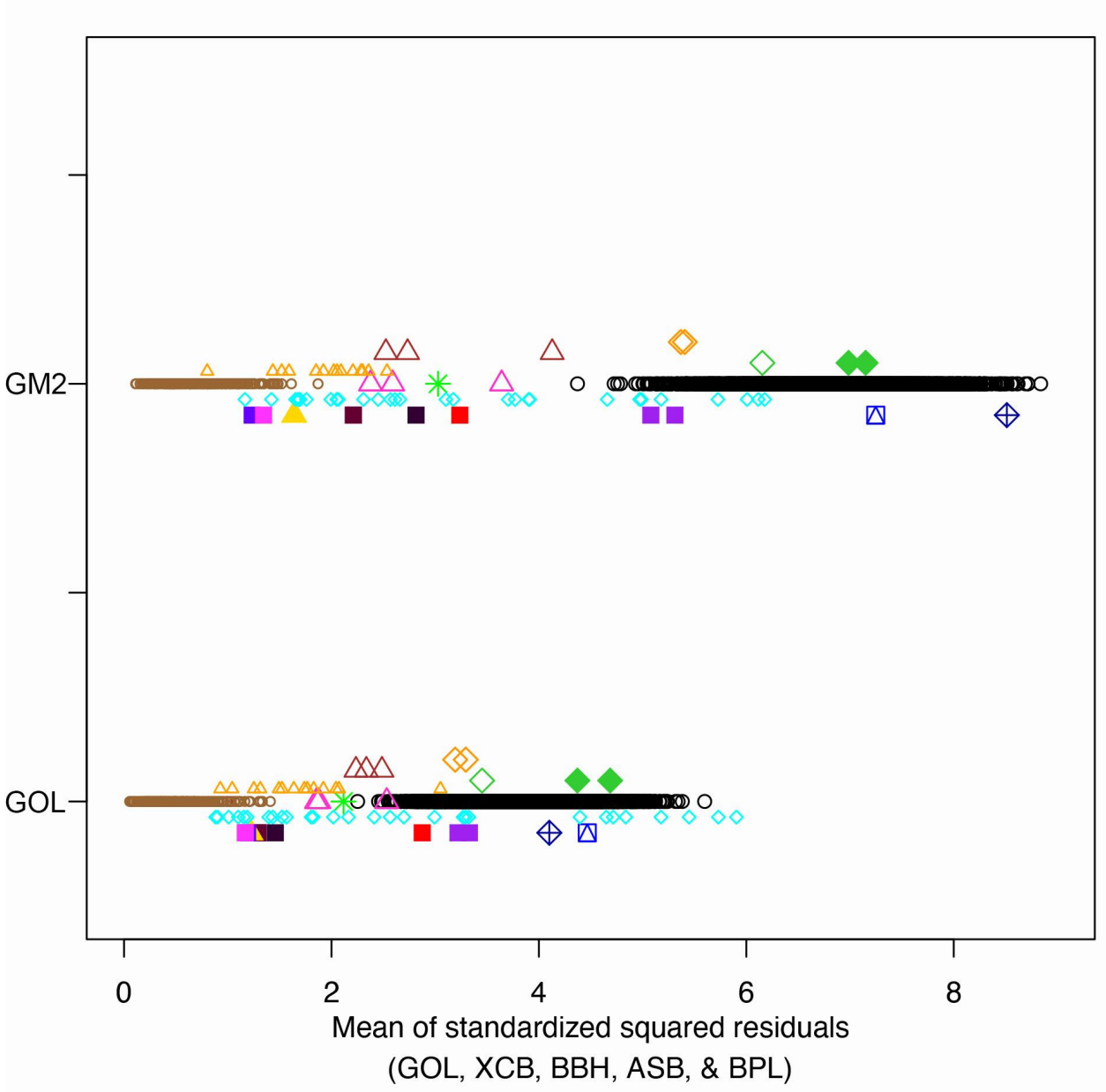

Figure 74. Visual representation of the mean of standardized squared residuals of the GM1 neurocranial variables (BNL removed) for fossil and extant taxa compared when fitted against the mean of standardized squared residuals of the GM1 neurocranial variables (BNL removed) for *Pan* and *Pongo* GM2 and GOL, GOL mean of standardized squared residuals axis excludes GOL. Symbols are the same as previous figures. (back to text).

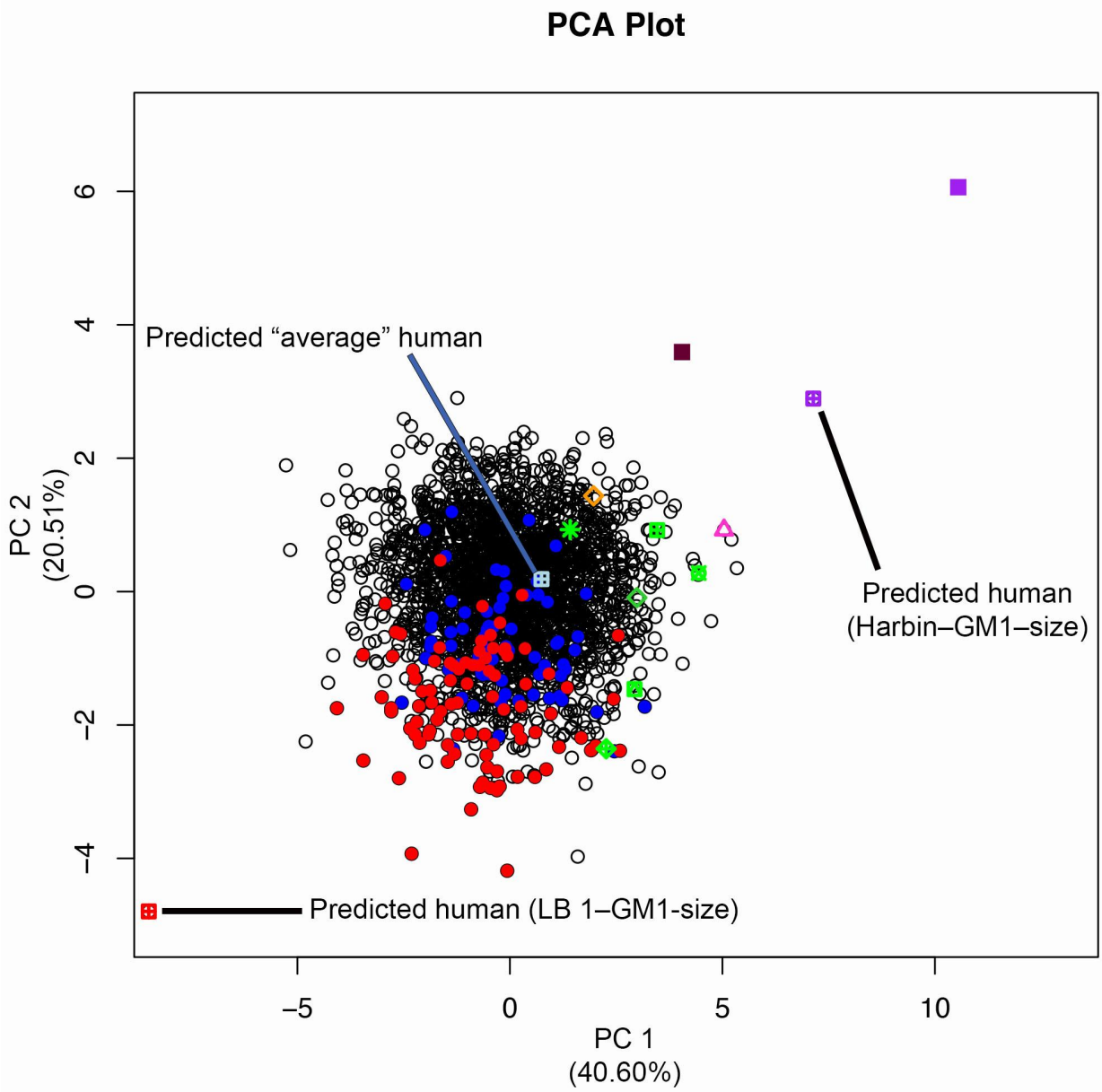

Figure 75. PCA components 1 and 2 of facial shape variables for recent modern humans and selected fossil hominins. Symbols are the same as in Figures 14 and 15 with the addition of a predicted human the size of the LB 1 cranium (red square with cross), a predicted human the size of the Harbin cranium (purple square with cross), and a predicted "average" recent modern human (light blue square with cross). (back to text).

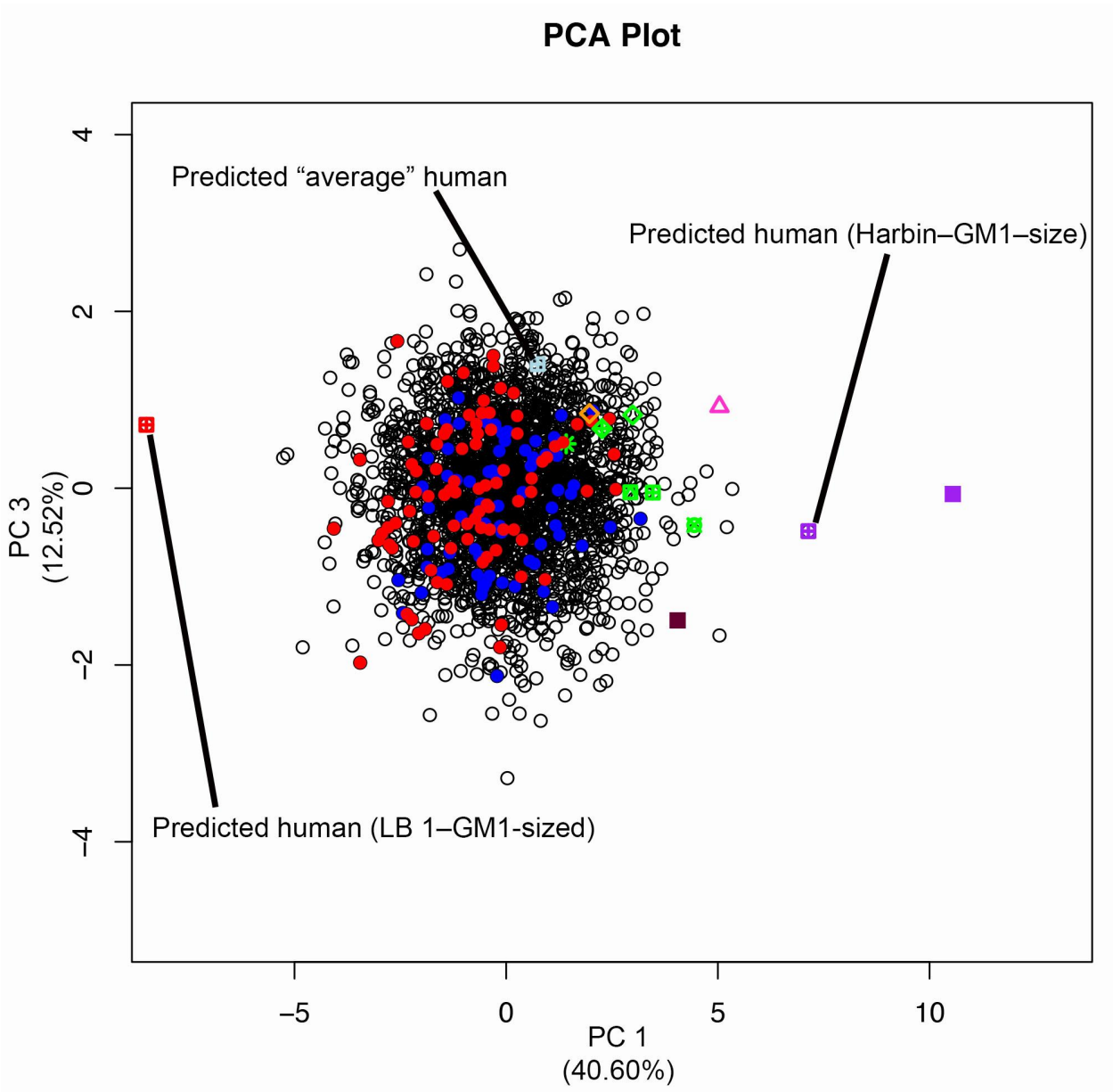

Figure 76. PCA components 1 and 3 of facial shape variables for recent modern humans and selected fossil hominins. Symbols are the same as in Figures 14 and 15 with the addition of a predicted human the size of the LB 1 cranium (red square with cross), a predicted human the size of the Harbin cranium (purple square with cross), and a predicted "average" recent modern human (light blue square with cross). (back to text).

References

Aiello, L., Dean, M.A., 1990. An introduction to human evolutionary anatomy. London: Academic Press.

Aiello, L.C., Wells, J.C.K., 2002. Energetics and the evolution of the genus *Homo*. Annu. Rev. Anthropol. 31, 323–338.

Antón, S.C., 2003. Natural history of *Homo erectus*. Yearbook of Phys. Anthropol. 46, 126–170.

Argue, D., Donlon, D., Groves, C., Wright, R., 2006., *Homo floresiensis*: Microcephalic, pygmoid, *Australopithecus*, or *Homo*? J. Hum. Evol. 51, 360–374.

Argue, D., Morwood, M.J., Sutikna, T., Jatmiko, Wahyu Saptomo, E., 2009. *Homo floresiensis*: A cladistic analysis. J. Hum. Evol. 57, 623–639.

Argue, D., Groves, C.P., Lee, M.S.Y., Jungers, W.L., 2017. The affinities of *Homo floresiensis* based on phylogenetic analyses of cranial, dental, and postcranial characters. J. Hum. Evol. 107, 107–133.

Arif, J., Kaifu, Y., Baba, H., Suparka, M.E., Zaim, Y., Setoguchi, T., 2002. Preliminary observations of a new cranium of *Homo erectus* (Tjg-1993.05) from Sangiran, Central Jawa. Anthropol. Sci. 110, 165–177.

Arsuaga, J.L., Martínez, I., Garcia, A., Lorenzo, C., 1997. The Sima de los Huesos crania (Sierra de Atapuerca, Spain). A comparative study. J. Hum. Evol. 33, 219–281.

Asfaw, B., Gilbert, H.W., Beyene, Y., Hart, W.K., Renne, P.R., WoldeGabriel, G., Vrba, E.S., White, T.D., 2002. Remains of *Homo erectus* from Bouri, Middle Awash, Ethiopia. Nature 416, 317–320.

Baab, K.L., McNulty, K.P., 2009. Size, shape, and asymmetry in fossil hominins: The status of LB 1 cranium based on 3D morphometric analyses. J. Hum. Evol. 57, 608–622.

Baab, K.L., McNulty, K.P., Harvati, K., 2013. *Homo floresiensis* contextualized: A geomorphic morphometric comparative analysis of fossil and pathological human samples. PLOS ONE 8, e69119.

Baab, K.L., 2016. The place of *Homo floresiensis* in human evolution. J. Anthropol. Sci. 94, 5–18.

Baab, K.L., Brown ,P., Falk, D., Richtsmeier, J.T., Hildebolt, C.F., Smith, K., Jungers, W., 2016. A critical evaluation of the Down Syndrome diagnosis for LB 1, type specimen of *Homo floresiensis*. PLOS ONE 11, e0155731.

Barr, A.W., Pobiner, B., Rowan, J., Du, A., Faith, J.T., 2022. No sustained increase in zooarchaeological evidence for canivory after the appearance of *Homo erectus*. Proc. Natl. Acad. Sci. 119, e2115540119.

Bastir, M., Rosas, A., 2016. Cranial base topology and basic trends in the facial evolution of *Homo*. J. Hum. Evol. 91, 26–35.

Benazzi, S., Bookstein, F.L., Strait, D.S., Weber, G.W., 2011. A new OH5 reconstruction with an assessment of its uncertainty. J. Hum. Evol. 61, 75–88.

Berger, L.R., Tobias, P.V., 1996. A chimpanzee-like tibia from Sterkfontein, South Africa and its implications for the interpretations of bipedalism in *Australopithecus africanus*. J. Hum. Evol. 30, 343–348.

Berger, L., de Ruiter, D.J, Churchill, S.E., Schmid, P., Carlson, K., Dirks, P.H.G.M, Kibii, J.M., 2010. *Australopithecus sediba*: A new species of *Homo*-like australopith from South Africa. Science 328, 195–204.

Bramble, D.M, Lieberman, D.E., 2004. Endurance running and the evolution of *Homo*. Nature 432, 345–352.

Broham, L., Cardillo, M., 2007. Primates follow the 'island rule': implications for interpreting *Homo floresiensis*. Biol. Lett. 3, 398–400.

Brown, F., Harris J., Leakey, R., Walker, A., 1985. Early *Homo erectus* from west Lake Turkana, Kenya. Nature 316, 788–792.

Brown, P., Sutikna B., Morwood, M.J., Soejono, R.P., Jatmiko, Wayhu Saptomo, E., Rokus Awe Due., 2004. A new small-bodied hominin from the Late Pleistocene of Flores, Indonesia. Nature 431, 1055–1061.

Brown, P., Maeda, T., 2009. Liang Bua *Homo floresiensis* mandibles and mandibular teeth: a contribution to the comparative morphology of a new hominin species. J. Hum. Evol. 57, 571–596.

Brown, P., 2012. LB 1 and LB 6 are not modern human (*Homo sapiens*) cretins. J. Hum. Evol. 62, 201–224.

Brunet, M., Guy, F., Pilbeam, D., Mackaye, H.T., Likius, A., Ahounta, D., Beauvilain, A., Blondel, C., Bocherens, H., Boisserie, J-R., De Bonis, L., Coppens, Y., Dejax, J., Denys, C., Duringer, P., Eisenmann, V., Fanone, G., Fronty, P., Geraads, D., Lehmann, T., Lihroeau, F., Louchart, A., Mahamat, A., Merceron, G., Mouchelin, G., Otero, O., Campomanes, P.P., De Leon, M.P., Rage, J-C., Sapanet, M., Schuster, M., Sudre, J., Tassy, P., Valentin, X., Vingaud, P., Viriot, L., Zazzo, A., Zollikofer, C., 2002. A new hominid from the Upper Miocene of Chad, Central Africa. Nature 418, 145–151.

Campione, N.E., Evans, D.C., 2012. A universal scaling relationship between the body mass and proximal limb bone dimensions in quadrupedal terrestrial tetrapods. BMC Biol. 10, 60.

Clarke, R.J., 1985. *Australopithecus* and early *Homo* in southern Africa. In: Delson, E. (Ed.), Ancestors: The hard evidence. Alan R. Liss, New York, pp. 171–177.

Clarke, R.J., 1990. The Ndutu cranium and the origin of *Homo sapiens*. J. Hum. Evol. 19, 699–736.

Condemi, S., 1992. Les hommes fossiles de Saccopastore. Cahier de paleoanthropology, C.N.R.S. Éditions, Paris.

Cook, R.W., Vazzana, A., Sorrentino, R., Benazzi S., Smith, A.L., Strait, D.S., Ledogar, J.A., 2021. The cranial biomechanics and feeding performance of *Homo floresiensis*. Interface Focus 11, 2020083.

Curnoe, D., Tobias, P.V., 2006. Description, new reconstruction, comparative anatomy, and classification of the Sterkfontein Stw 53 cranium, with discussions about the taxonomy of other southern African early *Homo* remains. J. Hum. Evol. 50, 36–77.

D'Août, K., Aerts, P., 2008. The evolutionary history of the human foot. In D'Août, K., Lescrenier, K., Van Gheluwe, B., De Clercq, D. (eds.): Advances in plantar pressure measurements in clinical and scientific research. Shaker Publishing, The Netherlands. pp. 44–68.

Daver, G., Guy, F., Mackeye, H.T., Likius, A., Boisserie, J-R., Moussa, A., Pallas, P., Vingaud, P., Clarisse, N.D., 2022. Postcranial evidence of late Miocene hominin bipedalism in Chad. Nature 609, 94–100.

Deagling, D.J., Patel, B.A., Jungers, W.L., 2014. Geometries and comparative biomechanics of *Hmom floresiensis* mandibles. J. Hum. Evol. 68, 36–46.

Delezene, L.K., 2015. Modularity of the anthropoid dentition: Implications for the evolution of the hominin canine honing complex. J. Hum. Evol. 86, 1–12.

Dembo, M., Matzke, N.J., Mooers, A.Ø., Collard, M., 2015. Bayesian analysis of morphological supermatrix sheds light on controversial fossil hominin relationships. Proc. R. Soc. B 282, 20150943.

Dembo, M., Radovčić, D., Garvin, H.M., Laird, M.F., Schroeder, L., Scott, J.E., Brophy, J., Ackermann, R.R., Musiba, C.M., de Ruiter, D.J., Mooers, A.Ø., Collard, M., 2016. The evolutionary relationship and age of *Homo naledi*: An assessment using dated Bayesian phylogenetic methods. J. Hum. Evol. 97, 17–26.

Denell, R., Roebroeks, W., 2005. An Asian perspective on early human dispersals from Africa. Nature 438, 1099–1104.

Détroit, F., Mijares, A.S., Corny, J., Daver, G., Zanolli, C., Dizon, E., Robles, E., Grün, R., Piper, P.J., 2019. A new species of Homo from the Late Pleistocene of the Philippines. Nature, 568, 181–186.

Dhona, M.S., Sanderson, R., López, S., France, J., 2018. Bivariate relationships incorporating method comparison: a review of linear regression methods. CAB reviews 11(28), 1–15.

Du, A., Zipkin, A.M., Hatala, K.G., Renner, E., Baker, J.L., Bianchi, S., Bernal, K.H., Wood, B.A., 2018. Patterns and process in hominin brain size evolution are scale-dependent. Proc. R. Soc. B 285, 20172738.

Elton, S., Bishop, L.C., Wood, B., 2001. Comparative context of Plio-Pleistocene hominin brain evolution. J. Hum. Evol. 41, 1–27.

Falk, D., Hildebolt, C., Smith, K., Morwood, M.J., Sutikna, T., Brown, P., Jatmiko, Wahyu Saptomo, E., Brunsden, B., Prior, F., 2005a. The Brain of LB 1, *Homo floresiensis*. Science 308, 242–245.

Falk, D., Hildebolt, C., Smith, K., Morwood, M.J., Sutikna, T., Brown, P., Jatmiko, Wahyu Saptomo, E., Brunsden, B., Prior, F., 2005b. Response to Comment on "The Brain of LB 1, *Homo floresiensis*". Science 310, 236c.

Falk, D., Hildebolt, C., Smith, K., Morwood, M.J., Sutikna, T., Jatmiko, Wahyu Saptomo, E., Brunsden, B., Prior, F., 2006. Response to comment on "The brain of LB 1, *Homo floresiensis*". Science 312, 999c.

Falk, D., Hildebolt, C., Smith, K., Morwood, M.J., Sutikna, T., Wahyu Saptomo, E., Imhof, H., Seidler, H., Prior, F., 2007. Brain shape in human microcephalics and *Homo floresiensis*. Proc. Natl. Acad. Sci. 104, 2513–2518.

Falk, D., Hildebolt, C., Smith, K., Jungers, W., Larson, S., Morwood, M.J., Sutikna, T., Jatmiko, Wahyu Saptomo, E., Prior, F., 2009a. The Type Specimen (LB 1) of *Homo floresiensis* did not have Laron Syndrome. Am. J. Phys. Anthropol. 140, 52–63.

Falk, D., Hildebolt, C., Smith, K., Morwood, M.J., Sutikna, T., Jatmiko, Wahyu Saptomo, E., Prior, F., 2009b. LB 1's virtual endocast, microcephaly, and hominin brain evolution. J. Hum. Evol. 57, 597–607.

Feuerriegel, E.M., Voisin, J-L., Churchill, S.E., Haeusler, M., Mathews, S., Schmid, P., Hawks, J., Berger, L.E., 2019. Upper limb fossils of *Homo naledi* from the Lesedi Chamber, Rising Star System, South Africa. PaleoAnthropology 2019, 311–349.

Gordon, A.D., Nevell, L., Wood, B., 2008. The *Homo floresiensis* cranium (LB 1): Size, scaling, and early *Homo* affinities. Proc. Natl. Acad. Sci. U.S.A 105, 4650–4655.

Grabowski, M., Hatala, K.G., Jungers, W.L., Richmond, B.G., 2015. Body mass estimates of hominin fossils and the evolution of human body size. J. Hum. Evol. 85, 77–93.

Green, D.J., Gordon, A.D., Rightmire, B.G., 2007. Limb-size proportions in *Australopithecus afarensis* and *Australopithecus africanus*. J. Hum. Evol. 52, 187–200.

Haeusler, M., McHenry, H.M., 2004. Body proportions of *Homo habilis* reviewed. J. Hum. Evol. 46, 433–465.

Haeusler, M., McHenry, H.M. 2007. Evolutionary reversals of limb proportions in early hominids? Evidence from KNM-ER 3735 (*Homo habilis*). J. Hum. Evol. 53, 383–405.

Harmand, S., Lewis, J.E., Feibel, C.S., Lepre, C.J., Prat, S., Lenoble, A., Boës, X., Quinn, R.L., Brenet, M., Arroyo, A., Taylor, N., Clément, S., Daver, G., Brugal, J-P., Leakey, L., Mortlock, R.A., Wright, J.D., Lokorodi, S., Kirwa, C., Kent, D.V., Roche, H., 2015. 3.3-million-year-old stone tools from Lomekwi 3, West Turkana, Kenya. Nature 521, 310–315.

Hawks, J., Elliot, M., Schmid, P., Churchill, S.E., de Ruiter, D.J., Roberts, E.M., Hilbert-Wolf, H., Garvin, H.M., Williams, S.A., Delezene, L.K., Feuerriegel, E.M., Randolph-Quinney, P., Kivell, T.C., Laird, M.F., Tawane, G., DeSilva, J.M., Bailey, S.E., Brophy, J.K., Meyer, M.R., Skinner, M.M., Tocheri, M.W., VanSickle, C., Walker, C.S., Campbell, T.L., Kuhn, B., Kruger, A., Tucker, S., Gurtov, A., Hlophe, N., Hunter, R., Morris, H., Peixotto, B., Ramalepa, M., van Rooyen, D., Tsikoane, M., Boshoff, P., Dirks, P.H.G.M., Berger, L.R., 2017. New fossil remains of *Homo naledi* from the Lesedi Chamber, South Africa. eLife, 6;e24232.

Holloway, R.C., 2015. The evolution of the hominid brain. In: Henke W., Tattersall, I., (eds.): Handbook of Paleoanthropology. Springer, pp. 1961–1987.

Holm, S., 1979. A simple sequentially rejective multiple test procedure. Scandinavian J. Stat. 6, 65–70.

Holowaka, N.B., Lieberman, D.E. 2018. Rethinking the evolution of the human foot: insights from experimental research. J. Exper. Biol. 221, jeb174425.

Howell, F.C., 1960. European and Northwest African Middle Pleistocene hominids. Curr, Anthropol. 1, 195–232.

Howells, W.,W., 1973. Cranial variation in man: A study by multivariate analysis of patterns of differences among recent human populations. Papers of the Peabody Museum of Archeology and Ethnology, vol. 67, pp. 259. Cambridge, Mass.: Peabody Museum.

Hunt, K.D., 1994. The evolution of human bipedality: ecology and functional morphology. J. Hum. Evol. 26, 183–202.

Jacob, T., Indriati, E., Soejono, R.P., Hsü, K., Frayer, D.W., Eckhardt, R.B., Kuperavage, A.J., Thorne, A., Henneberg, M., 2006. Pygmoid Australomelanesian *Homo sapiens* skeletal remains from Liang Bua, Flores: Population affinities and pathological abnormalities. Proc. Natl. Acad. Sci. U.S.A 103, 13421–13426.

Jungers, W.L., 1982. Lucy's limbs: Skeletal allometry and locomotion in Australopithecus afarensis. Nature 297, 676–678.

Jungers, W., Hancourt-Smith, W.E.H, Wunderlich, R.E., Tocheri, M.W., Larson, S.G., Sutikna, T., Rhokus Awe Due, Morwood, M.J., 2009a. The foot of *Homo floresiensis*. Nature 459, 81–84.

Jungers, W., Larson, S.G., Hancourt-Smith, W., Morwood, M.J., Sutikna, T., Rokhus A. D., Djubiantono. T., 2009b. Descriptions of the lower limb skeleton of *Homo floresiensis*. J. Hum. Evol. 57, 538–554.

Kaifu, Y., Aziz, F., Indriati, E., Jacob, T., Kurinawan, I., Baba, H., 2008. Cranial morphology of Javanese *Homo erectus*: New evidence for continuous evolution, specialization, and terminal extinction. J. Hum. Evol. 55, 551–580.

Kaifu, Y., Baba, H., Sutikna, T., Morwood, M.J., Kubo, D., Wahyu Saptomo, E., Jatmiko, Rokus, A. D., Djubiantono, T., 2011a. Craniofacial morphology of *Homo floresiensis*: description, taxonomic affinities, and evolutionary implication. J. Hum. Evol. 61, 644–682.

Kaifu, Y., Zaim, Y., Baba, H., Kurniawan, I., Kubo, D., Rizal, Y., Arif, J., Aziz, F., 2011b. New reconstruction and morphological description of a *Homo erectus* cranium: Skull IX (Tjg-1995.05) from Sangiran, Central Java. J. Hum. Evol. 61, 270–294.

Kaifu, Y., Kono, R.T., Sutikna, T., Wahyu Saptomo, E., Jatmiko, Awe Due, R., Baba, H., 2015a. Descriptions of the dental remains of *Homo floresiensis.* Anthropol. Sci. 123, 129–145.

Kaifu, Y., Kono, R.T., Sutikna, T., Wahyu Saptomo, E., Jatmiko, Awe Due, R., 2015b. Unique dental morphology of *Homo floresiensis* and its evolutionary implications. PLOS ONE 10, 1–27.

Kaifu, Y., Kurniawan, I., Kubo, D., Sudiyabudi, E., Putro, G.P., Prasanti, E., Aziz, F., Baba, H., 2015c. *Homo erectus* calvaria from Ngawi (Java) and its evolutionary implications. Anthropol. Sci. advanced publication.

Kaifu, Y., 2017. Archaic hominin populations in Asia before the arrival of modern humans: Their phylogeny and implications for the “Southern Denisovans”. Curr. Anthropol. 58, S418–S433.

Kilmer, J.T., Rodríguez, R.L., 2017. Ordinary least squares regression is indicated for studies of allometry. J. Evol. Biol. 30, 4–12.

Kimbel, W.H., Johanson, D.C., Coppens, Y., 1982. Pliocene hominid cranial remains from the Hadar Formation, Ethiopia. Am. J. Phys. Anthropol. 57, 453–499.

Kimbel, W.H., Johanson, D.C., Coppens, Y., 2004. The skull of *Australopithecus afarensis*. New York: Oxford University Press.

Kingslover, J.G., Koehl, M.A.R., 1985. Aerodynamics, thermoregulation and the evolution of insect wings: differential scaling and evolutionary change. Evolution 39, 488–504.

Kubo, D., Kono, R.T., Kaifu, Y., 2013. Brain size of *Homo floresiensis* and its evolutionary implications. Proc. R. Soc. B. 280, 20130338.

Kunze, J., Karakostis, F.A., Merker, S., Persani, M., Hotz, G., Tourloukis, V., Harvati, K., 2022. Entheseal patterns suggest habitual tool use in early hominins. PaleoAnthropology 2, 195–210.

Laird, M.Y., Schroeder, L., Garvin, H.M., Scoot, J.E., Dembo, M., Radovčić, D., Musiba, C.M., Ackermann, R.R., Schmid, P., Hawks, J., Berger, L.R., de Ruiter, D.J., 2017. The skull of *Homo naledi*. J. Hum. Evol. 104, 100–123.

Lahr, M.M., Foley, R., 2004. Human evolution writ small. Nature 431, 1043–1044.

Larson, S.G., Junger, W.L., Morwood, M.J., Sutikna, T, Jatmiko, Wahyu Saptomo, E., Rokus Awe Due, Djubiantono T., 2007. *Homo floresiensis* and the evolution of the hominin shoulder. J. Hum. Evol. 53, 718–731.

Larson, S.G., Jungers, W.L., Tocheri, M.W., Orr, C.M., Morwood, M.J., Sutikna, T., Rokus Due Awe, Djubiantono, T., 2009. Descriptions of the upper limb skeleton of *Homo floresiensis*. J. Hum. Evol. 57, 555–570.

Ledogar, J.A., Dechow, P.C., Wang, Q., Gharpure, P.H., Gordon, A.D., Baab, K.L., Smith, A.L., Weber, G.W., Grosse, I.R., Ross, C.F., Richmond, B.G., Wright, B.W., Byron, C., Wroe

S., Strait, D.S., 2016. Human feeding biomechanics: Performance, variation, and functional constraints. PeerJ 4: e2242.

Ledogar J.A., Benazzi, S., Smith, A.L., Weber, G.W., Carlson, K.B., Dechow, P.C., Grosse, I.R., Ross, C.F., Richmond, B.G., Wright, B.W., Wang, Q., Byron, C., Carlson, K.J., De Ruiter, D.J., Proyr McIntosh, L.C., Strait, D.S., 2017. The biomechanics of bony facial "buttresses" in South African australopiths: An experimental study using finite element analysis. Anat. Rec. 300, 171–195.

Leakey, R.E., Leakey, M.G., Walker, A.C. 1988. Morphology of *Turkanapithecus kalakolensis* from Kenya. Am. J. Phys. Anthropol. 76, 277–288.

Lieberman, D.E., 2005. Further fossil finds from Flores. Nature 437, 957–958.

Lieberman, D.E., Bramble, D.M., 2007. The evolution of marathon running. Sports Med. 288–290.

Lieberman, D.E., 2011. The Evolution of the Human Head. The Belknap Press of Harvard University.

Ligges, U., Mächler, M., 2003. Scatterplot3d - an R Package for Visualizing Multivariate Data. Journal of Statistical Software 8, 1–20.

Liu, W., Zhang Y., Wu, X., 2005. Middle Pleistocene human cranium from Tangshan (Nanjing), Southeast China: A new reconstruction and comparisons with *Homo erectus* from Eurasia and Africa. Amer. J. Phys. Anthropol. 127, 253–262.

Lockwood, C.A. 1999., Sexual dimorphism in the face of *Australopithecus africanus*. Amer. J. Phys. Anthropol. 108, 97–127.

Lockwood, C.A., Tobias, P.V., 1999. A large male hominin cranium from Sterkfontein, South Africa, and the status of *Australopithecus africanus*. J. Hum. Evol. 36, 637–685.

Lockwood, C.A., Menter, C.G., Moggi-Cecchi, J., Keyser, A.W., 2007. Extended male growth in a fossil hominin species. Science 318, 1443–1446.

Lordkipanidze, D., Vekua, A., Ferring, R., Rightmire, P.G., Zollikofer, C.P.E., Ponce de León, M.S., Agusti, J., Kiladze, G., Muskhelishvili, A., Nioradze, M., Tappen, M., 2006. A fourth hominin skull from Dmanisi, Georgia. Anat. Rec. A, 288A, 1146–1157.

Lovejoy, C.O., Suwa, G., Spurlock, L., Asfaw, B., White, T.D., 2009a. The pelvis and femur of *Ardipithecus ramidus*: The emergence of upright walking. Science 326, 71e1–6.

Lovejoy, C.O., Latimer, B., Suwa, G., Asfaw, B., White, T.D., 2009b. Combining prehension and propulsion: The foot of *Ardipithecus ramidus*. Science 326, 72e1–6.

MacFadden, B.J., 1986. Fossil horses from "Eohippus" (*Hyracotherium*) to *Equus*: Scaling, Cope's Law, and the evolution of body size. Paleobiol. 12, 355–369.

Marchi, D., 2015. Using the morphology of the hominoid distal fibula to interpret arboreality in *Australopithecus afarensis*. J. Hum. Evol. 85, 136–148.

Marzke, M.W., 1997. Precision grips, hand morphology, and tools. Amer. J. Phys. Anthropol. 102, 91–110

McCarthy, R., 2001. Anthropoid cranial base architecture and scaling relationships. J. Hum. Evol. 40, 41–66.

McDougall, I., Brown, F.H., Vasconcelos, P.M., Cohen, B.E., Thiede. D.S., Buchanan, M.J., 2012. New single crystal $^{40}Ar/^{39}Ar$ ages improve time scale for deposition of the Omo group, Omo – Turkana Basin. East Africa. J. Geol. Soc. 169, 213–226.

Morwood, M.J., Soejono, R.P., Roberts, R.G., Sutikna, T., Turney, C.S., Westaway, K.E., Rink, W.J., Zhao, J.-x., van den Bergh, G.D., Rokus Awe Due, Hobbs, D.R., Moore, M.W.,

Bird, M.I., Fifield, L.K., 2004. Archaeology and age of a new hominin from Flores in eastern Indonesia. Nature 431, 1087–1091.

Nagano, A., Umberger, B.R., Marzke, M.W., Gerritsen, K.G.M., 2005. Neuromusculoskeletal computer modeling and simulation of upright, straight-legged, bipedal locomotion of *Australopithecus afarensis* (A.L. 288-1). Amer. J. Phys. Anthropol. 126, 2–13.

Navarrete, A., van Schaik, C.P., Isler, K., 2011. Energetics and the evolution of human brain size. Nature 480, 91–93.

Ni, X., Ji, Q., Wu, W., Shao, Q., Ji, Y., Zhang, C., Liang, L., Ge, J., Guo, J., Li, J., Li, Q., Grün, R., Stringer, C., 2021. Massive cranium from Harbin in northeastern China establishes a new Middle Pleistocene human lineage. Innovation 2, 100130.

Ohman, J.C., Wood, C., Wood, B., Crompton, R.H., Günther, M.M., Yu, L., Savage, R., Wang, W., 2002. Stature-at-death of KNM-WT 15000. Hum. Evol. 17, 129–142.

Orr, C.M., Tocheri, M.W., Burnett, S.E., Awe Due R., Wahyu Saptomo, E., Sutikna, T., Jatmiko, Wasisto, Morwood, M.J., Jungers, W.L., 2013. New wrist bones from Liang Bua (Flores, Indonesia). J. Hum. Evol. 64, 109–129.

Pagel, M.D., Harvey, P.H., 1988. The taxon-level problem in the evolution of mammalian brain size: Facts and artifacts. Amer. Natur. 132, 344–359.

Pearson, O.M., Lieberman, D.E., 2004. The aging of Wolff's "Law": Ontogeny and responses to mechanical loading in cortical bone. Yearbook Phys. Anthropol. 47, 63–99.

Pérez-Claros, J.A., Jiménez-Arenas, J., Palmqvist P., 2015. Neurocranium versus face: A Morphometric approach with classical anthropometric variables for characterizing patterns of cranial integration in extant hominoids and extinct hominins. PLos ONE 10: e0131055.

Pérez-Claros, J.A., Palmqvist, P., 2022. Heterochronies and allometries in the evolution of the hominid cranium: A morphometric approach using classical anthropometric variables. PeerJ 10, e13991.

Pickford, M., Senut, B., Gommery, D., Treil, J., 2002. Bipedalism in *Orrorin tugenensis* revealed by its femora. C. R. Paleovol 1, 191–203.

Pilbeam, G., Gould, S.J., 1974. Size and scaling in human evolution. Science 186, 892–901.

Plummer, T.W., Oliver, J.S., Finestone, E.M., Ditchfield, P.W., Bishop, L.C., Scott A. Blumenthal, S.A., Lemorini, C., Caricola1, I., Bailey, S.E., Herries, A.I.R., Parkinson, J.A., Whitfield, E., Hertel, F., Kinyanjui, R.N., Vincent, T.H., Li, Y., Louys, J.,Frost, S.R., Braun, D.R., Reeves, J.S., Early, E.D.G., Onyango, B., Lamela-Lopez, R., Forrest, F.L., He, H., T.P., Frouin, M., Nomade S., Wilson, E.P., Bartilol, S.K., Rotich, N.K., Pott, R., 2023. Expanded geographic distribution of dietary strategies of the earliest Oldowan hominins and *Paranthropus*. Science 379, 561–566.

Pontzer, H., Roilan, C., Rightmire, P.G., Jashashvili, T., Ponce de León, M.S., Lordkipanidze, D., Zollikofer, C.P.E., 2010. Locomotor anatomy and biomechanics of the Dmanisi hominins. J. Hum. Evol. 58, 492–504.

Prabhat, A.M., Miller, C.K., Prang, T.C., Spear, J., Williams, S.A., DeSilva, J.M., 2021. Homoplasy in the evolution of modern human-like joint proportions in *Australopithecus afarensis*. eLife 10, e65897.

R Core Team., 2021. R: A language and environment for statistical computing. R Foundation for Statistical Computing, Vienna, Austria. URL https://www.R-project.org/.

Rak., Y., White, T.D., Howell, C.F., 1983. The Australopithecine face. Academic Press Inc.

Rak, Y., Marom, A., 2017. Opposing extremes of zygomatic bone morphology: *Australopithecus boisei* versus *Homo neanderthalensis*. Anat. Rec. 300, 152–159.

Rak, Y., Kimbel, W.H., Moggi-Cecchi, J., Lockwood, C.A., Menter, C., 2021. The DNH 7 skull of *Australopithecus robustus* from Drimolen (Main Quarry), South Africa. J. Hum. Evol. 151, 102913.

Richtsmeier, J.T., Walker, A., 1993. A morphometric study of facial growth. In Walker, A., Leakey, R., (eds.): The Nariokotome *Homo erectus* skeleton. Harvard University Press, pp. 409–430.

Richmond, B.G., Aiello, L.C., Wood, B.A., 2002. Early hominin limb proportions. J. Hum. Evol. 43, 529–548.

Richmond, B.G., Jungers, W.L., 2008. *Orrorin tugenesis* femoral morphology and the evolution of hominin bipedalism. Science 319, 1662–1665.

Rightmire, P.G., 1983. The Lake Ndutu cranium and early *Homo sapiens* in Africa. Amer. J. Phys. Anthropol. 61, 245–254.

Rightmire, P.G., Lordkipanidze, D., Vekua, A., 2006. Anatomical descriptions, comparative studies and evolutionary significance of the hominin skulls from Dmanisi, Republic of Georgia. J. Hum. Evol. 50, 115–141.

Ruff, C.B., Walker, A., 1993. Body size and body shape. In Walker, A., Leakey, R., (eds.): The Nariokotome *Homo erectus* skeleton. Harvard University Press, pp. 234–265.

Ruff, C., 2009. Relative limb strength and locomotion in *Homo habilis*. Amer. J. Phys. Anthropol., 138, 90–100.

Ruff, C.B., Burgess, M.L., Squyres, N., Junno, J-A., Trinkaus, E., 2018. Lower limb articular scaling and body mass estimation in Pliocene and Pleistocene hominins. J. Hum. Evol. 115, 85–111.

Ruff, C.B., Wood, B.A., 2023. The estimation and evolution of hominin body mass. Evol. Anthropol. 32, 223–237.

Ruxton, G.D., Wilkinson, D.M., 2011. Thermoregulation and endurance running in extinct hominins: Wheeler's models revisited. J. Hum. Evol. 61, 169–175.

Ryan, T.M., Carlson, K..J., Gordon, A.D., Jablonski, N., Shaw, C.N., Stock, J.T., 2018. Human-like hip joint loading in *Australopithecus africanus* and *Paranthropus robustus*. J. Hum. Evol. 121, 12–24.

Scardia, G., Neves, W.A., Tattersall, I., Blumrich, L., 2021. What kind of hominin first left Africa? Evol. Anthropol. 30, 122–127.

Shea, J.J., 2017. Occasional, obligatory, and habitual stone tool use in hominin evolution. Evol. Anthropol. 26, 200–217.

Selassie, Y., Suwa G., White, T.D., 2004. Late Miocene teeth from the Middle Awash, Ethiopia, and early hominid dental evolution. Science 303, 1503–1505.

Selassie, Y., Melillo, S.M., Vazzana, A., Benazzi. S., Ryan, T.M., 2019. A 3.8-million-year-old hominin cranium from Woranso-Mille, Ethiopia. Nature 573, 214–219.

Semaw, S., Renne, P., Harris, J.W.K., Feibel, C.S., Bernor, R.L., Fesseha, N., Mowbray, K., 1997. 2.5-million-year-old stone tools from Gona, Ethiopia. Nature 385, 333–336.

Singleton, M., 2012. Postnatal cranial development in Papionin primates: An alternative model for hominin evolutionary development. Evol. Biol. 39, 499–520.

Spence, A.J., 2009. Scaling in biology. Curr. Biol. 19, R57–61.

Spoor, F., Leakey, M.G., Gathogo, P.N., Brown, F.H., Antón, S.C., McDougall, I., C. Kiarie, Manthi, F.K., Leakey, L.N., 2007. Implications of new early *Homo* fossils from Ileret east of Lake Turkana, Kenya. Nature 448, 688–691.

Stelzer, S., Gunz, P., Neubauer, S., Spoor, F., 2017. Hominoid arcade shape: Pattern and magnitude of covariation. J. Hum. Evol. 107, 71–85.

Stern Jr., J.T., Susman, R.L., 1983. The locomotor anatomy of *Australopithecus afarensis*. Amer. J. Phys. Anthropol. 60, 279–317.

Susman, R.L., Stern, J.t., Jungers, W.L., 1984. Arboreality and bipedality in the Hadar hominids. Folia primatol. 43, 113–156.

Susman, R.L., 1998. Hand function and tool behavior in early hominids. J. Hum. Evol. 35, 23–46.

Suwa, G., Asfaw, B., Beyene, Y., White, T.D., Katoh, S., Nagaoka, S., Nakaya, H., Uzawa, K., Renne, P., Wolde, Gabriel, G., 1997. The first skull of *Australopithecus boisei*. Nature 389, 489–492.

Suwa, G., Kono, R.T., Simpson, S.W., Asfaw, B., Lovejoy, C.O., White, T.D., 2009. Paleobiological implication of the *Ardipithecus ramidus* dentition. Science 326, 94–99.

Traynor, S., Green, D.J., Hawks, J., 2022. The relative limb size of *Homo naledi*. J. Hum. Evol. 170, 103253.

Tobias, P.V., 1967. Olduvai Gorge: The cranium of *Australopithecus* (*Zinjanthropus*) *boisei*. Cambridge University Press.

Tocheri, M.W., Orr, C., Larson, S.G., Sutikna, T., Jatmiko, Wahyu Saptomo, E., Awe Due, R., Djubiantono, T., Morwood, M.J., Jungers, W.L., 2007. The primitive wrist of *Homo floresiensis* and its implications for hominin evolution. Science 317, 1743–1745.

Tocheri, M.W., Veatch, G., Jatmiko, Wahyu Saptomo, E., Sutikna T., 2022. *Homo floresiensis*. In Kim, N.C., Higham, C., (eds.): Oxford Handbook of Southeast Asian Archaeology. Oxford University Press, pp. 38–69.

van den Bergh, G.D., Kaifu, Y., Kurniawan, I., Kono, R.T., Brumm, A., Setiyabudi, E., Aziz, F., Morwood, M.J., 2016. *Homo floresiensis*-like fossils from the early Middle Pleistocene of Flores. Nature 534, 245–248.

Warton, D.I., Duursma, R.A., Falster, D.S. and Sara, S., 2012. smatr 3 - an R package for estimation and inference about allometric lines. Methods in Ecology and Evolution 3, 257–259.

Weaver, T.D., Stringer, C.B., 2015. Unconstrained cranial evolution in Neandertals and modern humans compared to common chimpanzees. Proc. R. Soc. B. 282: 20151519.

Weber, G.W., Krenn, V.A., 2017. Zygomatic root position in recent and fossil hominids. Anat. Rec. 300, 160–170.

Weidenreich, F., 1943. The skull of *Sinanthropus pekinensis*: A comparative study on a primitive hominid skull. Geological Survey of China.

Weston, E.M., Lister, A.M., 2009. Insular dwarfism in hippos and a model for brain size reduction in *Homo floresiensis*. Nature 459, 85–88.

White, C.R., Cassey, P., Blackburn, T.M., 2007. Allometric exponents do not support a universal metabolic allometry. Ecology 88, 315–323.

Wickham, H. 2016., ggplot2: Elegant Graphics for Data Analysis. Springer-Verlag New York.

Widianto, H., Zeitoun, V., 2003. Morphological description, biometry and phylogenetic position of the skull of Ngawi 1 (East Java, Indonesia). Inter. J. Osteoarch. 13, 339–351.

Will, M., Pablos, A., Stock, J.T., 2017. Long-term patterns of body mass and stature evolution within the hominin lineage. R. Soc. Open Sci. 4, 171339.

Wood, B., 1991. Koobi Fora Research Project, Volume 4: Hominid Cranial Remains. Clarendon Press, Oxford (England).

Wood, B., 2019. Human Evolution: A Very Short Introduction. 2nd edition. Oxford: Oxford University Press.

Yegian, A.K., Tucker, Y., Bramble, D.M., Liebrman, D.E., 2021. Neuromechanical linkage between the head and forearm during running. Amer. J. Phys. Anthropol. 174, 752–762.

Zhu, Z., Dennell, R., Huang, W., Wu, Y., Qui, S., Yang, S., Roa, Z., Hou, Y., Xie, J., Han, J., Ouyang, T., 2018. Hominin occupation of the Chinese Loess Plateau since about 2.1 million years ago. Nature 559, 608–612.